THE INTERACTION OF CLIMATE, TECTONICS, AND TOPOGRAPHY IN THE OLYMPIC MOUNTAINS OF WASHINGTON STATE: THE INFLUENCE OF EROSION ON TECTONIC STEADY-STATE AND THE SYNTHESIS OF THE ALPINE GLACIAL HISTORY

BY

JESSICA LYNN HELLWIG

THESIS

Submitted in partial fulfillment of the requirements
for the degree of Master of Science in Geology
in the Graduate College of the
University of Illinois at Urbana-Champaign, 2010

Urbana, Illinois

Adviser:

Assistant Professor Alison M. Anders

ABSTRACT

The interaction of climate, tectonics, and topography in the Olympic Mountains of Washington State is explored to determine the influence of glaciers on spatially variable erosion and rock uplift rates. As glaciers have long been present on the peninsula, could glacial erosion explain the observed pattern of rock uplift? A numerical model of glacial flow, ICE Cascade, is used to reconstruct the glacial extent of the Last Glacial Maximum for the first time. Modeled ice extent best matches observations when summer temperatures range from 7.0-8.0°C and precipitation is reduced to 0.4-0.8 times the modern. These values are consistent with paleoclimate records. Simulated glacial erosion based on a sliding law varies with observed trends in rock uplift rates across the peninsula. If erosion rates are assumed to equal rock uplift rates, as suggested by evidence of tectonic steady state in the region, a glacial erosion constant on the order of 10^{-5} is indicated based on modeled sliding rates in three valleys on the western side of the range.

These efforts are hampered by the lack of a glacial and paleoclimate record from the northern and eastern peninsula. A regional growth curve for lichenometric dating of neoglacial moraines is developed and applied to four moraines at the base of Royal Glacier on Mt. Deception. The moraines range in age from 1839±45, 1895±45, and 1963±45, to less than 20±45 years. The estimated equilibrium line altitude (ELA) for Royal Glacier during this time is 1774 m as compared with 1688 m for Blue Glacier in the western Olympics over the same period. A compendium of glacial deposits observed throughout the peninsula is also summarized so a broader picture of the alpine glacial extent and continental ice extent can be developed.

Overall, this work demonstrates that the sliding based glacial erosion model can explain the uplift pattern when the glacial erosion constant is on the order of 10^{-5} in three separate river valleys. Additional work on the northern and eastern sides of the peninsula would allow for a broader picture of the glacial history and provide a closer glacial erosion constant in the model. The culmination of work in these areas allows for a greater understanding of how climate, erosion, and tectonics interact on the Olympic Peninsula.

For Erin Kathryn Hellwig.

May you follow your dreams and know anything is possible.

ACKNOWLEDGEMENTS

These projects would not have been possible without the support of many people. I would like to thank my advisers, Alison Anders and Jonathan Tomkin, for their help and advice with the many aspects of this thesis. I would like to thank Geoffrey Poore for his help with the initial set-up of ICE Cascade and with the climate sensitivity analysis. Many thanks go to the many graduate students who have assisted me with this endeavor. Several people from Olympic National Park have been of great assistance with the field work portion of my thesis as well as with gathering further information on the peninsula: Jerry Freilich, Dave Conca, and Gay Hunter. Jon Reidel from the National Park Service assisted with the recognition of glacial geomorphic features and glacial extent on the peninsula. Bill Shelmerdine from Olympic National Forest assisted with locating William Long's papers. Dan and Birgitt Altmayer and Bridget Yuvan were of great assistance with the field work component of my thesis. This work was possible through grant #43713-G8 from the American Chemical Society and a Leighton Award and Wanless Fellowship from the Department of Geology at the University of Illinois. Finally, many thanks go to my parents and family for their support and love throughout this project.

TABLE OF CONTENTS

CHAPTER 1: INTRODUCTION AND BACKGROUND……1
1.1 Introduction……1
1.2 Background on the Olympic Peninsula……..3
1.2.1 Climate……4
1.2.2 Glacial Mechanics……...5
1.2.3 Glacial History……6
1.2.4 Geology……10
1.2.5 Accretionary Wedge/Topographic Steady State……...11
1.3 Outline……..14
1.4 Figures and Tables……...15

CHAPTER 2: NUMERICAL MODELING OF GLACIAL EXTENT AND EROSION.23
2.1 Introduction……..23
2.2 ICE Cascade Model……24
2.3 Sensitivity of Glacial Extent to Temperature and Precipitation……..29
2.4 Determination of Glacial Erosion with ICE Cascade……..31
2.4.1 Reference Case Set-up……..31
2.4.2 Results of Erosion at the Entire Range Scale……33
2.4.3 Comparison of Glacial Erosion and Uplift Within the Valleys……34
2.4.4 Variability of Glacial Erosion with Precipitation and Temperature for the Reference Case……...35
2.4.5 Using the Glacial Erosion to Constrain the Glacial Erosion Rule…36
2.5 Discussion and Conclusions……38
2.6 Figures and Tables……...42

CHAPTER 3: LICHENOMETRY: RECENT GLACIAL HISTORY OF ROYAL BASIN……...76
3.1 Introduction……..76
3.2 Lichenometry……...76
3.2.1 Introduction……...76
3.2.2 Lichen Biology……..77
3.2.3 Lichen Growth……..77
3.2.4 Lichen Measurement……79
3.3 Pacific Northwest Regional Growth Curve……79
3.4 Olympic National Park-Mount Deception Data……..83
3.5 Discussion……86
3.5.1 The Chronology of Royal Basin Compared to the Regional Glacial History……86
3.5.2 ELA Reconstructions……88
3.6 Conclusions……..93
3.7 Figures and Tables……...94

CHAPTER 4: CATALOG OF DESCRIPTIONS OF GLACIAL DEPOSITS IN THE OLYMPIC MOUNTAINS……..121

4.1 Introduction……121
4.2 Glacial Deposits and Features Recorded By William Long……..125
4.3 References of Deposits From Other Authors By William Long……183
4.4 Figures……188

CHAPTER 5: SUMMARY AND FUTURE WORK……..189
5.1 Hypotheses and Motivation……...189
5.2 Results……190
5.3 Future Work……...191

REFERENCES……194

APPENDIX A: SUMMARY OF CODES AND PROCESSES FOR TRANSFORMING THE ICE CASCADE DATA……...203
A.1 ICE Cascade Codes, Data, and Methods for Running……..203
A.2 Matlab Codes and Methods……...204
A.3 Matlab and ICE Cascade Codes……207

CHAPTER 1: INTRODUCTION AND BACKGROUND

1.1 INTRODUCTION

Recent research documents the theoretical possibility of interactions between climate, surface erosion, and rock uplift rates (Willett, 1999; Zeitler er al., 2001; Willett and Brandon, 2002; Koons et al., 2003; Hilley and Strecker, 2004; Whipple and Meade, 2004; Roe et al., 2006). One of the most striking aspects of this work is the suggestion that climate may influence mountain building not only by passively shaping topography, but also by actively influencing the rates and spatial patterns of tectonic deformation (Willett, 1999; Stolar et al., 2006). If so, the spatial and temporal variability in climate might be recorded by the variability in rock uplift rates. These ideas represent a significant shift in the conventional conception of mountain building.

Testing the possibility of climate-driven variability in rock uplift rates in real mountain ranges is challenging for several reasons. First, climate, erosion, and tectonics form a coupled system in which processes feedback on one another. For example, surface erosion rates depend on topography and are, therefore, influenced by rock uplift rates. Climate is also sensitive to both topography and rock uplift and hence surface erosion. These links make it difficult to determine causality as opposed to simply noting concurrent changes in climate, erosion, and rock uplift. Secondly, climate varies significantly in space and time, especially in mid-latitude mountain ranges during the Quaternary. Moreover, this variability in climate is generally not well constrained, especially at the spatial (1-100 km) and temporal scales (0.001-10 Ma) that matter for the topographic evolution of mountain ranges. Finally, thermochronologic data constraining rock uplift rates provide averages over relatively long timescales (0.1-10 Ma), which are difficult to compare with measures of erosion rates through cosmogenic methods or landform dating and analysis, which represent much shorter timescales (100-100,000 yrs).

The Olympic Mountains of Washington State provide a unique opportunity to test the hypothesis that climate-driven spatial variability in erosion rates can create spatial variability in rock uplift rates. The tectonic setting of the Olympic Mountains is an accretionary wedge which is well-described by the critical-taper wedge model of Dahlen

(1984). In such an orogen, the topographic form of the mountain range maintains a constant taper angle. Numerical studies of eroding critical wedge mountain ranges indicate that the spatial variability in surface erosion rates is balanced by spatial variability in rock uplift rates to maintain the taper angle (Stolar et al., 2006; Tomkin and Roe, 2007). In addition, the Olympic Mountains are thought to be in a steady-state in which the spatially-variable erosion and rock uplift patterns have been maintained in a close balance over several million years (Brandon et al., 1998; Pazzaglia and Brandon, 2001). The evidence for this balance comes from the agreement of fission-track cooling age reconstructions of long-term exhumation and radiocarbon dating of Quaternary fluvial terraces (Pazzaglia and Brandon, 2001). The uplift and exhumation are faster in the center of the range than at the edges with the rates of exhumation approximately 1 mm/yr in the center and 0.1 mm/yr on the flanks (Brandon, 2004). This well-established and steady, but spatially variable, pattern of rock uplift and surface erosion provides a natural laboratory for the study of the link between surface processes, climate, and tectonics.

The Olympic Mountains setting also provides a well-constrained spatially and temporally variable climate in which to observe the interactions between climate, surface processes, and rock uplift. The climate of the Olympic Mountains is characterized by a significant decrease in precipitation rates across the range from west to east. This spatial variability in the modern is closely associated with topography and is relatively insensitive to variability in atmospheric conditions from storm to storm (Anders et al., 2007; Minder et al., 2008). In addition, a simple, physically-based model of the precipitation pattern can reproduce observed spatial patterns in precipitation (Anders et al., 2007). The Olympic Mountains have also been extensively glaciated during the Quaternary and the impact of temporal variability in climate can be seen in the record of ice extent. Reconstructions of glaciers in several large valleys on the western side of the Olympic Mountains have been completed (Thackray, 1996, 2001). The modern orographic precipitation pattern in a maritime climate allows glaciers to exist at relatively low altitudes throughout the range. There are currently over sixty active glaciers in the range (Spicer, 1986).

Despite the persistent climate gradients and tightly constrained tectonic setting of the Olympic Peninsula, the spatially-variable erosion and rock uplift pattern in the Olympic Mountains remains poorly understood. In particular, the spatial variability in erosion rates is not consistent with the prominent stream power theory of fluvial incision rates (Tomkin et al., 2003). Can glacial erosion explain the observed pattern of rock uplift rates?

Glaciers can be highly effective agents of erosion (e.g., Hallet et al., 1996) and have been hypothesized to control the maximum topography of glaciated ranges (e.g., Porter, 1981). Numerical models indicate that glaciers focus erosion at high elevations and decrease mountain relief (Tomkin and Braun, 2002). Glaciated critical-taper wedges behave similarly to fluvially-eroded wedges in numerical models and both show the impact of climate on rock uplift rates (Tomkin and Roe, 2007).

The focus of this work is on the relationships between climate, glacial extent, long-term exhumation, and the spatial patterns of glacial erosion in the Olympic Mountains. The record of recent glaciations and glacial landforms will be examined and the spatial variability in the timing and extent of glaciers across the range will be compared with the modern climatic gradients. Using a numerical model of glacier flow, glaciers consistent with geomorphic and paleoclimate data pertaining to glacial extent and climatic conditions during the late Quaternary will be reproduced. Finally, a numerical model of glacial erosion is used to estimate the spatial distribution of erosion rates that would have been associated with the reconstructed glaciers.

1.2 BACKGROUND ON THE OLYMPIC PENINSULA

The Olympic Peninsula is the most northwestern portion of the contiguous United States. It is bounded by the Pacific Ocean to the west, the Strait of Juan de Fuca to the north, Puget Sound to the east, and the Chehalis River Valley lowland to the south (Figure 1.1). The peninsula is dominated by the Olympic Mountains, a rugged, deeply incised, 7700 km^2 mountain range. The mountains rise gradually from the Pacific coastal plain in the west to altitudes greater than 2000 m, remain high throughout the eastern portion of the range, and then drop drastically into the Puget and Juan de Fuca lowlands to the east. Mt. Olympus is the highest peak at 2432 m and lies in the center of the

peninsula, while Mt. Deception is the second highest peak at 2374 m and lies in the eastern portion of the range.

1.2.1 Climate

The Olympic Peninsula experiences a maritime climate with moderate temperatures and large annual precipitation totals (Spicer, 1986; Thackray, 2001; Anders et al., 2007). Southwesterly and westerly winds prevail during the fall and winter, or from October to March (winter precipitation), and these winds deliver moisture laden Pacific air masses (Spicer, 1986; Thackray, 2001). These air masses provide large amounts of precipitation to the peninsula, with 80% of the annual precipitation falling during this time (Spicer, 1986; Thackray, 2001). The precipitation varies depending on the altitude of the location on the peninsula. The winter precipitation mostly falls as rain at altitudes below 300 m, a mixture of rain and snow occurs between 300 m to 750 m, and snow occurs above 750 m (Spicer, 1986). Snowfall typically begins in October and the seasonal snowfall accumulation can last through June or July with the total snowfall ranging from 20-76 cm in the coastal regions gradually increasing with altitude to a maximum of approximately 1270 cm near the mountain crest (Spicer, 1986). Northwesterly and westerly winds prevail in the spring and summer and these winds are generated by a high pressure center that dominates the northern portion of the Pacific Ocean during this time leading to a summer dry season (Spicer, 1986). The Cascade Range to the east also protects the peninsula from the masses of cold, arctic air blown south from Canada in the winter and hot, dry air in the summer thus letting the Pacific Ocean moderate the temperatures.

Annual temperatures show little spatial variation except with elevation. In the coastal lowlands, the summer temperature varies from 10°C to 24°C and the winter temperature ranges from -2°C to 7°C (Spicer, 1986). Extreme temperatures occur when continental air masses are able to invade the Olympic Peninsula from the east, however, the Cascade Range generally blocks these air masses, preventing them from reaching the peninsula (Spicer, 1986; Anders et al., 2007). The temperature does vary with elevation at a lapse rate of 0.0063 °C/m (NOAA, 2007).

There are distinct variations in the amount of precipitation delivered to different parts of the Olympic Peninsula and the precipitation pattern varies from west to east across the Olympic Mountains (Figure 1.2). The total annual precipitation along the coast ranges from 1780-2540 mm/yr while the valleys on the western side receive more than 3175 mm/yr (Spicer, 1986). Mt. Olympus receives 4800-5080 mm/yr of precipitation, the greatest amount in the continental United States (Spicer, 1986). Northeast of Mt. Olympus the precipitation rates decrease drastically over a distance of less than 60 km with Port Angeles receiving 259 mm/yr and Sequim receiving 158 mm/yr (Spicer, 1986; Thackray, 1996). The precipitation pattern is due to orographic lifting and adiabatic cooling of the moist, maritime air crossing the mountain range (Spicer, 1986; Anders et al., 2007). As storms move into the coastal region of the peninsula from the Pacific Ocean, they reach the foothills of the mountains. The mountains force the clouds upward and as the air gets colder and air pressure decreases, the clouds are unable to retain the large amounts of moisture and release it to the valleys and peaks of the western side of the range. As the clouds reach the eastern side and begin to descend, they are already deprived of large amounts of moisture and experience further adiabatic warming and drying creating a rain shadow.

1.2.2 Glacial Mechanics

Glaciers form when the snowfall that occurs during winter exceeds the melt that occurs during the summer. Environmental variables including precipitation, temperature, altitude, and continentality influence glacial extent (Paterson, 1994; Ritter et al, 2002; Hooke, 2005). The gains and losses in ice thickness and extent that occur on a glacier correspond to the accumulation and ablation. Accumulation occurs mainly through snow falling on the glacier which is then slowly transformed into ice, but it can also occur through avalanches, the formation of frost on the glacier, the freezing of rain within the snowpack, the transportation of snow by wind, and many other processes (Paterson, 1994; Benn and Evans, 1998; Knight, 1999; Ritter et al, 2002). Ablation includes all of the processes whereby snow and ice are lost from the glacier. Some of these processes include melting, run-off, evaporation, sublimation, calving of icebergs, and the removal of snow by wind (Paterson, 1994; Knight, 1999; Ritter et al, 2002; Hooke, 2005). The

influence of these processes on a glacier have led to the divisional names of a glacier. The area of net accumulation on a glacier is known as the accumulation area. Gravitational forces move ice towards lower elevations where the annual melt exceeds the annual accumulation (Paterson, 1994; Hooke, 2005). This area is known as the ablation area.

The mass balance of a glacier is defined as the difference between the amounts of ablation and accumulation that occur over the entire glacier surface over a specific period of time, which is usually one year. A glacier is in steady state when it has a constant volume with the amount of ablation equaling that of the accumulation. Thus the mass balance is zero. If the accumulation is greater than the ablation, the mass balance has a positive value and the glacier is growing. If the accumulation is less than the ablation, the mass balance is negative and the glacier is shrinking (Paterson, 1994; Benn and Evans, 1998; Knight, 1999). The line that separates the accumulation and ablation areas is known as the equilibrium line. This line is determined at the end of the melting season and it is where the amount of ablation is equal to the amount of accumulation or the local annual mass balance is zero. Changes in climate can lead to changes in the altitude of the equilibrium line.

1.2.3 Glacial History

The Olympic Mountains have been extensively glaciated by alpine glaciers and 266 glaciers exist within the range with approximately 60 of them considered active at present (Spicer, 1986). The glaciers cover an area of 45.94 km^2 and comprise 9% of the glaciated area south of Alaska in the United States (Spicer, 1986). The glaciers are mainly cirque glaciers, but a few valley glaciers are also present in the wetter portions of the mountains. The glaciers exist at relatively low altitudes due to the abundant precipitation and maritime climate. The Olympic Mountains were never overrun by a continental glacier. Instead, the Cordilleran Ice Sheet flowed into the Strait of Juan de Fuca and Puget Sound and reached the eastern and northern sides of the Olympic range.

The Cordilleran Ice Sheet flanked the eastern and northern sides of the Olympic Mountains through the Puget and Juan de Fuca Lobes during the glacial maxima of the Quaternary Period (Figure 1.3). The mountain glaciers of the Olympics reached

maximum extents during the glacial maxima as well and greatly eroded the mountains through extensive valley glaciers (Crandell, 1965; Thorson, 1980; Porter and Swanson, 1998). The margin of the Cordilleran Ice Sheet that influences the Olympic Mountains originated in the Coast Ranges and Fraser Lowland of British Columbia, Canada, and during each of the glacial intervals the margin of the ice sheet advanced into northwestern Washington. During at least the last two glaciations, the Fraser and Salmon Springs, the ice sheet split into two major lobes. The Juan de Fuca Lobe moved west through the Strait of Juan de Fuca, across the continental ice shelf, and into the Pacific Ocean. The Puget Lobe advanced to the south into the Puget Lowland between the Olympic Mountains and the Cascade Range (Crandell, 1965; Thorson, 1980; Porter and Swanson, 1998).

The Quaternary history of the glacial advances for both the Cordilleran Ice Sheet and alpine glaciers has been examined in the region. The Puget Lobe has been greatly studied, especially for the most recent advances. The southeastern part of the Puget Lowland contains glacial strata that represent at least four major glaciations and are interbedded with nonglacial deposits (Crandell, 1965; Thorson, 1980; Porter and Swanson, 1998). The stratigraphic record has at least two glacial fluctuations for each major glaciation and the origin of the sediments can be determined by their lithology (Crandell, 1965; Thorson, 1980; Porter and Swanson, 1998). During interglacial periods drainage was through the Puget Lowland and into the Strait of Juan de Fuca (northward). However, during glacial maxima the Cordilleran Ice Sheet occupied the lowland and the drainage of meltwater was forced to the Chehalis River Valley in the southwest and drained west from there into the Pacific Ocean (Crandell, 1965; Thorson, 1980; Porter and Swanson, 1998).

The earliest recorded glaciations, the Orting and Puyallup Glaciations, occurred in the Early or Middle Pleistocene and show the advance and retreat of the Puget Lobe (Crandell, 1965; Thorson, 1980). The deposits are mainly in the southwestern portion of the Puget Lowland and consist of drift, till, and fluvial and lacustrine deposits. These glaciations are followed by the Salmon Springs Glaciation in the Late Pleistocene, during which there were two advances of both the Puget Lobe and the alpine glaciers with an interglacial period separating the advances (Crandell, 1965). The Fraser Glaciation

followed the Salmon Springs and this glaciation is divided into three stades: the Evans Creek, Vashon, and Sumas Stades. The Fraser Glaciation began with the alpine glaciers reaching a maximum extent in the Evans Creek Stade (Crandell, 1965; Thorson, 1980; Spicer, 1986). The alpine glaciers began to retreat before 15,000 years ago, in contrast, the Cordilleran Ice Sheet continued to grow, culminating with the Puget Lobe reaching a maximum extent during the Vashon Stade (Crandell, 1965; Thorson, 1980; Spicer, 1986). The Puget Lobe retreated during the Everson Interstade and a minor readvance followed in the Sumas Stade (Crandell, 1965). The Cordilleran Ice Sheet then dissipated, while the alpine glaciers continue to exist to the present time (Spicer, 1986). The glaciations and the corresponding major events are summarized in Table 1.1. The ages of the glaciations have been determined from radiocarbon dating of plant samples and pre- and post-glacial sediments (Crandell, 1965; Thorson, 1980; Porter and Swanson, 1998; Heusser et al., 1999).

The alpine glaciers of the Olympic Mountains developed into large valley glaciers that advanced and retreated during the glaciations. These glaciers together acted as a large snow and ice complex from which the valley glaciers drained (Crandell, 1965; Spicer, 1986; Heusser et al., 1999). The glaciers of the western and southern sides, which were flowing towards the Pacific Ocean, flowed onto the coastal plain of the southwestern Olympic Peninsula and merged to become broad piedmont lobes close to, or at, sea level (Crandell, 1965; Spicer 1986). Moraines mark the furthest extent of the valley glaciers in the river valleys. On the northern and eastern sides, the Cordilleran Ice Sheet interacted with the alpine glaciers making their extent much harder to determine (Crandell, 1965; Thorson, 1980; Spicer, 1986; Porter and Swanson, 1998; Heusser et al., 1999).

The interaction of the Cordilleran Ice Sheet and the alpine glaciers of the Olympic Mountains has not been well studied. The altitude of the ice surface for the Puget Lobe has been determined based on the altitude of glacial erratics, continental glacial drift height, and large-scale glacial erosional features (Crandell, 1965; Thorson, 1980; Spicer 1986; Porter and Swanson, 1998). The features have not been dated and thus can be difficult to correlate with the multiple glaciations. The Cordilleran Ice Sheet also dammed the valleys on the eastern and northern sides of the Olympics creating proglacial

lakes. These lakes had alpine glacial meltwater streams flowing into them that were sediment laden, which resulted in the deposition of large deltas (Crandell, 1965; Spicer 1986). The height of the lacustrine and delta deposits can help to determine how far the ice sheet reached into the valleys. Any moraines the alpine glaciers left in these lower altitudes would have been destroyed and where the two different sources of ice met in the valleys, no alpine moraines would have been deposited.

The western side of the Olympic Mountains had no ice sheet interacting with the alpine valley glaciers making it easier to interpret the glacial extent. Thackray (2001) discovered that the alpine glaciers in the Olympic Mountains descended into the valleys and coastal lowlands six times during the late Wisconsin Glaciation and deposited extensive geomorphic features and a stratigraphic record that contains abundant organic material. The Hoh and Queets River Valleys were examined as they had large glaciers repeatedly descend them to the coastal plain, erode material, and deposit thick sediment layers and landforms (Thackray, 2001). Postglacial shoreline erosion and fluvial incision have exposed both the glacial and nonglacial sedimentary sequences in stream cuts and sea cliffs in both river valleys (Thackray, 2001). Each advance consists of a thick advance outwash layer and a thin layer of ablation or lodgement till with thick lacustrine sediments appearing upvalley from end moraine dams (Thackray, 2001). The lacustrine sediments may contain plant material, wood, or seeds that can be radiocarbon dated and wood can also be found locally in till and outwash (Thackray, 2001). Sequences of landforms were also produced by each glaciation consisting of end moraines followed by proglacial outwash terraces (Thackray, 2001).

Thackray (2001) also examined the patterns of temperature that were inferred from pollen data and the glacier fluctuations and found that the Pacific moisture delivery was the dominant control on the Late Pleistocene glaciations and that the most extensive advances, the oldest ones, occurred during cool, wet periods while the younger, less extensive advances occurred during colder, drier periods. The ice volume of the last glacial maximum was limited by arid conditions that developed due to the atmospheric influences of the Cordilleran Ice Sheet (Thackray, 2001). The Puget Lobe of the Cordilleran Ice Sheet in the continental interior controlled the atmospheric circulation pattern over the Olympic Mountains at this time instead of the westerly air flow of the

maritime climate currently observed and this limited the moisture delivery to the Olympic Peninsula creating a cooler and drier climate (Heusser et al., 1999; Thackray, 2001). The mapping and dating of the morphologic and stratigraphic units of the river valleys allows for the determination of the glacial history on the western side of the Olympic range.

The glacial history of the eastern side of the range has been studied only minimally. William E. Long of the United States Forest Service examined neoglacial and Pleistocene glacial deposits throughout the Olympic Mountains. He describes both geomorphic features and deposits located in the valleys of the eastern and northern sides, however, while he suggests ages and reasons for the deposits and features, no absolute ages have been determined and no further research conducted. None of his work was published, but it does supply a starting base for determining the glacial history of the eastern Olympic Mountains. His work will be examined in a later chapter.

1.2.4 Geology

The Olympic Mountains are an accretionary wedge that is formed by the Juan de Fuca Plate subducting beneath the North American Plate. This subduction zone, known as the Cascadia Subduction Zone, has a length of 1300 km and reaches from Vancouver Island to northern California (Brandon et al, 1998; Brandon, 2004). The Juan de Fuca Plate is actively subducting at approximately 30 mm/yr and the surface trace of the subduction thrust is marine, approximately 80 km offshore, and lies at approximately 2500 m below sea level (Brandon, 2004). Due to the subduction and the accretionary wedge, there are two lithologic assemblages, the peripheral and core rocks, that can be found throughout the Olympic Mountains (Figure 1.4).

The peripheral rocks, known as the Coast Range Terrane, encompass the structural lid and they are stratigraphically continuous and unmetamorphosed. The terrane consists of oceanic crust which occurs as a landward-dipping unit in the Cascadia wedge with the accreted sediments extanding landward beneath the terrane (Brandon et al., 1998; Pazzaglia and Brandon, 2001). The oceanic crust was accreted onto the continent by either the collision of an intra-Pacific seamount province or by backarc or forearc rifting at the North American plate margin (Brandon et al., 1998). However, the terrane is clearly involved in the subduction related deformation, albeit at a slower rate of

deformation than that of the toe, and is thus a more evolved part of the accretionary wedge (Brandon et al., 1998; Pazzaglia and Brandon, 2001). The Coast Range Terrane is composed of a basal unit called the Crescent Formation and the overlying Peripheral Sequence. The Crescent Formation consists of pillowed and massive basalt flows that are cut by dikes and interbedded with pelagic limestone and mudstone (Brandon et al, 1998). The Peripheral Sequence consists of Eocene to lower Miocene marine clastic strata (Spicer, 1986; Brandon et al, 1998; Brandon, 2004). The Coast Range Terrane is separated from the core rocks by the Hurricane Ridge and Calawah faults and is folded into a horseshoe shaped belt that rings the core rocks on the northern, eastern, and southern sides of the Olympic Peninsula.

The core rocks are known as the Olympic Subduction Complex and they are mostly slightly metamorphosed. These rocks encompass the exposed accretionary wedge sediments produced by the subduction zone and the Complex is split into the Upper, Lower, and Coastal units. The Upper unit is composed of Eocene clastic sediments, mainly shale and sandstone from turbidite sequences, and Eocene pillow basalts (Brandon et al, 1998). The Lower unit consists of late Oligocene and early Miocene clastic sediments, once again mainly turbidite sandstones. The Coastal Unit is an accretionary unit composed of turbidite sequences of Miocene age with exotic blocks of Eocene age pillow basalts and sedimentary rocks occurring within it (Brandon et al, 1998; Brandon, 2004).

1.2.5 Accretionary Wedge/Topographic Steady State

Subduction zones do not completely remove the subducting plate from the surface of the earth. A portion of the plate gets left behind at the leading edge of the overriding plate as an accretionary complex that is composed of the sedimentary cover of the downgoing plate. The Juan de Fuca Plate is covered by approximately 2500 m of sediment and geophysical and geochemical evidence indicate that all of the incoming sedimentary section is accreted into the accretionary wedge, known as the Cascadia Wedge, while the underlying crust and mantle are subducted with a minor amount of underplating occurring (Brandon et al., 1998; Brandon, 2004).

The Cascade volcanic arc parallels the subduction zone and denotes where the subducting slab has reached a depth of approximately 100 km and melting begins. The forearc, or the region between the subduction zone and the arc, is marked by a low, which includes the Georgia Straits, Puget Sound, and Willamette Valley, and a high, which includes the Coast Ranges of Canada, Washington, and Oregon and the Olympic Mountains, and both the forearc high and low parallel the subduction zone. The forearc high is the crest of the Cascadia Subduction Wedge, which is represented by the Olympic Mountains, and it separates the pro-wedge to the west and the retro-wedge to the east (Brandon et al., 1998; Wegmann and Pazzaglia, 2002; Brandon, 2004). The structure of the accretionary wedge is contained in Figure 1.5. The distance between the subduction zone and the arc is greatest across the Olympic Mountains and this is due to the shallower dip of the subducting slab beneath the Olympics. The shallow dip also caused the Olympics to emerge above sea level before any other section of the forearc high, approximately 15 Ma, marking it as the most evolved section of the forearc high (Brandon, 2004). Erosion of the Olympic Mountains, which compose the accretionary wedge, is a large recycling system whereby the sediments eroded are transported to the ocean by rivers and once again are accreted to the wedge and uplifted to become part of the mountains again. Erosion acts as a driver of deformation, but also limits the growth of the wedge (Brandon, 2004). This is due to an accretionary wedge being characterized by a critical taper that has its cross-sectional geometry evolving in a self-similar pattern over long timescales (Dahlen, 1984).

The Olympic Mountains are in topographic steady state, which is defined by a balance in rates of erosion and rock uplift. Several methods have been used to determine the uplift and erosion rates. Apatite and zircon fission-track dating have been used over the entire peninsula to measure the exhumation rates (Brandon et al., 1998; Brandon, 2004). U-TH/He dating has also been used on the peninsula (Batt et al., 2001).

Calculating the incision rate of rivers is a method that can be used to estimate erosion rates. Incision is the rate at which rivers cut into the bedrock and it can be resolved by determining the age of former river channels. Remnants of old river channels, called straths, are flat, eroded surfaces that are cut into the bedrock and they are located in the hillslope above the current river channel. The age and height of the straths

above the modern river channel shows the amount of incision that has occurred. The Clearwater River in the Olympic Mountains has 60 straths from which incision rates were calculated. This is the only river in the Olympics that erosion rates can be determined in as the Clearwater River is unglaciated.

The incision and exhumation rates are similar even though they represent different processes and time intervals and this similarity suggests that the Olympic Mountains are in steady-state. The rates appear to have been in steady state since approximately 14 Ma (Brandon et al., 1998; Brandon, 2004). A map of the uplift is provided in Figure 1.6 and a profile of the uplift rates along the transect marked in Figure 1.6 is in Figure 1.7. The uplift and exhumation rates are faster along the center of the range than at the edges with the rates of exhumation approximately 1 mm/yr in the center and 0.1 mm/yr on the flanks (Brandon, 2004). The rates for both the Holocene and Pleistocene fluvial erosion also progressively increase in the upstream direction (Pazzaglia and Brandon, 2001; Wegmann and Pazzaglia, 2002).

For a wedge to achieve self-similar growth in the simplest way is by steady, constant uplift over the range and, without erosion, a spatially non-uniform rock uplift pattern would alter the wedge's geometry by destroying the critical taper and altering the surface uplift. It thus seems unlikely that tectonics could sustain non-uniform uplift over long time periods (Dahlen, 1984). However, recent work has shown a coupling between rock uplift and surface erosion at accretionary wedges (Whipple and Meade, 2004; Hilley and Strecker, 2004). Work in the Olympic Mountains suggests that orographic precipitation influences the large-scale structure of the range and the windward versus leeward distribution of uplift (Willett and Brandon, 2002). The Southern Alps of New Zealand also have thermochronologic data that indicate that the windward side of the range has faster rates of uplift (Batt et al., 1999). In the case of the Olympic Mountains, an orographic precipitation pattern is present and it likely influences the erosion rates and also makes it possible for glaciers to exist within the range. Examination of the fluvial erosion in the range indicates that fluvial erosion alone is not consistent with the observed pattern of exhumation (Tomkin et al., 2003). The Clearwater River has a downstream decrease in the rates of incision which a stream power based model of erosion is unable to reproduce (Tomkin et al., 2003). Another form of erosion must be significantly

contributing to the total erosion to have the Olympic Mountains be in steady state with a rock uplift rate that increases toward the center of the range.

1.3 OUTLINE

The interaction of climate, tectonics, and erosion is examined in the Olympic Mountains. A numerical model, ICE Cascade, is used to determine if the steady-state pattern observed in the Olympics is consistent with glacial erosion that has occurred due to late Cenozoic cooling. The glacial coverage of the Olympics at the LGM is modeled and the associated glacial erosion rates are compared with the uplift rates. Moraines from Royal Glacier on Mt. Deception in the eastern Olympic Mountains are dated using lichenometric techniques, contributing to the neoglacial history of the range. The reconstructed ice extent and equilibrium lines determined from the moraines allows for an investigation of the climate gradients across the region. The locations of glacial deposits in the eastern and northern sides of the range are compiled from the work of the few researchers who have examined this area. The combination of these investigations will allow for a more complete view of the interactions between erosion, tectonics, and climate on the Olympic Peninsula.

1.4 FIGURES AND TABLES

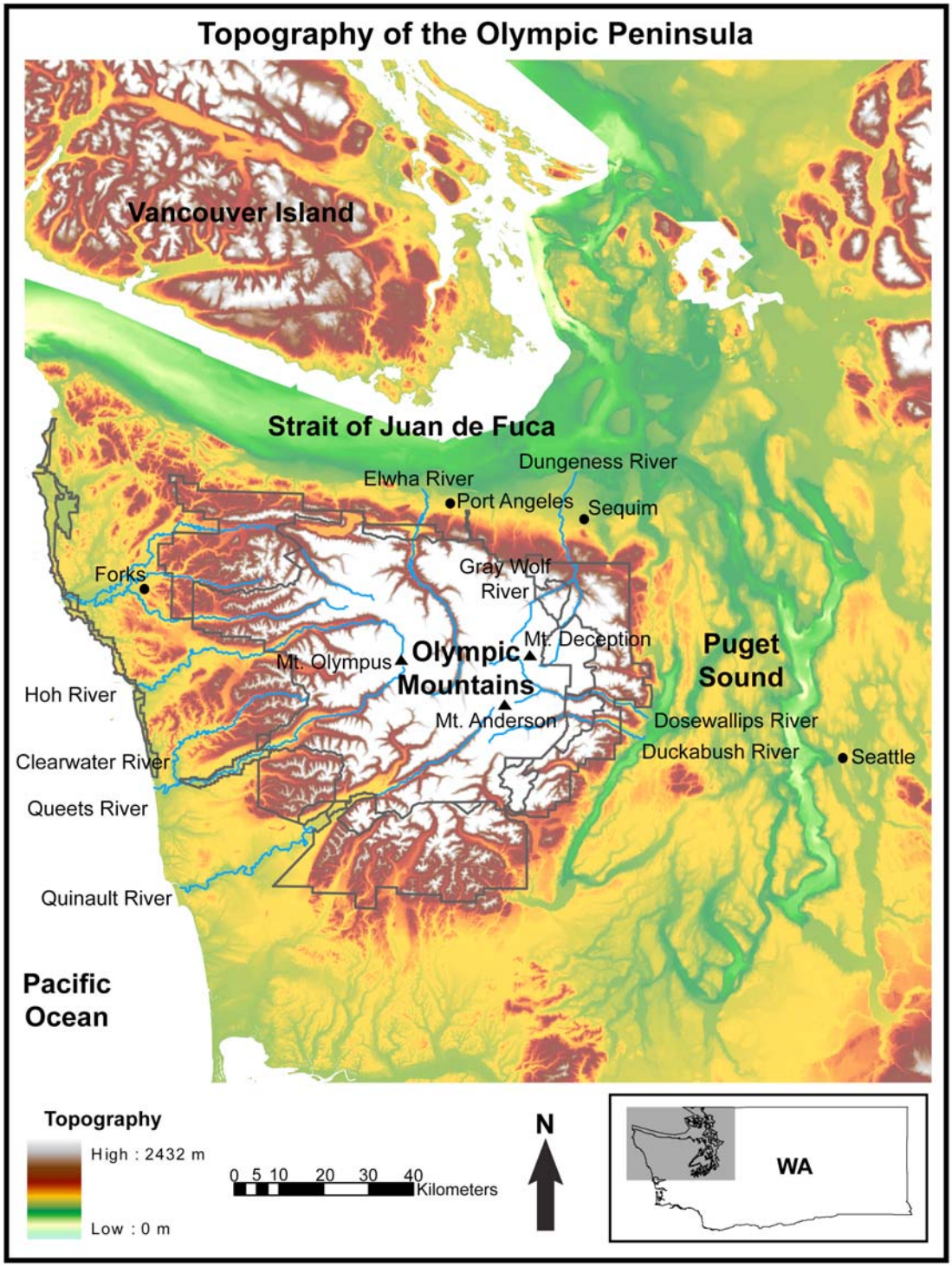

Figure 1.1. Topography of the Olympic Peninsula. Elevation is measured in meters with the grid in kilometers. Features relevant to this study are displayed on the topography.

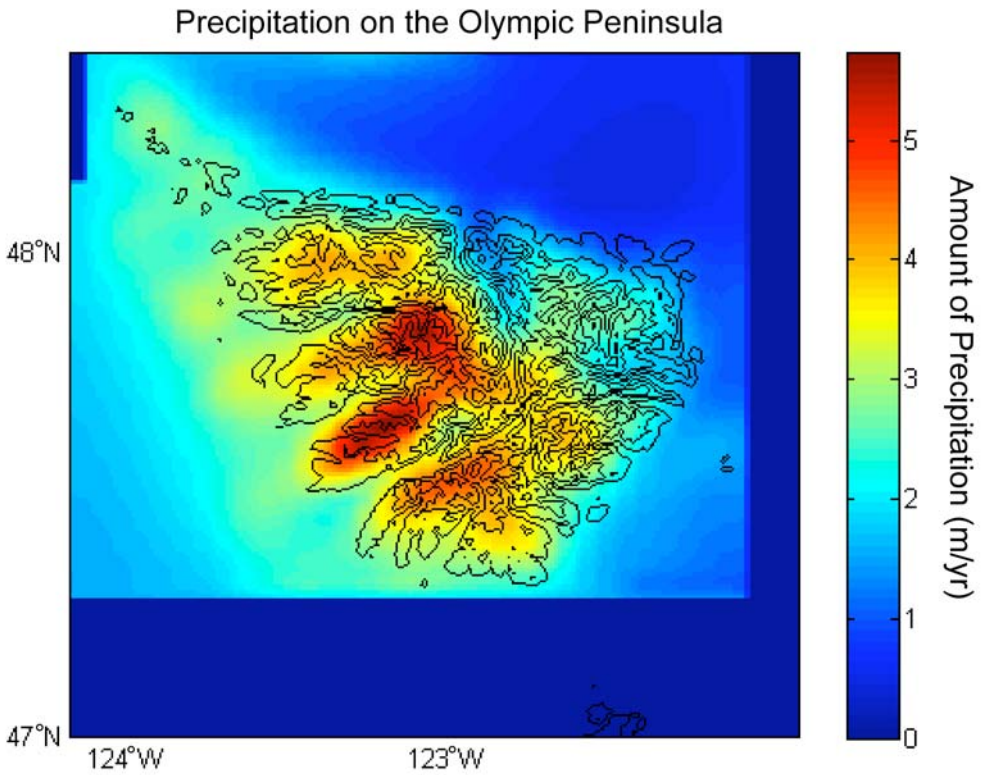

Figure 1.2. The precipitation across the Olympic Peninsula. The precipitation is measured in mm/yr and the orographic precipitation pattern can be observed. The topography is contoured in black.

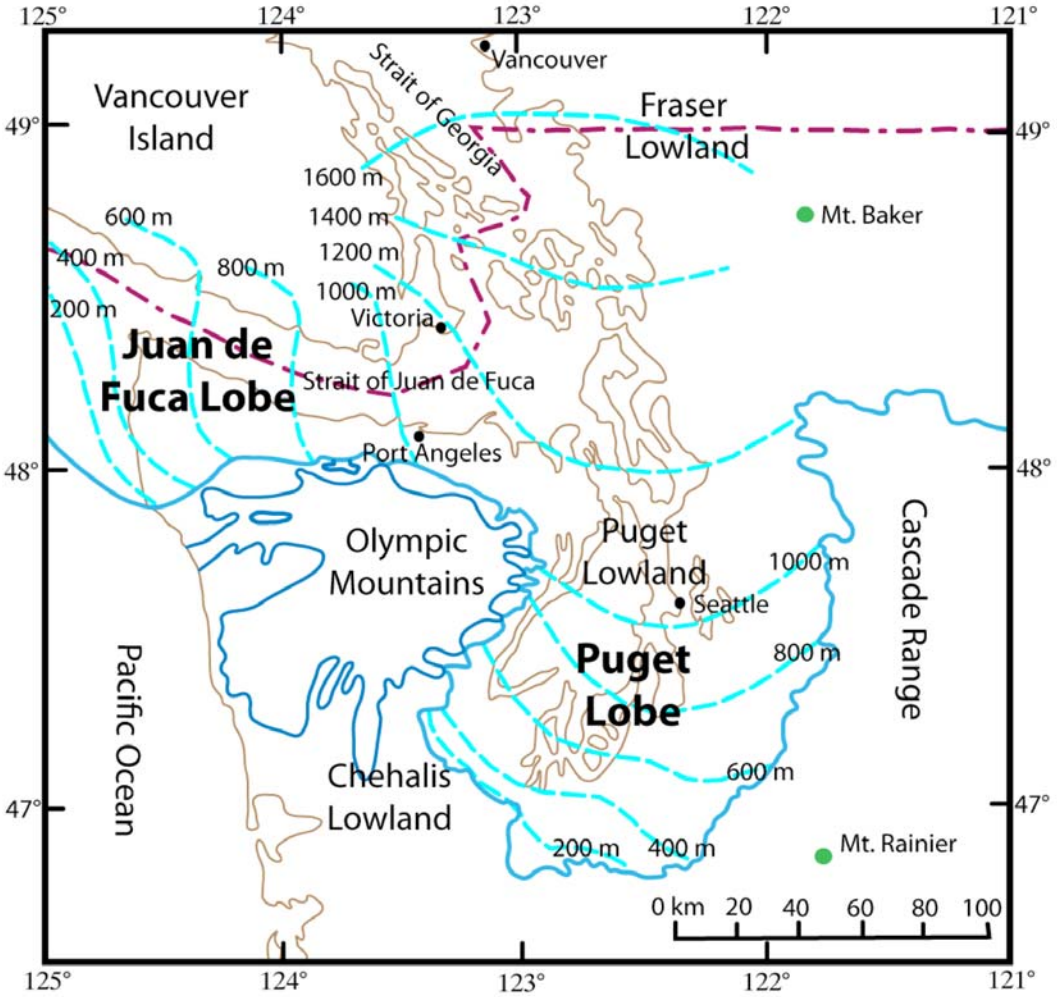

Figure 1.3. The glacial extent for the Cordilleran Ice Sheet's Puget Lobe and Juan de Fuca Lobe (light blue) and the maximum extent of the alpine glaciers in the Olympic Mountains (dark blue). The contours of the ice sheet are marked and based on Thorson (1980), Waitt and Thorson (1983), and Porter and Swanson (1998). Features mentioned in the text are included on the figure (based on Crandell, 1965; Heusser, 1972; Thorson, 1980; Waitt and Thorson, 1983; Porter and Swanson, 1998).

Glacial Chronology of Western Washington State			
Geologic Climate Unit		**Approximate Age (yr B.P.)**	**Major Events**
Fraser Glaciation		11,000-23,000	Marine Isotope Stage 2
	Sumas Stade	11,000-11,600	Minor readvance of Cordilleran Ice Sheet
	Everson Interstade	12,800-13,600	Juan de Fuca Lobe retreated and Puget Lobe recessed enough so marine water enters Puget Lowland
	Vashon Stade	14,000-17,000	Advance and recession of Cordilleran Ice Sheet; Puget Lobe reaches a max
	Unnamed Interstade	17,000-19,000	Recession of alpine glaciers
	Evans Creek Stade	19,000-23,000	Alpine glaciers advance to a max and retreat
Olympia Interglaciation		23,000-60,000	Fluvial and lacustrine sedimentation in Puget Lowland; Marine Isotope Stage 3
Possession Glaciation		60,000-75,000	Marine Isotope Stage 4
Whidbey Interglaciation		75,000-125,000	Marine Isotope Stage 5
Double Bluff Glaciation		150,000-250,000?	Marine Isotope Stage 6
Salmon Springs Glaciation			Two episodes of Cordilleran Ice Sheet advancement and recession; Two episodes of advancement and recession of alpine glaciers; Fluvial sedimentation in Puget Lowland inbetween the episodes
Puyallup Interglaciation			Lacustrine sedimentation in Puget Lowland with fluvial and mudflow aggradation in the southeastern section; Re-establishment of northwest flowing rivers
Stuck Glaciation			Two episodes of advancement and retreat of Cordilleran Ice Sheet
Alderton Interglaciation			Re-establishment of northwest flowing rivers; Fluvial and mudflow aggradation in southeastern Puget Lowland
Orting Glaciation			Two episodes of advancement and retreat of Cordilleran Ice Sheet

Table 1.1. The glacial chronology of western Washington State. Major events and approximate ages of events are listed (Crandell, 1965; Thorson, 1980; Thackray, 1996).

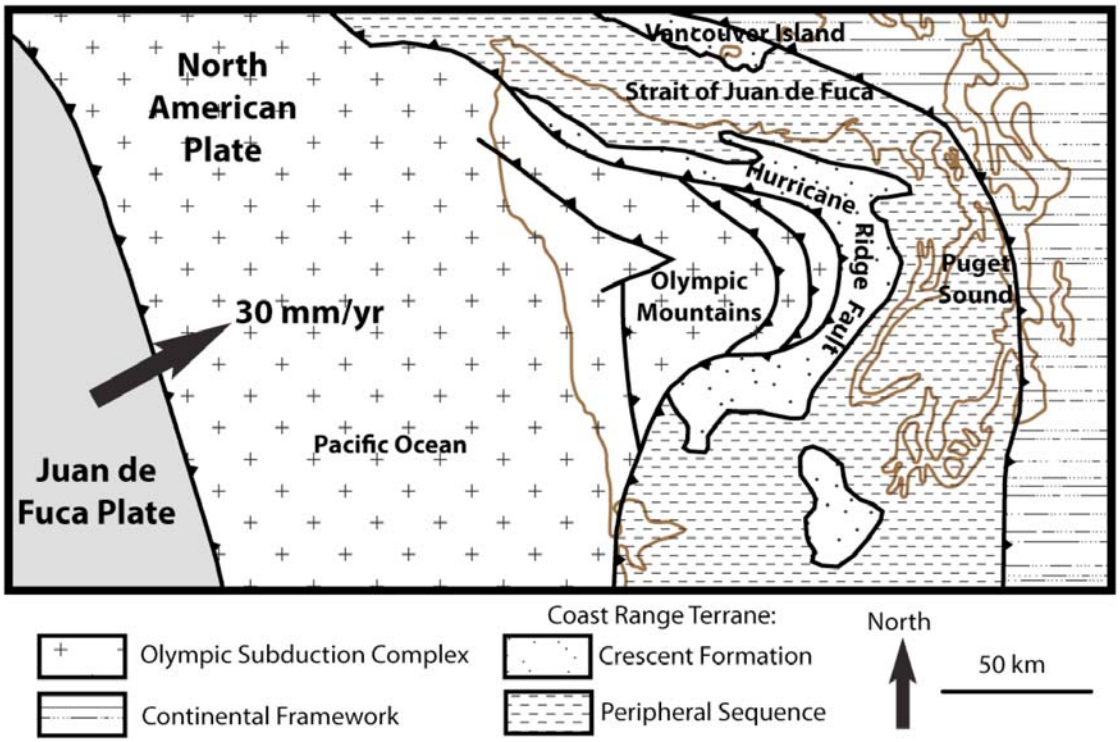

Figure 1.4. The geology of the Olympic Peninsula and the location of the Juan de Fuca Subduction Zone. The units are listed in the legend and are described in the text (based on Garcia, 1996; Brandon et al., 1998; Brandon, 2004).

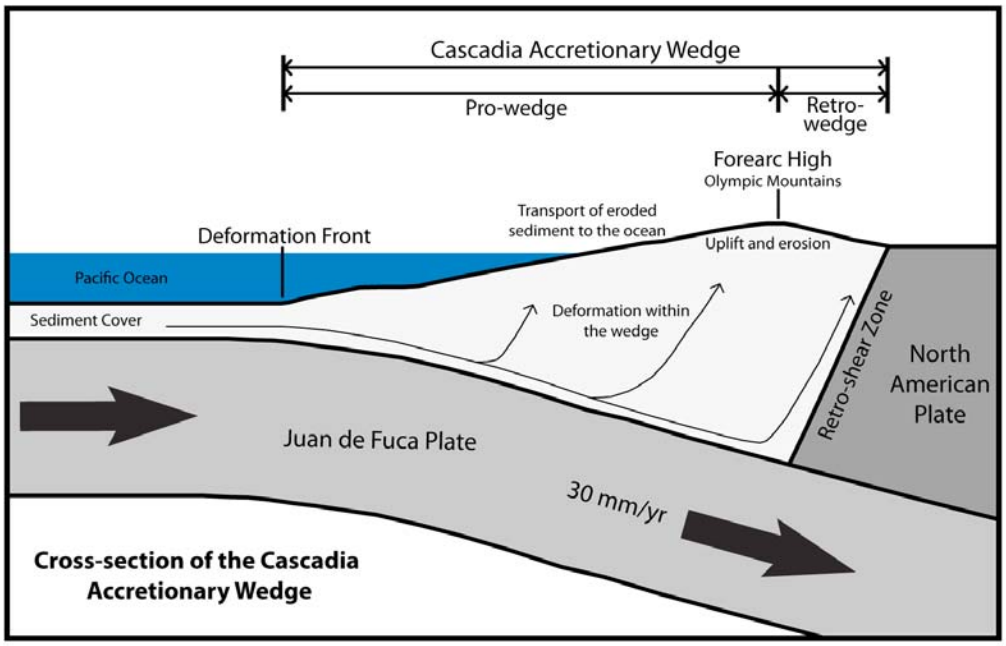

Figure 1.5. The structure of the Cascadia Accretionary Wedge and the Juan de Fuca Subduction Zone. The plate is subducting at 30 mm/yr and the sediment cover has a thickness of 2500 m. Sediment is accreted, deformed, and uplifted in the wedge and then eroded and transported back to the ocean to be recycled once again (based on Brandon et al., 1998; Pazzaglia and Brandon, 2001; Brandon, 2004).

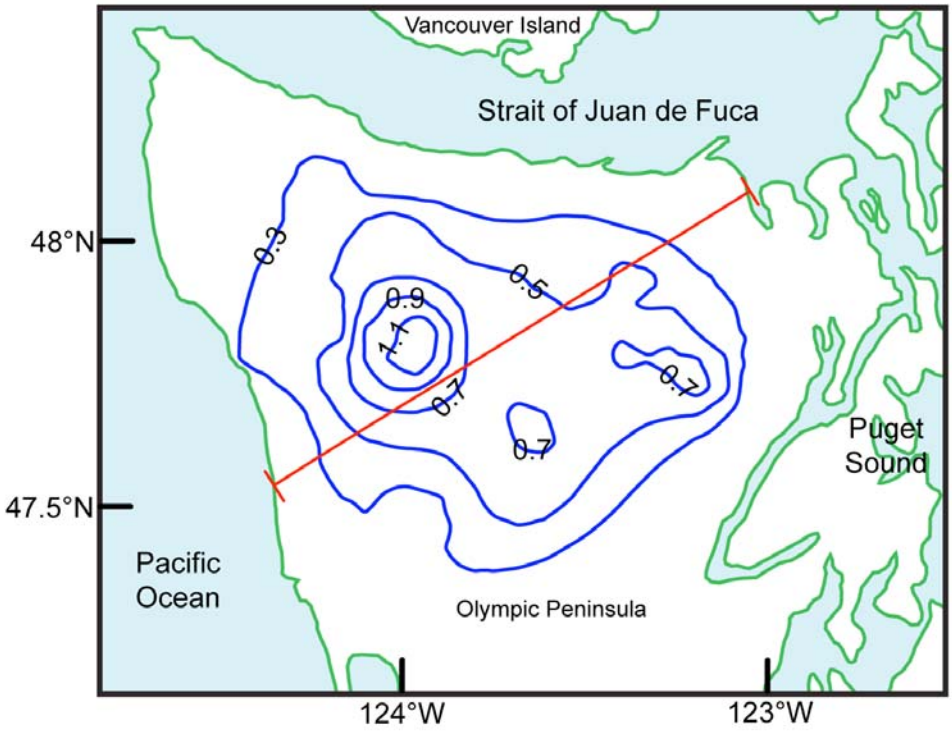

Figure 1.6. The spatial pattern of uplift on the Olympic Peninsula. The uplift is measured in mm/yr and is denoted by the blue contours. The transect denoted by the red line is the profile of the uplift used in the following figure. The fastest rates occur within the western Olympics (adapted from Brandon et al., 1998).

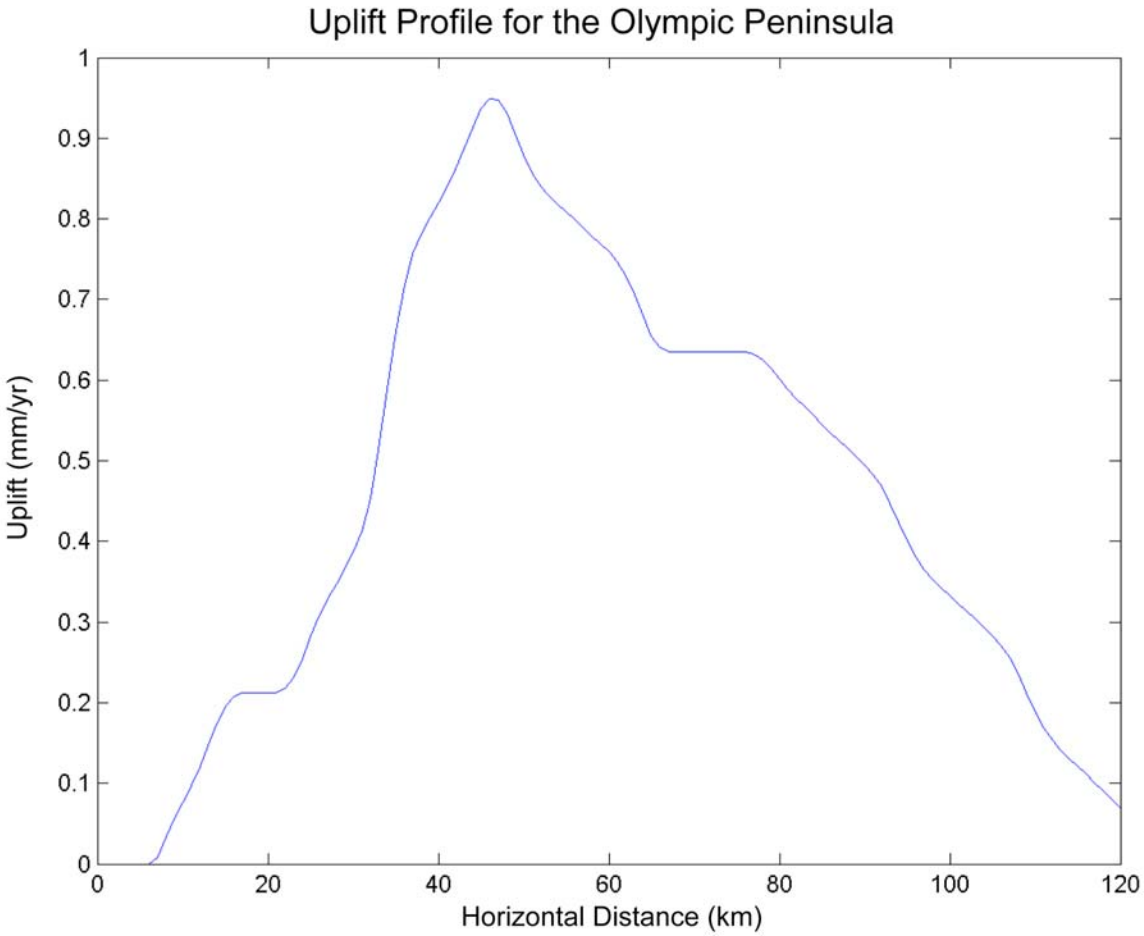

Figure 1.7. The uplift across the Olympic Mountains of Washington State. Uplift is measured in mm/yr and is measured along the red transect in Figure 1.6.

CHAPTER 2: NUMERICAL MODELING OF GLACIAL EXTENT AND EROSION

2.1 INTRODUCTION

A surface processes model, ICE Cascade, is used to examine the effect glaciation has on erosion and uplift. The highly glaciated Olympic Mountains of Washington State are an accretionary wedge with spatially non-uniform rock uplift rates. The Olympics are in steady-state with rock uplift rates equal to erosion rates over timescales of 10^5-10^6 years (Brandon et al., 1998). However, models of fluvial erosion cannot produce spatial variability consistent with the spatial variability in rock uplift rates (Tomkin et al., 2003). This study investigates whether spatial patterns of glacial erosion are similar to spatial patterns in rock uplift. If so, it suggests that spatially non-uniform rock uplift rates in the Olympic Mountains are a consequence of glacial erosion brought on by late Cenozoic cooling.

The ICE Cascade model will be used to model both the ice extent and erosion. ICE Cascade is a numerical model that simulates glacial, fluvial, and hillslope erosion to examine long-term landscape evolution (Braun et al., 1999; Tomkin and Braun, 2002; Tomkin, 2007). Glacial erosion is explicitly calculated by ICE Cascade as a function of ice evolution in a two-dimensional, finite difference model (Tomkin, 2007). The time-averaged glacial erosion rate depends on the extent and duration of glaciations, i.e., the glacial history of the Olympic Mountains. This history is approximated by a single glacial cycle and therefore requires that ICE Cascade be able to simulate the glacial and interglacial ice extent. Precipitation and temperature changes are imposed in order to determine the sensitivity of modeled ice extent to climatic parameters. Given this sensitivity, an entire glacial cycle is simulated and the modeled pattern of glacial erosion can be compared to the spatial pattern of uplift.

Two specific hypotheses are addressed that relate climate, glacial extent and erosion, and spatial patterns of rock uplift in the Olympic Mountains:

1. ICE Cascade can simulate past glacial extent with plausible values of climatic parameters, and,

2. Sliding-law based glacial erosion patterns are similar to the observed spatial patterns in rock-uplift rates.

2.2 ICE CASCADE MODEL

ICE Cascade is a surface process model designed to model the effect of glacial erosion on the large-scale geomorphology of active mountain ranges (Braun et al., 1999). Unless otherwise noted, the model formulation used here is identical to Tomkin and Braun (2002) and Tomkin (2007). A summary of the constants and the corresponding values used in the model are recorded in Table 2.1.

Glaciers erode through a variety of processes including abrasion, chemical weathering, subglacial water erosion, and plucking. In mountain settings, however, the direct action of glacial ice on the bed likely dominates (Hallet, 1979; Lliboutry, 1994; Hallet et al., 1996). The process of abrasion, in particular, has received considerable study and ICE Cascade idealizes glacial erosion in the form of a glacial abrasion model. If sediment accumulates beneath the glacier, it protects the bed, limiting the effectiveness of abrasion (Bennett and Glassner, 1996). ICE Cascade neglects this effect and uses a simple, but physically based model in which glacial erosion is dependent only on the sliding velocity (Braun et al., 1999; Tomkin and Braun, 2002). The lack of glacial storage of sediments limits the model to hard-bed systems including mountain settings where the glacial storage of sediments is negligible compared to the size of the orogen (Tomkin, 2007). The glacial erosion has the form:

$$\left(\frac{\partial h}{\partial t}\right)_g = K_g \left|\mathbf{u}_s\right|^l \qquad (2.1)$$

where h is the topographic height, $\partial h/\partial t$ is the glacial erosion rate, and K_g and l are constants. This equation was proposed by Hallet (1979). It represents the general form of the abrasion law and is appropriate for any erosion mechanism that scales with basal velocity (Hallet, 1979; Hallet, 1996). Numerical modeling, theory, and field evidence all suggest that l=1 (Hallet, 1979; Harbor, 1992b; Humphrey and Raymond, 1994). The glacial erosion constant, K_g, is approximately 10^{-4}, based on field evidence (Humphrey

and Raymond, 1994). In this study $\partial h/\partial t$ is computed, but not applied, so the glaciers do not actually erode the landscape. Therefore, what I term modeled glacial erosion is actually the modeled potential for glacial erosion.

Glacial erosion is based on the ice sliding velocity, which, in turn, depends on the extent and thickness of the ice. Therefore, an ice dynamics model is needed to model glacial erosion. ICE Cascade uses a vertically integrated ice mass conservation equation to determine the thickness of the ice, h_{ice}:

$$\frac{\partial h_{ice}}{\partial t} = \nabla \cdot \mathbf{F} + M \tag{2.2}$$

where $\mathbf{F}$ is the vertically integrated mass flux ($\mathbf{F}=h\mathbf{u}$, where $\mathbf{u}$ is the vertically integrated horizontal ice velocity) and M is the mass balance (Paterson, 1994). Mass balance includes the two dominant processes that determine the net accumulation and ablation in temperate, alpine glaciers: surface accumulation and basal melting (Braun et al., 1999).

The ice velocity, $\mathbf{u}$, is the sum of both the deformation velocity, $\mathbf{u_d}$, and the sliding velocity, $\mathbf{u_s}$:

$$\mathbf{u} = \mathbf{u_d} + \mathbf{u_s} \tag{2.3}$$

It is assumed that the horizontal derivatives of the ice stress and velocity are small compared to the vertical derivatives and thus the longitudinal strain rates can be ignored (the “shallow-ice approximation”) so the velocities have the following form:

$$\mathbf{u_d} = \frac{2A_d\beta_c}{n+2}(\rho g)^n h_{ice}^{(n+1)} \left|\nabla(h+h_{ice})\right|^{(n-1)} \nabla(h+h_{ice}) \tag{2.4}$$

$$\mathbf{u_s} = \frac{A_s\beta_c}{N-P}(\rho g h_{ice})^n \left|\nabla(h+h_{ice})\right|^{(n-1)} \nabla(h+h_{ice}) \tag{2.5}$$

where ρ is the ice density, g is the acceleration due to gravity, β_c is the constriction factor, n is the ice flow exponent, A_d is the deformation constant, A_s is the sliding parameter, N is

the ice overburden pressure, and P is the basal water pressure with A_d and n defining the power-law rheology and strain rate for ice:

$$\dot{\varepsilon} = A_d \sigma^n \tag{2.6}$$

where σ^n is the stress (Hutter, 1983; Knap et al., 1996). The values of A_d and n are determined from a review of field data and experimental results by Paterson (1994). Although A_d is temperature dependent, it is reasonable to treat it as a constant when the ice temperature does not vary significantly. In particular, this assumption is reasonable for valley glaciers and temperate ice caps because the ice everywhere is at or near the melting point (Braun et al., 1999; Tomkin and Braun, 2002).

The expression for the sliding velocity was developed by Bindschadler (1983) and is supported by laboratory tests and empirical fits of the recorded basal velocity of glaciers (Budd et al., 1979; Bindschadler, 1983; Harbor, 1992a). The value of A_s depends on the site and varies by more than an order of magnitude between different glaciers (Bindschadler, 1983). ICE Cascade uses a value for A_s that was calculated by Budd et al. (1979) and agrees reasonably well with the data in Paterson's (1994) review of the ratio of basal to surface velocities. In addition, if ice is frozen to the bedrock, basal sliding ceases and this appears to be an important control on the pattern of glacial erosion in numerical models (Oerlemans, 1984; Drewry, 1986). However, models of alpine glacial erosion are not thermally controlled and in the present study alpine glaciations and ice caps are examined so no basal freezing occurs (Harbor et al., 1988; Tomkin and Braun, 2002; Tomkin, 2007).

Following the work of Knap et al. (1996), it is assumed that basal water pressure is equal to 20% of the ice overburden pressure. This assumption does not account for the complex spatial and temporal variations in water pressure that occur underneath flowing glaciers, and I note that it is likely that changes in the flow and pressure of subglacial water do influence the rate of glacial erosion (Drewry, 1986; Iverson, 1991; Harbor, 1992b; Humphrey and Raymond, 1994; Alley et al., 2003; Tomkin, 2007). ICE Cascade averages over the short-term water pressure variations. This simplification is similar to the assumptions made in many fluvial incision models which use an average flow and

neglect stochastic and threshold effects of water flow despite the fact that they may be important (e.g., Howard and Kerby, 1983; Tucker and Bras, 2000). The effects of subglacial water pressure variations on glacial erosion rates remain unconstrained and, therefore, the possible error in using our model of glacial erosion is studied.

When ice flows down glacial valleys, the deformation and sliding velocities are influenced by the presence of valley walls constricting the ice flow (Tomkin and Braun, 2002). This effect is incorporated into the model by scaling the ice velocities by a "constriction factor," β_c, which has the following form:

$$\beta_c = \frac{1}{1 + k_c \frac{\partial^2 h}{\partial x_f^2}} \tag{2.7}$$

where k_c is the constriction constant and $\partial^2 h / \partial^2 x_f$ is the second derivative of the bedrock topography in a direction normal to the direction of ice flow (Braun et al., 1999; Tomkin and Braun, 2002).

The mass balance term, M, is the sum of the surface accumulation, M_a, and the melting rate at the surface, M_m (Braun et al., 1999; Tomkin and Braun, 2002). M_a is equivalent to the local precipitation rate and if the surface temperature is at or below zero the precipitation is added as ice instead of water (Braun et al., 1999; Tomkin and Braun, 2002). M_m is the assumed to be proportional to the difference between the surface temperature, T_s, and the temperature above zero (Braun et al., 1999; Tomkin and Braun, 2002). No melting occurs if T_s is less than or equal to zero, but if T_s is greater than zero:

$$M_m = -\alpha_1 T_s \tag{2.8}$$

where α_1 is the ablation constant and it is estimated by Kerr (1993). The temperature across the model depends on the time and altitude and has the following form:

$$T_s = T_0(t) - \alpha_2 (h + h_{ice}) \tag{2.9}$$

where T_0 is the temperature at sea level and α_2 is the lapse rate (Braun et al., 1999; Tomkin and Braun, 2002).

The spatial grid has a one kilometer resolution and time steps of approximately one year are used, which corresponds to those of modern fluvial process models (Stolar et al., 2006; Tomkin, 2007). With a grid spacing of one kilometer, an implicit assumption is being made that the major agents of glacial erosion are features that are as large as, or larger than, the valley glaciers and ice caps and, therefore, the grid size. This is an appropriate assumption for orogen scale investigations. The larger ice structures will be dominant in the reconstructions of the ice since the LGM and can still exist in glacially active areas today with model simulations supporting the assumption (Braun et al., 1999; Tomkin, 2007).

Subgrid scale behavior may be especially important when considering glacial erosion in regions of relatively thin ice. The assumption that ice is evenly distributed across the grid scale works well for thick ice, but is weak when only a small amount of ice is present at a node. For example, ice on isolated peaks is much more plausibly characterized by both icy and rocky areas within a 1 km^2 area (Tomkin, 2007). Therefore, as glacial erosion is nonlinear with the ice thickness, thin ice regions may be insufficiently eroded in the model.

Runaway erosion can occur at individual nodes in a glacial model because the vertical stresses are ignored in the two-dimensional ice flow equations thus producing overly smooth ice surfaces (Tomkin, 2007). Due to this effect, it is possible that an ice covered node which is a topographic minimum may have almost the same glacial height as the surrounding nodes. In that case, the ice thickness at the low node may be much greater than for surrounding nodes and, therefore, the local glacial erosion rate would be faster than for neighboring nodes (Tomin, 2007). If compensatory ice flow from the surrounding ice nodes works to keep the thickness constant while the node erodes, a positive feedback develops where the topographic minimum is exaggerated and the erosion rate and ice thickness increase (Tomkin, 2007). The feedback rarely occurs and can usually be avoided by using a smaller timestep so the ice surface is more accurately calculated. However, the nonlinear nature of this feedback makes its occurrence unpredictable (Tomkin, 2007).

2.3 SENSITIVITY OF GLACIAL EXTENT TO TEMPERATURE AND PRECIPITATION

I will first test the hypothesis that the glacial coverage of the Olympic Mountains through a glacial-interglacial cycle can be modeled with ICE Cascade. This involves attempting to reproduce the observed last glacial maximum (LGM) ice extent with ICE Cascade and determining the sensitivity of the ice extent to precipitation and temperature. This is the first time ICE Cascade has been used to simulate former glaciers on real topography at high spatial resolution.

ICE Cascade requires the topography and climate parameters as inputs. The 1/3 arcsecond NED digital topography (USGS, 2007) for the Olympic Peninsula was resampled to produce a 1 km resolution digital elevation model (Figure 2.1). A 1 km resolution map of climatological precipitation rates based on numerical weather modeling provides the relative differences in precipitation rates across the region (Figure 2.2) (Anders et al., 2007). This spatial pattern of precipitation is scaled by a factor, P_f, to allow for changes in the overall amount of precipitation:

$$a(i,j) = preciprate\_spatial(i,j) \times P_f \tag{2.10}$$

where *a(i,j)* is the precipitation, P_f is the precipitation factor, and *preciprate_spatial(i,j)* is the orographic precipitation pattern. Temperature is assumed to vary with elevation according to a fixed lapse rate of 0.0063°C/km, based on five modern temperature records from the Olympic Peninsula (NOAA, 2007). Sea level temperature (SLT) is 16°C at present and is decreased to simulate glacial conditions (Heusser et al., 1999). The ablation constant for a maritime climate, such as is found on the Olympic Peninsula, is 1.5 (Kerr, 1993).

ICE Cascade is run with the topography held constant for a given sea level temperature and precipitation factor until glaciers reach a steady state. This is accomplished within 5,000 model years for all simulations presented. The modeled ice extent as formed under current climate conditions is compared to that of the modern glacial extent (Figure 2.3). No glacial ice is formed in the model, which is consistent with

the 1 km resolution of the model and the diminutive and retreating glaciers found today; glaciers are not in steady state in the modern climate (Conway et al., 1999).

To estimate the LGM climate parameters, the modeled ice extent is compared with the geologic records of the LGM ice position. The locations of the LGM ice margin in the Hoh, Queets, and Quinault Valleys in the western Olympic Peninsula have been established through the mapping and dating of glacial deposits (Figure 1.1) (Thackray, 2001). An additional constraint on ice extent comes from the lack of LGM glacial deposits in the Clearwater River Valley in the western Olympic Peninsula (Pazzaglia and Brandon, 2001). The LGM deposits used to constrain the model are recorded in Figure 2.3. No glacial deposits have been dated on the eastern or northern sides and the alpine ice in these areas also interacted with the Cordilleran Ice Sheet making it difficult to determine the true alpine ice extent. A metric based on the agreement between the modeled ice and the geologic record of LGM glacial deposits in these four river valleys determines the best fitting model runs of the climate parameters. For each record of LGM position, the along-valley distance from the LGM deposit to the modeled ice margin is calculated. The model misfit is defined as the sum of these distances (Figure 2.4). Modeled ice that overshoots the LGM ice position is given the same penalty as ice that undershoots the position. For the Clearwater River, the modeled ice tends to spill into the headwaters and a penalty is given if the ice extends downstream into the valley. As a note, geomorphic evidence shows ice may have spilled into the headwaters of the valley during the late Quaternary (Tomkin et al., 2003).

The sensitivity of the ice extent to the precipitation factor and sea level temperature was examined. A wide range of parameter space was studied: sea level temperature was varied from 4.0-16.0°C with increments of 0.5°C and the precipitation factor was varied from 0.25-1 with increments of 0.25. The best fitting model runs occur for sea level temperatures between 6.0-8.0°C and a precipitation fraction between 0.2-0.6 (Figure 2.5). In the region of parameter space with low misfit values additional parameter sets were examined, specifically, sea level temperatures from 6.0-8.5°C with increments of 0.2°C and precipitation fractions between 0.2-0.8 with an increment of 0.1. A narrow range of variables produces glacial extents in the western Olympics similar to those observed at the last glacial maximum: sea level temperatures between 6.0°C and 7.5°C

and a precipitation fraction between 0.2 and 0.6 (Figure 2.6). The ice extent and ice thickness for one of these cases are shown in Figures 2.7 and 2.8.

An independent constraint on sea level temperature and precipitation comes from a paleoclimate reconstruction based on pollen data from the Humptulips River Valley on the southwestern side of the Olympic Peninsula (Heusser et al., 1999). This record suggests that at the LGM precipitation was 1/3-1/2 of the current and the summer temperature was depressed ≥5°C from the modern sea level temperature (current SLT:14-16°C) (Heusser et al., 1999). The model climatic parameters that best reproduce the observed ice extent correlate very well with the paleoclimate record (Figure 2.6). The agreement between the best fit parameters and the paleoclimate observations increases confidence that ICE Cascade reasonably simulates the glacial extent in general.

The ice extent is more sensitive to temperature than to the precipitation fraction. This suggests that ablation is the dominant mechanism constraining ice extent on the Olympic Peninsula. The maritime climate and specifically the ablation constant of 1.5 may be an important factor in causing this temperature sensitivity.

The range of precipitation factors with low model misfit indicates that a range of ice thicknesses could still produce similar ice extent. The ice thickness will influence the sliding velocities and thus the erosion rates. Therefore, variability in modeled glacial erosion rates within the best fitting region of parameter space is expected.

The narrow range of temperatures in the low model misfit region could provide an additional constraint for the LGM climate. Existing paleoclimate data only constrains a minimum decrease from the modern sea level temperature. Numerical models of glacial extent have been used to constrain past climates (Kuhlemann et al., 2008). A more precise precipitation pattern could improve efforts to model glacial ice extent. In addition, geologic constraints on the ice thickness would also better constrain the model.

2.4 DETERMINATION OF GLACIAL EROSION WITH ICE CASCADE

2.4.1 Reference Case Set-up

ICE Cascade can generate the observed ice extent of the LGM with the appropriate climatic parameters. Therefore, it is reasonable to compare the predicted

spatial pattern of erosion to the spatial pattern of uplift. The LGM ice extent occurs at a sea level temperature of 7.2°C and a precipitation factor of 0.4. This case is shown in Figure 2.5 with a magenta circle and will be the reference case for the study of the glacial erosion examination. The glacial erosion is modeled over the glacial cycle in order to capture the changes in glacial extent over time. The glacial erosion is calculated every timestep, but is not applied to the topography. The topography is held fixed and the total potential for glacial erosion over the glacial-interglacial cycle is tracked.

To simulate the glacial cycle, temperatures are decreased from modern to LGM according to the following equation:

$$temps = \left(SLT_{\mathbf{modern}} - 0.0063 \times ht\right) - \left(\left(\frac{\left(SLT_{\mathbf{modern}} - SLT_{\mathbf{LGM}}\right)}{t_{final}}\right) \times time\right) \qquad (2.11)$$

where *temps* is the surface temperature, SLT_{modern} is the sea level temperature of today, which is 16.0°C, SLT_{LGM} is the sea level temperature at the LGM as determined by the reference case (7.2°C), 0.0063°C/km is the lapse rate, *ht* is the elevation of the topography including the ice thickness, t_{final} is the duration of the run in model years (100,000 yrs), and *time* is the time at which the temperature is being calculated. This temperature variability produces glaciers that grow to the LGM extent during the run. The precipitation is determined from Equation 10 wherein, if temperature is greater than 0°C, the precipitation falls as rain and is factored into the material lost from a glacier and if the temperature is less than 0°C, the precipitation falls as snow and adds to the mass of the glacier.

The growth of the glaciers in the Olympic Mountains to their full LGM extent is recorded in Figure 2.9. The corresponding thickness of the ice is in Figure 2.10. The figures demonstrate the full impact of the ice over the glacial cycle.

In the reference case model run, unreasonably fast sliding velocities were observed at a few points. These are numerical instabilities that result from coarse grid resolution, large precipitation rates, and long timescales. The artifacts either occurred in regions with naturally high sliding rates or in isolated positions with neighbors that have slow sliding rates. To eliminate these instabilities, a cap was placed on the sliding

velocities in the model. Sliding velocities of approximately 1000 m/yr might not be unphysical, but velocities greater than 5,000 m/yr are extremely unlikely in the Olympic Mountains. Thus, sliding velocities greater than 5,000 m/yr were deemed unphysical and set to zero. Sliding velocities between 500 m/yr and 5,000 m/yr were set to 500 m/yr. This limit on sliding velocity influenced only the numerical instabilities and preserved the sliding velocity patterns observed prior to the initiation of the cap (Figure 2.11).

2.4.2 Results of Erosion at the Entire Range Scale

Glacial erosion is calculated for the reference case according to Equation 2.1 with the standard glacial erosion constants of K_g, with a value of 10^{-4}, and l, with a value of one. The erosion pattern of the reference case is shown in Figure 2.12. The fastest erosion rates are located in the Hoh Valley on the western side of the Olympic Mountains, where the fastest uplift rates are also observed (Figure 1.6). Valleys have faster modeled glacial erosion rates than peaks and ridges, where the erosion rate is slow and does not vary smoothly.

The average erosion rate across the Olympic Mountains is compared to the uplift pattern along a transect from SW to NE (Figure 2.13). The erosion rate is greater than the rock uplift rate, but the spatial patterns are similar. The northern and eastern sides of the Olympic Mountains should not be examined in much detail as the alpine ice extent in these valleys is unconstrained and the Cordilleran Ice Sheet likely influenced glacial extent, and therefore, glacial erosion rates.

To illustrate the spatial variability within the Olympic Mountains, the rock uplift rates and modeled glacial erosion rates are compared in map view (Figure 2.14). The highest rock uplift rates do not occur in the center of the range or where the highest elevations occur. Instead, the fastest rock uplift rates occur partway up the Hoh Valley. The fastest modeled erosion occurs within the valleys and the fastest erosion rates occur in the Hoh Valley. It is expected that the valleys would have faster glacial erosion rates than the ridges due to the much larger ice thickness in the valleys. Slope processes including mass wasting erode the ridges and are not included in the modeled glacial erosion rates. Glacial erosion is expected to impact the ridges indirectly. Multiple local maxima in glacial erosion rates can be seen in each of the river valleys on the western

side of the Olympic Mountains. This is the result of tributary valleys feeding into the main valley. The erosion rate also varies from north to south with the maximum amounts of erosion occurring in the northern valleys. Glacial erosion rates and rock uplift rates are regressed on one another (Figure 2.15) giving an r-squared value of 0.0679, which demonstrates that the data has very poor pixel-by-pixel correlation. The lack of correlation between glacial erosion rates and rock uplift rates is expected because glacial erosion is not acting everywhere. Instead, glacial erosion is expected to lower the valley floors and the ridges will be forced to follow at a similar pace due to the limited strength of rocks to hold steep slopes. Therefore, this study will focus on the spatial patterns of modeled glacial erosion rates and rock uplift rates within three valleys.

2.4.3 Comparison of Glacial Erosion and Uplift Within the Valleys

The modeled glacial erosion rates and rock uplift rates in the Hoh, Queets, and Quinault River Valleys on the western side of the Olympic Peninsula are compared to evaluate the hypothesis that glacial erosion rates and rock uplift rates have similar spatial patterns of variability. Figure 2.16 compares the erosion rates averaged over the glacial cycle at points on the valley floors in each of the river valleys and across the entire peninsula to each other and with the uplift pattern. The fastest erosion rates occur in the Hoh Valley. In all three valleys, the modeled glacial erosion rates are significantly faster than the rock uplift rates.

Erosion rates and rock uplift rates are compared along the longitudinal profiles for the three valleys (Figures 2.17-2.19). The erosion rate pattern in the Hoh Valley resembles the pattern of rock uplift rates, but the erosion rates are much faster than the uplift rates. The fastest erosion rates correspond to the area of maximum uplift rates. Linear regression of erosion rates on rock uplift rates in the Hoh Valley yield an r-squared value of 0.67, which demonstrates a degree of correlation. Rock uplift rates and glacial erosion rates also have similar spatial patterns in the Queets Valley and modeled erosion rates are much faster than rock uplift rates. There is more variability in the erosion rates than in the uplift rates. Linear regression of the erosion rates and the uplift rates in the Queets Valley yield an r-squared value of 0.45, which shows some degree of relationship. Modeled glacial erosion rates in the Quinault Valley are also faster than rock

uplift rates. However, the erosion pattern and uplift pattern do not resemble each other in this valley and linear regression gives an r-squared value of only 0.17.

2.4.4 Variability of Glacial Erosion with Precipitation and Temperature for the Reference Case

How sensitive are the modeled glacial erosion rates in the Hoh, Queets, and Quinault Valleys to changes in temperature and precipitation? ICE Cascade can simulate the observed ice extent at LGM with a range of temperature and precipitation values. The glacial erosion rates for the entire range of climatic parameters are compared with the reference case described above. To do this analysis, the model was run many times. To decrease the time required for each model run, the model timesteps are increased by a factor of 10 (from one year to ten years), which decreases the runtime from approximately two days to around four hours. To determine the impacts of this change in timestep, select runs are compared with the original, higher time resolution simulations. There is little effect on erosion rates: the modeled erosion rates are within 5% of each other on average (Figure 2.20). The largest difference is 13% and this occurs in a section of the Quinault Valley. Due to this support, the model is run for 10,000 yrs instead of the full glacial cycle.

The influence of precipitation and temperature variations on the total erosion rates and patterns for the entire range and for the three chosen valleys is quantified. To examine the influence the temperature has on the erosion rates, the precipitation fraction is held at 0.6 while the temperature is varied from 7.0-8.0°C. The erosion rates produced are compared to each other for the entire range (Figure 2.21). Lower temperatures produce slower modeled erosion rates. It was found that the erosion rates for the various temperature runs vary by a factor of 26-34% per degree Celsius. To examine how the precipitation influences the erosion rates, the temperature is held at 8.0°C while the precipitation factor varies from 0.4-0.8. The erosion rates produced are compared in Figure 2.22 for the entire range. Less precipitation produced lower modeled glacial erosion rates and it is observed that a halving of the precipitation decreases the erosion rates by 24-37%. The relationship between glacial erosion rates and precipitation is similar to the theoretical square root relationship predicted by Tomkin and Roe (2007) for

high sloped, mixed sliding and deformation critical wedges like the Olympic Mountains, which would predict a decrease in erosion rates of 29% for a halving of precipitation rates.

Each of the valleys provides the same results as that of the entire range and it is observed that the overall change in the amount of erosion is not that large and the spatial pattern does not change. In particular, decreasing the temperature and precipitation within reasonable bounds does not bring the modeled glacial erosion rates into agreement with the rock uplift rates.

2.4.5 Using the Glacial Erosion to Constrain the Glacial Erosion Rule

The correlation between the spatial patterns of modeled glacial erosion rates and measured rock uplift rates suggests that these data sets provide an opportunity to calibrate the glacial erosion constant. To my knowledge, this is the first attempt to validate the sliding law for the glacial erosion rates on geologic timescales. The glacial erosion constant, K_g, is estimated to be between 10^{-4} and 10^{-5} (Humphrey and Raymond, 1994). The exponent in the sliding law, l, is suggested to have a low value between 1 and 2 according to numerical work by Harbor (1992b) and theory supports this low value regardless of the erosion mechanism (Hallet, 1979). Since the Olympic Mountains are in steady state, I assume that the rock uplift rates and glacial erosion rates on the Olympic Peninsula are equal. In particular, I assume that modeled glacial erosion rates in large valleys are equal to local rock uplift rates. Therefore, the local rock uplift rates within the valleys are assumed to be the true glacial erosion rates. These rates are compared with glacial erosion rates based on modeled sliding from ICE Cascade. The constants, K_g and l, are varied to produce different models of glacial erosion. The model which best matches the true glacial erosion rates is found. Instantaneous glacial sliding rates from the reference model are available at ten equally-spaced time steps. For each of these ten sets of conditions, modeled glacial erosion rates have the form:

$$\dot{e}_t(x) = K_g s_t(x)^l \tag{2.12}$$

where for each point on the valley long profile, x, $\dot{e}_t$ is the erosion rate at time t, and s_t is the sliding rate at time t. Long-term glacial erosion rates are assumed to be the average of the instantaneous rates at these ten time steps. Therefore, the long-term glacial erosion rate is:

$$\dot{e}(x) = \frac{\sum_{t=1}^{10} \dot{e}_t(x)}{10} = K_g \times \frac{\sum_{t=1}^{10} s_t(x)}{10} \tag{2.13}$$

This modeled long-term glacial erosion rate is compared to the measured true glacial erosion rate. The misfit is defined as:

$$m = \sqrt{\frac{\sum_{x=1}^{n} \left(\dot{e}(x) - E(x)\right)^2}{n-2}} \tag{2.14}$$

where $E(x)$ is the true erosion rate at each point along the valley profile and n is the number of points in the valley profile. The best fitting values for the model parameters are found by minimizing this misfit. Note that the measured and modeled erosion rates along the valley profiles are not strictly independent of each other, which precludes standard statistical analysis.

Initially, l is held constant at one and K_g is allowed to vary for each of the valleys examined. One point in the Hoh Valley is subject to persistent numerical instability due to unusually high slopes around it and this point is eliminated from the following analysis. Modeled erosion rates and true erosion rates are compared in the Hoh Valley (Figure 2.23), the Queets Valley (Figure 2.24), and the Quinault Valley (Figure 2.25). In all three valleys, the best fit for K_g is significantly less than 10^{-4}, ranging from 8.859e-6 to 1.206e-5 (Table 2.2). The misfits for these cases are given in Table 2.3 and range from approximately 32-78% of the true value of the erosion rate. The narrow range of best fit values for K_g across three valleys supports the classical glacial erosion law. In addition, note that the best fitting values for K_g are within the range estimated by Humphrey and Raymond (1994): 10^{-4} to 10^{-5}.

If both K_g and l are allowed to vary, the misfits are somewhat reduced. l is allowed to vary from 0.1-2.0. The best fitting cases are found for the Hoh Valley (Figure 2.26), the Queets Valley (Figure 2.27), and the Quinault Valley (Figure 2.28). The magnitude of K_g in these cases is not comparable to other cases because a variable l implies that the units of K_g are also variable. In all three valleys, the best fitting values for l are much less than one (Table 2.3). For the Hoh and Quinault Valleys, the misfit is significantly lower when l is allowed to vary, while in the Queets Valley the improvement is slight.

Finally, l is set equal to zero and K_g is allowed to vary. This scenario represents the possibility that glacial sliding is not a good predictor of glacial erosion rates, but that the presence of glacial ice alone might provide a reasonable model. The results of this analysis differ from valley to valley. In the Hoh and Quinault Valleys (Figures 2.29 and 2.31), the misfit is larger than for finite variable l. In the Queets Valley (Figure 2.30), however, the lowest misfit occurs when l is zero. This disagreement from valley to valley might be explained by the lack of true erosion rate measurements in the Queets and Quinault Valleys. These valleys have fewer measurements of rock uplift rates than the Hoh Valley (Brandon et al., 1998). In addition, the modeled glacial ice in the Queets Valley characteristically did not reach the dated end moraines under the climatic conditions that produced the best fit overall. This failure of the model in the Queets Valley suggests that local glacial processes here are not well-resolved by the reference case ICE Cascade simulation.

2.5 DISCUSSION AND CONCLUSIONS

ICE Cascade successfully reproduces the observed ice extent for the LGM when summer sea level temperatures are between 7.0-8.0°C and precipitation rates are 0.4-0.8 of the modern precipitation rates. This is the first time that ICE Cascade has been used to simulate observed glacial extent in detail for a real mountain range. Moreover, the climate parameters that reproduce the observed ice extent also match the paleoclimate reconstructions from pollen data in the Humptulips River Valley. The accord between model climate parameters and paleoclimatic estimates indicates that standard ice model mechanics in ICE Cascade are sufficient to describe the glacial history of the Olympic

Mountains. In addition, the hypothesis that ICE Cascade can simulate the observed ice extent with plausible climate parameters is supported.

The ice extent is more sensitive to temperature and less sensitive to precipitation, with temperature varying the erosion rates by a factor of 26-34% per degree Celsius. A halving of the precipitation decreases the erosion rates by a factor of 24-37%. Each of the valleys provides the same results as that of the entire range. It is observed that the overall change in the amount of erosion is not large and the spatial pattern of the erosion does not change. In particular, decreasing the temperature and precipitation within reasonable bounds does not bring the modeled glacial erosion rates into agreement with the rock uplift rates.

Modeled glacial erosion rates vary in a manner consistent with the observed rock uplift rates within three large valleys on the western side of the Olympic Peninsula. These valleys sample a range of values for average uplift rates from 0.75 mm/yr for the Hoh Valley, to 0.62 mm/yr for the Queets Valley, to 0.51 mm/yr for the Quinault Valley. Glacial erosion rates are predicted to be the fastest in the Hoh Valley where the observed rock uplift rates are also the fastest. In each valley, the spatial pattern of modeled glacial erosion rates resembles the observed pattern of rock uplift rates. However, the rock uplift rates are significantly slower than modeled glacial erosion rates with standard sliding law coefficients of K_g equal to 10^{-4} and l equal to one. Varying the amount of precipitation and temperature in the range of the best fitting cases produced by the LGM climate sensitivity analysis does not alter the spatial pattern of erosion, just the magnitude. The similar spatial patterns in modeled glacial erosion and rock uplift supports the hypothesis that sliding law based glacial erosion patterns are similar to observed rock uplift patterns in the Olympic Mountains. However, the fact that the glacial erosion rates are consistently faster than the rock uplift rates suggests that the standard sliding law might be improved upon.

The glacial erosion sliding law is calibrated over long time periods by assuming that the glacial erosion rates are equal to the measured rock uplift rates. This assumption is partially justified by the strong evidence for steady state topography in the Olympic Mountains (Brandon, 2004) and by the failure of the stream power based fluvial incision models to match rock uplift rate patterns (Tomkin et al., 2003). To perform this

calibration, values are found for the parameters K_g and l which minimize the misfit between the modeled erosion rates and the observed rock uplift rates. In each of the three valleys studied, if l is held fixed at one, the best fitting K_g is on the order of 10^{-5}. The consistency between the valleys with this value for K_g and the fact that its magnitude is within the range supported by observations (Humphrey and Raymond, 1994) suggests that the glacial erosion sliding law with K_g equal to 10^{-5} is a reasonable model for glacial erosion of the Olympic Mountains. This model allows for long-term steady state between glacial erosion and rock uplift rates.

If both K_g and l are allowed to vary, lower misfits between the modeled erosion rates and the observed uplift rates are found when l is less than one. These low values are not supported by the theory of abrasion-based erosion (Hallet, 1979). Additionally, the best fitting values for l vary from valley to valley. Low values for l suggest that either the sliding law based erosion may not be a good model for long-term glacial erosion or the assumption that glacial erosion rates are equal to rock uplift rates is not valid. If the influence of subglacial water and water pressure variability on glacial erosion are significant, then one might expect to get an unphysical estimate for l from the calibration estimate. It is also possible that long-term erosion rates in the Olympic Mountains are not dominated by glacial erosion and, therefore, that the assumption that glacial erosion and uplift are equal may not be reasonable. The relatively coarse sampling of long-term rock uplift rates and the fact that points within the valleys are not independent might also hamper the calibration.

I suggest that the lack of uplift data in the Queets and Quinault Valleys is a significant factor in producing a poor fit between modeled erosion rates and rock uplift rates and in generating low estimated values for l. In the Queets and Quinault Valleys, there are only a few measurements of rock uplift rates (Brandon et al., 1998). In contrast, uplift rates are better constrained in the Hoh Valley and the correlation between uplift rates and erosion rates is better. There are additional errors in the calibration due to the uncertainty in rock uplift rate measurements (Brandon et al., 1998). Additionally, ice extent in the Queets Valley does not match geomorphic records for the climate conditions which match ice in three other locations. The failure of ICE Cascade to fit the Queets Valley could result from errors in precipitation estimates for this region or from changes

in the valley topography since the LGM. The orographic precipitation pattern is likely to have errors in excess of 10% for the modern climate (Anders et al., 2007) and may not represent the spatial variability in precipitation during glacial conditions, especially when the continental ice was present in the region.

If glacial erosion rates and rock uplift rates are equal and the sliding law model is sufficient, the various uncertainties in the data are expected to generally increase misfits and may reduce the dependency between the model parameters and observations. This may result in a calibrated value for l that is lower than it should be. I argue that the sliding law for glacial erosion is plausible given the uncertainties. The similarity in the fitted K_g values for l equal to one in three river valleys lends support to this claim. It is expected that the uncertainty in the data could produce a factor of two change in the misfit following Tomkin et al. (2003). Thus, the relatively small decreases in misfit when l is allowed to vary in the Hoh and Queets Valleys suggest that the l equal to one case and the l equal to 0.4 or zero cases are equivalent and that a sliding law based glacial erosion model is supported. In contrast, in the Quinault Valley a very low l produces a very large decrease in misfit, suggesting that an l less than one case represents a true improvement in the model.

Finally, only glacial erosion is considered and fluvial and hillslope erosion processes are neglected. It is expected that fluvial erosion rates are less important than glacial erosion rates during the Quaternary and note that stream-power based models of fluvial incision have been unable to reproduce the observed spatial pattern of rock uplift rates (Tomkin et al., 2003). However, fluvial and hillslope erosion clearly have contributed to the erosion of the Olympic Peninsula and their omission may increase the degree of misfit. In particular, the processes that control valley wall slope failure may influence overall erosion in the Olympic Mountains. The debris produced along valley walls may become entrained by glaciers and influence its ability to erode the bed through the production of tools and protection from erosion analogous to fluvial bed armoring (Bennett and Glassner, 1996). A more complete model of erosion might allow for a more conclusive test of the relationship between rock uplift rates and erosion rates in the Olympic Mountains.

2.6 FIGURES AND TABLES

Model Parameter Values		
Symbol	**Parameter Name**	**Value/Units**
A_d	Deformation constant	2.5×10^{-16} m^6 s^{-1} N^{-3}
A_s	Sliding parameter	1.8×10^{-10} m^8 s^{-1} N^{-3}
α_1	Ablation constant	1.5 m yr^{-1} °C^{-1}
α_2	Lapse rate	0.0063°C/m
β_c	Constriction factor	
g	Acceleration due to gravity	9.81 m s^{-2}
h	Topographic height	m
h_{ice}	Ice thickness	m
ht	Topographic height plus ice thickness	m
K_g	Glacial erosion constant	10^{-4}
k_c	Constriction constant	10^5 m
κ	Thermal diffusivity of ice at 0°C	1.09×10^{-6} m^2 s^{-1}
l	Exponent of glacial erosion	1
M_a	Rate of accumulation	m yr^{-1}
M_m	Rate of ablation	m yr^{-1}
N	Ice overburden pressure	
n	Ice flow exponent	3
P	Basal water pressure	
ρ	Density of ice	910 kg m^{-3}
T or T_0	Sea level temperature	°C or 16°C
T_b	Basal temperature	°C
T_s	Surface temperature	°C

Table 2.1. Summary of the parameters, constants, and variables used in the model and their corresponding values and units.

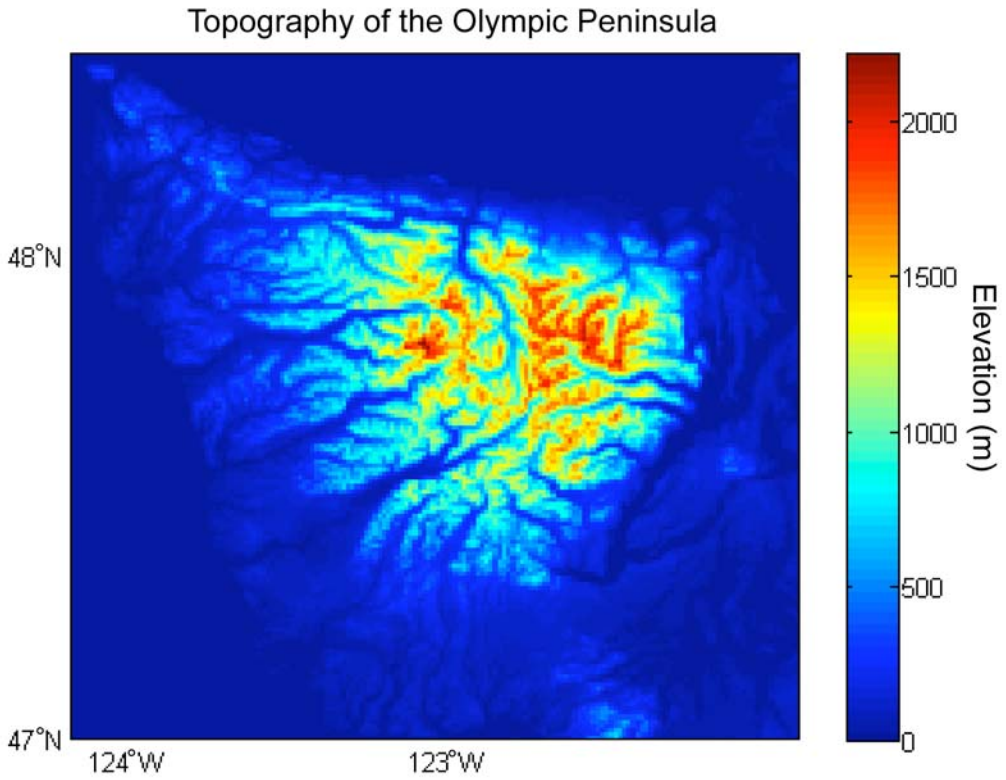

Figure 2.1. The topography of the Olympic Peninsula as it appears in ICE Cascade. The topography is measured in meters and the grid is 1 km by 1 km.

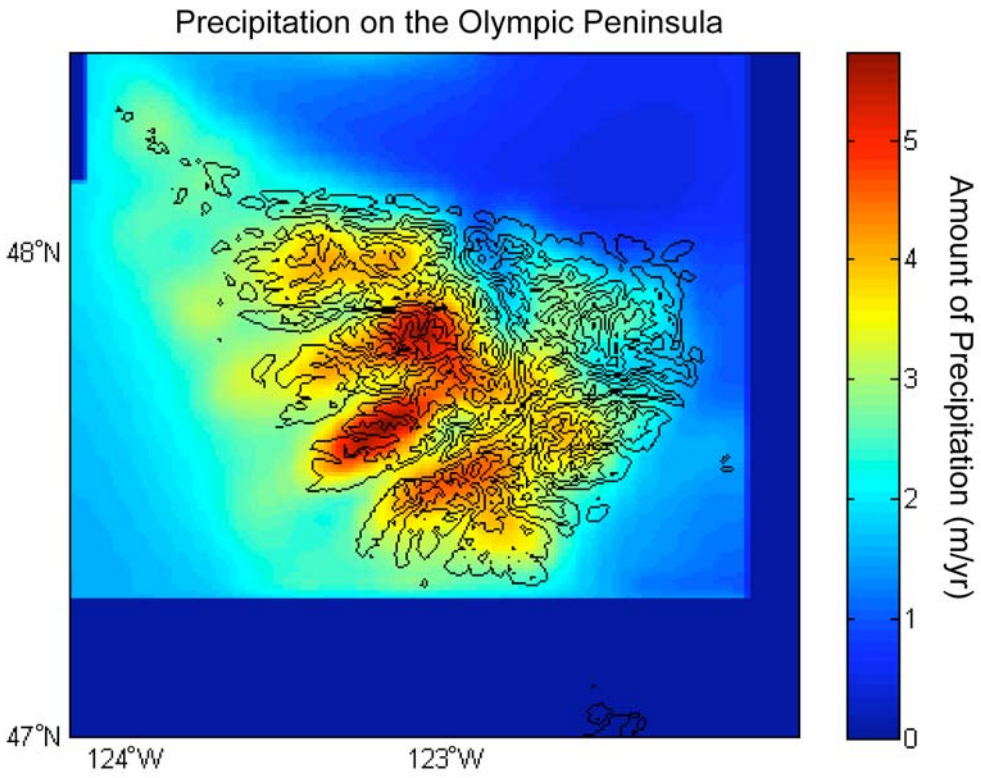

Figure 2.2. The orographic precipitation pattern of the Olympic Mountains as it appears in ICE Cascade. The precipitation is measured in meters/year and the grid is 1 km by 1 km.

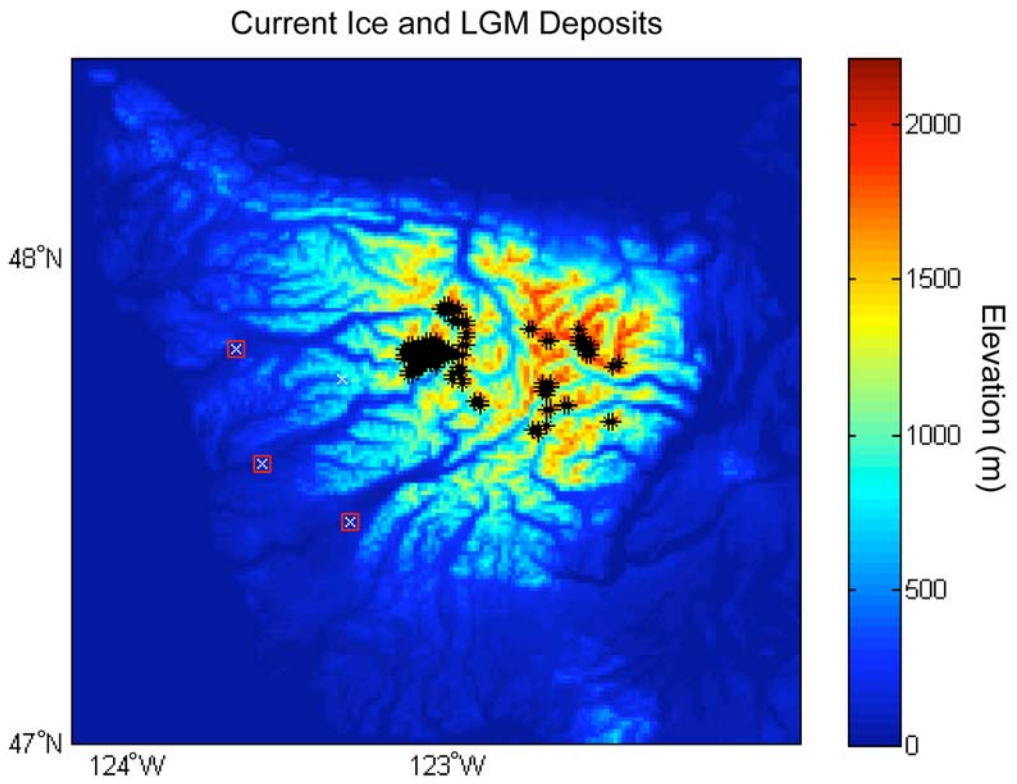

Figure 2.3. The current ice extent and the LGM deposits used in ICE Cascade to determine the sensitivity for the Olympic Peninsula. The current ice extent is marked by black asterisks and the LGM deposits are marked by magenta squares.

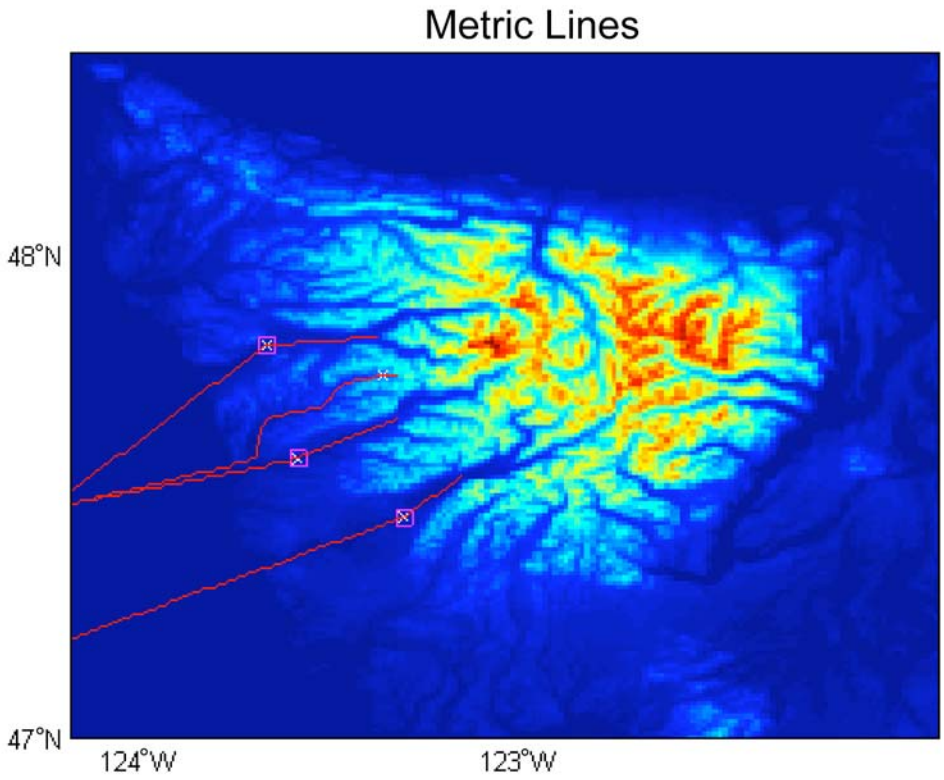

Figure 2.4. The lines used in the metric for determining the misfit of the modeled ice extent with the dated geomorphic deposits of the LGM ice extent are shown as the red lines. The pink squares mark the LGM deposits and the white x's are the dated LGM deposits used by the metric.

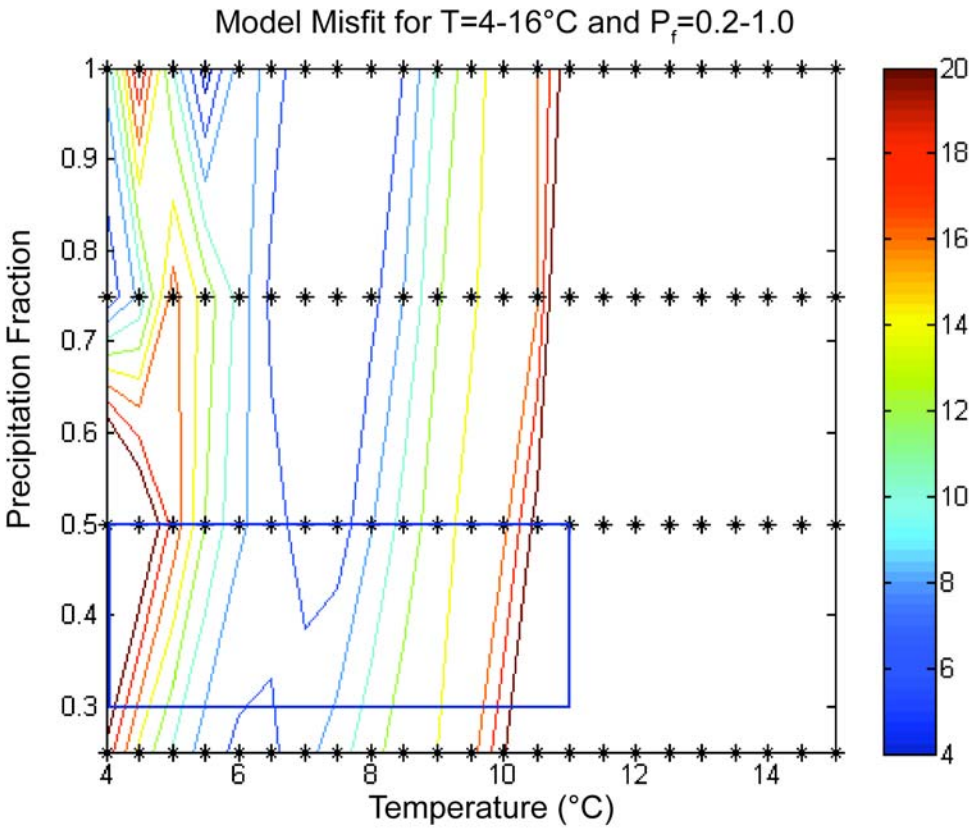

Figure 2.5. Metric of the ice extent in the Hoh, Queets, Clearwater, and Quinault River Valleys at the LGM for the Olympic Mountains' alpine glaciers. The ablation constant is 1.5, temperature ranges from 4.0-16.0°C, and the precipitation fraction ranges from 0.2-1.0 of the modern precipitation. The black asterisks represent each of the model runs used in the metric. The best fitting region has temperatures from 6.0-8.0°C and a precipitation fraction of 0.2-0.8 of the modern precipitation. The blue box represents the best fitting climate parameters based on paleoclimate data.

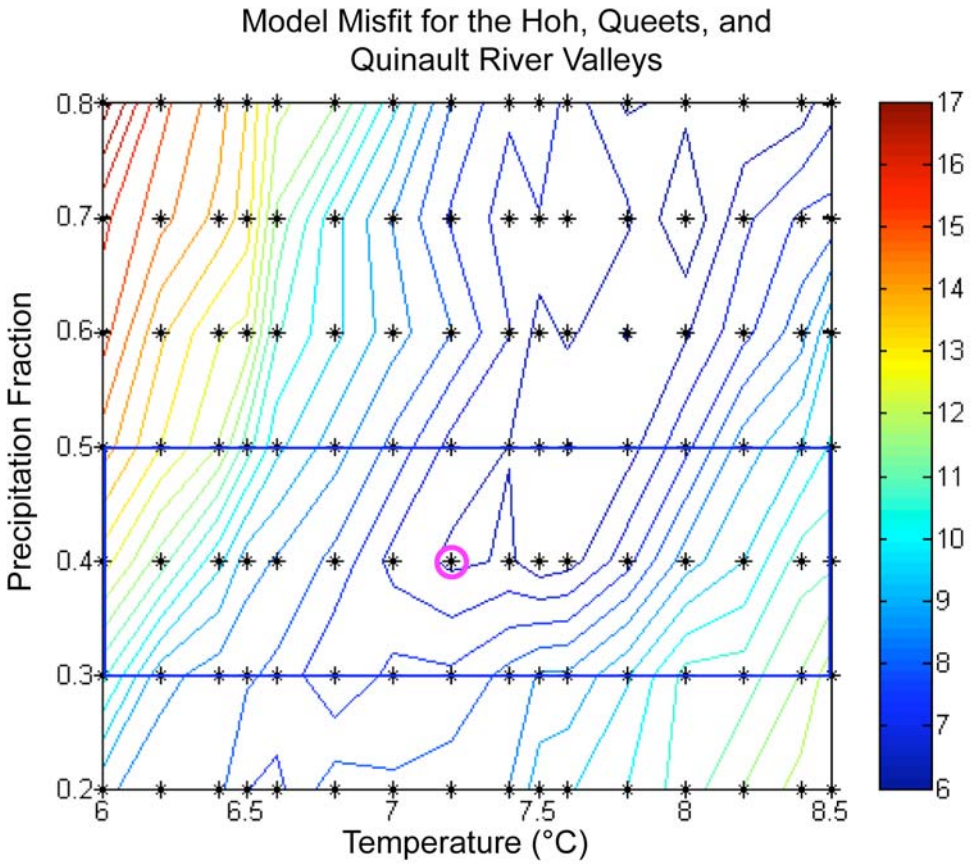

Figure 2.6. Metric of the ice extent in the Hoh, Queets, Clearwater, and Quinault River Valleys at the LGM for the Olympic Mountains' alpine glaciers. The ablation constant is 1.5, temperature ranges from 6.0-8.5°C, and the precipitation fraction ranges from 0.2-0.8 of the modern precipitation. The magenta circle denotes the best fitting case used throughout this chapter and the blue box denotes the paleoclimate estimates for the LGM climate.

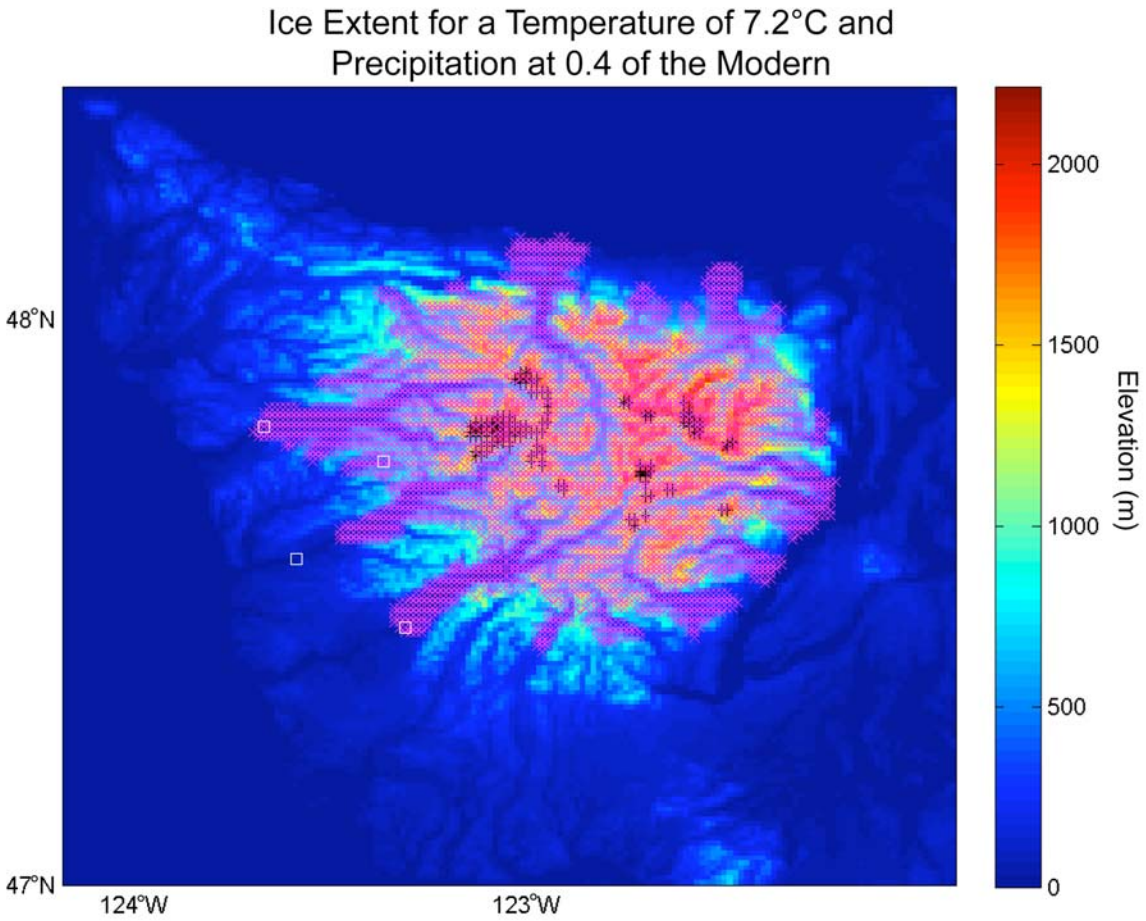

Figure 2.7. The maximum ice extent from ICE Cascade as compared to the LGM deposits for the best fitting case with a temperature of 7.2°C, the precipitation fraction at 0.4 of the modern precipitation, and an ablation constant of 1.5. The modeled ice extent is marked by magenta asterisks, the current ice extent is marked by black asterisks, and the LGM deposits are marked by white squares.

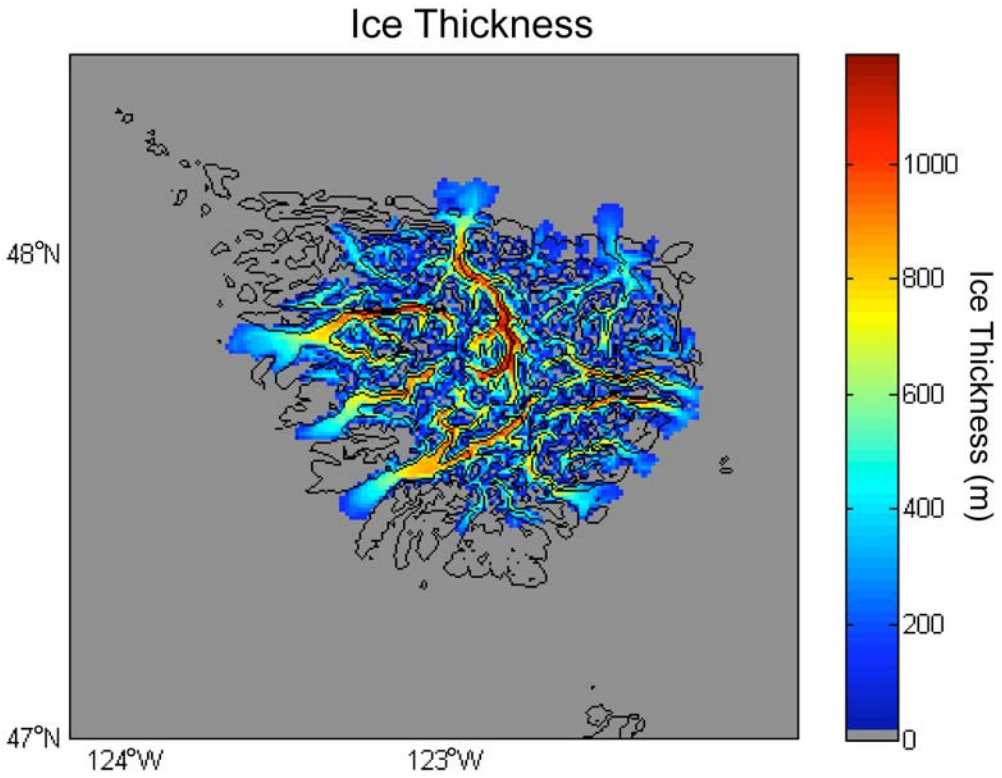

Figure 2.8. Ice thickness for the best fitting case at maximum ice extent with a temperature of 7.2˚C and precipitation at 0.4 of the modern. The ice thickness is measured in meters and the contours mark the topography.

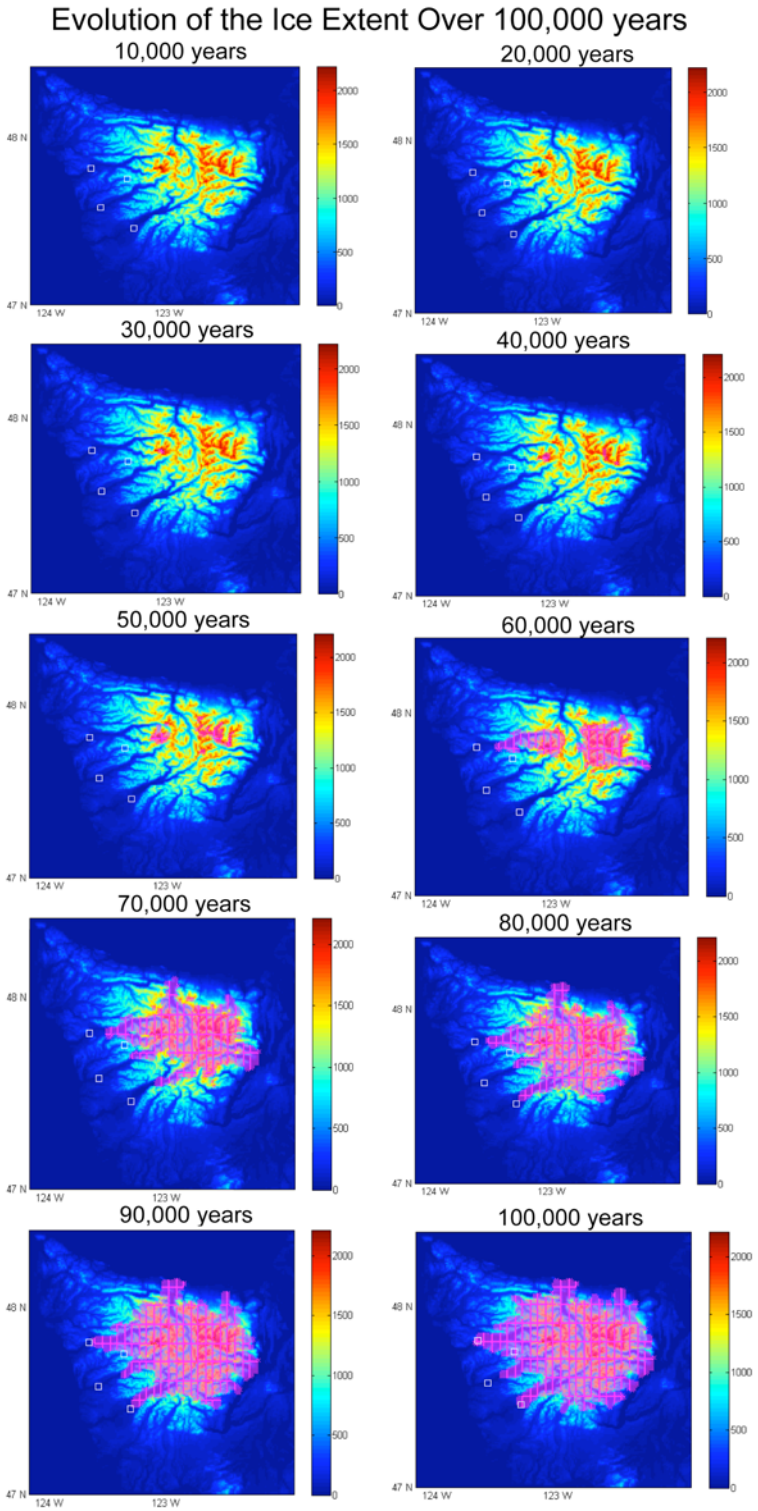

Figure 2.9. The evolution of ice extent from ICE Cascade for the best fitting case with a temperature of 16-7.2˚C and precipitation at 0.4 of the modern. The modeled ice extent is marked by magenta asterisks and the LGM deposits are marked by white squares. The topography is measured in meters. The ice extent is recorded every 10,000 years for the 100,000 year glacial cycle.

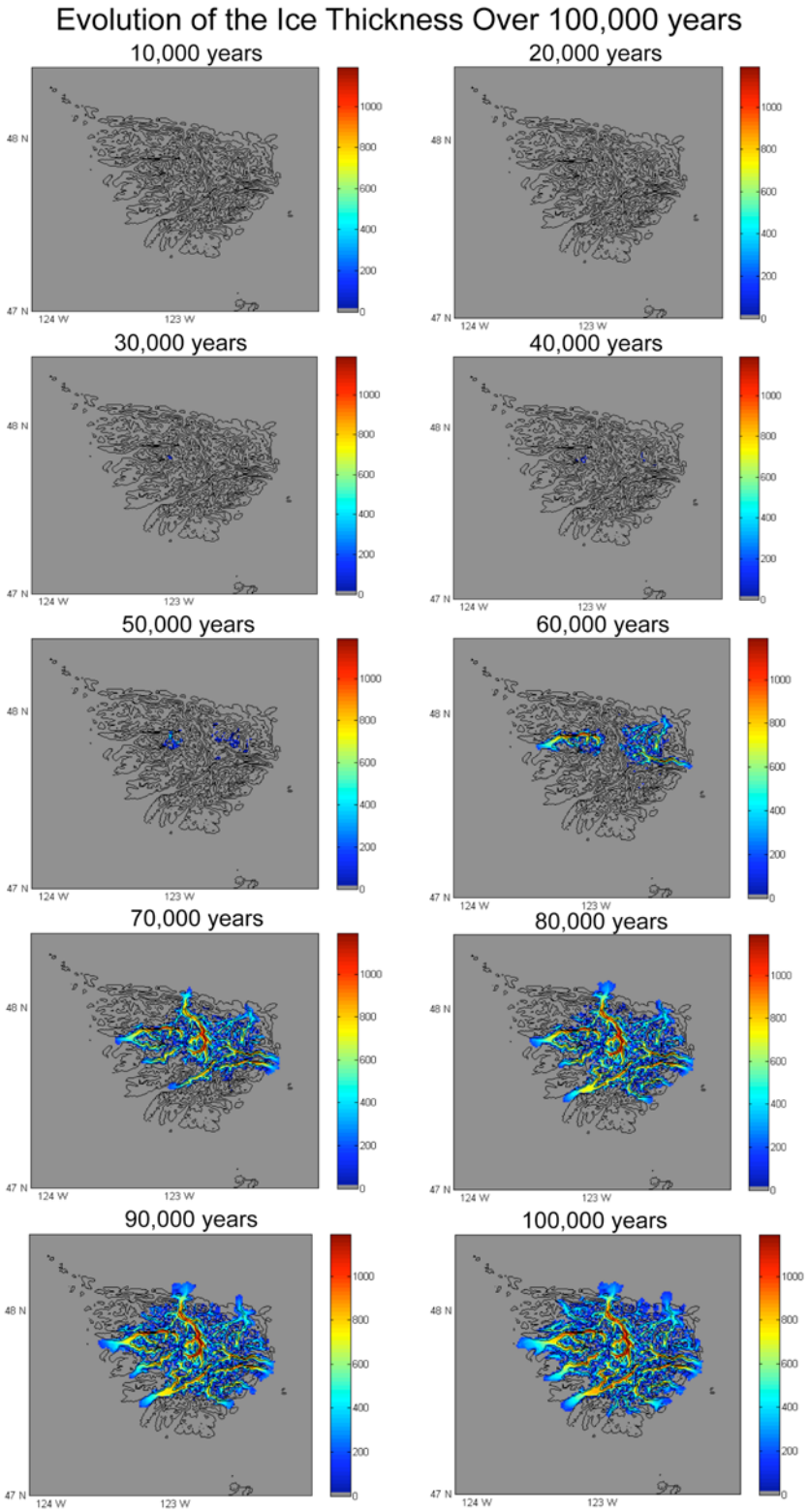

Figure 2.10. The evolution of the ice thickness for the best fitting case with a temperature of 16-7.2˚C and precipitation at 0.4 of the modern. The ice thickness is measured in meters and the contours mark the topography. The ice thickness is recorded every 10,000 years for the 100,000 year glacial cycle.

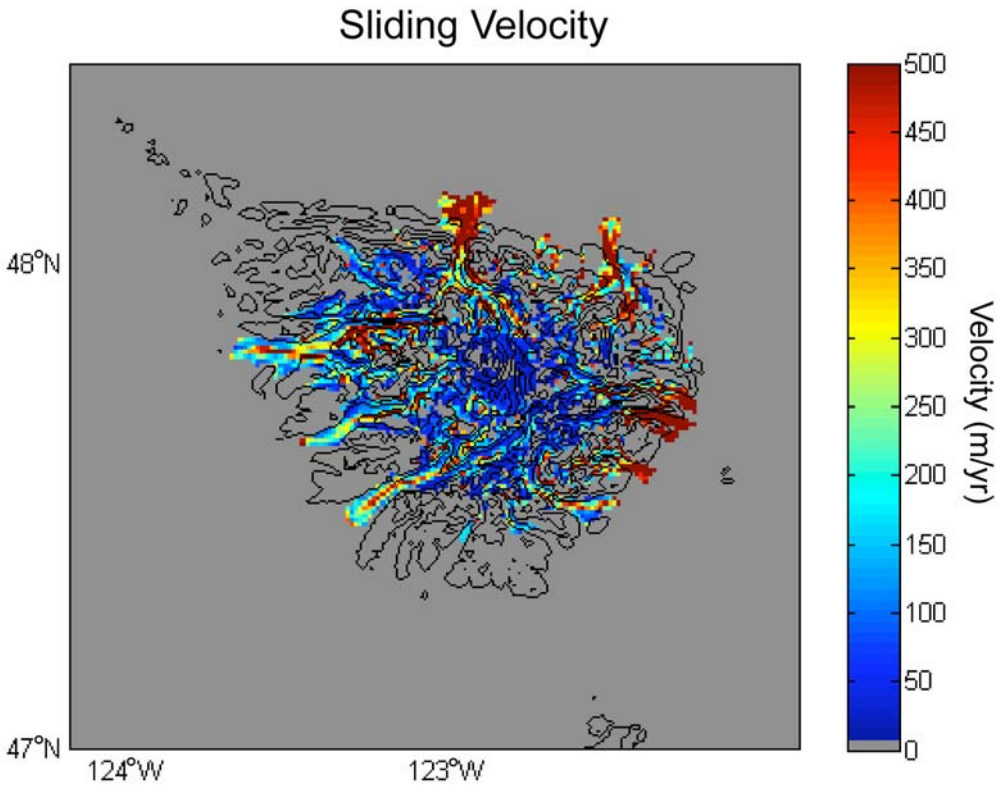

Figure 2.11. The spatial pattern of the sliding velocity at maximum glacial extent throughout the Olympic Peninsula. The sliding velocity is measured in meters per year and the contours denote the topography. The valleys on the western side of the peninsula are examined for their erosion because the valleys on the eastern and northern sides interacted with the Cordilleran Ice Sheet and their ice extent and corresponding velocities are unknown.

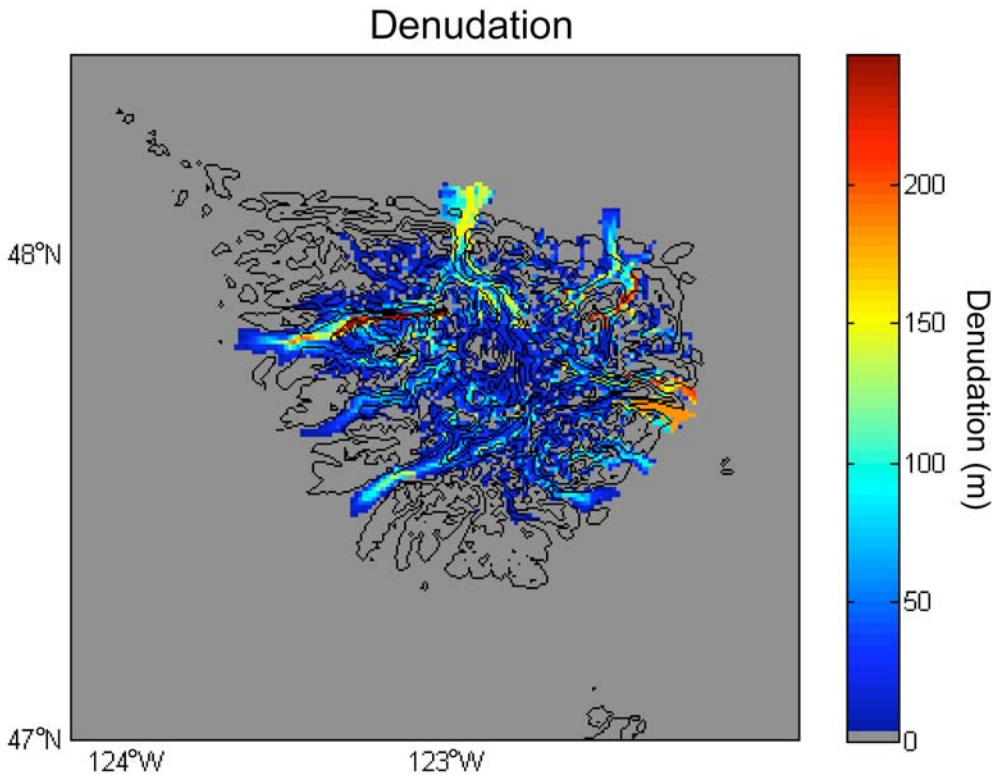

Figure 2.12. The glacial erosion pattern produced by ICE Cascade for the Olympic Mountains over 100,000 years. The erosion is measured in meters and the topography is marked by the black contours. The fastest erosion occurs in the Hoh River Valley.

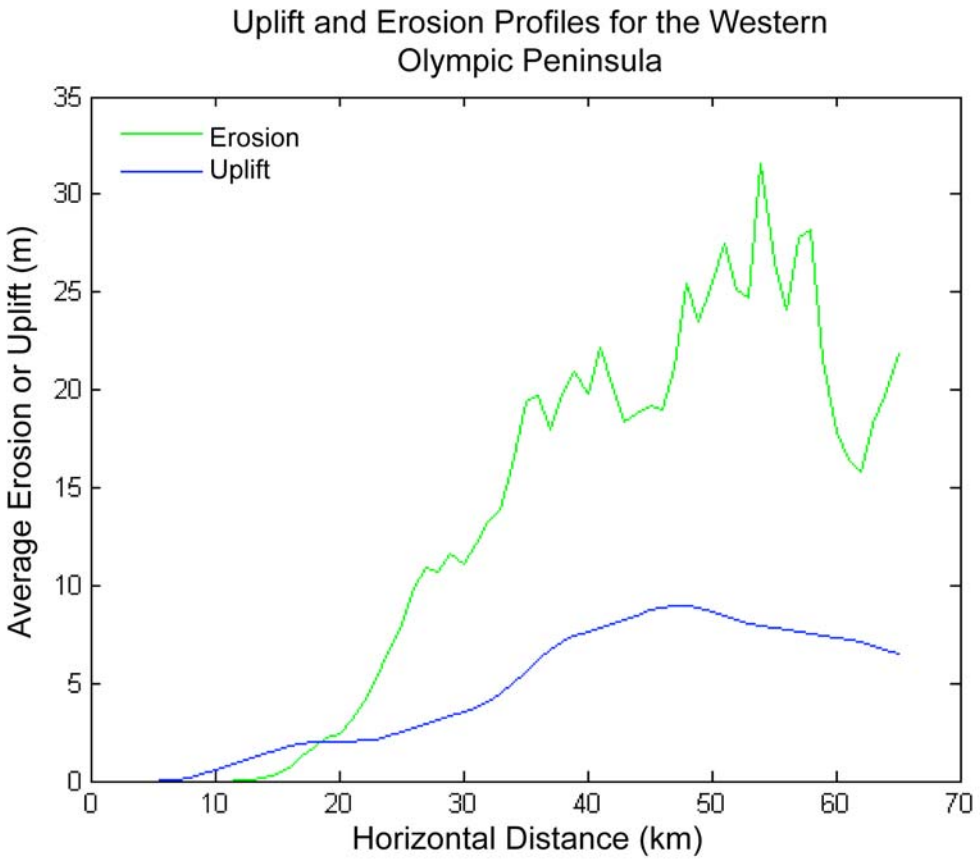

Figure 2.13. The average glacial erosion profile over the Olympic Mountains as compared to the uplift from the profile provided by Brandon et al. (1998) in Figure 1.7. The uplift is in blue and the erosion is in green. The erosion is greater than the uplift as the magnitude of the patterns is different, but the overall pattern is similar.

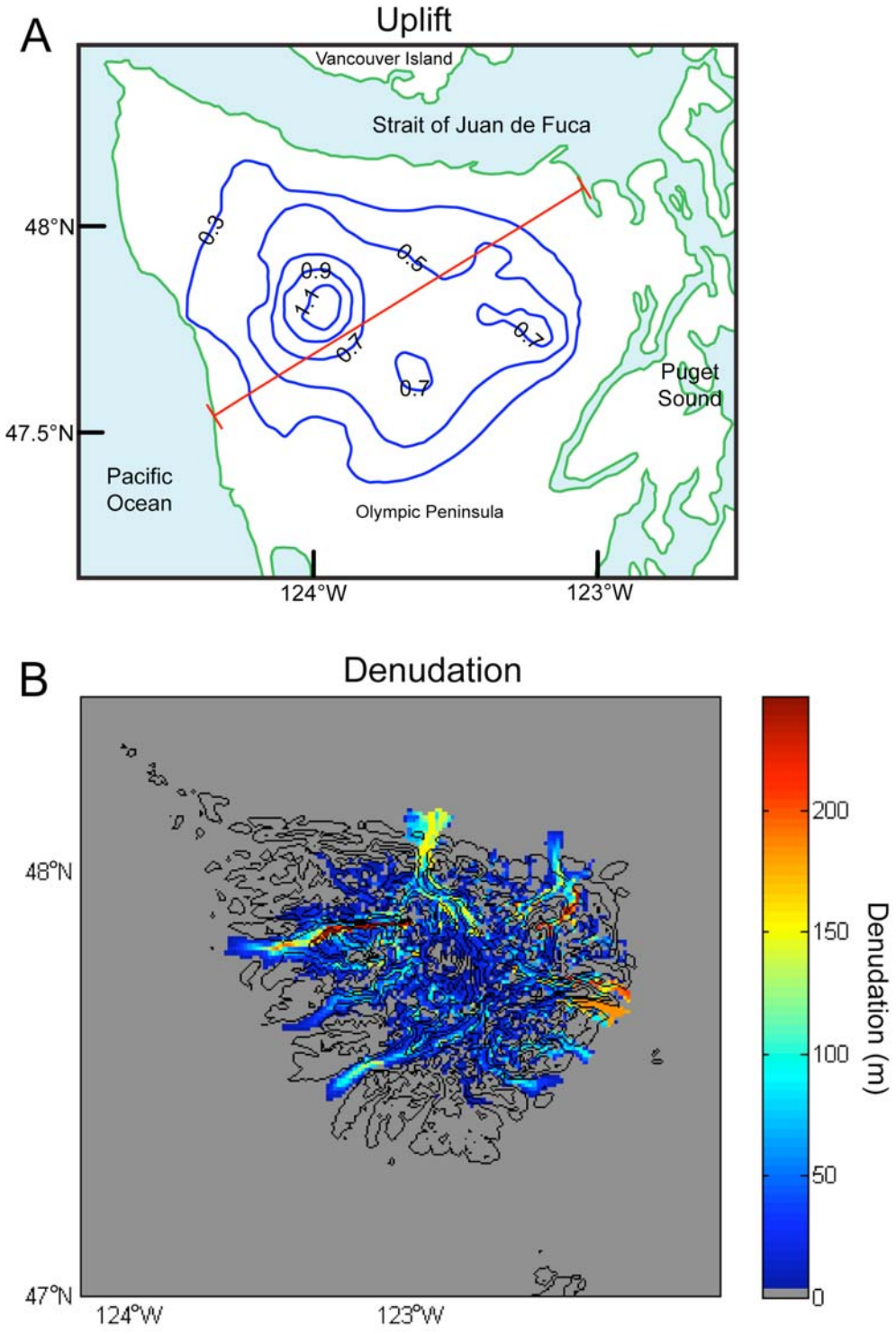

Figure 2.14. Comparison of the total erosion pattern produced by the glacial erosion in ICE Cascade and the contoured uplift pattern for the Olympic Peninsula. The uplift (A) and erosion (B) rates vary north to south. The highest areas of erosion occur in the river valleys. The highest uplift rates occur in the Hoh River Valley, where the highest erosion also occurs (adapted from Brandon et al., 1999).

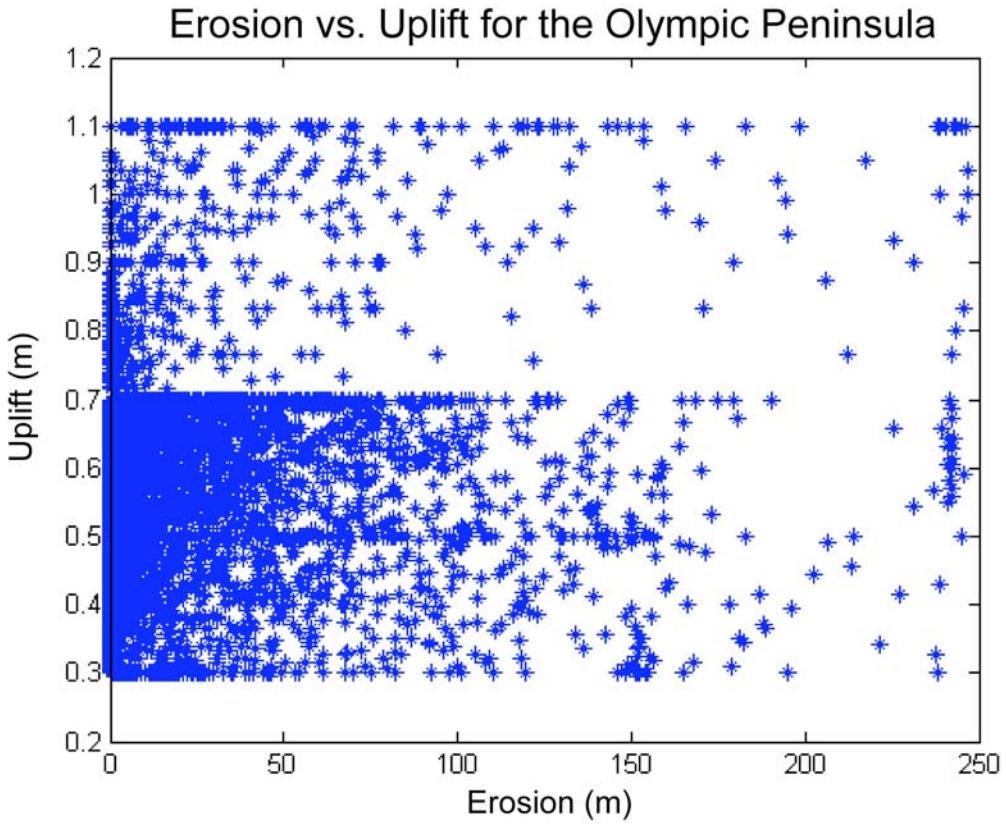

Figure 2.15. Regression of the total erosion against the total uplift across the entire Olympic Peninsula. Both the uplift and erosion are measured in meters. The r-squared has a value of 0.0679 and this is expected as glaciers do not erode everywhere on the peninsula.

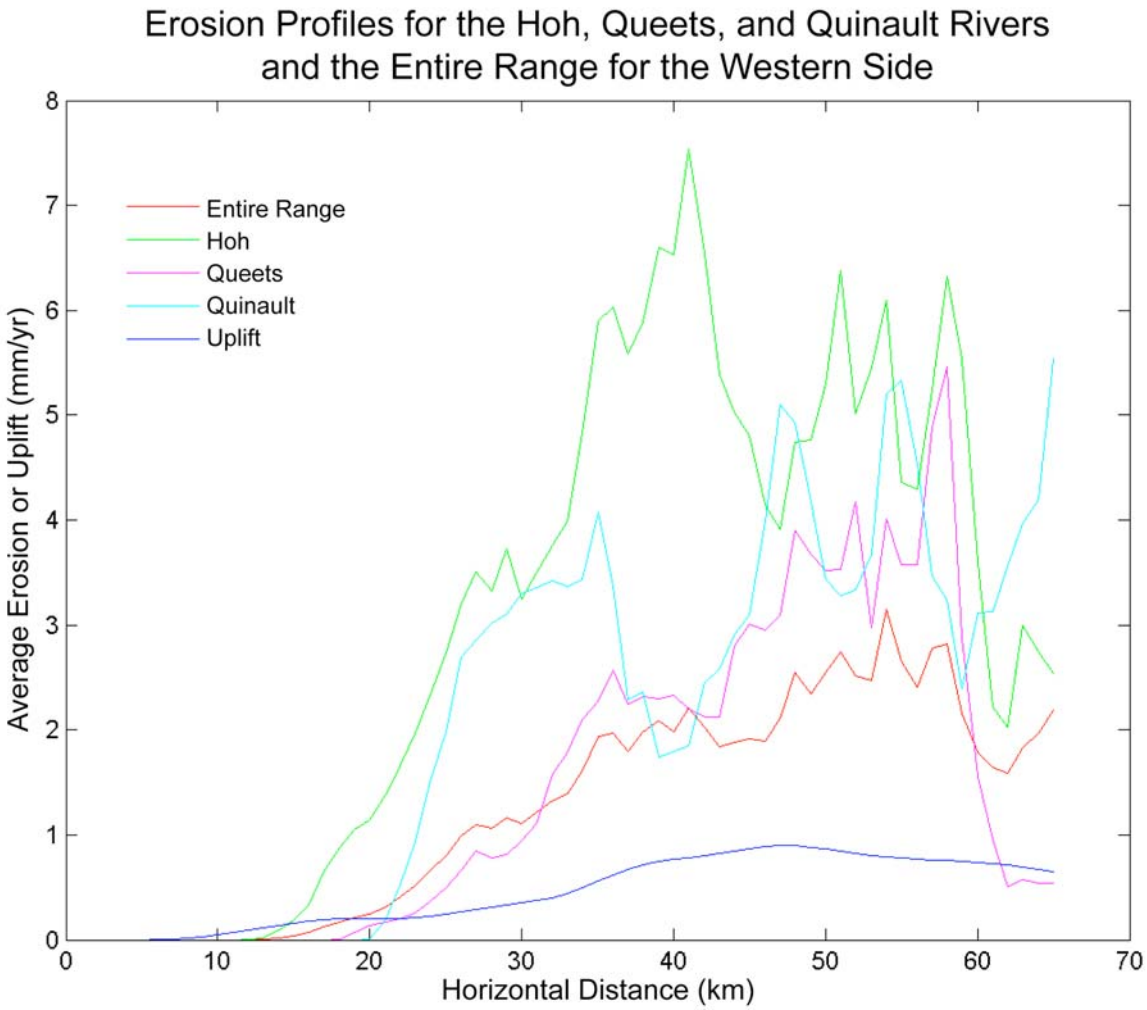

Figure 2.16. The erosion profiles in the Hoh, Queets, and Quinault River Valleys and across the entire range as compared to each other and the uplift profile. The highest erosion occurs in the Hoh River Valley and the magnitudes of all of the erosion profiles are greater than the uplift profile, though the patterns of all are similar.

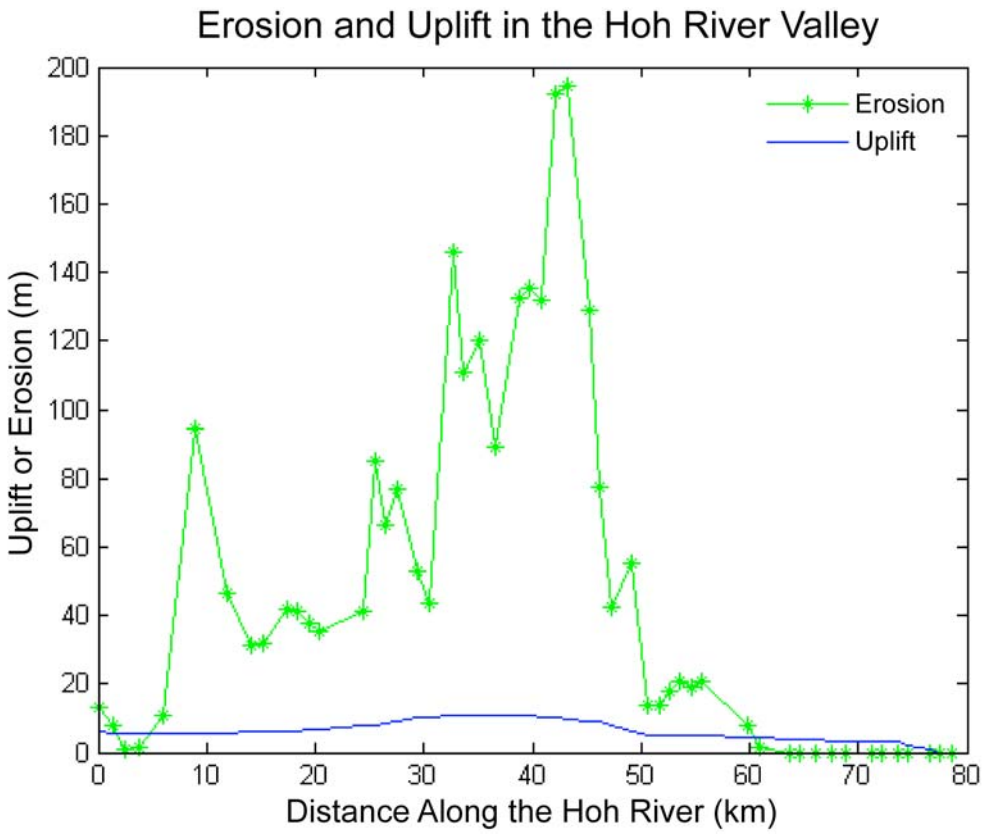

Figure 2.17. Comparison of the erosion and uplift along the longitudinal profile of the Hoh River Valley. The erosion pattern in the Hoh River Valley correlates well with the pattern of uplift, but the magnitudes of the two parameters are different, with the erosion being higher than the uplift. Regression of the data provides an r-squared value of 0.6695, which shows that they correlate fairly well.

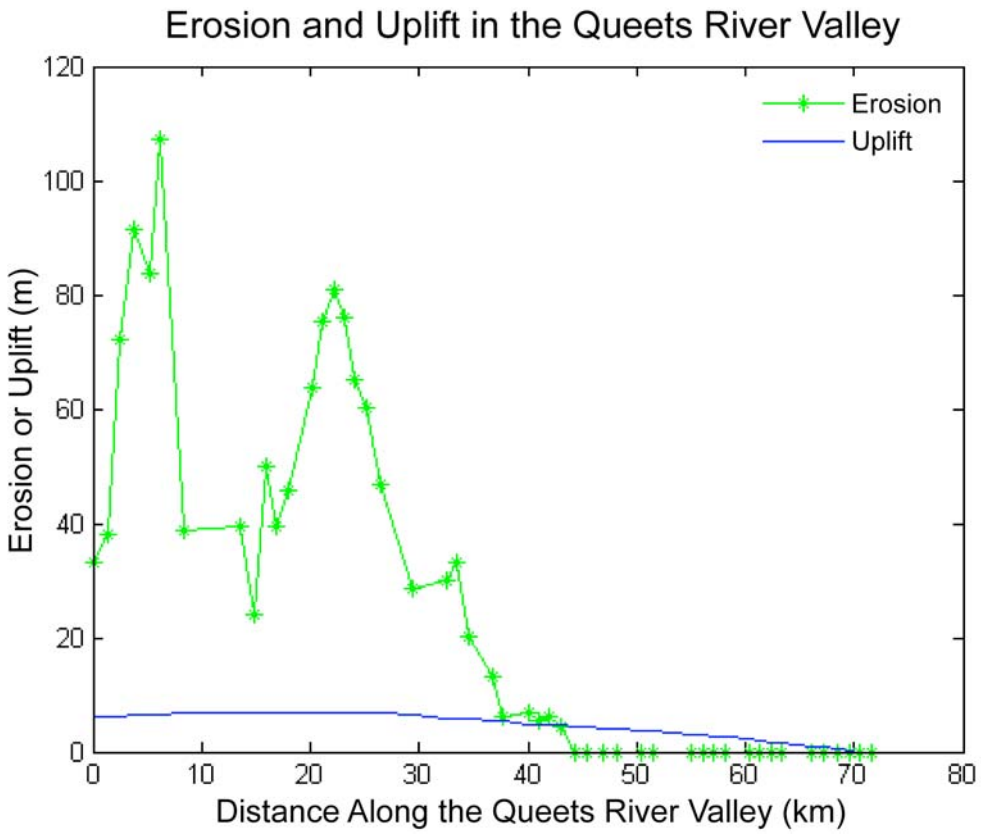

Figure 2.18. Comparison of the erosion and uplift along the longitudinal profile of the Queets River Valley. The erosion pattern in the Queets River Valley correlates with the pattern of uplift, but the magnitudes of the two parameters are different, just like in the Hoh River Valley, with the erosion being higher than the uplift. There is also more variability in the erosion rates than there are in the uplift rates. Regression of the data provides an r-squared value of 0.4536, which shows that they correlate fairly well.

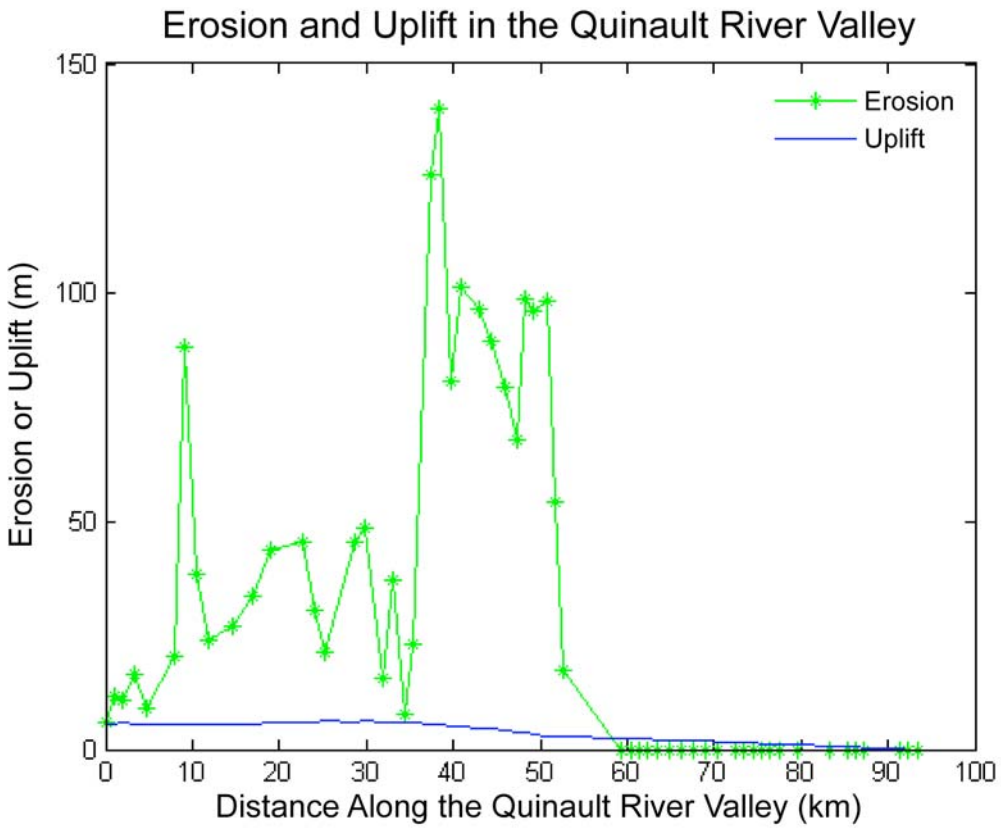

Figure 2.19. Comparison of the erosion and uplift along the longitudinal profile of the Quinault River Valley. The erosion pattern in the Quinault River Valley does not resemble the uplift pattern very well and the magnitudes of the two parameters are different, just like in the Hoh and Queets River Valleys, with the erosion being higher than the uplift. Regression of the data provides an r-squared value of 0.1669, which supports the idea that they do not correlate well.

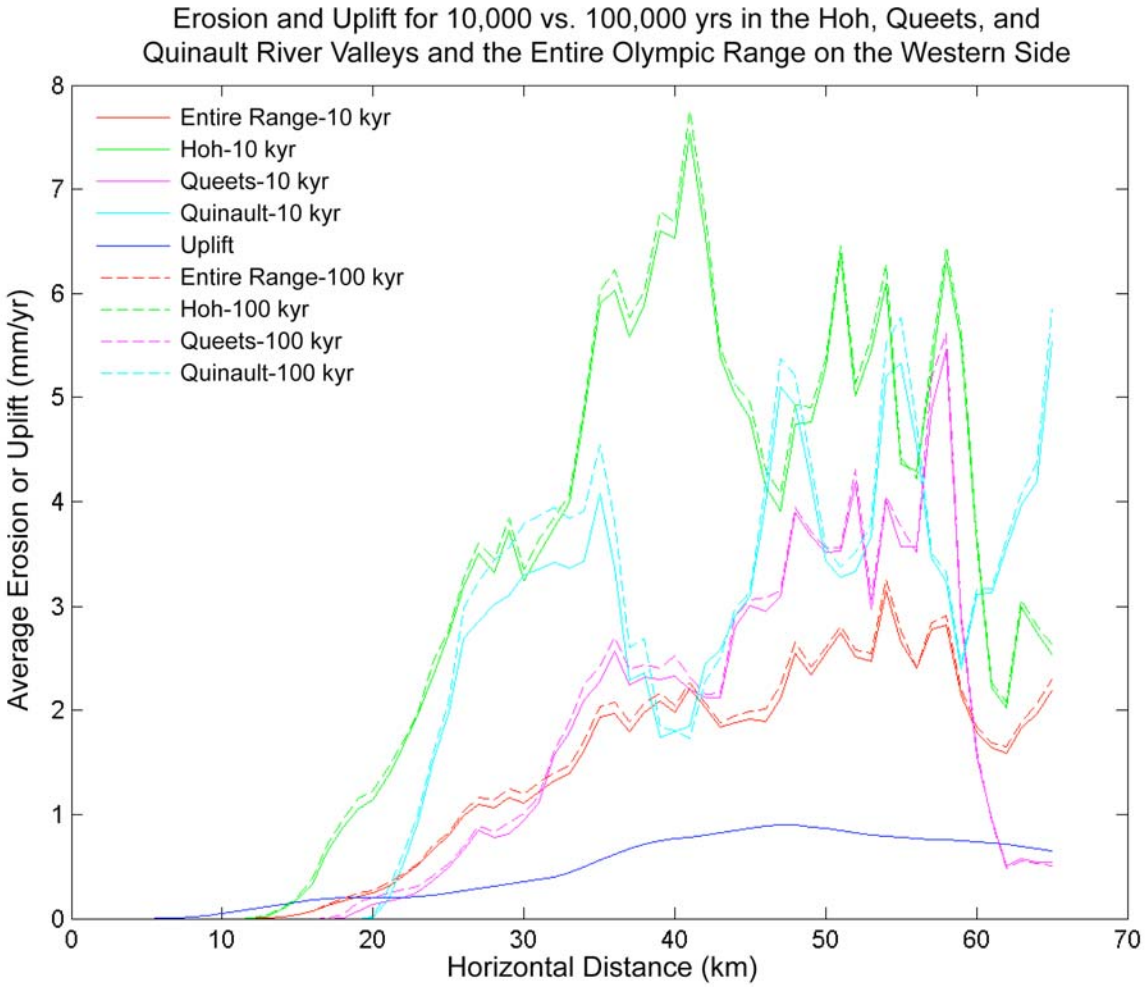

Figure 2.20. Comparison of the erosion profiles for the entire range and the Hoh, Queets, and Quinault River Valleys on the western side of the peninsula to determine if there is a difference in the amount of erosion produced in a 10,000 year run in ICE Cascade as compared to a 100,000 year run. The erosion rates are within 5% of each other with the largest difference occurring in a section of the Quinault River Valley with a difference of 13%. For the majority of the time, the two erosion patterns correlate very well and because of this, the model is run for 10,000 yrs instead of the full glacial cycle.

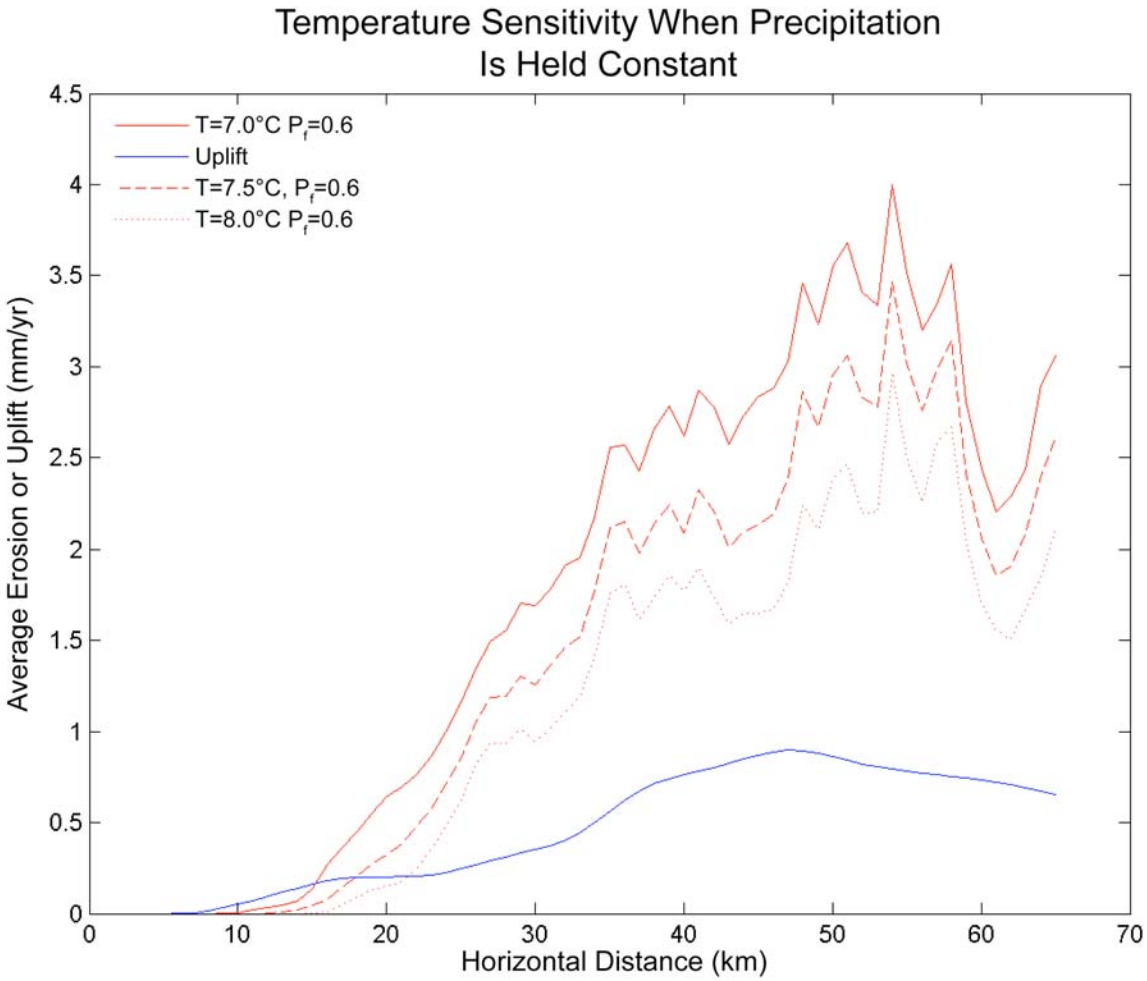

Figure 2.21. The sensitivity of ICE Cascade to different values of temperature when the precipitation is held constant at 0.6 of the modern precipitation. The temperature varies from 7.0-8.0°C and the uplift is marked by the blue line. The temperature varies by 26-34% per degree Celsius.

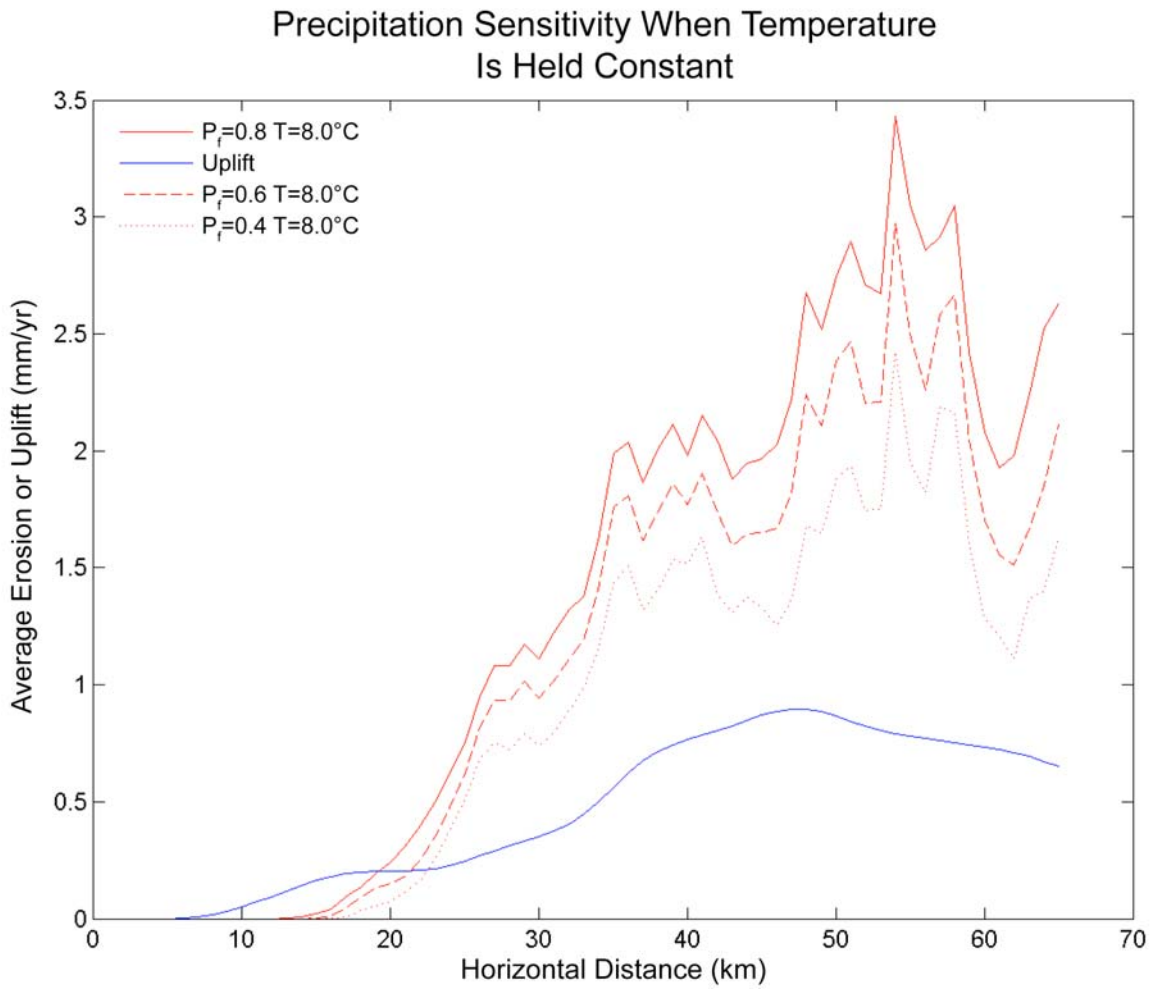

Figure 2.22. The sensitivity of ICE Cascade to different values of precipitation when temperature is held constant at 8.0°C. The precipitation varies from 0.4-0.8 of the modern precipitation and the uplift is marked by the blue line. The precipitation varies by 24-37%.

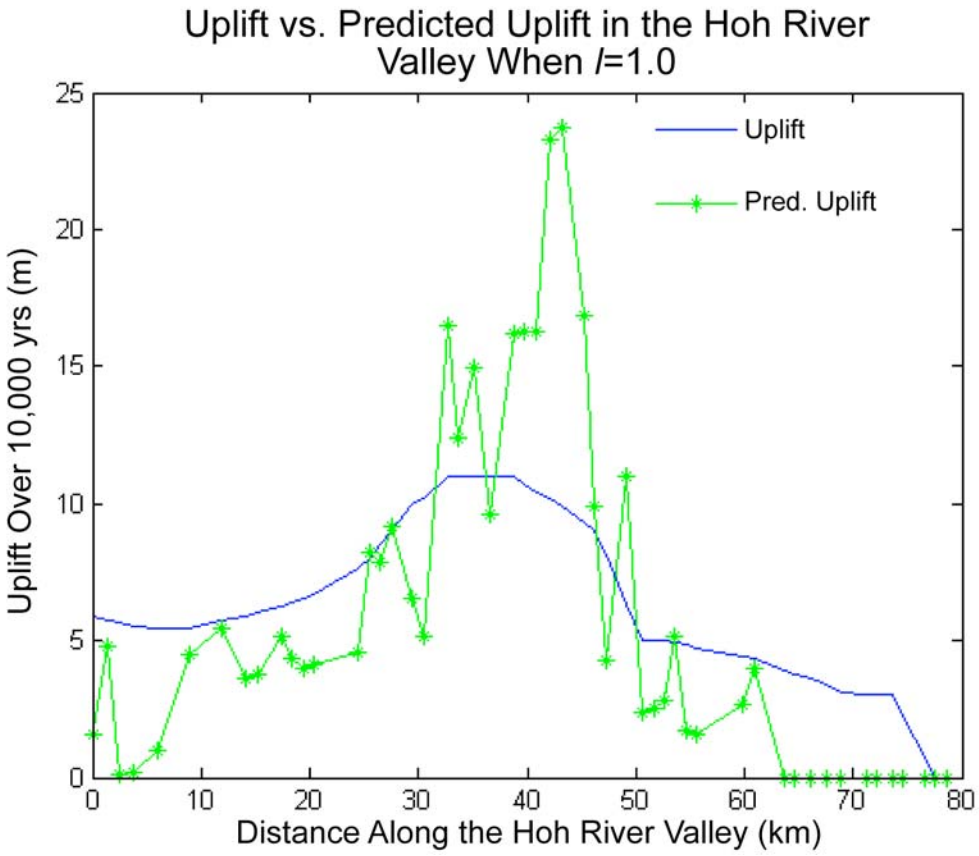

Figure 2.23. The predicted uplift pattern for the best fitting K_g when l is held at one for the Hoh River Valley. The patterns correlate well and the K_g is found to be 1.206e-5. The misfit is 4.62857 m and the average predicted uplift of 7.4478 m closely matches the average observed uplift of 7.4495 m.

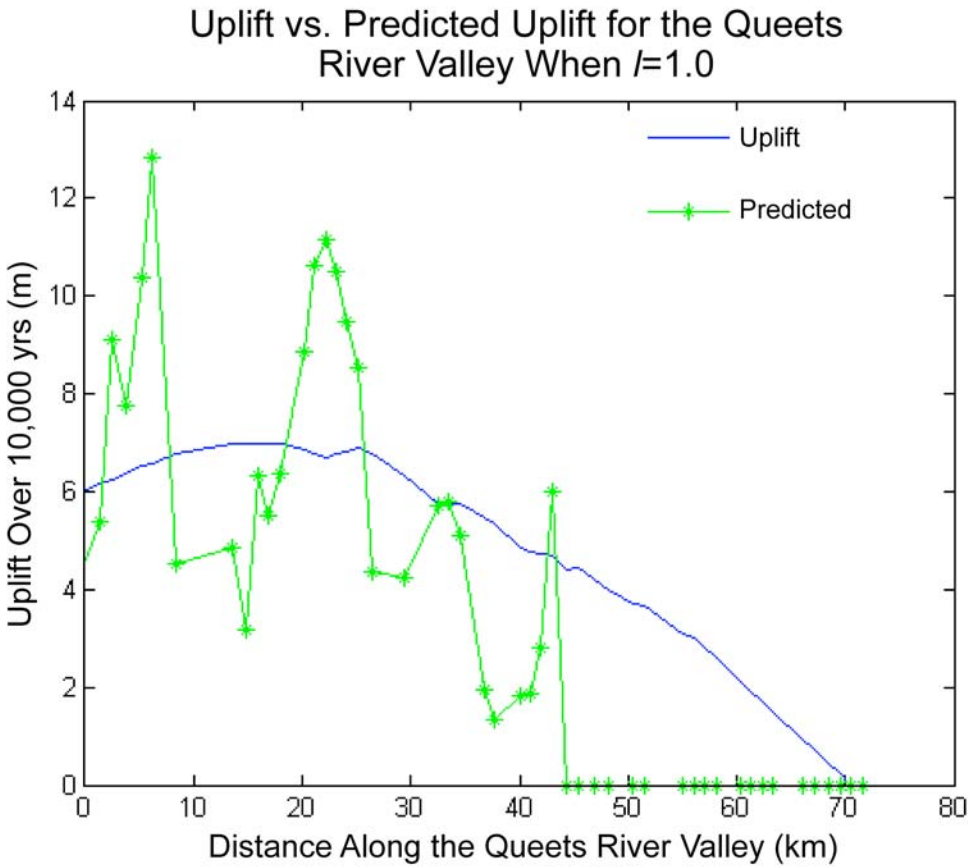

Figure 2.24. The predicted uplift pattern for the best fitting K_g when l is held at one for the Queets River Valley. The patterns correlate, but not as well as that of the Hoh River Valley. The K_g is found to be 1.219e-5 and the misfit is 2.847 m. The average predicted uplift of 6.2357 m closely matches the average observed uplift of 6.2341 m.

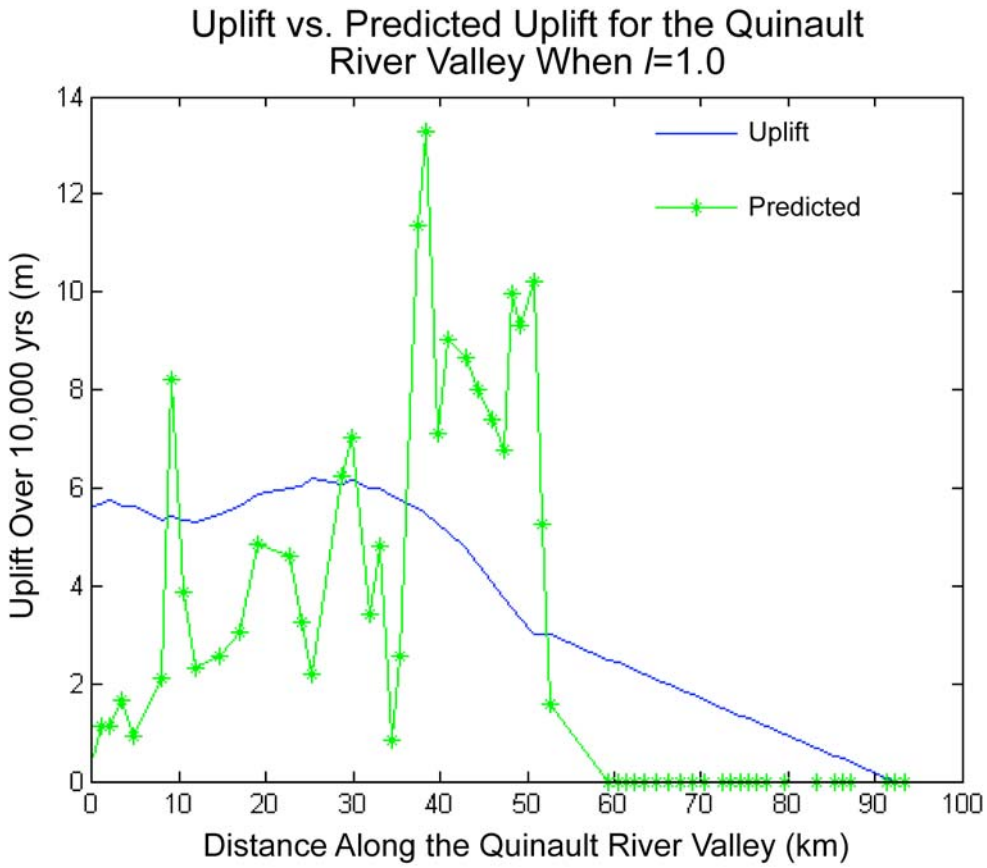

Figure 2.25. The predicted uplift pattern for the best fitting K_g when l is held at one for the Quinault River Valley. The Quinault has the least well-correlated data from all three river valleys. The K_g is found to be 5.104e-6 and the misfit is 4.0336 m. The average predicted uplift of 5.14625 m closely matches the average observed uplift of 5.14624 m.

K_g, l, and r^2 Values for the Hoh, Queets, and Quinault Rivers								
Hoh River			**Queets River**			**Quinault River**		
K_g	l	r^2	K_g	l	r^2	K_g	l	r^2
4.967×10^{-8}	2.0	0.3923	5.727×10^{-8}	2.0	0.0327	2.986×10^{-8}	2.0	0.1241
8.708×10^{-8}	1.9	0.4106	9.906×10^{-8}	1.9	0.0427	5.349×10^{-8}	1.9	0.1296
1.523×10^{-7}	1.8	0.43	1.709×10^{-7}	1.8	0.0551	9.56×10^{-8}	1.8	0.1348
2.658×10^{-7}	1.7	0.4505	2.941×10^{-7}	1.7	0.0703	1.704×10^{-7}	1.7	0.1396
4.627×10^{-7}	1.6	0.4723	5.046×10^{-7}	1.6	0.0887	3.03×10^{-7}	1.6	0.1438
8.031×10^{-7}	1.5	0.4955	8.636×10^{-7}	1.5	0.1109	5.371×10^{-7}	1.5	0.1472
1.39×10^{-6}	1.4	0.5201	1.474×10^{-6}	1.4	0.1375	9.486×10^{-7}	1.4	0.1495
2.398×10^{-6}	1.3	0.5462	2.51×10^{-6}	1.3	0.1688	1.67×10^{-6}	1.3	0.1506
4.124×10^{-6}	1.2	0.5738	4.261×10^{-6}	1.2	0.2054	2.926×10^{-6}	1.2	0.15
7.067×10^{-6}	1.1	0.6028	7.215×10^{-6}	1.1	0.2475	5.104×10^{-6}	1.1	0.1472
1.206×10^{-5}	1.0	0.633	1.219×10^{-5}	1.0	0.2952	8.859×10^{-6}	1.0	0.1417
2.051×10^{-5}	0.9	0.6641	2.053×10^{-5}	0.9	0.348	1.529×10^{-5}	0.9	0.1328
3.47×10^{-5}	0.8	0.6954	3.45×10^{-5}	0.8	0.4053	2.623×10^{-5}	0.8	0.1196
5.843×10^{-5}	0.7	0.7258	5.783×10^{-5}	0.7	0.4654	4.47×10^{-5}	0.7	0.1011
9.785×10^{-5}	0.6	0.7534	9.669×10^{-5}	0.6	0.5263	7.563×10^{-5}	0.6	0.0761
1.629×10^{-4}	0.5	0.775	1.613×10^{-4}	0.5	0.5854	1.27×10^{-4}	0.5	0.0447
2.691×10^{-4}	0.4	0.7849	2.683×10^{-4}	0.4	0.6396	2.114×10^{-4}	0.4	0.0119
4.411×10^{-4}	0.3	0.772	4.454×10^{-4}	0.3	0.6862	3.49×10^{-4}	0.3	0.0036
7.16×10^{-4}	0.2	0.714	7.375×10^{-4}	0.2	0.7226	5.707×10^{-4}	0.2	0.106
1.149×10^{-3}	0.1	0.5729	1.219×10^{-3}	0.1	0.7474	9.245×10^{-4}	0.1	0.3878
7.45×10^{-4}	0		6.234×10^{-4}	0		5.146×10^{-4}	0	

Table 2.2. The K_g and l values with the corresponding r-squared values when K_g and l are allowed to vary in the glacial erosion rule (Equation 2.1) to determine the best fitting correlation between the uplift and erosion patterns in the Hoh, Queets, and Quinault River Valleys.

Values for the Best Fitting Cases in the Valleys			
River	K_g	l	**Misfit (%)**
Hoh River	1.206e-5	1.0	62.13%
	2.691e-4	0.4	28.28%
	7.35e-4	0	31.56%
Queets River	1.219e-5	1.0	45.67%
	1.219e-3	0.1	32.33%
	6.2375e-4	0	12.61%
Quinault River	8.859e-6	1.0	78.38%
	9.245e-4	0.1	16.34%
	5.15e-4	0	19.71%

Table 2.3. Values for K_g, l, and the misfit for the best fitting cases for each of the river valleys that are discussed in the text.

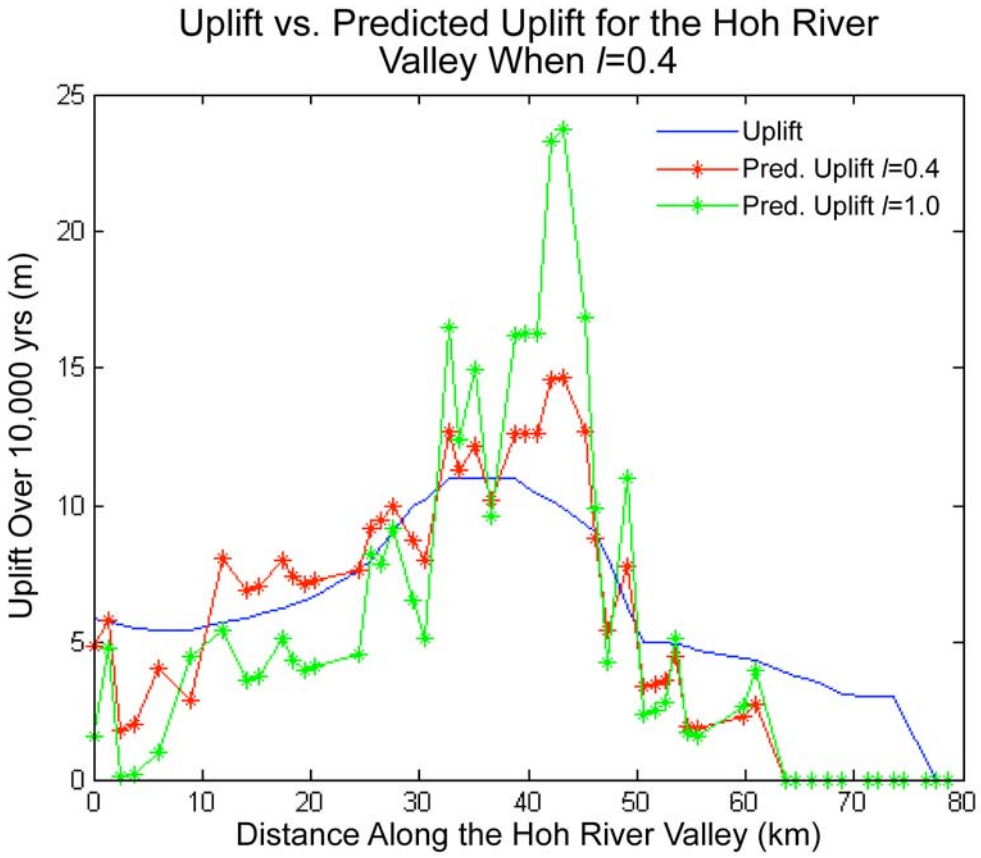

Figure 2.26. Comparison of the uplift (blue line), predicted uplift when *l* is one (green line), and the predicted uplift when *l* is 0.4 and K_g is 2.691e-4 for the Hoh River Valley. The predicted uplift for the varying *l* correlates very well with the uplift profile and also matches the magnitude.

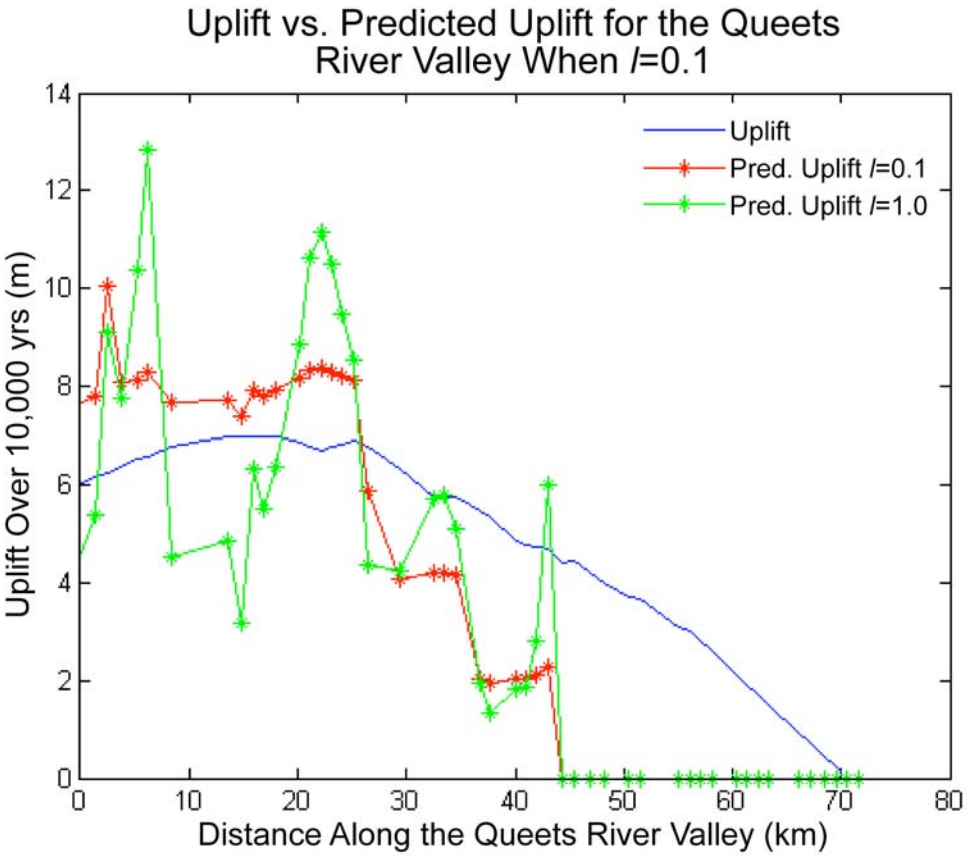

Figure 2.27. Comparison of the uplift (blue line), predicted uplift when l is one (green line), and the predicted uplift when l is 0.1 and K_g is 1.219e-3 for the Queets River Valley. The predicted uplift for the varying l correlates with the uplift profile, though there are some slight differences in the pattern and the increases/decreases in the profile. It also matches the magnitude.

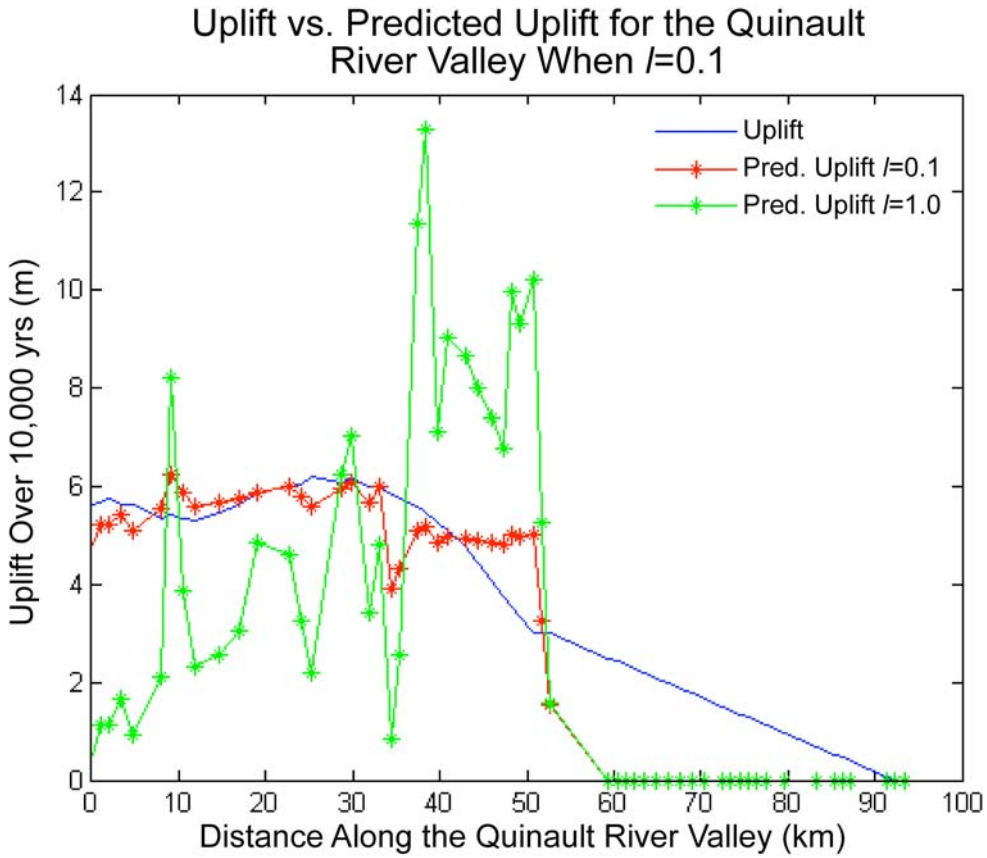

Figure 2.28. Comparison of the uplift (blue line), predicted uplift when *l* is one (green line), and the predicted uplift when *l* is 0.1 for the Quinault River Valley. The predicted uplift for the varying *l* best correlates with the uplift profile for this case, though the data for the Quinault River does not correlate well. It also matches the magnitude. The *l* equal to 0.1 has a K_g value of 9.245e-4.

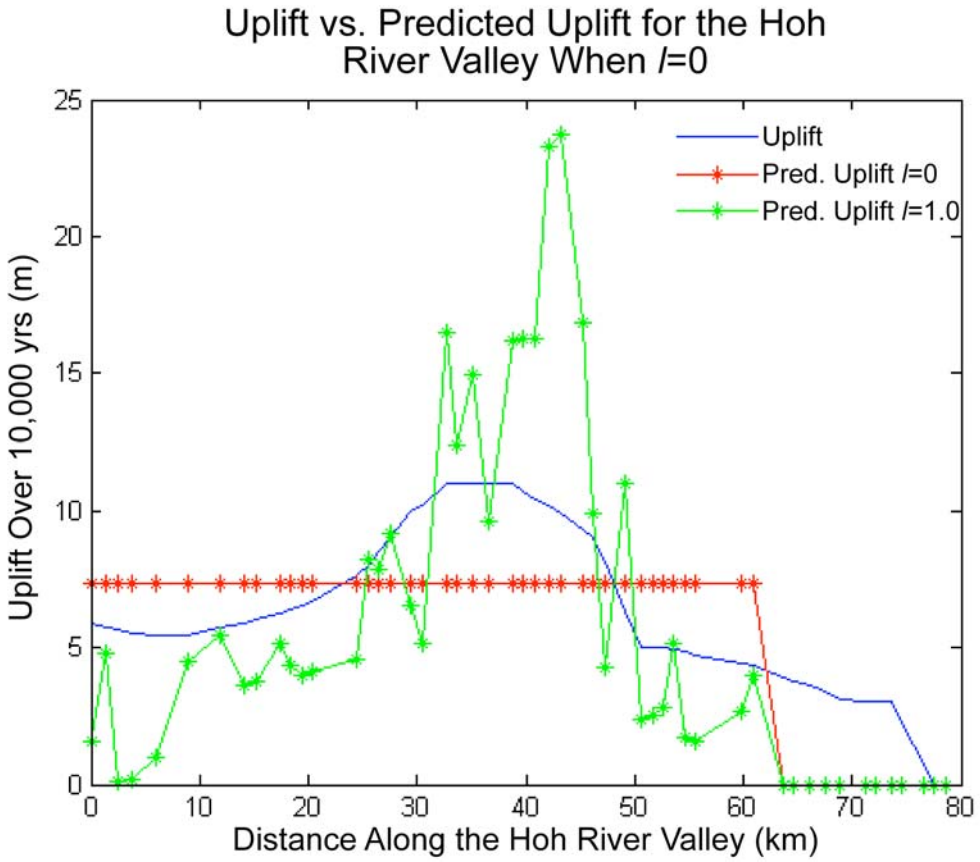

Figure 2.29. Comparison of the uplift (blue line), predicted uplift when *l* is one (green line), and the predicted uplift when *l* is zero for the Hoh River Valley. The *l* equal to zero case has a K_g value of 7.35e-4 and a misfit of 2.3508 m. The average predicted uplift is 7.35 m while the average observed uplift is 7.4495 m.

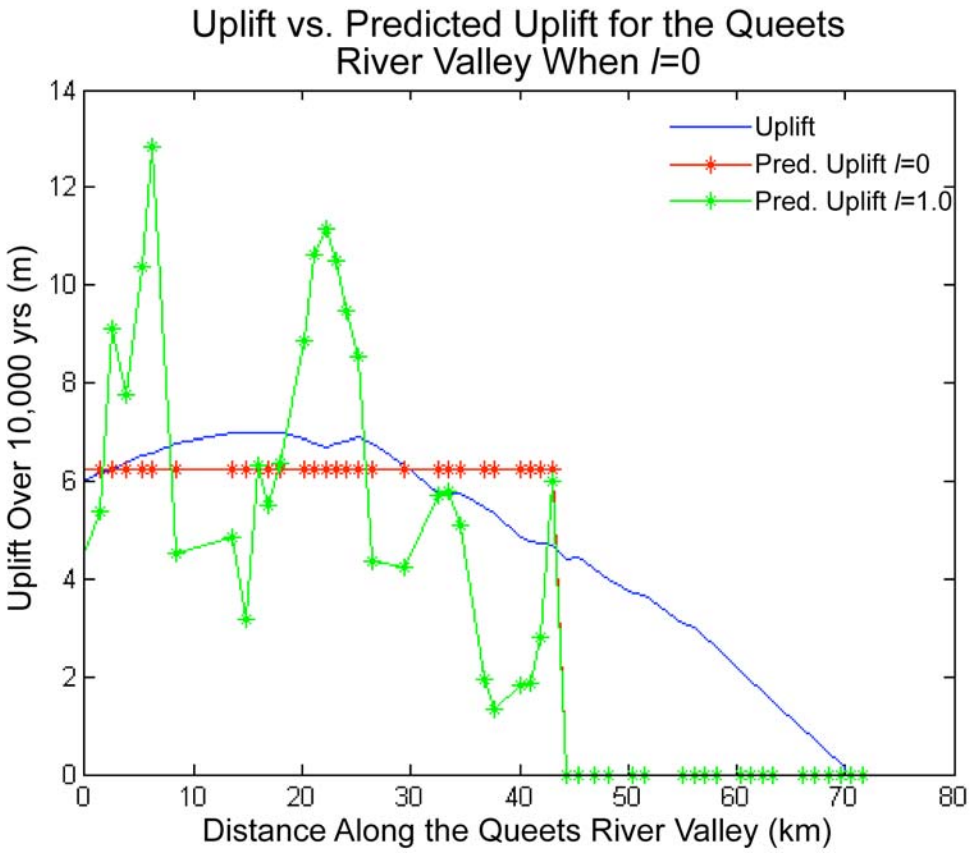

Figure 2.30. Comparison of the uplift (blue line), predicted uplift when *l* is one (green line), and the predicted uplift when *l* is zero for the Queets River Valley. The *l* equal to zero case has a K_g value of 6.2375e-4 and a misfit of 0.7859 m. The average predicted uplift is 6.2375 m while the average observed uplift is 6.2341 m.

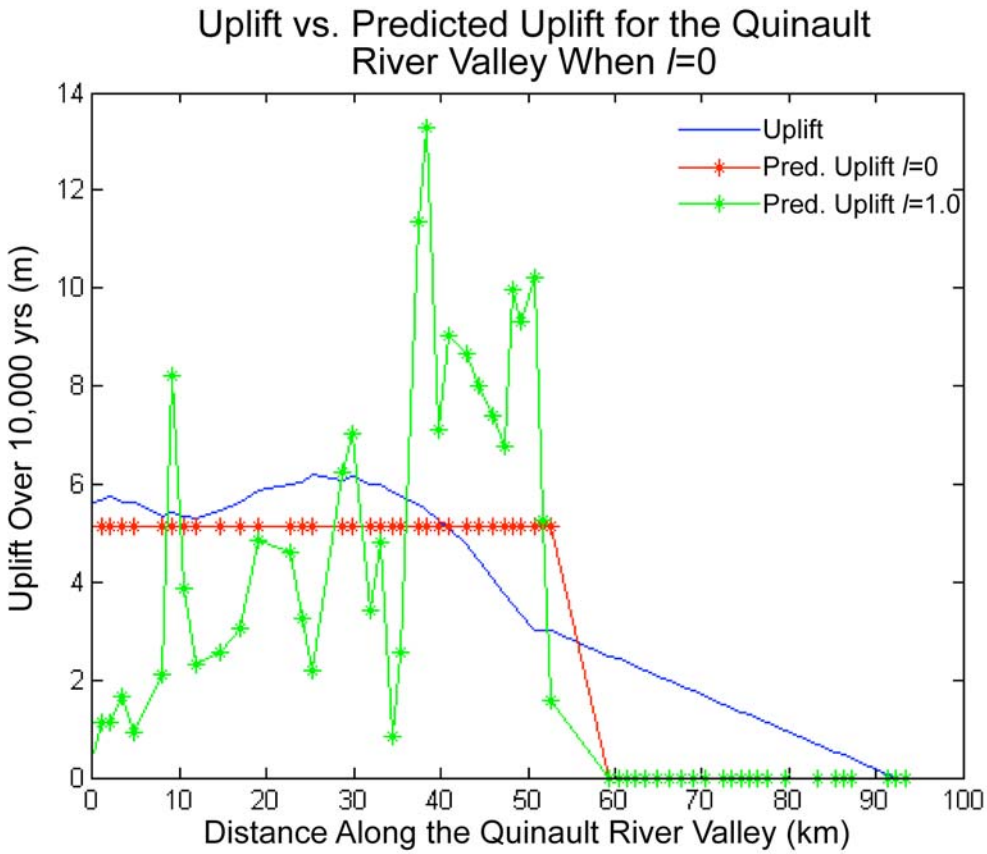

Figure 2.31. Comparison of the uplift (blue line), predicted uplift when *l* is one (green line), and the predicted uplift when *l* is zero for the Hoh River Valley. The *l* equal to zero case has a K_g value of 5.15e-4 and a misfit of 1.01439 m. The average predicted uplift is 5.15000007 m while the average observed uplift is 5.14624 m.

CHAPTER 3: LICHENOMETRY: RECENT GLACIAL HISTORY OF ROYAL BASIN

3.1 INTRODUCTION

The climatic asymmetry of the Olympic Mountains is presumed to influence the glacial history of the region and differences between the western and eastern sides of the range are expected. The western side of the range has detailed radiocarbon, lichenometric, and dendrochronologic dates constraining the fluctuations of the ice-margin since the late Pleistocene for the Hoh, Queets, Quinault, and Clearwater River Valleys (Heusser, 1974; Thackray, 2001). In contrast, the eastern side of the range has very little data to document former ice positions or glacial maxima. This study constrains the recent glacial history of Royal Basin in the eastern Olympic Mountains through lichenometric dating of moraines.

Lichenometry is a dating technique that uses the size of lichens to date surfaces. If the relationship between the size and age of a lichen can be determined, then the minimum age of the surface can be calculated. Several lichenometric studies have been conducted in the Pacific Northwest, but no growth curve, which connects the size of the lichen diameter to the age of the surface, has been developed for the Olympic Mountains. A regional growth curve is created using data from regions with similar environmental characteristics to the Olympic Mountains. This growth curve is applied to lichens on four moraines located at the base of Royal Glacier on Mt. Deception to determine the recent glacial advances or still-stands. The equilibrium line altitudes are reconstructed and compared with those of Blue Glacier on the western side of the Olympic Mountains.

3.2 LICHENOMETRY

3.2.1 Introduction

Lichenometry has been used to date relatively recent glacial and alpine features up to 1,000 years old, but it is most often used for dating features that formed during the past 500 years (Porter, 1981; Armstrong, 2004). Lichenometric dating is used when the time spans involved are too short for dating techniques such as radiocarbon dating and when dendrochronology and human artifacts are unavailable (Porter, 1981; Bull, 1996;

Bull and Brandon, 1998; O'Neal and Schoenenberger, 2003; Muller, 2006). Lichens are typically used to date surfaces that formed due to natural phenomena in order to determine the time elapsed since a certain event took place. Some examples are rockfalls, glacial moraines, mud flows, river flooding, periglacial surfaces, lake and sea level changes, talus stabilization, and other geomorphic features (Porter, 1981; Bull and Brandon, 1998; O'Neal and Schoenenberger, 2003; Armstrong, 2004; Muller, 2006).

3.2.2 Lichen Biology

Lichens are not plants or individual organisms, but are a symbiotic community between a fungus and algae. Their complex biological system makes them difficult to classify. The fungus produces a thallus or body part that houses the algae (DePriest, 1994). There are three morphological types of thalli and these are crustose, foliose, and fruticose. A foliose lichen is leaf-like in appearance and structure and attaches to the substrate with small root-like features. A crustose lichen is crust-like, flaky, and tightly attaches to or embeds in a surface. A fruticose lichen is shrub-like with a stalk or thallus that attaches to the substrate at a single point and forms a branched structure (DePriest, 1994; Armstrong, 2004). Crustose lichens are typically used in lichenometric studies as they grow radially over the substratum, attach tightly to the surface, have slow growth rates, and live for very long periods of time (Armstrong, 2004).

Most lichenometric studies use lichens from the genus *Rhizocarpon*, which are crustose lichens of a yellow-green color (Armstrong, 2004). *Rhizocarpon* are abundant in arctic and alpine environments, have slow growth rates, and have a long duration of life (Armstrong, 2004; Larocque and Smith, 2004). *Rhizocarpon geographicum* is one of the first species to appear on a newly established surface. It has a bright green color bordered by black spores and it resembles a map when several lichens grow next to each other. A *Rhizocarpon* lichen that was used in this study can be seen in Figure 3.1.

3.2.3 Lichen Growth

Lichens experience four phases of growth: colonization, great growth, uniform growth, and slow growth. Colonization is the amount of time that occurs between the exposure of the surface and the appearance of the first lichen to grow on the surface. It

involves the delivery of the spores to the surface, the establishment of a symbiotic relationship between the fungi and an algae, and the growth of the lichen to a size that is visible (Porter, 1981; Bull and Brandon, 1998). Colonization is a function of the size of the surface area that is available for colonization with a larger surface having a higher probability of receiving an initial spore in a shorter amount of time. Following the colonization time is a period of rapid growth that varies in length for different regions. This "great growth period" has growth proceeding at a logarithmic rate and it ends when the diameter of the lichen reaches between 10 and 20 mm (Porter, 1981; Bull and Brandon, 1998; O'Neal and Schoenenberger, 2003). After this phase the lichen experiences a uniform growth phase where the growth rate is linear. A subsequent slow growth phase follows these three phases of growth during which the growth rate decreases until the lichen dies (Porter, 1981; O'Neal and Schoenenberger, 2003). All of these phases are influenced in their duration and rate by environmental properties which include substrate lithology and age, the degree of weathering, precipitation availability, the duration of snow cover, altitude, temperature, and competition with other plants (Innes, 1984, 1985a; Porter, 1981; Bull and Brandon, 1998; O'Neal and Schoenenberger, 2003; Armstrong, 2004; Laroque and Smith, 2004).

To date lichens, a relationship between the size and age of a lichen needs to be determined. The growth rate of a lichen is hard to determine directly because of the long time interval needed to accomplish this task. A more difficult, but direct method involves measuring individual lichen diameters over a course of several years to determine the growth rate of the species (Porter, 1981; Armstrong, 2004; Larocque and Smith, 2004; Allen and Smith, 2007). This data can be used to create a growth curve and provide the age of the surface. Otherwise, lichens can be measured on surfaces of a known age such as gravestones, buildings, rock walls, mine soil heaps, and other similar features or well-dated geomorphic events like avalanches and rock slides (Porter, 1981; Bull and Brandon, 1998; Armstrong, 2004; Muller, 2006). The sensitivity of lichen growth to environmental factors implies that a local calibration is needed to use lichenometry in a particular region (Porter, 1981; Bull and Brandon, 1998; O'Neal and Schoenenberger, 2003).

3.2.4 Lichen Measurement

Lichens do not always grow equally in all directions so typically the largest diameter of an individual lichen is measured (Porter, 1981; Armstrong, 2004; Larocque and Smith, 2004). A digital caliper is used to measure the diameter. However, lichens can grow into each other and fuse together making it difficult to determine if a large lichen is a single individual. Studies use two methods for collecting and analyzing lichen data. One method is to find the single largest lichen on the surface being dated. This lichen is considered to be the oldest as its advantageous location on the rock surface allowed for colonization prior to other lichens (Porter, 1981; Bull and Brandon, 1993; Larocque and Smith, 2004; Muller, 2006). This lichen diameter is then used in conjunction with a growth curve to yield an age for the surface. This method is subject to error, however, because the largest lichen may be composed of several smaller lichens that merged together.

An alternate method uses the many individual lichens that form the population on the surface being considered. A large surface is divided into many smaller sections, for example, individual boulders on a moraine or talus slope. The largest lichen in each section is measured. A frequency histogram of the largest lichens is then made and it is expected to have a normal distribution (Brandon and Bull, 1998; Armstrong, 2004; Larocque and Smith, 2004). If the distribution is not normal, the large outliers are eliminated until the distribution is normal. This process eliminates lichens that might have merged together and formed unexpectedly large lichens. This data can then be used to create growth curves or determine the age of an unknown surface (Brandon and Bull, 1998; Armstrong, 2004; Larocque and Smith, 2004). This is the method used to collect lichen data in Royal Basin in the Olympic Mountains.

3.3 PACIFIC NORTHWEST REGIONAL GROWTH CURVE

Lichenometry would be useful in determining the most recent glacial extent in the eastern Olympic Mountains. No growth curve exists for this range, however, lichenometric studies from the Pacific Northwest provide data on lichen growth under environmental conditions similar to those in the Olympic Mountains. The growth curves for several areas in the region are compared to constrain the variability in growth rates

across the region. A combined growth curve is developed using all available data and is applied to the eastern Olympic Mountains.

Several growth curves have been developed in the Pacific Northwest. A growth curve for Mt. Rainier, Mt. Hood, and Mt. Baker, which are located in the Cascade Range of Washington and northern Oregon, was developed by Porter (1981) and refined by O'Neal and Schoenenberger (2003). Larocque and Smith (2004) calibrated lichen growth in the Mount Waddington area of the Coast Mountains of British Columbia, Canada. In addition, a growth curve for Strathcona Provincial Park on Vancouver Island, British Columbia, Canada, has been developed (Lewis and Smith, 2004). The data collection methods varied between the different studies. The single largest lichen was found and measured for each surface in two of the studies (Porter, 1981; O'Neal and Schoenenberger, 2003; Lewis and Smith, 2004). In contrast, Larocque and Smith (2004) use the method chosen by this study in which thirty lichens were measured and a test for the normality of the distribution was conducted. The lichen thallus data used to produce these growth curves is given in Table 3.1 and the data are plotted with their fitted growth curves in Figure 3.2.

All of the study areas used the lichen genus *Rhizocarpon* (all presumed *geographicum,* except for two lichens from the Mount Waddington Area study which were *macrosporum*) in their studies (Porter, 1981; O'Neal and Schoenenberger, 2003; Larocque and Smith, 2004; Lewis and Smith, 2004). Each study area has slightly different environmental conditions and generally similar growth rates. In addition, the environmental properties of the study areas span the precipitation, temperature, altitude, and lithology of Royal Basin in the Olympic Mountains making it reasonable to use a regional growth curve. The environmental properties for each location, including Royal Basin, are provided in Table 3.2.

In order to estimate the growth rates for the Olympic Mountains, a regional growth curve based on all of the available calibration points in the Pacific Northwest was developed. Bull and Brandon (1998) have developed an equation that incorporates the first three basic phases of lichen growth and have used this to describe the growth curve. The equation is as follows:

$$D = D_0\left(1 - e^{-K(\tau-\tau_0)}\right) + C(\tau - \tau_0) \quad (3.1)$$

where D is the size of the largest lichen in millimeters, τ is the substrate exposure age in years, τ_0 is the mean colonization time, D_0 is the excess lichen size produced by the great growth phase, K is the nonlinear component of the growth rate during the great growth phase, and C is the constant growth rate during the uniform growth phase (Bull and Brandon, 1998). The data sets used to create a growth curve that can be calibrated by this equation must include multiple thalli from both the great growth and uniform growth phases (Bull and Brandon, 1998). However, if the data sets consist of mainly thalli measurements from the uniform growth phase, a linear regression method of the following form can be substituted instead:

$$D = A + B\tau \quad (3.2)$$

where D is the dependent variable, τ is the independent variable, and A and B are fit parameters that have the following form based on Equation 3.1:

$$A = D_0 - C\tau_0 \quad (3.3)$$

$$B = C \quad (3.4)$$

(Bull and Brandon, 1998).

Only three points from the published Pacific Northwest data represent the colonization time, great growth, and slow growth phases. Since this number is too small to be used to create an accurate fit with Equation 3.1, the three points were eliminated and the combined curve was fit with a linear regression. The resulting combined curve can be seen in Figure 3.3. A 95% confidence interval was determined by using the variance, which has the following form:

$$\hat{\sigma}^2 = \frac{RSS}{n-2} = \ldots = \frac{1}{n-2}\left[\sum\left(y_i - \bar{y}\right)^2 - \frac{\left(\sum\left(x_i - \bar{x}\right)\left(y_i - \bar{y}\right)\right)^2}{\sum\left(x_i - \bar{x}\right)^2}\right] \quad (3.5)$$

where n is the sample size and:

$$RSS = SYY - \frac{SXY^2}{SXX} \tag{3.6}$$

$$SXX = \sum \left(x_i - \bar{x} \right)^2 \tag{3.7}$$

$$SYY = \sum \left(y_i - \bar{y} \right)^2 \tag{3.8}$$

$$SXY = \sum \left(x_i - \bar{x} \right)\left(y_i - \bar{y} \right) \tag{3.9}$$

$$\bar{x} = \frac{\sum x_i}{n} \tag{3.10}$$

$$\bar{y} = \frac{\sum y_i}{n} \tag{3.11}$$

A prediction interval is needed to determine the confidence interval and the predicted value has the following form:

$$\tilde{y}_* = \hat{\beta}_0 + \hat{\beta}_1 x_* \tag{3.12}$$

where $\hat{\beta}_0$ is the y intercept value, $\hat{\beta}_1$ is the slope, the x_* is the known value, and the $\tilde{y}_*$ represents the predicted value. The prediction interval is determined by the uncertainty:

$$P.I. = \tilde{y}_* \pm t\left(\frac{\alpha}{2}, n-2 \right) \times se\left(\tilde{y}_* \right) \tag{3.13}$$

where:

$$se\left(\tilde{y}_* \right) = \sqrt{\hat{\sigma}^2 \left(\frac{1}{n} + \frac{\left(x_* - \bar{x} \right)^2}{SXX} + 1 \right)} \tag{3.14}$$

For the regional growth curve, the equation of the linear fit is:

$$y = 0.3054x + 10.003 \quad (3.15)$$

with an r-squared value of 0.9139. The t-value for a 95% confidence interval for a sample size n-2=63 is 2.296. The resultant 95% confidence intervals can be observed in Figure 3.3. The combined fits and r-squared values of both the regional and individual study curves are located in Figure 3.4. From this plot, it can be observed that the regional growth curve is not controlled by a single site because there are relatively old lichens at each of the individual sites. The error provided by the 95% confidence intervals is large, approximately 45 years, however, the individual curves have errors from 10 to 80 years so the error on the growth curve is reasonable (Larocque and Smith, 2004). Overall, the fit of the combined curve is good, especially with an r-squared value of 0.9139 and thus it should be able to accurately describe the Olympic Mountains lichen data.

3.4 OLYMPIC NATIONAL PARK-MOUNT DECEPTION DATA

Royal Basin, on the eastern edge of Olympic National Park, was selected for a study of the recent glacial extent (Figure 3.5). Four moraines are observed at the base of Royal Glacier on Mount Deception and they lie at elevations between 1767.8 m and 1755.6 m. The moraines are composed of large boulders that are primarily basalt and metamorphosed marine sedimentary rocks. The moraines can be seen in Figures 3.6 through 3.11. The largest lichens, believed to be of the species *Rhizocarpon geographicum*, growing on the surfaces of the four moraines were measured with a digital caliper that has an error of ± 0.1 mm. The lichens were evaluated by separating each moraine into 10 sections and measuring the largest lichens found in each section along the surface. The data was compiled to determine the largest lichen thalli present on each moraine. 60 lichen diameters were measured for each moraine, except for the moraine closest to Royal Glacier, which had no lichens growing on it. The data for the lichen sizes found on each moraine is located in Table 3.3.

A Shapiro-Wilk normality test was conducted to determine if any of the lichen populations were not normally distributed by following the methodology of Larocque and

Smith (2004). Frequency histograms for each lichen population were developed to evaluate the normality of the distribution and the normality test was then conducted on the population to eliminate erroneously large lichens.

The Shapiro-Wilk normality test computes the W statistic (Shapiro and Wilk, 1965). The W statistic is scale and origin invariant and is effective for both small (n<20) and large samples (Shapiro and Wilk, 1965). The Shapiro-Wilk test tests the null hypothesis that a sample of size *n* with $x_1, x_2, \ldots, x_n$ comes from a normal distribution. The W statistic has the form:

$$W_{test} = \frac{\left(\sum_{i=1}^{k} a_{n-i+1}\left(y_{n-i+1} - y_i\right)\right)^2}{\sum_{i=1}^{n}\left(y_i - \bar{y}\right)^2} = \frac{b^2}{S^2} \tag{3.16}$$

The test is conducted by first ordering the observations to obtain an ordered sample $y_1 \leq y_2 \leq \ldots \leq y_n$. S^2 is calculated by the following equation:

$$S^2 = \sum_{i=1}^{n}\left(y_i - \bar{y}\right)^2 \tag{3.17}$$

where $\bar{y}$ is the sample mean:

$$\bar{y} = \frac{\left(y_1 + \ldots + y_n\right)}{n} \tag{3.18}$$

If *n* is even, *b* is then computed using the following form:

$$b = \sum_{i=1}^{k} a_{n-i+1}\left(y_{n-i+1} - y_i\right) \tag{3.19}$$

where $n=2k$ and the values of a_{n-i+1} are provided in a statistical table for the W test statistic (Shapiro and Wilk, 1965). If n is odd, b is also computed from Equation 3.19, with the exception that $n=2k+1$ instead. The W test statistic can then be computed by dividing b^2 by S^2. An alpha level (denoted α), or significance level, must be chosen. If the p-value is greater than the chosen alpha level or the W test statistic is greater than the W_α (as determined from a statistical table for the W test statistic), the distribution is normal and the null hypothesis that the data come from a normal distribution is not rejected. If the p-value is less than the chosen alpha level or the W test statistic is less than the W_α, the null hypothesis is rejected and the distribution is not normal (Shapiro and Wilk, 1965).

For the study of the moraines in Royal Basin, an alpha level of 0.05 was selected. The results of the Shapiro-Wilk normality tests are contained in Table 3.4. If the distribution was not normal, the largest lichen diameter was eliminated. The frequency histograms developed for each of the moraines can be seen in Figures 3.12, 3.13, and 3.14. On the outermost moraine, one large lichen measurement was discarded to obtain a normally distributed lichen population. On the second outermost moraine, the four largest lichen diameters were discarded to produce a normally-distributed population. The third outermost moraine had a normal distribution when the normality test was applied.

The regional growth curve for the Pacific Northwest discussed in Section III was applied to estimate the ages of the moraines in Royal Basin. The ages of the four moraines are estimated to be 170 years (1839), 114 years (1895), 46 years (1963), and less than 46 years (or younger than 1963) for the innermost moraine with no measurable lichens. Lichens have a colonization time between 5 to 20 years and in the Pacific Northwest it has been observed that lichens typically colonize a surface in 10 to 20 years, so the youngest moraine must be a maximum of 20 years old. The error on the ages is found from the 95% confidence intervals on the regional growth curve with a maximum error of 43 years. This is reasonable based on the error of the individual growth curves and the good fit of the regional growth curve. A summary of the ages for the moraines is located in Table 3.5.

3.5 DISCUSSION

3.5.1 The Chronology of Royal Basin Compared to the Regional Glacial History

In general, recent glacial variability in the Pacific Northwest has occurred simultaneously across the region. A study of the late Holocene glacial fluctuations on Mt. Rainier found that glaciers were at or near their late Neoglacial maximum extents in the late 18th or early 19th centuries (Burbank, 1981, 1982). The glaciers on Mt. Hood and Mt. Baker both have a general pattern of retreat from 1902 through the mid-1940's, advances from the mid-1940's through the mid-1970's, and retreat from the mid-1970's to the mid-1990's (Harper, 1993; Lillquist and Walker, 2006). In the western Olympic Mountains, the most complete glacial chronology is derived from Blue Glacier.

Blue Glacier is one of several glaciers that ring Mt. Olympus, the highest peak in the Olympic Mountains (Figure 3.15). It is 4.2 km long, 4.3 km^2 in area, and it ranges in altitude from 1275 to 2350 m. Blue Glacier experiences a temperate, maritime climate and lies in the area of heaviest annual precipitation on the Olympic Peninsula. Large annual precipitation rates allow Blue Glacier to extend to relatively low and warm altitudes, ensuring that annual ablation rates are also large (Spicer, 1989). The high rates of mass turnover at Blue Glacier make it sensitive to minor variability in climate (Spicer, 1989).

Blue Glacier has been the subject of a long history of research that developed as part of the International Geophysical Year, 1957-1958, when annual studies began on the glacier. Due to these investigations, a detailed history of the terminus position has been compiled (Figure 3.16). Terminal moraines indicate that around the year 1815, the termini of both Blue and the neighboring White Glacier were joined in Glacier Creek after the ice descended a steep cliff (Heusser, 1957; Spicer, 1989). Blue Glacier recessed from this maximum position with occasional standstills or minor readvances in the late 19th and early 20th centuries (Heusser, 1957; Spicer, 1989). Between 1815 and 1900 the glacier receded approximately 2800 ft and the ice stabilized around the year 1900 (Heusser, 1957; Spicer, 1989). About the year 1920, the glacier again receded, retreating more than 1400 m by the 1950's (Spicer, 1989; Conway et al., 1999). A minor advance

occurred in the 1980's, but recent data has indicated that the glacier is once again retreating (Conway et al., 1999; Rasmussen and Conway, 2001).

The ages of the moraines in Royal Glacier can be compared with the ages of the terminus positions of Blue Glacier. The Royal Basin moraines date from 1839, 1895, 1963, and younger than 1963. The moraine from 1839 occurs in the period of unknown glacier length from Blue Glacier. The moraine from 1895 occurs when Blue Glacier has reached a standstill that lasts until around 1920. The 1963 moraine occurs when Blue Glacier is in retreat and this retreat is followed by a minor readvance in the 1980's. As the youngest moraine cannot be dated, it is difficult to compare with the Blue Glacier record. The lack of correlation between the Blue Glacier record and the moraines in Royal Basin could reflect the uncertainty in the ages of the Royal Basin moraines. Alternatively, the climates of the western and eastern Olympics could vary independently in such a way that glacier mass balances are not impacted in the same way on both sides of the range. Study of additional glaciers on both sides of the Olympics could distinguish between these two possibilities. The changes in the equilibrium line altitudes inferred from the glacier positions will be used to further explore the possibility of different climatic trends across the Olympic Peninsula.

The glacial recession that occurred on Blue Glacier from the 1920's to the 1940's was observed to be the result of increased temperature and decreased precipitation according to weather stations in the valleys of the Olympic Mountains (Heusser, 1957; Spicer 1986; Spicer 1989). This trend was afterwards reversed with a cooler, wetter climate resulting in standstills or markedly decreased retreat of the glaciers (Heusser, 1957; Spicer 1986; Spicer 1989). Only three glaciers on Mt. Olympus have shown advances since this change. The most recent climate changes in western Washington have been determined by Conway et al. (1999) and Rasmussen and Conway (2001) and they have observed that temperatures have increased by 1.2°C since 1948 with most of the warming occurring during the winter months with a 3.3°C increase in the average winter temperature. Precipitation was found to have decreased, especially in the winter months, and when this is combined with the winter temperature increase, the rain versus snow precipitation mix has been altered and the annual snowfall near the terminus has decreased by more than 500 mm since 1948 (Conway et al., 1999; Rasmussen and

Conway, 2001). With these changes in mind, the most recent advance of Blue Glacier in the 1980's might not show up for Royal Glacier as the great difference in precipitation and larger accumulation area of Blue Glacier make the ELA and glacier mass balance more susceptible to small fluctuations in precipitation than Royal Glacier, which experiences only the major climatic shifts in increased temperature and decreased precipitation resulting in overall glacial recession.

3.5.2 ELA Reconstructions

The mass balance of a glacier is defined as the difference between the amounts of ablation and accumulation that occur on a glacier measured over a specific period of time, which is usually one year. The accumulation area is where material is added to the glacier and the ablation area is where material is removed from the glacier. Accumulation and ablation vary across the surface of the glacier. A glacier is in steady state when it has a constant volume with the amount of ablation equaling that of the accumulation. If the accumulation is greater than the ablation, the mass balance has a positive value and the glacier is growing. If the accumulation is less than the ablation, the mass balance is negative and the glacier is shrinking (Paterson, 1994; Benn and Evans, 1998; Knight, 1999). The line that separates the accumulation and ablation areas is known as the equilibrium line.

The equilibrium line altitude (ELA) of a glacier is the elevation at which the annual mass balance is zero: above this altitude there is net accumulation of ice, below it there is net loss of ice. The firn line, which is the lower limit of snow at the end of the melting season, is often used as a marker of the ELA on modern glaciers (Porter, 2001; Osipov, 2004). The difference between the modern ELA and an ELA of some earlier time is called the equilibrium line depression and it is used as an indicator of climate change (Porter, 2001). The ELAs indicated by the moraines in Royal Basin will be compared with the previous reconstructions of the ELAs in the Olympic Mountains in order to assess the impact of spatial variability in precipitation on the recent history of glacial extents.

The mass balance of a glacier and the subsequent fluctuations of the ELA are controlled by climatic processes and the precipitation and temperature are the most

important of these factors. Therefore, the modern and paleo-ELAs can serve as proxy records of changes in precipitation and temperature. The primary controls on the ELA in the mid-latitudes are winter precipitation, which dominates accumulation, and summer temperature, which dominates ablation (Leonard, 1989). Other factors like windiness, cloudiness, and shading may be important, however, work in the Cascade Range indicates that temperature and precipitation account for more than 90% of the variance in the equilibrium line (Leonard, 1989). Detailed mapping of modern and paleo-ELAs and their corresponding variations may provide information on the changing climatic patterns, for example, changes in precipitation sources and wind direction (Leonard, 1984).

Spatial variability in the ELA across the Olympic Mountains has previously been studied for both modern glaciers and for inferred Quaternary average positions (Porter, 1964; Spicer 1986). Porter (1964) connected the lowest, north-facing cirques in the Olympic Mountains and observed that the surface defined increases in elevation with distance from the Pacific coast, presumably as a result of the decrease in precipitation across the region (Figure 3.17). A surface connecting the snowlines of modern glaciers also increases in elevation with distance from the coast, but much less steeply (Porter, 1964). In the northeastern corner of the Olympic Mountains, the two surfaces intersect and the lowest cirques are currently occupied by glacier ice (Porter, 1964).

Spicer (1986) used aerial photography to determine the mean glacial altitude, used as a proxy for the ELA, for 31 active glaciers across the Olympic Mountains. The glacial histories resolved from moraines of 10 of the 31 glaciers were used to determine the mean altitudes for modern, neoglacial (or since the most recent glacial period, the Wisconsin glaciation), and early 20th century surfaces (Figure 3.17) (Spicer, 1986). The mean altitude of modern glaciers rises approximately 12 m/km from the southwest to the northeast (Spicer, 1986). Mean glacial altitude for the neoglacial maximum increases at approximately 66 m/km or 5.5 times the present gradient (Spicer, 1986). Once again, the variations in the glacial mean altitudes were attributed to the variations in precipitation across the range.

The changes in the slope of the ELA across the Olympic Mountains over time have been attributed to changes in precipitation and/or temperature (Porter, 1964, Spicer,

1986). Porter (1964) hypothesized that the Olympic Mountains may have experienced a significant reduction in precipitation that offset the effects of lower temperatures locally during the glacial maxima. This hypothesis remains untested, but suggests an important difference in the behavior of glaciers on the western side of the Olympic Mountains versus the eastern side. To examine the variability of the ELAs across the Olympic Range, the recent changes in the ELA in Royal Basin will be compared with the detailed record from Blue Glacier on the western side of the Olympic Mountains.

The ELAs implied by the moraines of Royal Glacier were reconstructed using the Accumulation-Area Ratio, or AAR, method. The AAR is a ratio of the glaciers accumulation area to the total area of the glacier (Porter, 2001; Osipov, 2004; Ramage et al., 2005). Studies conducted on modern glaciers have shown that glaciers under steady state conditions in the mid-latitudes have AARs of approximately 0.65 ± 0.05, which means that the accumulation area accounts for approximately two-thirds of the glacier's total area (Porter, 2001; Osipov, 2004; Ramage et al., 2005; Stansell et al., 2007). To estimate the ELA with the AAR method, the former extent of the glacier is determined from glacial geologic features such as moraines (Porter, 2001; Osipov, 2004; Ramage et al., 2005). An initial, estimated ELA is then determined using the Altitude Ratio method, which states that the ratio of a glacier's altitude above the equilibrium line to the total altitudinal range is 0.5 (Porter, 2001; Osipov, 2004; Ramage et al., 2005). Contours of the glacier's surface are then drawn and these are based on the principles of glacier flow in which contours are concave in the accumulation area and convex in the ablation area, with the degree of convexity or concavity increasing with escalating distance from the equilibrium line (Porter, 2001; Osipov, 2004; Ramage et al., 2005). The results of this work for the moraines at the base of Royal Glacier can be seen in Figure 3.18. Following this step, the area between each pair of successive contours is measured and then used to generate a cumulative curve that depicts the glacier's area versus altitude distribution (Porter, 2001; Osipov, 2004; Ramage et al., 2005; Stansell et al., 2007). The cumulative curves for the moraines at the base of Royal Glacier are located in Figures 3.19, 3.20, 3.21, and 3.22. An AAR of 0.65 is then used to determine the ELA on the plot with the error being derived from a range of AAR values, for example ±0.05 or ±0.10 (Porter, 2001; Osipov, 2004; Ramage et al., 2005). The ELAs for each of the moraines at the base

of Royal Glacier are located in Table 3.6. The moraines show that the ELA for Royal Glacier was close to 1772 m four times in the last 200 years.

A detailed history of the ELAs of Blue Glacier in the western Olympic Mountains is available. Spicer (1989) reconstructed the ELA by using the mean glacial altitude as a proxy for the ELA. The ELA has also been recorded almost annually with the research that began in the 1950's on the glacier. By combining the datasets, the paleo-ELAs of Blue Glacier are resolved and they are compared with the paleo-ELAs for Royal Glacier in Figure 3.23.

The ELAs from the moraines in Royal Basin from 1895 and 1963 can be directly compared to ELAs of Blue Glacier. In the 1890's, the ELA for Royal Glacier was 1769 m while at Blue Glacier it was 118 m lower at 1651 m. In the 1960's, the ELA of Royal Glacier was 1776 m and Blue Glacier had an ELA 131 m lower at 1645 m. It can be observed additionally, that the ELAs for both Blue and Royal Glacier were close to the same value over the same period of time. The moraines of Royal Glacier have an average ELA of approximately 1772 m over the 200 year time span while over the same 200 years, the ELA of Blue Glacier is approximately 1688 m. The difference in the average ELAs for the two glaciers over this time period is the climate gradient. For the last 200 years the lowest moraine-forming ELA is approximately 1764 m for Royal Glacier, while for the same time period Blue Glacier is approximately 1614 m for similar methods of ELA reconstruction. When these two ELAs are connected, a climate gradient of 5 m/km can be observed across the range. This climate gradient primarily reflects changes in precipitation across the Olympic Mountains. Blue Glacier receives approximately 5 meters per year of precipitation while Royal Glacier receives only approximately 0.5 meters per year. The difference in the precipitation is responsible for the difference in the ELAs. As the elevations are quite similar with Mt. Olympus at 2432 m elevation and Mt. Deception at 2374 m elevation (approximately 1275 to 2350 m for Blue Glacier and 1743 to 2310 m for Royal Glacier) the temperature should be approximately the same for both glaciers.

The climate gradient determined from Blue and Royal Glaciers can be compared to the work of Porter (1964) and Spicer (1986). Porter's Pleistocene line has a slope of 20 m/km while the modern line has a slope of 8 m/km. Spicer's neoglacial line has a slope of

9 m/km, the early 20th Century line has a slope of 9 m/km, and the modern line has a slope of 7 m/km (Porter, 1964; Spicer, 1986). These data suggest a trend towards a decreasing climate gradient over time. During the Pleistocene the climate was colder and drier than the present climate (Heusser et al., 1999). The Pacific moisture delivery is provided by westerly air flow in the maritime climate currently observed in the Olympics. Pollen data and the glacial records on the western side of the range have shown that the Pacific moisture delivery was impeded during the last glacial maximum where glacier advances were mainly limited by a drier climate (Heusser et al., 1999; Thackray, 2001). The Puget Lobe of the Cordilleran Ice Sheet in the continental interior controlled the atmospheric circulation pattern over the Olympic Mountains at this time instead of the westerly air flow of the maritime climate currently observed and this limited the moisture delivery to the Olympic Peninsula (Heusser et al., 1999; Thackray, 2001). This reduction in precipitation from the Cordilleran Ice Sheet would have lead to even greater differences in the precipitation pattern during the last glacial maximum. As glaciers respond slowly to changes in climate, it would result in the gradually gentler slopes we observe in Porter and Spicer's work and the Royal and Blue Glacier climate gradient determined by the author.

Future work could focus on the orographic precipitation pattern as its influence on the modern mass balances of the glaciers within the Olympic Mountains could be seen. By examining the paleo-ELAs for all of the glaciers within the mountains, the existence and extent of the orographic precipitation pattern at the time of the last glacial maximum could be determined. In addition to the east to west side comparisons of the climate of the Olympic Mountains, the glacial history of the eastern side of the range could be better constrained. By locating and dating moraines throughout the region, the glaciers could be reconstructed and the full history of glaciations and climatic changes could be documented for the eastern Olympics. This information would be an invaluable contribution to the determination of the overall history of this range.

Also, the benefits would extend to the glacial erosion model I am using, as a more precise resolution of the erosion from having dated constraints on ice extent would allow for a more accurate comparison of the erosion with the uplift to determine why the Olympic Mountains are in steady state. The climate changes discovered by this work

could also help us to learn about what is currently happening and what may happen in the future with glacial extent in this range as our climate is currently changing in new ways with the full impacts having yet to be seen.

3.6 CONCLUSIONS

Lichenometric studies from various locations in the Pacific Northwest were combined to develop a regional growth curve that was applied to four moraines at the base of Royal Glacier on Mount Deception in the Olympic Mountains. The moraines were found to date from 1839, 1895, 1963, and younger than 1963. The determination of the ages for the four moraines allows for the beginning of the glacial recession history of Royal Glacier on Mount Deception to be determined and allows for the comparison of the eastern and western sides of the range.

The fluctuations of the length of Royal Glacier can be compared with those of Blue Glacier. The ELAs for the Royal Glacier moraines were reconstructed and compared with the ELAs for neoglacial moraines of Blue Glacier. The ELAs of the moraines of Royal Glacier were reconstructed using the AAR method. The ELAs were determined to be 1764 m for the 1839 moraine, 1769 m for the 1895 moraine, 1776 m for the 1963 moraine, and 1788 m for the moraine that is younger than 1963. These ELAs are close to the same value four times in the last 200 years, while over the same period of time the ELA of Blue Glacier is approximately 1688 m. The difference in the average ELAs for both Blue and Royal Glaciers over this time period is the climate gradient. The slope of this climate gradient is similar to both Porter's (1964) and Spicer's (1986) modern climate gradients and differs greatly from Porter's (1964) Pleistocene climate gradient implying a change in the climate in the Pleistocene as compared to the current climate.

3.7 FIGURES AND TABLES

Figure 3.1. A *Rhizocarpon geographicum* lichen that was observed on the moraines at the base of Royal Glacier on Mt. Deception. The digital calipers are used as a scale. Photograph by J. Hellwig.

Lichen Thallus Data and Surface Ages for the Locations Used in This Study						
Mts. Rainier, Hood, and Baker			**Mt. Waddington**		**Strathcona Provincial Park**	
Location	**Thallus Diameter (mm)**	**Surface Age (yr)**	**Thallus Diameter (mm)**	**Surface Age (yr)**	**Thallus Diameter (mm)**	**Surface Age (yr)**
Mt. Baker	39	77	13	20.00	3.2*	3
Mt. Baker	35.5	75	14	23	11.8	10
Mt. Baker	31.1	62	13.1	23	10.1	11
Mt. Baker	0*	8	13	25	11.9	15
Mt. Baker	29.2	62	13.2	26	13.4	16
Mt. Baker	49.9	97	14	27	15.7	17
Mt. Baker	50	97	12.5	27	18.7	20
Mt. Hood	70	189	14.5	28	22.2	22
Mt. Hood	55	122	15	28	23.9	27
Mt. Hood	27	62	19	35	22.6	29
Mt. Hood	21	55	17	36	22.2	31
Mt. Rainier	35.9	84	25	55	20.9	33
Mt. Rainier	16.7	33	27	62	27.1	45
Mt. Rainier	40.4	86	31.5	100	29.7	55
Mt. Rainier	36	82	35	111	31	64
Mt. Rainier	20.9	46	34.4	136	36.5	66
Mt. Rainier	63	145	40	165	32.7	67
Mt. Rainier	59	135	85*	680	34.1	69
Mt. Rainier	31.9	59			34	72
Mt. Rainier	31.3	57			36	82
Mt. Rainier	27.2	51			36.5	83
Mt. Rainier	11.8	26			40.2	89
					32.8	52
					25.6	40
					42.7	100
					97.4	288
					96.6	290
					78	220

Table 3.1. Lichen thallus data and equivalent ages for Mt. Rainier, Mt. Hood, and Mt. Baker, Mount Waddington, and Strathcona Provincial Park (From Porter, 1981; O'Neal and Schoenenberger, 2003; Larocque and Smith, 2004; Lewis and Smith, 2004). The asterisks mark the points that were removed from the growth curve for the linear fit of the uniform growth phase.

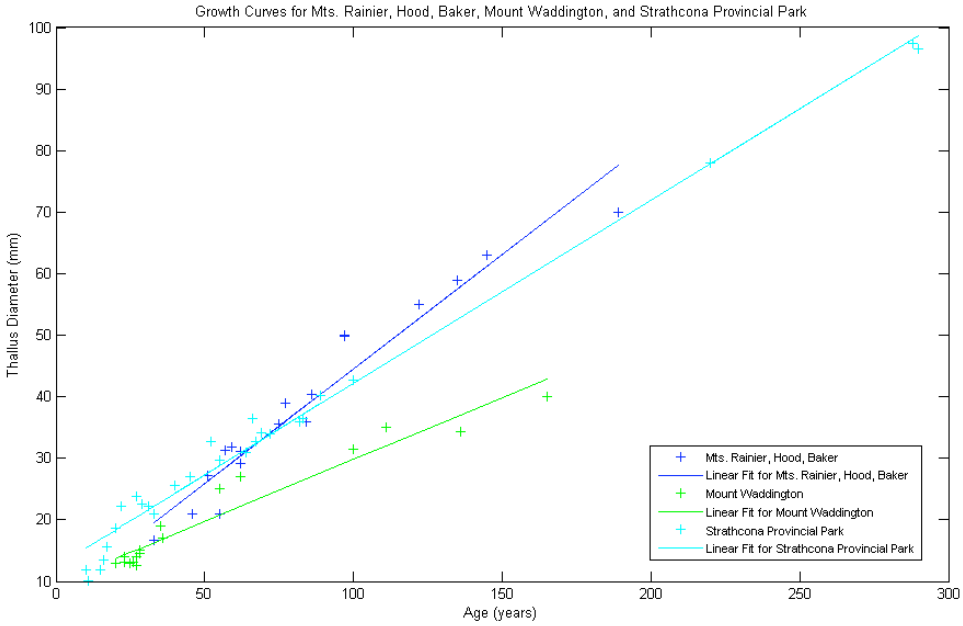

Figure 3.2. Plot of the growth curves and the corresponding linear fits that are used in this study (Data from Porter, 1981; O'Neal and Schoenenberger, 2003; Larocque and Smith, 2004; Lewis and Smith, 2004).

Variables for the Correlation of the Growth Curves to Mt. Deception					
Location	**Elevation (m)**	**Precipitation (m/yr)**	**Temperature (°C)**	**Substrate Lithology**	**Latitude/ Longitude**
Mt. Deception	1755-1767	0.5	1	Basalt, Marine Rhythmites, Slate, Sandstone, Siltstone	47°49’ N 123°13’ W
Mt. Rainier	1000-2000	2.63±1	3.4	Andesite Granodiorite	46°50’ N 122°45’ W
Mt. Hood	1000-2000	2.667	5.56	Andesite Granodiorite	45°22’ N 121°42’ W
Mt. Baker	1000-2000	2.6	5	Andesite Granodiorite	48°45’ N 121°50’ W
Mt. Waddington Area	55-1675	0.334-1.677	2.2-7.9	Granite, Andesite, Gneiss, Granodiorite	51°14-36’ N 124°30’-126° W
Strathcona Provincial Park	165-1325	2.62	3	Not provided	49°40’ N 125°40’ W

Table 3.2. The variables used to correlate the moraines on Mt. Deception with the other areas from which growth curves were developed (From Porter, 1981; O’Neal and Schoenenberger, 2003; Larocque and Smith, 2004; Lewis and Smith, 2004).

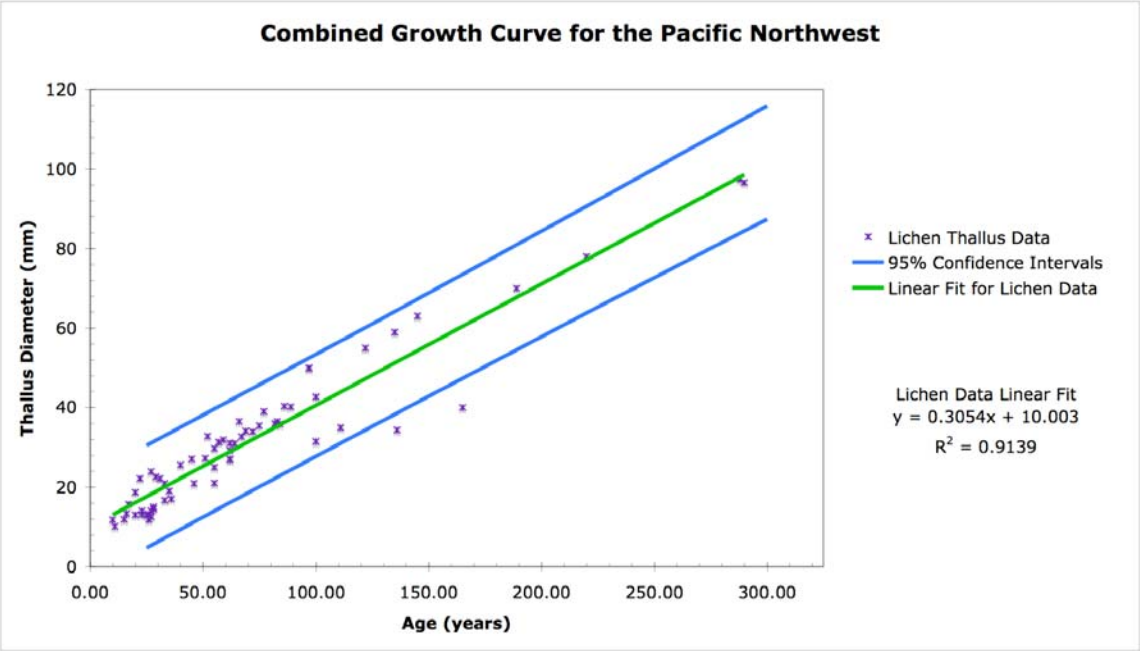

Figure 3.3. Plot of the regional or combined growth curve and the corresponding linear fit and 95% confidence interval (Data from Porter, 1981; O'Neal and Schoenenberger, 2003; Larocque and Smith, 2004; Lewis and Smith, 2004).

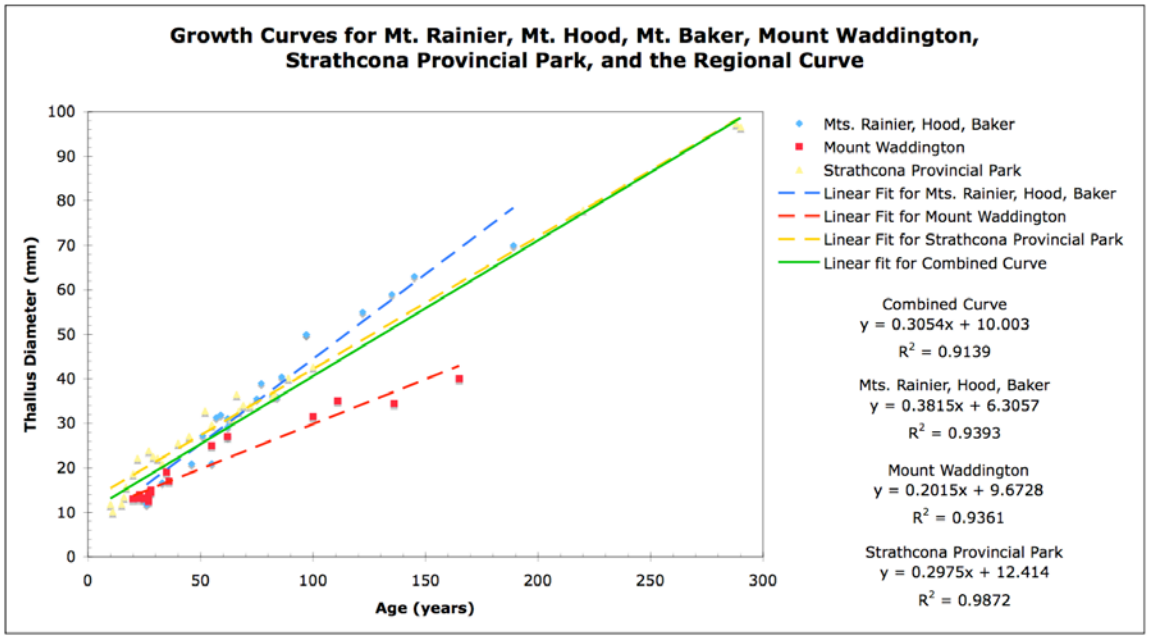

Figure 3.4. Plot of growth curves that are used in this study along with the corresponding linear fits, equations, and r-squared values for the fits (Data from Porter, 1981; O'Neal and Schoenenberger, 2003; Larocque and Smith, 2004; Lewis and Smith, 2004).

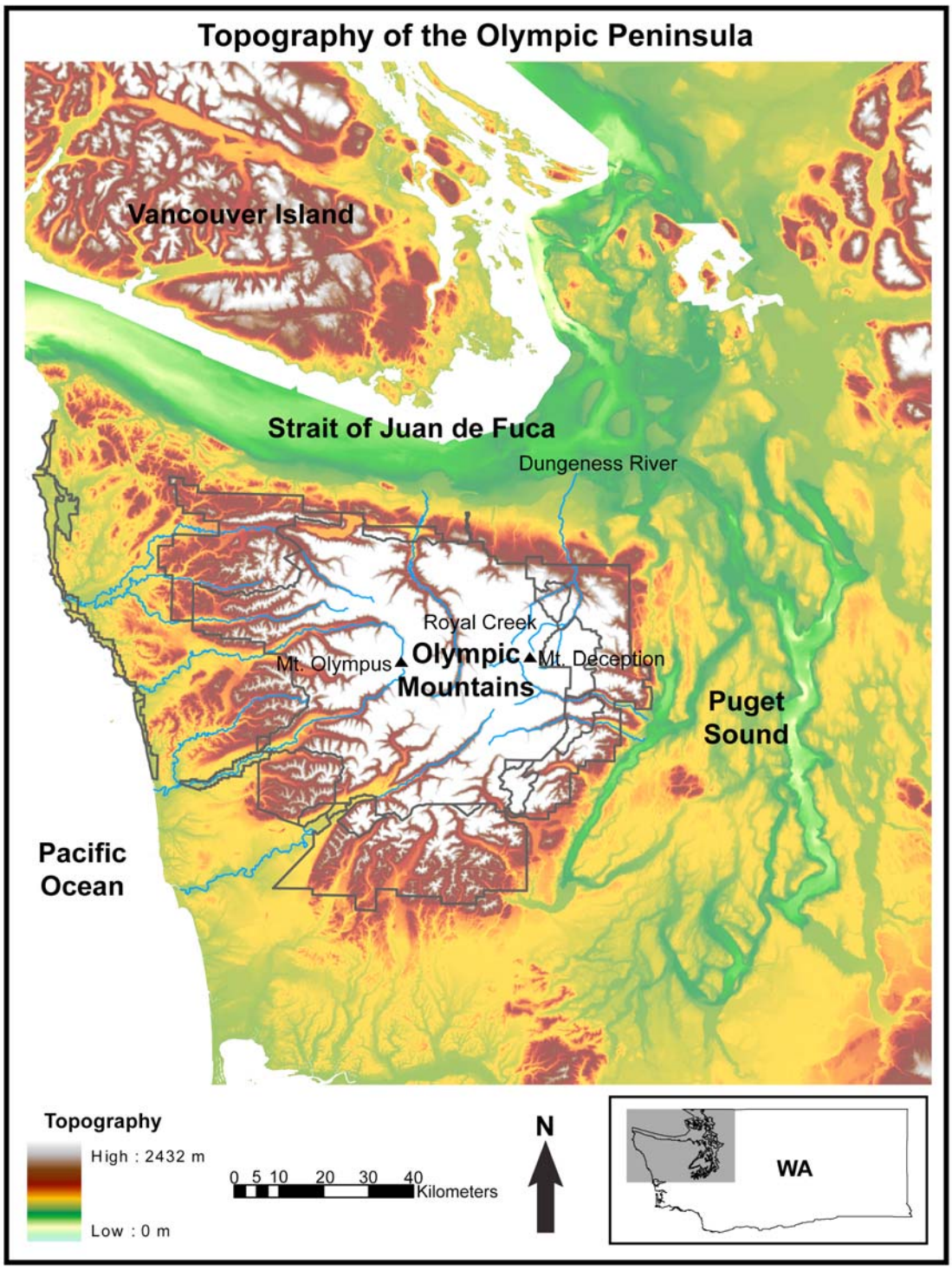

Figure 3.5. The location of places used in this study is underlain by the topography of the Olympic Mountains. The elevation is measured in meters.

Figure 3.6. The summit of Mount Deception and three of the outermost moraines used in this study. Photograph by J. Hellwig.

Figure 3.7. Moraines in the Upper Royal Basin composed of boulders and gravel. Photograph by J. Hellwig.

Figure 3.8. Mount Deception and two of the moraines used in this study. Photograph by J. Hellwig.

Figure 3.9. Scale photograph of the third outermost moraine. Photograph by J. Hellwig.

Figure 3.10. Mount Deception and the third outermost moraine. Photograph by J. Hellwig.

Figure 3.11. The lateral moraine and three of the outermost moraines blending into it. Photograph by J. Hellwig.

Table 3.3. Lichen Thallus measurements for the four moraines studied in Upper Royal Basin. The thallus measurements marked by an asterisk were removed from the distribution so the data would fit a normal distribution.

Lichen Thallus Measurements for Mount Deception			
1st Outermost Moraine (mm)	**2nd Outermost Moraine (mm)**	**3rd Outermost Moraine (mm)**	**4th Outermost Moraine (mm)**
66.51*	49.33*	23.95	No measurable lichens found on the moraine
61.85	48.45*	23.56	
53.53	47.02*	23.21	
50.1	46.71*	22.4	
49.57	44.73	21.34	
48.67	42.85	21.13	
46.4	42.27	20.44	
45.99	39.89	20.4	
45.92	37.22	20.12	
45.63	36.15	19.6	
44.73	36.04	19.23	
44.67	35.73	18.72	
44.64	35.67	18.46	
44.41	35.45	18.12	
44.24	35.36	17.52	
43.44	34.14	17.05	
42.05	34.12	16.69	
41.66	33.86	16.41	
41.58	33.78	16.4	
41.58	33.77	16.34	
40.95	33.5	15.65	
40.94	33.12	15.56	
40.59	32.79	15.33	
40.34	32.68	15.26	
39.86	31.72	14.92	
39.86	31.4	14.76	
39.22	31.07	14.34	
39.01	30.95	14.21	
39.01	30.69	13.88	
38.79	30.56	13.74	
37.68	30.4	13.66	
37.5	30.24	13.42	
37.36	30.16	13.25	
37.2	30.15	12.92	
36.57	29.97	12.82	
36.52	29.86	12.76	
36.42	29.84	12.59	
36.34	29.46	12.54	
36.07	29.43	12.53	
35.84	29.22	12.4	
35.58	29.15	12.23	
35.18	28.99	12.22	
34.83	28.99	12.14	
34.78	28.35	12	
34.18	27.98	11.93	
34.09	27.91	11.78	

33.68	27.76	11.61	
33.6	27.62	11.19	
33.57	27.48	10.85	
33.1	26.99	10.82	
32	26.54	10.3	
31.2	26.41	9.96	
30.02	26.23	9.69	
29.68	25.73	9.52	
28.7	25.68	9.42	
28.59	25.51	9.21	
28.27	25.38	8.92	
27.19	23.08	8.57	
26.29	22.61	7.74	
23.61	20.31	6.99	

Table 3.3 (cont.). Lichen Thallus measurements for the four moraines studied in Upper Royal Basin. The thallus measurements marked by an asterisk were removed from the distribution so the data would fit a normal distribution.

Shapiro-Wilks Normality Test Results					
Alpha=0.05					
	Run 1	Run 2	Run 3	Run 4	Run 5
1st Outermost Moraine	W=0.9477 p-value= 0.01210	W=0.9799 p-value= 0.4344 Normal			
2nd Outermost Moraine	W=0.9142 p-value= 0.0004511	W=0.9249 p-value= 0.001352	W=0.9368 p-value= 0.004724	W=0.9514 p-value= 0.02265	W=0.9665 p-value= 0.1209 Normal
3rd Outermost Moraine	W=0.9632 p-value= 0.06787 Normal				

Table 3.4. Results for the Shapiro-Wilks Normality Test for the moraines of Royal Glacier. W is the test statistic and the alpha is 0.05. For the distribution to be normal the p-value must be greater than alpha. When not normal, the largest diameter was eliminated and the test run again.

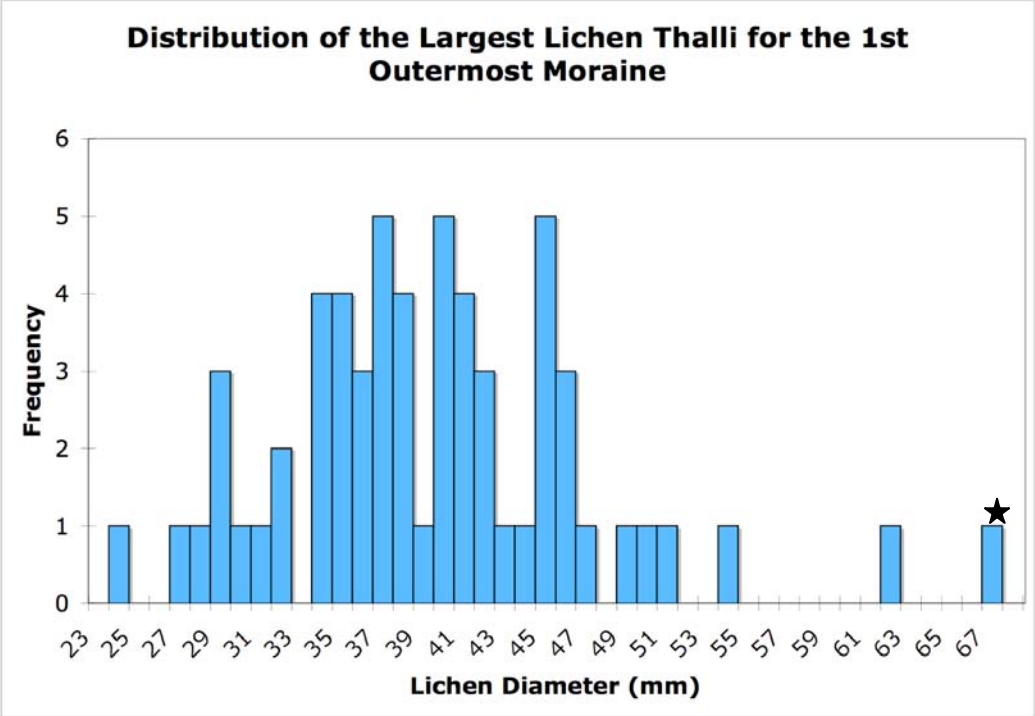

Figure 3.12. Frequency histogram of the largest lichen diameters from the 1st Outermost Moraine at the base of Royal Glacier on Mt. Deception. This data is normally distributed when the lichen diameters marked with an asterisk are removed.

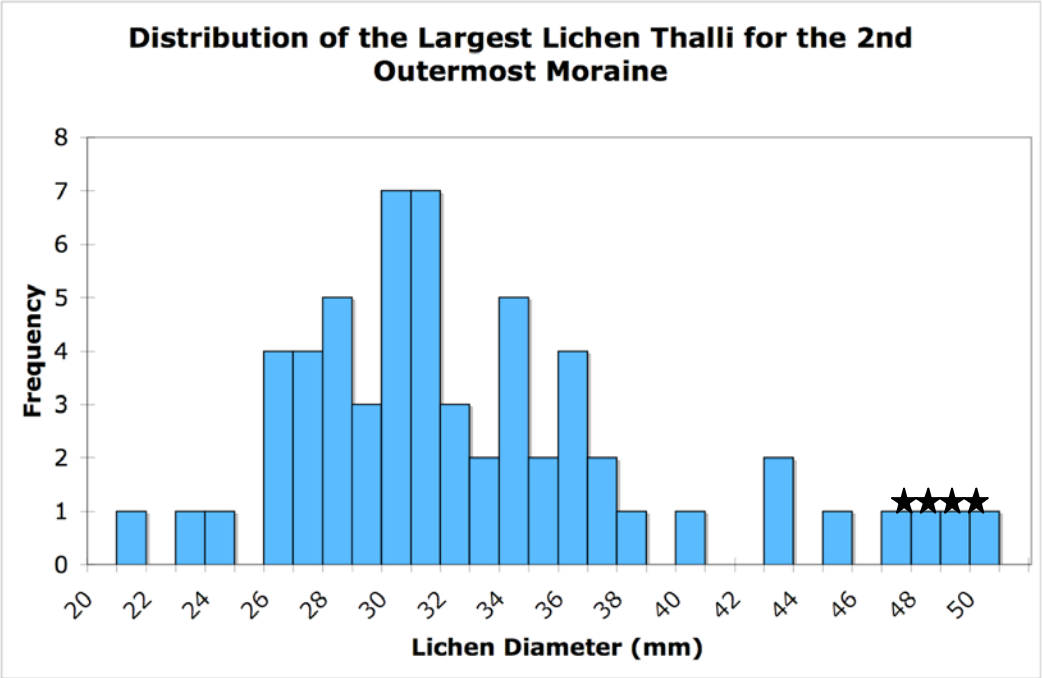

Figure 3.13. Frequency histogram of the largest lichen diameters from the 2nd Outermost Moraine at the base of Royal Glacier on Mt. Deception. This data is normally distributed when the lichen diameters marked with an asterisk are removed.

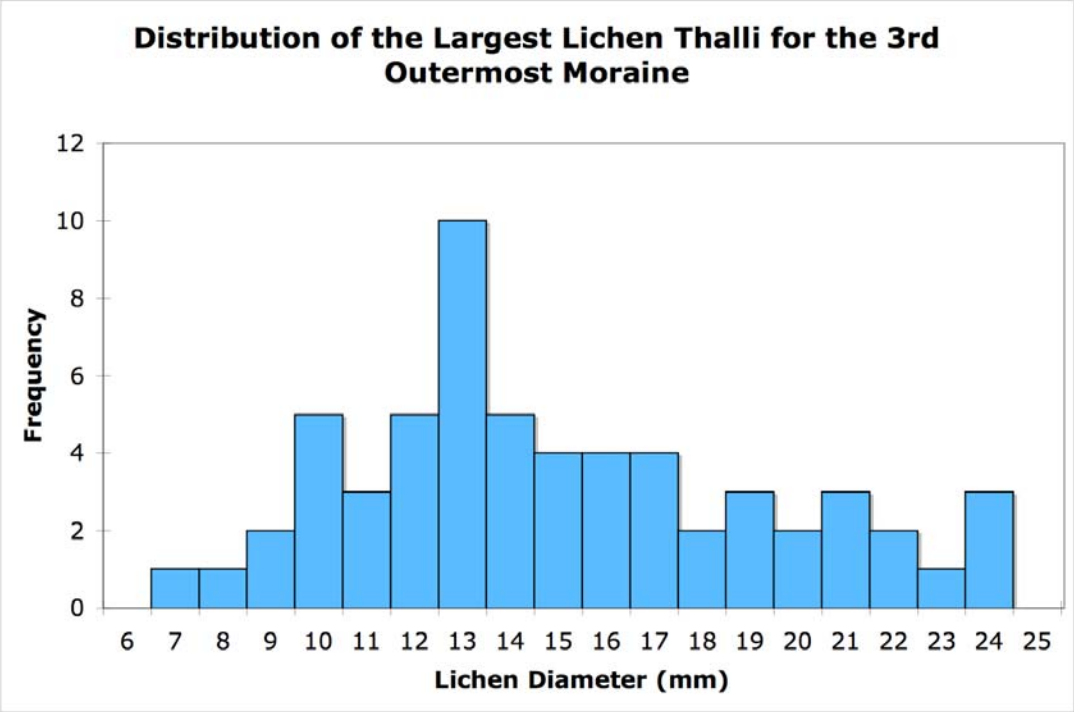

Figure 3.14. Frequency histogram of the largest lichen diameters from the 3rd Outermost Moraine at the base of Royal Glacier on Mt. Deception. This data is normally distributed when the lichen diameters marked with an asterisk are removed.

Equivalent Surface Ages from the Growth Curves				
	Surface Age (yr) with the Corresponding Year in Parentheses			
	Regional Growth Curve	**Mt. Rainier, Mt. Hood, Mt. Baker**	**Strathcona Provincial Park**	**Mount Waddington Area**
1st Outermost Moraine Largest Thallus: 61.85 mm	170 (1839)	146 (1863)	166 (1843)	259 (1750)
2nd Outermost Moraine Largest Thallus: 44.73 mm	114 (1895)	101 (1908)	109 (1900)	174 (1835)
3rd Outermost Moraine Largest Thallus: 23.95 mm	46 (1963)	46 (1963)	39 (1970)	71 (1938)
4th Outermost Moraine Largest Thallus: None to Measure	<46 (<1963)			

Table 3.5. The largest lichen thalli measurements from the moraines at the base of Royal Glacier on Mt. Deception and the corresponding surface ages and dates from each of the growth curves. The errors for each of the moraine ages were developed from the spread of ages calculated using each of the growth curves and the 95% confidence interval.

Figure 3.15. Blue Glacier on Mount Olympus. Blue Glacier is located in the center of the picture. Photograph by J. Hellwig

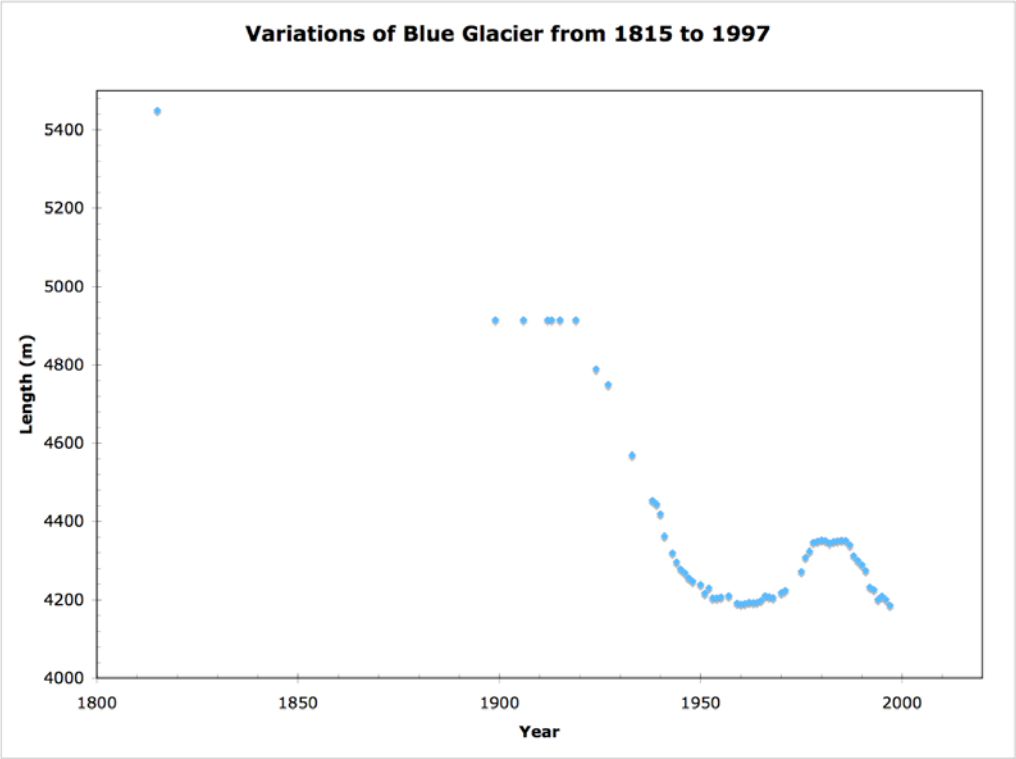

Figure 3.16. The length variations of Blue Glacier from 1815 to 1997. The advances and retreats that have occurred over the glacier are summarized in the text (Spicer, 1989; Conway et al., 1999).

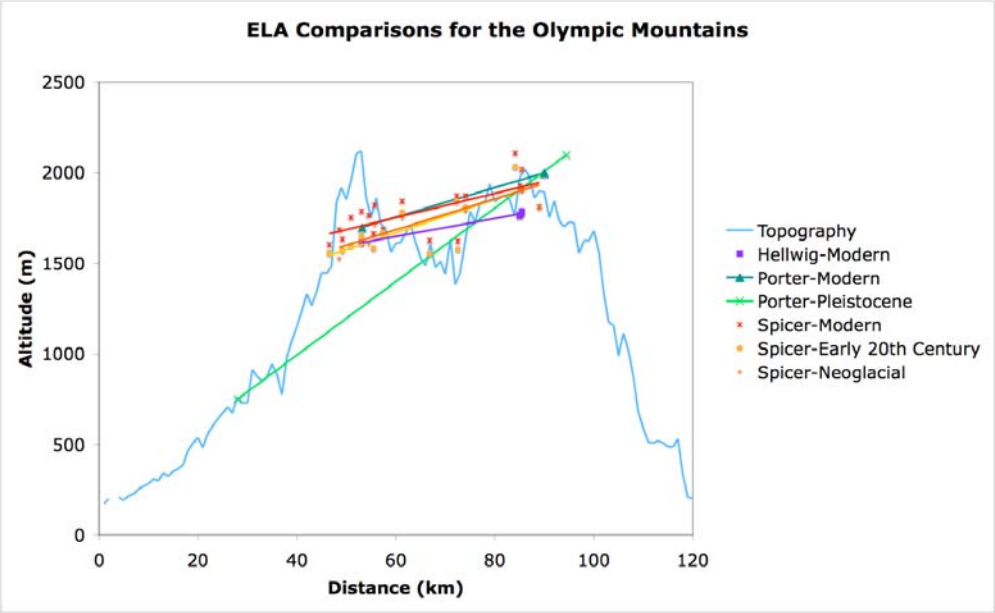

Figure 3.17. ELA comparisons based on the work of Porter (1964) for modern and Pleistocene variations and Spicer (1986) for modern, early 20th century, and neoglacial mean glacial altitude variations. Mean glacial altitude can be used as a proxy for the ELA. The ELAs for the reconstructed Royal Glacier are included (Porter, 1964; Spicer 1986).

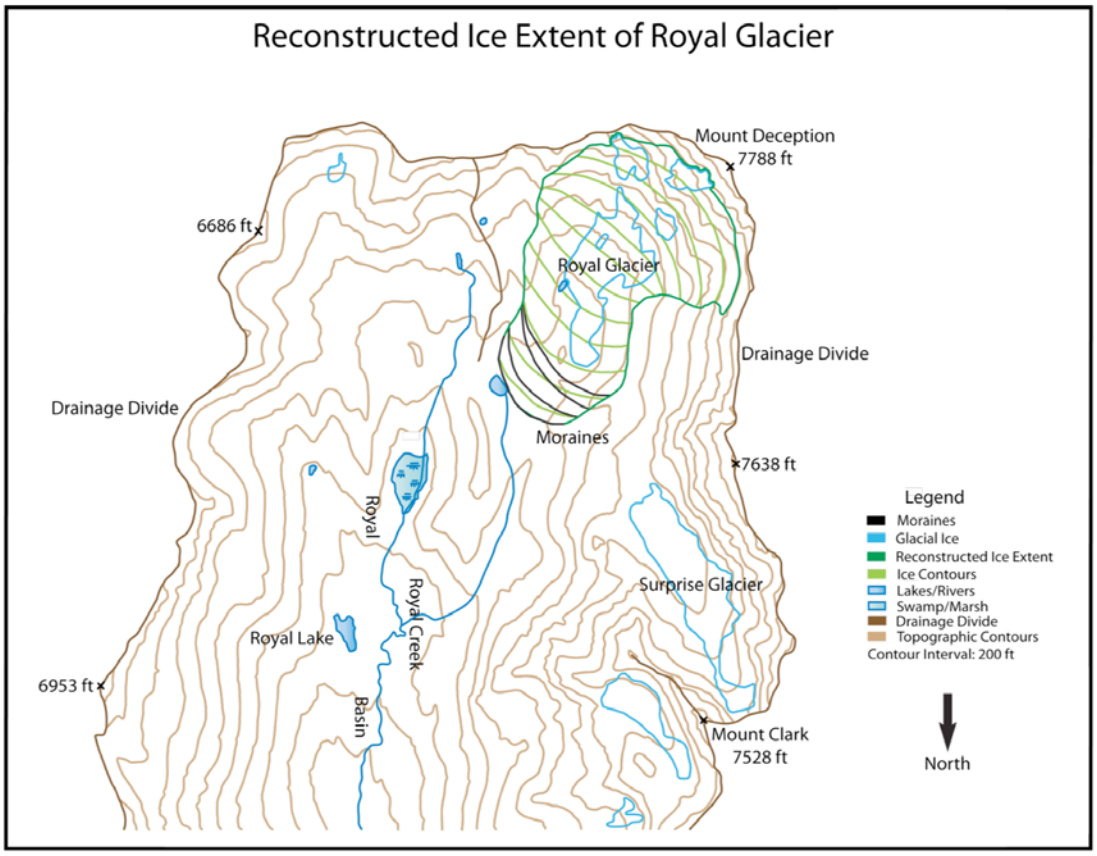

Figure 3.18. The reconstructed ice extent for Royal Glacier based on the moraines using the AAR method. The ice contours for use with the cumulative area curve are marked in light green and the contour interval for the topography is 200 ft.

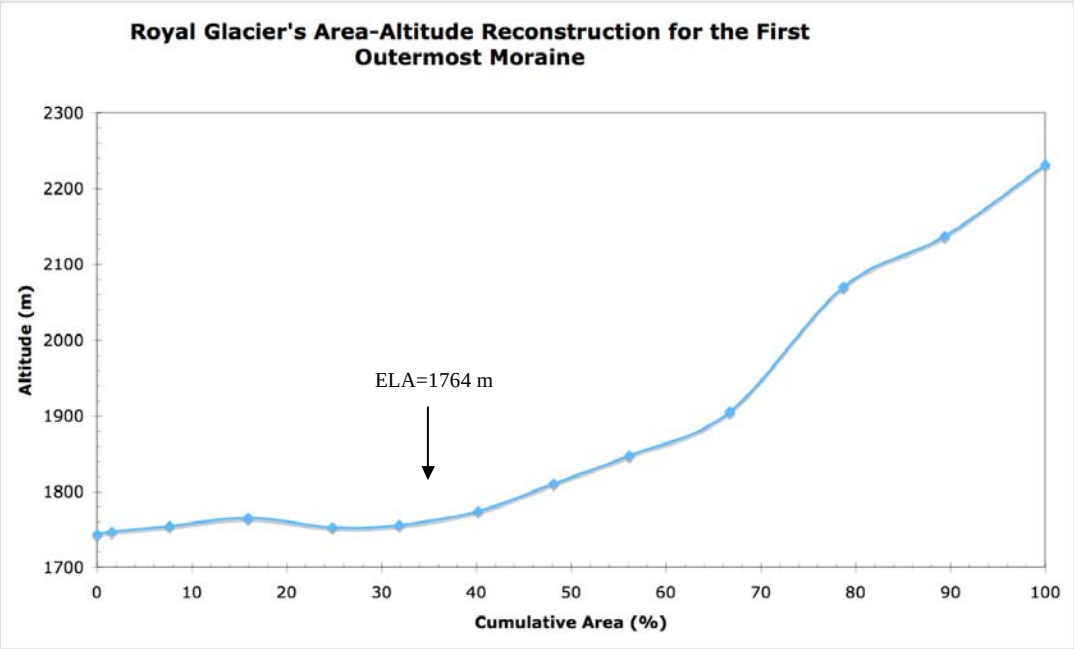

Figure 3.19. Reconstructed area-altitude profile from the first outermost moraine of Royal Glacier. The ELA of the reconstructed glacier is at 1764 m.

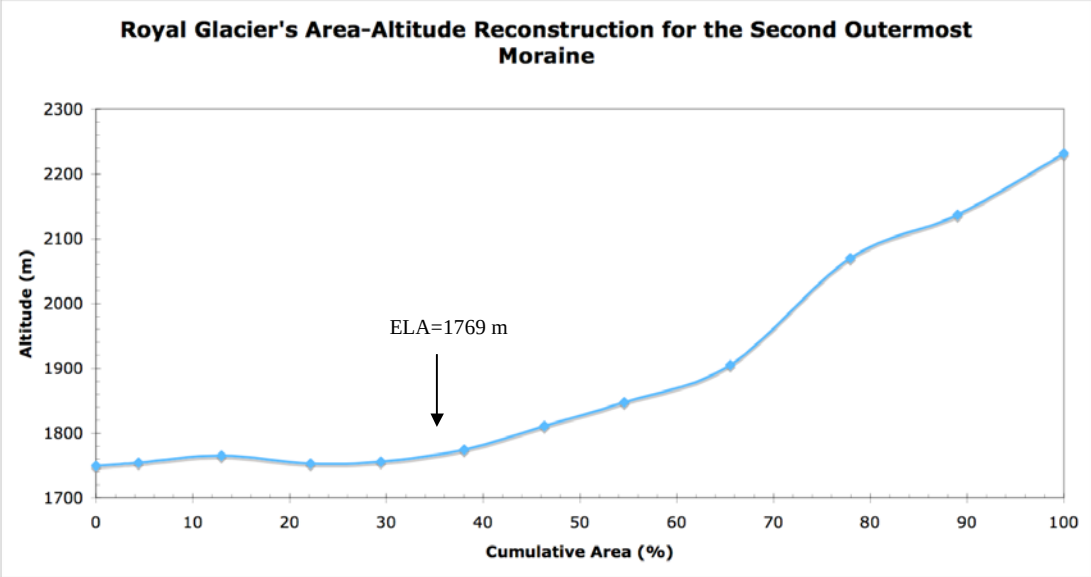

Figure 3.20. Reconstructed area-altitude profile from the second outermost moraine of Royal Glacier. The ELA of the reconstructed glacier is at 1769 m.

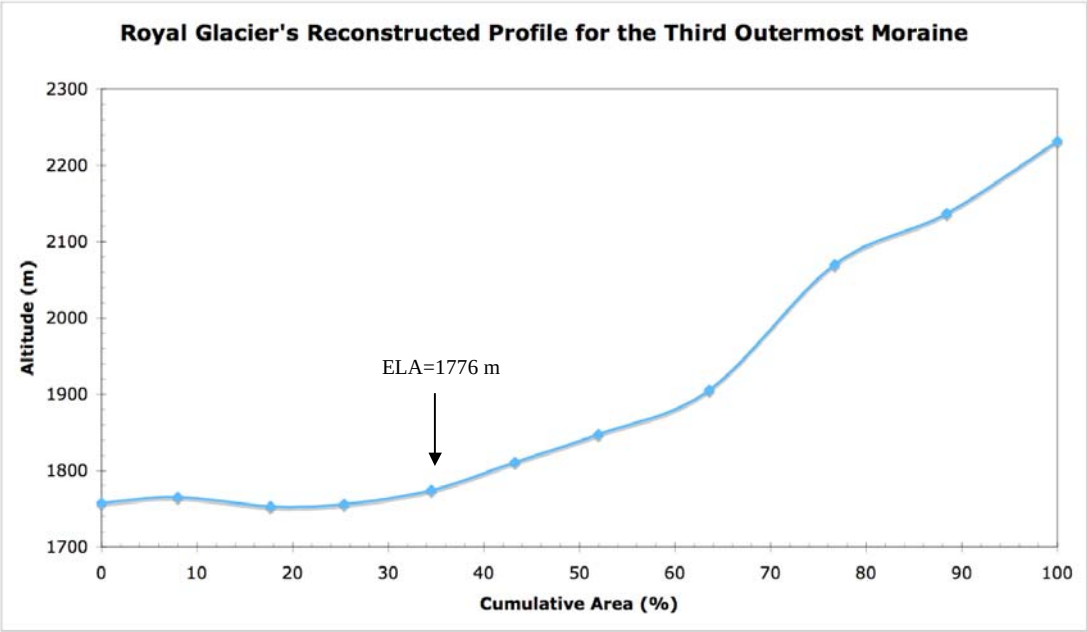

Figure 3.21. Reconstructed area-altitude profile from the third outermost moraine of Royal Glacier. The ELA of the reconstructed glacier is at 1776 m.

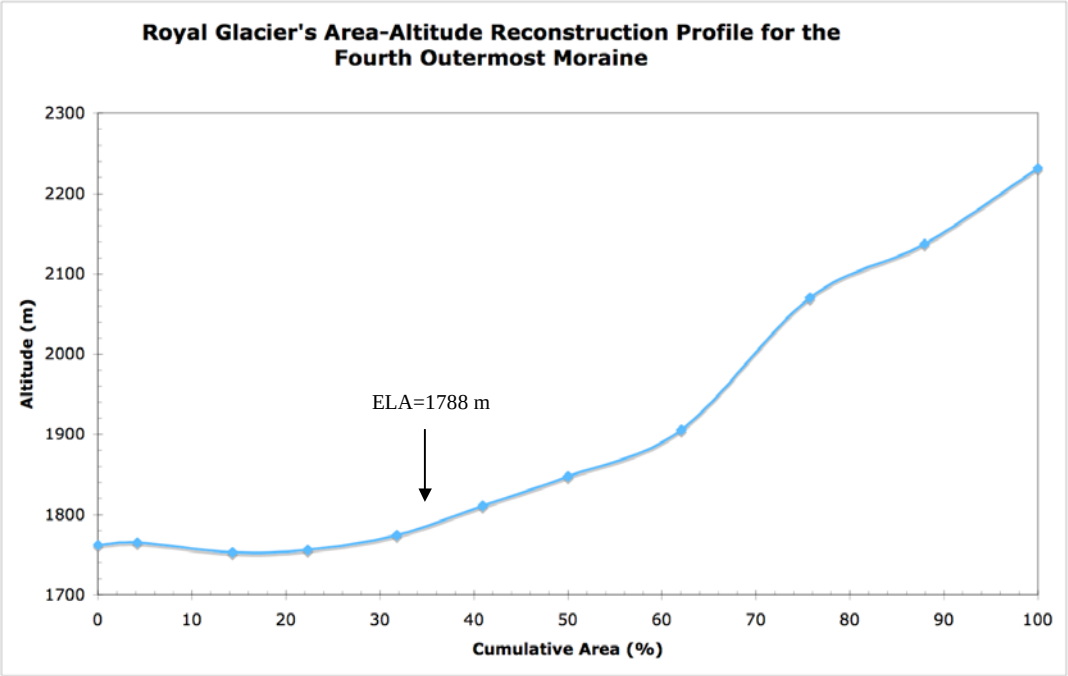

Figure 3.22. Reconstructed area-altitude profile from the fourth outermost moraine of Royal Glacier. The ELA of the reconstructed glacier is at 1788 m.

Equilibrum Line Altitudes for the Reconstructed Royal Glacier		
Moraine	**ELA (m)**	**ELA (ft)**
1st Outermost Moraine	1764	5786
2nd Outermost Moraine	1769	5802
3rd Outermost Moraine	1776	5825
4th Outermost Moraine	1788	5865

Table 3.6. Equilibrium line altitudes for the reconstructed Royal Glacier based on the four moraines present at the base of the glacier.

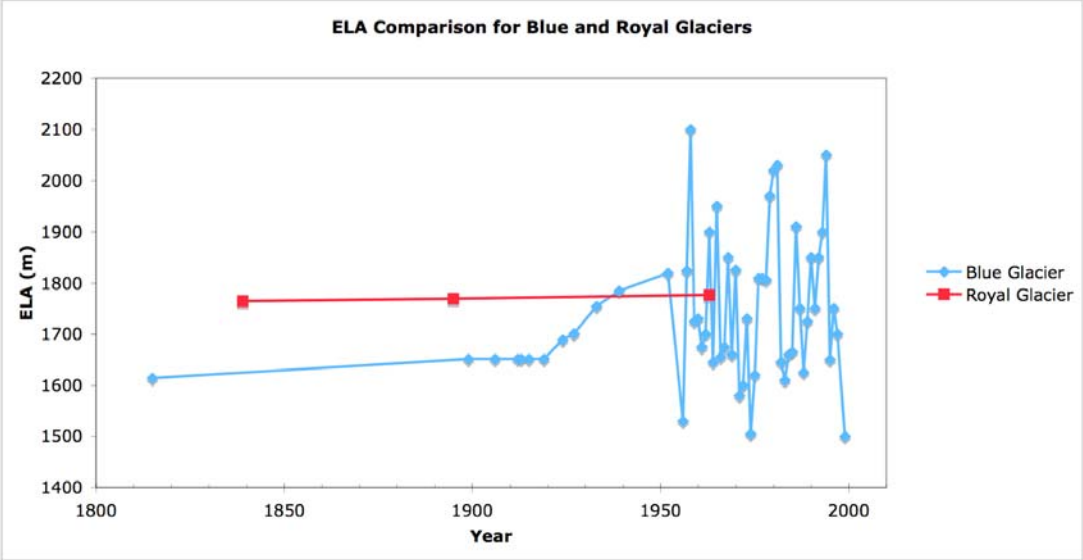

Figure 3.23. The comparison for the paleo-ELAs of Blue Glacier and Royal Glacier. The ELAs for Royal Glacier were determined by reconstructing the ice extent based on the moraines examined. The ELAs for Blue Glacier were determined from annual measurements and the reconstructed mean glacial altitudes (Spicer, 1989; University of Washington, 2005).

CHAPTER 4: CATALOG OF DESCRIPTIONS OF GLACIAL DEPOSITS IN THE OLYMPIC MOUNTAINS

4.1 INTRODUCTION

A small number of researchers have examined the glacial history of the eastern Olympic Mountains of Washington State. Chief among these is William A. Long who worked for the United States Forest Service at Olympic National Forest and was based in Olympia, Washington. He explored the river valleys on the northern and eastern sides of the Olympic Peninsula in addition to a few river valleys on the southeastern, southwestern, and northwestern portions of the peninsula. Long made notes of his observations of the glacial geology in these areas and recorded exposures, bedrock, and geomorphic features during the 1970's. He assembled his notes into papers that recorded these features and provided an estimated age for each of them. Long's papers have gone unpublished, but copies exist at Olympic National Park, Port Angeles, Washington, and at Olympic National Forest, Olympia, Washington. His work is unpublished and it has been summarized here for use in this project and future access.

Long separated the glacial deposits into several different age groups that follow:

Fraser Glaciation: 10 kyr-29 kyr (youngest)

Sumas Stade: 10 kyr-11 kyr

Everson Interstade (short, nonglacial): 11 kyr-13 kyr

Vashon Stade: 13 kyr-18 kyr

Evans Creek Stade: 18 kyr-29 kyr

Olympic Interglaciation or Erosion Interval (Nonglacial interval): 18-29kyr

Salmon Springs Glaciation: 29-40 kyr

Puyallup Nonglacial Interval

Stuck Glaciation

Alderton Nonglacial Interval

Orting Glaciation (oldest)

(Long, SSVCIOM). Long also recognized three episodes of Neoglacial activity and they are (from oldest to youngest): Royal, Constance, and Deception (Long, NNOMW). These intervals were separated by a milder period in which the glaciers in this area of the Olympic Mountains were smaller (Long, NNOMW). The majority of the deposits he

locates are from the Salmon Springs Glaciation, the Fraser Glaciation-Evans Creek and Vashon Stades, and Neoglacial times. A further breakdown and updated version of the glaciation chronology appears in Table 1.1.

Long describes the deposits left behind by both the continental and alpine ice. The continental ice deposits contain granitic stones and high-grade metamorphic rocks derived from the Canadian Rockies. These rocks are not native to the Olympic Mountains - the alpine glaciers originated in the Olympics and carry the basalt and sedimentary rocks that are native to the range (Long, GGEOPW; Long, GGNOP; Long, NNOMW; Long, GGSOPW; Long, GSRVNOPW; Long, GHRDBSOPW; Long, SSVCIOM). Long describes the deposits in his own terms and usually refers to them as being till or drift. He defines drift to be all rock material transported by glacial ice, all deposits made by glacial ice, and all deposits that are predominantly of glacial origin that are made in the sea or in bodies of glacial meltwater, whether they were transported by the water or rafted in icebergs. It includes till, scattered rock fragments, and stratified drift (Long, SSVCIOM). He defines till as a direct glacial deposit that was carried and deposited by glacial ice. The sediment lacks stratification and size sorting and water has played a minor role in its deposition (Long, SSVCIOM).

Long separated the deposits he observed into either continental or alpine deposits. He estimated the age of the deposits based on the degree of weathering, till composition, the arrangement of features/deposits, the weathering characteristics, the spatial relationships, granite weathering ratios, and the granite surface boulder frequency. From these observations, Long created a description for the types of till or drift he associated with each stade or glaciation.

Alpine glaciers originated in the Olympic Mountains and transported and deposited darker basalt and sedimentary rocks that are native to the range. Very few granites and other northern stones appear in these deposits. These rocks were likely picked up by the alpine glaciers as they moved into areas previously covered by the Cordilleran Ice Sheet and re-deposited at the outer limit of the glacial extent (Long, GGSOPW; Long, SSVCIOM).

Salmon Springs continental till is usually buried under soil and vegetation and is widely scattered on the steep slopes of the mountain front. It occurs in small isolated

patches and widely scattered erratics, which are mostly rounded cobbles and pebbles. The valley glaciers that acted concurrently with the Salmon Springs Puget ice would have prevented the Puget ice from entering the valleys and depositing erratics within them. This is why there is an almost total lack of drift in the valleys and why little or no granite is found in Evans Creek glacial deposits. Salmon Springs Puget Drift occurs mostly in interfluves or high on valley walls and surface granite boulders are rare (Long, GGEOPW; Long, GGNOP; Long, NNOMW; Long, GGSOPW; Long, GSRVNOPW; Long, GHRDBSOPW; Long, SSVCIOM).

Vashon continental drift usually has strong morphological expression and is widespread. There are many moraines from this time and they constitute barriers across valley floors. The drift always contains both fresh and decomposed granitic stones either at the surface or in cutbank exposures at most any altitude along the Olympic Mountain front. There are many granite boulders on the surface of deposits of Vashon drift while in Salmon Springs drift surface boulders are rare to absent. This is either because Vashon continental ice picked up most of the granite scattered on the mountain front by the Salmon Springs ice (hence the mixed fresh and decomposed clasts) or a large percentage of the Salmon Springs surface granite had completely disintegrated before the Vashon ice arrived. The continental ice flowed south from Vancouver Island and the Coast Mountains of Canada and was forced high into the north trending valleys and along the ridges of the east-trending valleys because the force of the ice flow was less in the east-trending valleys than north trending valleys. The ice was lower and its gradient much higher in the north-trending valleys so the ice pushed 2-3 times as far up the north-trending valleys as it did up the east-trending valleys, which face Hood Canal. Granitic stones decrease in the deposits upvalley depending on how far up the valley the ice reached because the lobe incorporated the Olympic bedrock and local alluvium into its load as it moved south and west (Long, GGEOPW; Long, GGNOP; Long, NNOMW; Long, GGSOPW; Long, GSRVNOPW; Long, GHRDBSOPW; Long, SSVCIOM).

The glacial geologic features observed by William Long are summarized into two lists from the seven papers that were located. The lists are split into two tables: the first records deposits and geomorphic features examined by William Long and the second records deposits referenced by William Long from other papers. As only one of the

papers has a date, the papers are referenced according to their titles, which are abbreviated to the following forms:

GGEOPW: Glacial Geology of the Eastern Olympic Peninsula, Washington

GGNOP: Glacial Geology of the Northern Olympic Peninsula

GGSOPW: Glacial Geology of the Southeastern Olympic Peninsula, Washington

GHRDBSOPW: Glaciations in the Humptulips River Drainage Basin, Southwestern Olympic Peninsula, Washington

NNOMW: Neoglaciation in the Northeastern Olympic Mountains, Washington

SSVCIOM: Salmon Springs and Vashon Continental Ice in the Olympic Mountains and Relation of Vashon Continental to Fraser Olympic Ice

GSRVNOPW: Glaciations of the Sitkum River Valley, Northwestern Olympic Peninsula, Washington

The age of the feature as determined by William Long, a brief description of it, its location with approximate latitude and longitude coordinates, and whether it lies on federal or public land is also noted. The deposits are separated according to the river valley they lie in. In addition, a map of all of the moraines separated according to their ages is shown in Figure 4.1. The spread of moraines in the valleys indicates the extent of the alpine glaciers and continental ice over time. The concentration of moraines indicates the ample amount of glacial deposits recorded in these valleys.

4.2 GLACIAL DEPOSITS AND FEATURES RECORDED BY WILLIAM LONG

What	Description	Where	Location	Age	Source
Continental Ice Extent	About 1 mile south of Vance Creek the upper limit of the ice sheet reached a 2,100 ft altitude at the crests of faceted ridge spurs		Vance Creek-South Fork Skokomish River Valley Lat: 47°47′30″ Long: 123°19′00″	Salmon Springs	Long, GGSOPW
Drift	The distribution of drift deposits in upper Vance Creek indicate that the Puget Lobe reached within half a mile of the head of Vance Creek during its maximum advance and terminated at an altitude of 1,225 ft; road cut exposures just below the upstream crossing of Vance Creek show nonstratified gravel with granitic stones	Olympic National Forest	Vance Creek-South Fork Skokomish River Valley Lat: 47°20′30″ Long: 123°21′30″	Salmon Springs	Long, GGSOPW
Erratics	On lower Vance Creek near the mouth of Nicklund Creek scattered erratic gravel on the north valley wall and a 10 ft boulder with a rounded outline lie near the top of the east valley wall at an altitude of 1,760 ft on upper Nicklund Creek and were carried by the Puget Lobe ice	Olympic National Forest	Vance Creek-South Fork Skokomish River Valley Lat: 47°20′30″ Long: 123°21′30″	Salmon Springs	Long, GGSOPW
Granite Boulders and Pebbles	Many rounded granite, pebble to small boulder size stones were found on the valley walls of Rock Creek to a height of 1,525 ft within half a mile of the valley head; road cuts expose a few glacially striated basalt stones	Olympic National Forest	Rock Creek-South Fork Skokomish River Valley Lat: 47°24′00″ Long: 123°25′30″	Salmon Springs	Long, GGSOPW
Granite Pebbles	Above the Vashon terminal moraine in Rock Creek, stream alluvium contains granitic pebbles as high as 1,250 ft	Olympic National Forest	Rock Creek-South Fork Skokomish River Valley Lat: 47°24′00″ Long: 123°25′30″	Salmon Springs	Long, GGSOPW
Puget Lobe Drift	On the east end of the ridge between Rock Creek and the South Fork of the Skokomish River, road cutbanks exposed the upper limit of a small body of weathered drift at a height of 1,975 ft	Olympic National Forest	Rock Creek-South Fork Skokomish River Valley Lat: 47°24′00″ Long: 123°25′30″	Salmon Springs	Long, GGSOPW
Alpine Till	Alpine till was found at points near Cedar Creek in the South Fork Valley;	Olympic National Forest	Cedar Creek-South Fork Skokomish River Valley	Salmon Springs	Long, GGSOPW

What	Description	Where	Location	Age	Source
	exposures along a logging road above the mouth of Cedar Creek on the east side reveal 15 ft of moderately weathered till, oxidized through the full exposure, clasts are greywacke, sandstone, and basalt with well-striated stones, fine surface cracks, and exfoliation in thin layers in the basalt; lies between altitudes of 1,600-1,800 ft		Lat: 47°29′00″ Long: 123°25′00″		
Alpine Till and Lateral Moraine	In Brown Creek Valley up to a height of 1,500 ft, logging road cutbanks exposed an alpine till with striated basalt clasts; it lies at the south end of a huge lateral moraine embankment that extends across and fills the broad saddle at the head of Brown Creek so the till must be older	Olympic National Forest	Brown Creek-South Fork Skokomish River Valley Lat: 47°27′30″ Long: 123°15′00″	Salmon Springs	Long, GGSOPW
Alpine Till	Formless deposits of till are located on the eastern wall of Cedar Creek valley and on both walls of the lower South Fork; this till occupies an intermediate position between a weathered pre-Fraser alpine till higher and Fraser end moraines lower	Olympic National Forest	Cedar Creek-South Fork Skokomish River Valley Lat: 47°29′00″ Long: 123°25′00″	Evans Creek	Long, GGSOPW
Alpine Till	Logging road cutbanks along the east side of Cedar Creek expose a compact till with numerous faceted and striated sandstone and basalt clasts ranging in size from pebbles to boulders 6 ft in diameter; most stones are firm, unweathered, oxidation up to 8 ft into the till, below the oxidized zone the till is gray in color; this till is also exposed at the head of Cedar Valley at an altitude of 1,450 ft	Olympic National Forest	Cedar Creek-South Fork Skokomish River Valley Lat: 47°29′00″ Long: 123°25′00″	Evans Creek	Long, GGSOPW
Alpine Till	A short glacier in upper Le Bar Creek valley overflowed the 2,000 ft high col opposite the mouth of Cedar Creek and probably merged with the South Fork glacier	Olympic National Forest	Le Bar Creek-South Fork Skokomish River Valley Lat: 47°25′15″ Long: 123°20′30″	Evans Creek	Long, GGSOPW

What	Description	Where	Location	Age	Source
Lateral Moraine	The North Fork Glacier built a huge lateral moraine in and across the Brown Creek saddle lying between the North and South Forks in the vicinity of Lake Cushman; landslides and road cuts on the Brown Creek flank expose up to 300 ft of alpine drift composed entirely of Olympic rock types; striated and faceted surfaces are retained on many boulders and stones but they are a little decayed; the top 10 ft of till is oxidized reddish-brown and grades down into unweathered till which is yellow-brown to gray; the broad crest is at 1,650 ft altitude and is strewn with till boulders	Olympic National Forest	Brown Creek-South Fork Skokomish River Valley Lat: 47°27′30″ Long: 123°15′30″	Evans Creek	Long, GGSOPW
Puget Lobe Drift	The upper limit of Vashon drift lies at a height of 1,250 ft on the east end of the ridge between Rock Creek and the South Fork of the Skokomish River	Olympic National Forest	Rock Creek-South Fork Skokomish River Valley Lat: 47°24′00″ Long: 123°25′30″	Vashon	Long, GGSOPW
Puget Lobe Drift	Near the mouth of Vance Creek valley near Lake Haven, drift extends up to an altitude of 1,500 ft and the road along the south side of Vance Creek exposes continental drift at several places; at a point 2 miles above the mouth of the valley the drift drops below the level of the road at the 1,200 ft contour	Olympic National Forest	Vance Creek-South Fork Skokomish River Valley Lat: 47°18′15″ Long: 123°18′30″	Vashon	Long, GGSOPW
Terminal Moraine	The terminal moraine of the Vance Creek tongue of Puget ice is 3 miles above the valley mouth where the moraine extends 3,000 ft or more along the creek; composed of gray drift consisting of unconsolidated sandy gravel with lenses and beds of fine sand and silt; the crest reaches an altitude of 1,175 ft or 500 ft above the creek and forms a gravel ridge ~1,000 ft long; the road	Olympic National Forest	Vance Creek-South Fork Skokomish River Valley Lat: 47°21′11″ Long: 123°21′33″	Vashon	Long, GGSOPW

What	Description	Where	Location	Age	Source
	on the north side of the valley cuts through the moraine revealing 30 ft of strongly deformed laminated clay and silt deposited in an ice-margin lake				
Lake Sediments	An exposure of undeformed lake fines is in a road cutbank half a mile above the terminal moraine from above	Olympic National Forest	Vance Creek-South Fork Skokomish River Valley Lat: 47°18′15″ Long: 123°18′30″	Vashon	Long, GGSOPW
Terminal Moraines	Large, well-formed terminal moraines from the Puget Lobe lie at midpoint in Vance and Rock Creeks; the moraine in Vance Creek is 3 miles above the valley mouth and the crest lies 500 ft above the stream at an altitude of 1175 ft; the road along the north side of Vance Creek cuts through the moraine and exposes 30 ft or more of strongly deformed laminated clays and silts which were deposited by an ice-margin lake and deformed by fluctuations of the ice terminus; the moraine on Rock Creek is a mile above the valley mouth, its crest lies at an altitude of 1150 ft, and is similar in form and morphology to the moraine in Vance Creek	Olympic National Forest	Vance and Rock Creeks-South Fork Skokomish River Valley Vance Creek Lat: 47°21′11″ Long: 123°21′33″ Rock Creek Lat: 47°22′30″ Long: 123°19′39″	Vashon	Long, GGSOPW
Terminal Moraine	A readvance of the Puget ice barely overrode the 1,062 ft saddle between the Cushman and Dennie Ahl Hills and left a moraine on the south end of Cushman Hill at 1,225 ft; the glacier pushed a half mile into the South Fork Skokomish River valley and left the moraine on thick glacial lake sediments at the mouth of Brown Creek valley; moraine is composed of unconsolidated water-worn stones rich in granites and must have been deposited in the lake as no stream channel cuts into the lake sediments beyond the	Olympic National Forest	Dennie Ahl Hill-South Fork Skokomish River Valley Lat: 47°25′52″ Long: 123°15′00″	Vashon	Long, GGSOPW

What	Description	Where	Location	Age	Source
	moraine; the lake sediments consist of bedded sand, gravel, and laminated clay and silt seen where the stream and slumps have exposed 75 ft of sediment; no foreign stones were found in the sediments which were supplied by Brown Creek and mass wasting of the valley walls				
Recessional Meltwater Channel	Bingham Creek Channel extends from Vance Creek over Windy Siding to the East Fork of the Satsop River; Vashon ice allowed the 600 ft col at Windy Siding to be used as an outlet to the glacial lake at Vance Creek;	Olympic National Forest	Satsop River-South Fork Skokomish River Valley Lat: 47°22′30″ Long: 123°27′00″	Vashon	Long, GGSOPW
Recessional Meltwater Channel	Winter Creek Channel begins at the 450 ft col 3 miles east of Windy Siding and was near the southwest margin of the Vashon glacier; meltwater flowed in a southeast direction; thick moraine deposits at the mouth of the channel are very irregular in frontal outline and the surface is pocked with kettles, some containing small ponds; opposite the mouth of the channel, kettles in thick drift occur almost to the floor of the Skokomish valley and channels across the embayment discharged into the valley when the ice front lay slightly north of the valley; the floor of the open end of the channel lies 350-400 ft above the nearly flat floor of the Skokomish valley	Olympic National Forest	Satsop River-South Fork Skokomish River Valley Lat: 47°22′30″ Long: 123°27′00″	Vashon	Long, GGSOPW
Recessional Meltwater Channel	Channel bends and steep margining bluffs developed in Vashon drift above the basalt occur along both rims of the South Fork Skokomish River gorge and mark the course of a meltwater channel that begins half a	Olympic National Forest	Steel Bridge-South Fork Skokomish River Valley Lat: 47°22′00″ Long: 123°16′45″	Vashon	Long, GGSOPW

What	Description	Where	Location	Age	Source
	mile north of the Steel Bridge crossing the gorge and extends south 3 miles; the winding South Fork gorge, which is 300 ft deep, crosses the channel several times indicating it was cut later than the functioning of the meltwater channel				
Recessional Meltwater Channel	Vashon recessional meltwater left the South Fork through 3 short channels through the hills; the channels combine in Flat Creek and the single channel extends south over an 850 ft col down Fir Creek into the Skokomish valley	Olympic National Forest	Flat Creek-South Fork Skokomish River Valley Lat: 47°22′00″ Long: 123°18′30″	Vashon	Long, GGSOPW
Kettles and Esker	The lowland drift plain in the Skokomish embayment is pitted with kettles, some as large as 75 ft deep and 300 ft across, occurring both singly and in groups; the drift is trenched and terraced by meltwater streams and built during the shrinkage of the Puget Lobe; a sinuous esker half a mile long and 50 ft high lies on the drift plain just north of the Dennie Ahl seed orchard	Olympic National Forest	Dennie Ahl Seed Orchard-South Fork Skokomish River Valley Lat: 47°23′00″ Long: 123°15′30″	Vashon	Long, GGSOPW
Bedrock Gorge	The South Fork Gorge is cut in basalt bedrock as much as 350 ft deep beneath the base of Vashon Puget recessional outwash sand and gravel and was produced by postglacial incision of the river on buried rock hills	Olympic National Forest	South Fork Skokomish River Valley Lat: 47°22′00″ Long: 123°16′45″	Post-glacial	Long, GGSOPW
Terraces	Postglacial incision of the river lowered the level of the lake in the South Fork; stream terraces flank the mountain valley of Le Bar Creek and are cut in the Vashon drift fill of the valley; they probably record the variations in the lake level	Olympic National Forest	Le Bar Creek-South Fork Skokomish River Valley Lat: 47°25′15″ Long: 123°20′30″	Post-glacial	Long, GGSOPW
Moraines	Moraines were deposited by the alpine ice within two miles of the Puget ice limit by the South Fork glacier;	Olympic National Forest	Cedar Creek-South Fork Skokomish River Valley Lat: 47°26′37″	Vashon	Long, GGSOPW

What	Description	Where	Location	Age	Source
	the outermost moraine lies 9.5 miles from the cirques at the valley head and across the mouth of Cedar Creek valley; the moraine rises 400 ft above the present river level and has a crestal altitude between 1,000-1,250 ft; the moraine has been breached by the river and road cutbanks expose basalt-sandstone till containing boulders up to 8 ft in diameter; on the downstream side the moraine grades into poorly sorted and poorly stratified boulder gravel which passes into sandy gravel outwash in which the river has cut a terrace for nearly two miles on the south side of the river; sediment in the terrace includes 150 ft of sandy gravel overlying 20-30 ft of massive to bedded clay, silt, and fine sand underlain by 100 ft of gravel which indicates a glacial lake formed when the Vashon Puget ice entered and dammed the valley		Long: 123°24′09″		
Glacial Lake	A lake with a surface elevation of approximately 900 ft was dammed by the outermost moraine from the above description; exposures of up to 20 ft of bedded clay and silt are seen near the base of the moraine and behind the moraine near the mouth of Church Creek; the lake beds are exposed to an altitude of 875 ft at which point they extend below the river and are covered by modern alluvium	Olympic National Forest	Cedar Creek-South Fork Skokomish River Valley Lat: 47°29′00″ Long: 123°25′00″	Vashon	Long, GGSOPW
Moraine	A smaller moraine lies just behind the outermost moraine from above; a wide moat 50 ft deep lies between them; the moraine has a crestal altitude between 1,000-1,100 ft; granitic stones lie on the moraine	Olympic National Forest	Cedar Creek-South Fork Skokomish River Valley Lat: 47°26′37″ Long: 123°24′10″	Vashon	Long, GGSOPW

What	Description	Where	Location	Age	Source
	surfaces, but are not mixed in with the morainal sediments; the erratics are thought to have been berg-rafted in a glacial lake dammed in the valley by the Puget Lobe				
Lateral Moraine	About a mile above Pine Creek the South Fork glacier built a lateral moraine 250 ft high across the hanging mouth of Church Creek, which lies 500 ft above the floor of the South Fork valley; the crest lies at an altitude between 1,200-1,300 ft and it is a rounded ridge a half mile long; road cuts reveal faceted and striated stones; Church Creek has cut through the moraine and incised a slotlike gorge 60-75 ft down into the underlying basalt bedrock	Olympic National Forest	Church Creek-South Fork Skokomish River Valley Lat: 47°27′33″ Long: 123°20′26″	Vashon	Long, GGSOPW
Moraine	The innermost terminal moraine in the South Fork Skokomish River lies 3 miles above the outermost one at Cedar Creek; the South Fork glacier reached 1,000 ft and was 5 miles long; on the downstream side the moraine grades into an outwash body 2 miles long that forms terrace segments along the south side of the valley	Olympic National Forest	Cedar Creek-South Fork Skokomish River Valley Lat: 47°26′22″ Long: 123°23′14″	Vashon	Long, GGSOPW
Morainal Debris	The glacier on Pine Creek advanced a little more than two miles from the cirque headwall and terminated near a 1,300 ft altitude, a mile away from the South Fork glacier; chaotic morainal debris holds in Pine Lake at an altitude of 1,750 ft and covers a mile long stretch of the valley floor below the lake; during the dry season the lake level is low and the outlet is dry and through the dam water seeps to form lower Pine Creek; during the wet season the lake level is high and drainage is from the surface	Olympic National Forest	Pine Creek-South Fork Skokomish River Valley Lat: 47°25′55″ Long: 123°28′35″	Vashon	Long, GGSOPW

What	Description	Where	Location	Age	Source
Puget Lobe Drift	Four miles north of Dow Mountain a small body of drift was exposed along the upper Lilliwaup Rd. to an altitude of 2,375 ft, which suggests that the Puget ice reached the north side of the mouth of the North Fork	Olympic National Forest	North Fork Skokomish River Valley Lat: 47°16′30″ Long: 123°14′00″	Salmon Springs	Long, GGSOPW
Striations	A saddle on the ridge between the North Fork and a branch of Washington Creek was overflowed by the North Fork Glacier; striations on rounded knobs of basalt are directed through the saddle	Olympic National Forest	Washington Creek-North Fork Skokomish River Valley Lat: 47°34′45″ Long: 123°11′00″	Salmon Springs	Long, GGSOPW
Lateral Moraines	Opposite the Brown Creek saddle on the north valley wall above mid-Lake Cushman are 2 short morainal ridges that were built along the lateral margin of the North Fork Glacier; the crests lie at a height of 2,000 ft; the larger outer moraine is about 800 ft long and 20-30 ft high; faceted and striated stones and several basalt blocks have diameters between 10-20 ft; 2 shallow depressions that contain water are between the ridges	Lake Cushman State Park	North Fork Skokomish River Valley Lat: 47°29′29″ Long: 123°14′41″	Evans Creek	Long, GGSOPW
Puget Lobe Till	Vashon Puget till occurs on Dow Mountain and the mountain slopes west and north of the Lake Cushman reservoir indicating that Puget ice reached at least as far upvalley as mid-Lake Cushman and extended across the lake and halfway up Cushman Hill	WA State Dept. of Natural Resources	Dow Mountain-North Fork Skokomish River Valley Lat: 47°24′30″ Long: 123°11′30″	Vashon	Long, GGSOPW
Puget Lobe Till	On Dow Mountain granite bearing drift occurs up to an altitude of 1,900 ft	WA State Dept. of Natural Resources	Dow Mountain-North Fork Skokomish River Valley Lat: 47°24′30″ Long: 123°11′30″	Vashon	Long, GGSOPW
End Moraine	A granite bearing segment of a Vashon end moraine lies at 1,750 ft on the east side of Cushman Hill 2.5 miles from Dow Mountain	WA State Dept. of Natural Resources	Dow Mountain-North Fork Skokomish River Valley Lat: 47°15′22″ Long: 123°28′22″	Vashon	Long, GGSOPW
Puget Lobe	On the north valley wall at	WA State	Dow Mountain-North	Vashon	Long,

What	Description	Where	Location	Age	Source
Till	points 6 miles north of Cushman Dam a Vashon till is exposed in cutbanks along the Mt. Ellinor Rd. up to an altitude of 1,750 ft	Dept. of Natural Resources	Fork Skokomish River Valley Lat: 47°29′30″ Long: 123°15′30″		GGSOPW
Lateral Moraine	The North Fork Skokomish glacier left a huge lateral morainal embankment in and across the Brown Creek saddle, which lies between the North and South Forks of the Skokomish River; artificial and natural exposures show the deposit is up to 350 ft thick; composed of local rock types – mainly fine-grained, hard basaltic rocks - striated and faceted surfaces are present on many boulders; the broad crest is strewn with many boulders and lies at 1,650 ft elevation at the lowest point in the saddle	Olympic National Forest	Brown Creek Saddle-North Fork Skokomish River Valley Lat: 47°26′00″ Long: 123°15′00″	Vashon	Long, SSVCIOM
Granite Erratics	No granite was found in the North Fork Skokomish Valley; granite erratics found on the east side of Big Creek up to 1,750 ft, but no granite was found on the opposite slope less than a mile away	WA State Dept. of Natural Resources	Big Creek-North Fork Skokomish River Valley Lat: 47°28′30″ Long: 123°12′00″	Vashon	Long, GGSOPW
Morainal Drift	Two well-defined morainal segments are located on a bench on the west side of Big Creek and were deposited by an alpine glacier; the outer moraine is 1,000 ft in length, 20-30 ft high, and the crest rises from an altitude of 1,975 ft in the northeast to 2,050 ft in the southwest; faceted and striated basalt stones are found in the moraines and several basalt boulders with diameters between 10 and 20 ft are located in them; two shallow depressions with water are between the moraines	WA State Dept. of Natural Resources	Big Creek-North Fork Skokomish River Valley Lat: 47°28′15″ Long: 123°12′53″	Vashon	Long, SSVCIOM
Granite Erratics	Farthest upvalley occurrence in the North Fork Skokomish River of granites is 7.5 miles west of Hood Canal at the Lake Cushman narrows	WA State Dept. of Natural Resources	Lake Cushman-North Fork Skokomish River Valley Lat: 47°27′15″ Long: 123°15′00″	Vashon	Long, GGSOPW

What	Description	Where	Location	Age	Source
	where Puget till overlies a thick deposit of laminated lake clays; the Puget Lobe dammed a lake in the valley when it entered and deposited clays which have till overlying them from where the ice advanced and deposited till over the lake beds				
Absence of Foreign Stones/ Merger of Glacial Ice	The merger of the North Fork alpine glacier and the Puget Ice is indicated by the abrupt absence of foreign stones beyond mid-Lake Cushman and the ice height on the valley walls	WA State Dept. of Natural Resources	Lake Cushman-North Fork Skokomish River Valley Lat: 47°27′15″ Long: 123°15′00″	Vashon	Long, GGSOPW
Moraine and Till	The North Fork Skokomish glacier deposited a terminal moraine over Puget till at mid-Lake Cushman; as the lake narrows clay-rich Puget till overlies laminated lake fines visible only during minimum reservoir storage; the Puget drift was overridden and deformed by an active valley glacier; till ~100 ft thick underlies an alpine terminal moraine and overlies the Puget till; the alpine till contains many smoothed, faceted, and striated basalt boulders and has no foreign stones; rounded basaltic knobs with larger striae and small grooves are seen above the moraine along the north shore of the lake and are probably from the moraine damming old Lake Cushman and explains why no granitic stones are found on the lakeward slope	WA State Dept. of Natural Resources	Lake Cushman-North Fork Skokomish River Valley Lat: 47°28′33″ Long: 123°15′00″	Vashon	Long, GGSOPW
Terminal Moraine	An alpine terminal moraine lies at Dead Horse Hill six miles behind the mid-Lake Cushman moraine; it is composed of huge angular boulders mostly of basalt and its hummocky surface is at 940 ft and rises 50 ft above the river	WA State Dept. of Natural Resources	Lake Cushman-North Fork Skokomish River Valley Lat: 47°30′09″ Long: 123°18′55″	Vashon	Long, GGSOPW

What	Description	Where	Location	Age	Source
Moraines	Small, fresh, well-defined moraines post-dating the late Fraser alpine moraines lie between altitudes of 4,800-5,200 ft on the north side of the ridge connecting Mounts Henderson and Skokomish; the till is fresh and the highest moraines are nonvegetated, consist of coarse angular rubble, and lie adjacent to small existing ice and snow bodies; outer moraines are sparsely to moderately vegetated and support some small conifers; the till and the altitudes indicate a recent deposition and suggest the moraines are neoglacial	Olympic National Park/ Olympic National Forest	Mts. Henderson and Skokomish-North Fork Skokomish River Valley Lat: 47°35′30″ Long: 123°18′25″	Neo-glacial	Long, GGSOPW
Alpine Glacier	A small glacial ice body lies on the north side of Mt. Skokomish (6,434 ft) at the head of the North Fork Skokomish River; the glacier lies between 5,500-6,000 ft, has crevasses, and is the only identifiable body of glacial ice remaining in the Skokomish drainage	Olympic National Park	Mt. Skokomish-North Fork Skokomish River Valley Lat: 47°34′00″ Long: 123°18′00″	Neo-glacial	Long, GGSOPW
Possible Alpine Glacier	On the north side of Mt. Henderson a snow bank fronted by an exceedingly youthful moraine with unstable slopes may conceal glacial ice	Olympic National Park	Mt. Henderson-North Fork Skokomish River Valley Lat: 47°35′14″ Long: 123°18′40″	Neo-glacial	Long, GGSOPW
Striations	Rounded basalt hillocks are covered in striations in a broad 2,100 ft saddle from the North Fork Skokomish Glacier	Olympic National Forest	Hamma Hamma River Valley Lat: 47°33′30″ Long: 123°11′30″	Salmon Springs	Long, GGEOPW
Striations	A basaltic till with well-striated stones is exposed in a roadcut in upper Washington Creek, near the junction with Jefferson Creek	Olympic National Forest	Washington Creek-Hamma Hamma River Valley Lat: 47°38′00″ Long: 122°07′30″	Salmon Springs	Long, GGEOPW
Alpine Till	An alpine basaltic till 10 ft thick containing well-striated stones is exposed in cutbanks along road No. 2469 just above its junction with road No. 2441 at Jefferson Creek; no granite is in the deposits	Olympic National Forest	Washington Creek-Hamma Hamma River Valley Lat: 47°32′00″ Long: 123°08′30″	Evans Creek	Long, SSVCIOM

What	Description	Where	Location	Age	Source
	at Washington Creek				
Alpine Till	A compact alpine till is exposed in road cutbanks in the Washington Creek valley indicating that a small glacial system occupied the valleys and these joined with a larger glacier descending Jefferson Creek valley; glacier smoothed surfaces are common along the valley walls up to 800-1,000 ft above the present stream and the postglacial incision has deepened the valley floors so little or no semblance of the broad glaciated floor remains	Olympic National Forest	Washington Creek-Hamma Hamma River Valley Lat: 47°32′00″ Long: 123°08′30″	Evans Creek	Long, SSVCIOM
Delta	A high delta lies on the south side of the mouth of the Hamma Hamma River; the top of the delta is at 300 ft, which is 80 ft higher than the level of Glacial Lake Hood (220 ft); foreset beds slope east at 28° so the source lay to the west; granitic stones are common; foreset beds can be up to 4 ft in thickness suggesting rapid deposition; the bedding has a graded aspect with a thin layer of sand at the base grading into coarse gravel followed by a rather sharp contact with the base of a fine layer of sand-the change is probably related to seasonal melting of an alpine glacier sending sediment down the river	River Mouth	Hamma Hamma River Valley Lat: 47°34′00″ Long: 123°02′30″		Long, GGEOPW and Long, SSVCIOM
Alpine Terminal Moraine	An alpine terminal moraine lies 2 miles above Cabin Creek on the Hamma Hamma River	Olympic National Forest	Hamma Hamma River Valley Lat: 47°35′58″ Long: 123°09′14″		Long, GGEOPW
Delta Slumping	The west side of the delta appears to have slumped post-glacially and left great masses of sediment in chaotic disarray on the flat floor of the Hamma Hamma River estuary; the slump extends 3,500 ft along the delta's backside, is 2,500 ft wide, and 150-200 ft thick; Long does not believe this is	River Mouth	Hamma Hamma River Valley Lat: 47°34′00″ Long: 123°02′30″	Vashon to Post-Glacial	Long, SSVCIOM

What	Description	Where	Location	Age	Source
	a slump as the sediments are characterized by intersecting ridges and deep depressions with steep sideslopes, but rather to lateral incision of the river as a mile above the delta the river has cut a 300 ft deep gorge in bedrock since the glacial recession; as the river would have incised laterally over the delta, the surface of the delta would have eroded from the top down and the stream would have carried the sediments away easily; a detached mass of ice could have filled the estuary so the deltaic sediments were deposited on it and then later dropped to the floor when the ice melted				
Arcuate Moraine Set	Whitehorse Creek is a minor tributary of the Hamma Hamma River and Lake of the Angels is drained by it; this lake is dammed by an arcuate moraine set at an altitude of 4,850 ft; there are 3 closely spaced moraines covered by heather	Olympic National Park/ Forest	Whitehorse Creek-Hamma Hamma River Valley Lat: 47°35′51″ Long: 123°16′17″	Constance	Long, NNOMW
Continental Drift/ Granite Erratics	Continental drift and granite erratics are exposed in road cutbanks on the west side of Waketikeh River Valley along Forest Road 2402 at an altitude of 2,625 ft	Olympic National Forest	Waketikeh River Valley Lat: 47°36′30″ Long: 123°03′30″	Salmon Springs	Long, GGEOPW
Granite Erratics	On the west slope of Waketikeh valley are granitic stones that lie above the Vashon deposits	Olympic National Forest	Waketikeh River Valley Lat: 47°36′30″ Long: 123°03′30″	Salmon Springs	Long, GGEOPW
Moraine Deposits	Morainal deposits with 6 foot diameter boulders are located at 1,850 ft on the west side of Waketikeh Creek valley where Kelly Road crosses the west branch of the creek	Olympic National Forest	Waketikeh River Valley Lat: 47°37′15″ Long: 123°02′24″	Vashon Stade	Long, GGEOPW
Continental Drift/ Granite Erratics	Continental drift and granite erratics are on top of Webb Mountain at 2,775 ft; it was overridden	Olympic National Forest	Webb Mountain Lat: 47°36′30″ Long: 123°01′30″	Salmon Springs	Long, GGEOPW
Granite Erratic	A 5-foot granite boulder lies at the upper Webb Mountain Road at 2,250 ft altitude	Olympic National Forest	Webb Mountain Lat: 47°36′30″ Long: 123°01′30″	Fraser	Long, GGEOPW
Continental	Continental drift is exposed	Olympic	Webb Mountain	Vashon	Long,

What	Description	Where	Location	Age	Source
Drift	in road cutbanks between 2,000-2,100 ft on Webb Mountain	National Forest	Lat: 47°36′30″ Long: 123°01′30″	Stade	GGEOPW
Continental Drift/ Granite Erratics	Continental drift and granite erratics are at the head of the South Fork Fulton Creek between 2,600 and 2,800 ft	Olympic National Forest	Fulton Creek Valley Lat: 47°37′00″ Long: 123°03′30″	Salmon Springs	Long, GGEOPW
Continental Drift/ Granite Erratics	Drift is exposed on the north side of the ridge facing the South Fork Fulton Creek 0.5 miles northwest of Webb Mountain up to an altitude of 2,950 ft	Olympic National Forest	Fulton Creek Valley Lat: 47°39′30″ Long: 123°01′30″	Salmon Springs	Long, GGEOPW
Erratics and Striated Stones	Erratics and striated basalt boulders are located up to an elevation of 2,400 ft on the north side of Fulton Creek	Olympic National Forest	Fulton Creek Valley Lat: 47°39′30″ Long: 123°01′30″	Vashon Stade	Long, GGEOPW
Puget Lobe Drift	A patch of Salmon Springs drift is located a mile east of North Rock between 2,600 and 2,800 ft	Olympic National Forest	North Rock-Divide between the Hamma Hamma and Duckabush Rivers Lat: 47°39′00″ Long: 123°03′15″	Salmon Springs	Long, SSVCIOM
Erratics	Erratics lie 200 ft higher at the same location above from Salmon Springs ice	Olympic National Forest	Mt. Jupiter Ridge-Duckabush River Valley Lat: 47°40′30″ Long: 123°03′30″	Salmon Springs	Long, GGEOPW
Terrace Remnants of the Drift Plain	Terrace remnants of the Puget Lowland drift plain have their best exposures on the south side of the river and extend 3.2 miles into the valley to an elevation of 450 ft	Olympic National Forest	Duckabush River Valley Lat: 47°42′30″ Long: 123°00′00″	Salmon Springs	Long, GGEOPW
Alpine Till	Till exposed in road cuts along the south side of the Duckabush River 2 miles from Hood Canal was deposited by an alpine glacier that extended beyond the mouth of the valley; the till lies just inside the Olympic National Forest boundary and it lies 400 ft above the valley floor at ~500 ft above sea level; the till is clay-rich, compact, brown, and composed mostly of basalt with many striated stones and no granite	Olympic National Forest	Duckabush River Valley Lat: 47°40′00″ Long: 122°56′30″	Evans Creek	Long, SSVCIOM
Erratics	Granite erratics are located on the east end of the Mt. Jupiter ridge at an elevation	Olympic National Forest	Mt. Jupiter Ridge-Duckabush River Valley	Vashon Stade	Long, GGEOPW

What	Description	Where	Location	Age	Source
	between 2,600 and 2,700 ft		Lat: 47°40′30″ Long: 123°03′30″		
Granite Erratics	Granite erratics are found up to 2,900 ft on the Mount Jupiter Trail (east end) along the drainage divide between the Duckabush and Dosewallips Rivers	Olympic National Forest	Drainage Divide of Dosewallips and Duckabush Rivers Lat: 47°44′30″ Long: 123°01′30″	Salmon Springs	Long, GGEOPW
Granite Erratics	Erratics as high as 3,450 ft are on the peak between Buck Mountain and Mt. Turner along the drainage divide between the Dosewallips and Big Quilcene Rivers	Olympic National Forest	Drainage Divide of Dosewallips and Big Quilcene Rivers Lat: 47°39′30″ Long: 122°56′00″	Salmon Springs	Long, GGEOPW
Alpine Glacier Extent, Striations, Breccia Erratics	About six miles above the mouth of the Dosewallips River the alpine glacier overflowed the broad 2,450-3,100 ft high saddle between the river and Rocky Brook and spilled through Rocky Brook valley; glacially striated basalt stones are observed in cutbanks along the upper Rocky Brook Road as high as 3,100 ft on the north valley wall and several large boulders (up to 35 ft across) of green volcanic breccia are there as well	Olympic National Forest	Rocky Brook-Dosewallips River Valley Lat: 47°48′30″ Long: 122°57′00″	Evans Creek	Long, SSVCIOM
Olympic Alpine Till	A compact alpine till occurs in lower Rocky Brook valley and is overlain in places by Vashon Puget drift	Olympic National Forest	Rocky Brook-Dosewallips River Valley Lat: 47°48′30″ Long: 122°57′00″	Evans Creek	Long, SSVCIOM
Granite Stones and Basalt Blocks	At the north side of the mouth of the Dosewallips River the Vashon glacier reached within 100 ft of the summit of Mt. Turner and left granite and basalt blocks	Olympic National Forest	Dosewallips River Valley Lat: 47°43′30″ Long: 123°03′00″	Vashon	Long, GGEOPW
Vashon Ice Limit Exposure	0.5 miles west of Mt. Turner on Jackson Creek Rd. a road cut exposes the Vashon ice limit; one mile west of Mt. Turner at the 2,000 ft saddle at the junction of Jackson Creek and Rocky Brook Roads, no evidence of Vashon ice exists	Olympic National Forest	Dosewallips River Valley Lat: 47°43′30″ Long: 123°03′30″	Vashon	Long, GGEOPW
Continental Till	One mile west of the previous site's saddle, a road cut exposes 25 ft of Puget till	Olympic National Forest	Dosewallips River Valley Lat: 47°43′30″	Vashon	Long, GGEOPW

What	Description	Where	Location	Age	Source
	where the Vashon glacier terminated		Long: 123°03′30″		
Glacial Lake Sediments	Vashon ice dammed a lake 2 miles long in Rocky Brook and road cut exposures show stratified sand and gravel with clay and silt lenses; granitic stones decrease in percentage from 5% at the downvalley end to none at the upvalley end	Olympic National Forest	Rocky Brook-Dosewallips River Valley Lat: 47°42′00″ Long: 123°04′30″	Vashon	Long, GGEOPW
Granite Boulders	Granite boulders lie at 3,400 ft altitude on the east face of Buck Mountain marking the upper limit of Vashon Puget ice	Olympic National Forest	Buck Mountain-Dosewallips River Valley Lat: 47°45′30″ Long: 122°56′45″	Vashon	Long, GGEOPW
Moraine	Constance Lake drains into the Dosewallips River and the lake appears to be dammed in part by a moraine and in part by a bedrock barrier at 4,650 ft	Olympic National Park	Constance Creek-Dosewallips River Valley Lat: 47°44′57″ Long: 123°07′57″	Royal	Long, NNOMW
Protalus Rampart Ridges and Moraines	On upper Constance Creek just above Constance Lake vegetated protalus rampart ridges parallel cliff bases at almost right angles to moraines at 4,650 ft	Olympic National Park	Constance Creek-Dosewallips River Valley Lat: 47°45′09″ Long: 123°08′28″	Constance	Long, NNOMW
Moraine	A moraine lies at an altitude of 5,750 ft on the northeast side of Mt. Mystery, it is triple crested, and 20-30 subtle recessional moraines lie behind the large moraine	Olympic National Park	Dosewallips River Valley Lat: 47°48′25″ Long: 123°13′27″	Deception	Long, NNOMW
End Moraine	A blocky end moraine at an altitude of 5,500 ft crosses the valley floor in upper Constance Creek from Debris Glacier	Olympic National Park	Constance Creek-Dosewallips River Valley Lat: 47°45′47″ Long: 123°08′18″	Deception	Long, NNOMW
Basaltic Till	A basaltic till with a cement hard enough so the till stands in cliffs 20 ft high with scattered surface granite stones is exposed in the Big Quilcene River Valley one-half mile above Tunnel Creek and in road cutbanks on the north wall of Tunnel Creek for a distance two miles above the Big Quilcene River; granite is only found a very short distance up this valley	Olympic National Forest	Tunnel Creek-Big Quilcene River Valley Lat: 47°48′00″ Long: 122°58′30″	Evans Creek	Long, GGEOPW and Long, SSVCIOM
Alpine	Alpine drift lies at the mouth	Olympic	Tunnel Creek-Big	Evans	Long,

What	Description	Where	Location	Age	Source
Drift	of Tunnel Creek valley on the north side and reaches a height of 1,700 ft; the drift consists of basalt in boulder-gravel form with striated stones and overlies 10-15 ft of laminated glacial lake clays and silts which in turn rest upon basalt bedrock; drift is probably a part of an end moraine deposited by Evans Creek ice whose eastern limit is unknown because the terminal deposits are buried by Vashon drift	National Forest	Quilcene River Valley Lat: 47°48′00″ Long: 122°58′30″	Creek	GGEOPW
Alpine Drift and Stratified Sediment	A formless deposit of alpine till and stratified sediment is exposed in river cutbanks on the north side of the valley; the deposit is underlain by bedded glacial lake fines; interpreted as the deposit of a lake dammed by an alpine terminal moraine subsequently buried by Vashon drift	Olympic National Forest	Big Quilcene River Valley Lat: 47°51′00″ Long: 122°58′30″	Evans Creek	Long, GGEOPW
Puget Drift	Puget drift containing many large granite boulders is located on lower Tunnel Creek Road 2767 just before Deserter Creek at an altitude of 1,600 ft; no deposits are found west of Deserter Creek which must delimit the westward extent of Puget ice in the lower Big Quilcene River valley	Olympic National Forest	Big Quilcene River Valley Lat: 47°47′30″ Long: 122°58′30″	Fraser	Long, GGEOPW
Granite Erratics/ Puget Ice Extent	Abundant granite occurs upvalley to the mouth of Tunnel Creek, but only one granite stone was found as far as a quarter of a mile inside the valley mouth; indicates a possible merging of the alpine and continental ice in lower Tunnel Creek	Olympic National Forest	Big Quilcene River Valley Lat: 47°47′30″ Long: 122°58′30″	Fraser	Long, GGEOPW
Basaltic Till	A compact basaltic till with striated stones is exposed at several places in road cutbanks along the north wall of the Tunnel Creek valley	Olympic National Forest	Big Quilcene River Valley Lat: 47°47′30″ Long: 122°58′30″	Fraser	Long, GGEOPW
No Glacial Deposits	The Tunnel Creek and Big Quilcene glaciers did not merge because the two mile	Olympic National Forest	Big Quilcene River Valley Lat: 47°47′30″ to	Fraser	Long, GGEOPW

What	Description	Where	Location	Age	Source
	stretch of the Big Quilcene valley between Tunnel and Townsend Creek is V-shaped in cross profile and appears to be a river-made landform		47°51′00″ Long: 122°58′30″		
Granite Erratics	Granite erratics were found over all parts of the southern half of the Quilcene Range which has a maximum elevation of 3,269 ft	Olympic National Forest	Quilcene Range-Big Quilcene River Valley Lat: 47°48′00″ Long: 122°58′00″	Fraser	Long, GGEOPW
Granite Erratics	Granite erratics occur to a height of at least 3,400 ft on the south end of Green Mountain indicating that Puget ice was 300-500 ft thick over the Quilcene Range south of Green Mountain	Olympic National Forest	Green Mountain-Big Quilcene River Valley Lat: 47°50′30″ Long: 122°58′30″		Long, GGEOPW
Granite Float Boulders	The Puget Lobe dammed a large glacial lake in the drainage of the Big Quilcene River and fingers of it reached into Tunnel and Townsend Creek valleys; granite float boulders were found up to 2,700 ft in upper Townsend Creek	Olympic National Forest	Townsend and Tunnel Creeks-Big Quilcene River Valley Lat: 47°51′00″ Long: 122°58′30″	Fraser	Long, GGEOPW
Glacial Lake Deposits	Glacial lake deposits occur in Townsend Creek from a point above Singing Creek downvalley to Forest Road 272; the deposits consist of bedded or massive clay and silt overlain by stratified basaltic sand and pebble-cobble gravel	Olympic National Forest	Townsend Creek-Big Quilcene River Valley Lat: 47°51′00″ Long: 122°58′30″	Fraser	Long, GGEOPW
End Moraine	The terminal position of Townsend Glacier is marked by an alpine end moraine composed of large volcanic blocks and rubble forming knobs and intersecting ridges enclosing depressions; the moraine covers a mile stretch of the valley floor and was deposited by a glacier 3 miles long that reached an elevation of 2,650 ft	Olympic National Forest	Big Quilcene River Valley Lat: 47°51′23″ Long: 123°00′35″	Fraser	Long, GGEOPW
Glacial Sediments	A sequence of glacial sediments exposed in cutbanks along the lower Pipeline Rd. near the mouth of the Big Quilcene valley include: a lower unit of		Big Quilcene River Valley Lat: 47°46′00″ Long: 122°51′30″	Fraser	Long, GGEOPW

What	Description	Where	Location	Age	Source
	massive-laminated clay and silt 20 ft thick, a middle unit of gray clay-rich till about 10 ft thick, and an upper unit of bedded sand and gravel at least 30 ft thick; the lower unit was deposited by a lake dammed in the valley by the Puget Lobe, the middle unit was deposited by Puget ice advancing up the valley as it contains granitic stones and striated basalts, and the upper unit is alpine and continental outwash deposited during the retreat of the Puget ice				
Glacial Sediment	At the mouth of Penny Creek by the U.S. Fish Hatchery, a borrow pit exposed more than 100 ft of glacial sediment that has bedding in the gravels with a dip lying at right angles to the plane surface of the beds with the dip in the same direction as the flow of Penny Creek; when Puget ice blocked the valley drainage both the Big and Little Quilcene Rivers used Penny Creek as an outlet and the crossbedding and horizontal bedding in the sediments show this	Olympic National Forest	Penny Creek-Big Quilcene River Valley Lat: 47°49′30″ Long: 122°55′00″	Fraser	Long, GGEOPW
End Moraine	A moraine of late Fraser age is found blocking the mouth of the South Branch of Tunnel Creek; drift comprising the moraine is exposed in a slump beside Tunnel Creek and the sediments are unweathered, gray, and composed of non-sorted volcanic debris loosely held in a sandy matrix	Olympic National Forest	South Branch of Tunnel Creek-Big Quilcene River Valley Lat: 47°47′22″ Long: 123°01′46″	Late Fraser	Long, GGEOPW
End Moraine	A forested ridge in the valley of the South Branch of Tunnel Creek could be a terminal moraine at an altitude near 2,700 ft at a point 3.25 miles from the headwall drainage divide; above the moraine the stream is not cut into bedrock and	Olympic National Forest	South Branch of Tunnel Creek-Big Quilcene River Valley Lat: 47°46′42″ Long: 123°03′58″	Fraser	Long, GGEOPW

What	Description	Where	Location	Age	Source
	has rock knobs with smooth surfaces and rounded outlines while below it is a box-like gorge with steep rock sides				
Terminal Moraine	A ridge segment of a terminal moraine is located on the north side of the Big Quilcene River 2 miles above Townsend Creek; the crest of the moraine lies at 2,100 ft and under it is 20 ft of evenly laminated yellowish-brown clay interpreted as the deposit of a lake dammed by the moraine	Olympic National Forest	Big Quilcene River Valley Lat: 47°49′34″ Long: 123°01′12″	Fraser	Long, GGEOPW
Terminal Moraines	On upper Townsend Creek is a completely preserved, bouldery moraine that crosses the valley and dams Sink Lake; the crest reaches a height of 3,075 ft and lies 200 ft above its outside base; a second moraine lies just behind the outer one and both moraines lie within 2 miles of cirque headwalls on Welch Peaks	Olympic National Forest	Townsend Creek-Big Quilcene River Valley Lat: 47°51′32″ Long: 123°01′13″	Fraser	Long, GGEOPW
Moraine	In upper Tunnel Creek a densely forested moraine lies at an altitude of 4,050 ft and dams a small lake; within 2 miles of cirque headwalls	Olympic National Forest	Tunnel Creek-Big Quilcene River Valley Lat: 47°50′00″ Long: 123°04′00″	Late Fraser	Long, GGEOPW
Moraine	A bouldery moraine supports old-growth conifers and lies at an altitude of 4,400 ft in the valley of the South Branch of Tunnel Creek; it lies within 2 miles of cirque headwalls	Olympic National Forest	South Branch of Tunnel Creek-Big Quilcene River Valley Lat: 47°47′30″ Long: 123°04′00″	Fraser	Long, GGEOPW
Granite Erratics	Erratics are found up to 3,450 ft on the northeast ridge of Buck Mountain	Olympic National Forest	Buck Mountain-Big Quilcene River Valley Lat: 47°45′30″ Long: 122°56′30″	Vashon	Long, GGEOPW
Vashon Puget Lobe Extent	Vashon Puget Lobe overrode Walker Mountain and advanced 4 miles into the Big Quilcene River valley	Olympic National Forest	Big Quilcene River Valley Lat: 47°47′30″ Long: 122°57′00″	Vashon	Long, GGEOPW
Merging of Alpine and Puget ice	An absence of erratics above Tunnel Creek indicates a possible merging of alpine and Puget ice	Olympic National Forest	Big Quilcene River Valley Lat: 47°47′30″ Long: 122°58′30″	Vashon	Long, GGEOPW
Granite Erratics	Granite erratics are in the lower Big Quilcene drainage	Olympic National	Big Quilcene River Valley	Vashon	Long, GGEOP

What	Description	Where	Location	Age	Source
	from the presence of the Puget Lobe: i) northeast ridge of Buck Mountain, 3,400 ft; ii) top of Mt. Walker, 2,804 ft; iii) Big Quilcene Lookout, 3,250 ft; iv) Rocky Brook Pass, 2,800 ft; v) log skid road a mile north of Rocky Brook Pass, 3,175 ft; vi) Deserter Creek, 1,600 ft; vii) Townsend Creek at road crossing, 2,300 ft; viii) south end of Green Mountain, 3,400 ft; ix) east flank of Green Mountain, 3,450 ft; x) south end of Mt. Zion ridge, 3,450 ft; xi) north end of Mt. Zion ridge, 3,550 ft	Forest	Lat: 47°47′30″ to 47°51′30″ Long: 122°58′30″ to 122°51′30″		W
Terminal Deposits of Puget Lobe	Terminal deposits of the Puget Lobe consisting of Vashon drift composed of deformed lake sediments and till reaching a height of 2,300 ft on the west valley wall of Townsend Creek is exposed in cutbanks on Townsend Creek by Forest Service Road 272	Olympic National Forest	Townsend Creek-Big Quilcene River Valley Lat: 47°50′30″ Long: 122°58′30″	Vashon	Long, GGEOPW
Glacial Sediment Sequence	A sequence of glacial sediments exposed in high cutbanks along the lower Pipeline Road near the mouth of the Big Quilcene River valley includes: a. a lower unit of massive to laminated clay and silt about 20 ft thick b. a middle unit of gray clay-rich till about 10 ft thick c. an upper unit of bedded sand and gravel at least 30 ft thick The underlying unit is distorted in places and interpreted to have been deposited in a lake dammed in the valley by the advancing Puget Lobe; the middle unit is Puget till containing granitic rock types and many well-striated basaltic stones deposited by Vashon ice that pushed up	Olympic National Forest	Big Quilcene River Valley Lat: 47°47′00″ Long: 122°52′00″	Vashon	Long, SSVCIOM

What	Description	Where	Location	Age	Source
	the valley and overrode the lake beds; the upper unit is a local alpine outwash deposited after the retreat of Vashon Puget ice from the valley				
Alpine Outwash	Below the mouth of Tunnel Creek the outwash contains granitic stones that were derived from Vashon recessional drift in the lower Big Quilcene River valley, but beyond the Vashon ice limit in lower Tunnel Creek no foreign stones were found in the alpine outwash	Olympic National Forest	Tunnel Creek-Big Quilcene River Valley Lat: 47°48′30″ Long: 122°58′30″	Vashon	Long, SSVCIOM
Bedrock Gorge	Below the mouth of Tunnel Creek, the Big Quilcene River has cut a 250 ft deep gorge in basalt bedrock beneath the Vashon Puget drift; as the Puget Lobe retreated, the ice stood in the Big Quilcene embayment which is defined by the Quilcene Range to the west, Mt. Walker on the east, and Walker Pass and Buck Mountain on the south; due to the ice tongue, the river became marginal around it and the former channel filled with drift and the river incised the bedrock on which it was now stuck; the gorge entrance is just upstream from Mile And A Half Creek and the former channel is a little less than 100 ft above the river level at the gorge		Big Quilcene River Valley Lat: 47°51′45″ Long: 123°02′30″	Vashon to Post-Glacial	Long, SSVCIOM
Gravel Body	A long gravel slope at the mouth of the Big Quilcene River valley descends from an altitude of 260 ft to tidewater at Quilcene Bay; delta foreset bedding exists in the gravel; a cutbank by U.S. Highway 101 just north of the confluence of Penny Creek with the Big Quilcene River shows the internal structure with the gravel exposed to a depth of 65 ft and the top 30 ft appearing to		Big Quilcene River Valley Lat: 47°51′45″ Long: 123°02′30″	Vashon to Post-Glacial	Long, SSVCIOM

What	Description	Where	Location	Age	Source
	be topset beds laid down when the river flowed into a glacial lake (these foresets consist chiefly of boulders); Glacial Lake Hood had two levels-220 ft and 120 ft-and the 165 ft altitude of the foreset beds does not correlate-perhaps a separate, smaller glacial lake was here; the lower foreset beds consist of coarser sediment (pebble-cobble size) and have ~5% northern origin stones so the conditions at deposition of the two foreset groups are different				
Moraine	A cirque on the northeast side of Welch Peaks is the source of Townsend Creek and has a small end moraine 30 ft high that is breached and supports a dense forest; it is at 5,400 ft in altitude	Olympic National Forest	Townsend Creek-Big Quilcene River Valley Lat: 47°51′16″ Long: 123°03′17″	Royal	Long, NNOMW
Glacial Extent	Abundant surface basalt boulders are located at an altitude of 5,150 ft near the entrance to the V-shaped gorge cut in bedrock by the South Fork of the Big Quilcene River and this likely marks the ice extent in this valley	Olympic National Forest	Big Quilcene River Valley Lat: 47°46′30″ Long: 123°05′00″	Royal	Long, NNOMW
End Moraine	An end moraine composed of angular basalt boulders up to 5 ft in diameter lies at an altitude of 4,050 ft and dams a shallow lake on the North Fork of Tunnel Creek	Olympic National Forest	North Fork of Tunnel Creek-Big Quilcene River Valley Lat: 47°46′45″ Long: 123°06′11″	Royal	Long, NNOMW
End Moraine	A densely vegetated end moraine composed of huge basalt blocks and rubble encloses a large depression on the valley floor at an altitude of 4,400 ft on the South Fork of Tunnel Creek	Olympic National Forest	South Fork of Tunnel Creek-Big Quilcene River Valley Lat: 47°48′08″ Long: 123°06′08″	Royal	Long, NNOMW
Moraine-like Ridges	At mid-lake on Lower Charlia Lake on Mt. Constance lie 3-4 short, very bouldery ridges which may mark the terminal position of the glacier; the ridges dip beneath the lake which lies at an altitude of 5,450 ft and	Olympic National Forest	North Fork of Tunnel Creek-Big Quilcene River Valley Lat: 47°48′02″ Long: 123°07′34″	Royal	Long, NNOMW

What	Description	Where	Location	Age	Source
	drains into the North Fork of Tunnel Creek				
Moraine	A second moraine lies behind the previous deposit in this valley of Royal age; it is completely preserved, rises 100 ft above its base, sparsely vegetated, and lies at 5,500 ft in elevation	Olympic National Forest	Townsend Creek-Big Quilcene River Valley Lat: 47°51′12″ Long: 123°03′18″	Constance	Long, NNOMW
Terminal Moraines	Above upper Charlia Lake a northeast facing cirque contains a broad, multiple ridged terminal moraine that dams the lake at 5,700 ft	Olympic National Forest	North Fork of Tunnel Creek-Big Quilcene River Valley Lat: 47°48′02″ Long: 123°07′47″	Constance	Long, NNOMW
Moraine	The South Branch of Tunnel Creek has a mass of hummocky morainal debris 0.75 miles from the head of the valley which appears to be a moraine	Olympic National Forest	South Fork of Tunnel Creek-Big Quilcene River Valley Lat: 47°48′01″ Long: 123°06′15″	Constance	Long, NNOMW
Moraine	An adjacent cirque 1,500 ft east of the above moraine has an unbreached arcuate moraine composed of boulders up to 50 ft in diameter on its lip at an altitude of 4,750 ft; it supports conifers where a little soil has developed	Olympic National Forest	South Fork of Tunnel Creek-Big Quilcene River Valley Lat: 47°48′15″ Long: 123°06′35″	Constance	Long, NNOMW
Moraine	Above upper Charlia Lake a northeast facing cirque contains a very fresh moraine just beyond the valley headwall that is composed of unstable basaltic debris at 6,300 ft	Olympic National Forest	North Fork of Tunnel Creek-Big Quilcene River Valley Lat: 47°47′47″ Long: 123°07′56″	Deception	Long, NNOMW
Moraines	A massive end moraine dams a lake below Constance Glacier at an altitude of 5,200 ft; it is triple crested and supports vegetation on the outside slope, but the inner slope is barren; 3 fresh moraines 3-6 ft high lie right at the terminus of the glacier	Olympic National Forest	North Fork of Tunnel Creek-Big Quilcene River Valley Lat: 47°46′49″ Long: 123°07′17″	Deception	Long, NNOMW
Terminal Moraine of Puget ice	The Puget Lobe pushed 2.5 miles into the Little Quilcene valley and terminated along Deadfall Creek leaving a terminal moraine which forms a continuous gravel ridge on the northwest slope for 1 mile; it has a rounded crest 75-100 ft high rising	Olympic National Forest	Deadfall Creek-Little Quilcene River Valley Lat: 47°53′10″ Long: 122°58′46″	Fraser	Long, GGEOPW

What	Description	Where	Location	Age	Source
	from an altitude of 1,700 ft beside the river to 2,500 ft at the upper end; exposures at Deadfall Creek show that the moraine has stratified sediment with bedding parallel to the slope; a road cutbank at the lower end shows a compact, clay rich gray till with faceted and striated stones; sediment is sand and pebble to boulder gravel with erratic stones and a few large granite boulders; several large kettles exist on the surface				
Glacial Lake	The Puget Lobe dammed a lake in the valley and the sediments deposited are up to 150 ft thick and composed of clay, silt, sand, and pebble gravel which is mostly of local basaltic rock material and a small amount of granite	Olympic National Forest	Little Quilcene River Valley Lat: 47°53′30″ Long: 123°01′30″	Fraser	Long, GGEOPW
Granite Erratics	North of Deadfall Creek continental ice rose high enough in Gold Creek to spill over Bon Jon Pass at 2,975 ft and into the Little Quilcene River; the granite distribution indicates ice was barely 300 ft thick over it	Olympic National Forest	Little Quilcene River Valley Lat: 47°55′30″ Long: 123°00′30″	Fraser	Long, GGEOPW
Continental Drift	The 3,100 ft col a mile east of Bon Jon pass contains continental drift up to 350 ft above it on the south end of Mt. Zion ridge	Olympic National Forest	Little Quilcene River Valley Lat: 47°55′30″ Long: 122°59′00″	Fraser	Long, GGEOPW
Granite Erratic	The highest granite erratic was found at an altitude of 3,550 ft on the northwest projecting ridge of Mt. Zion at the point where the ice sheet turned with the Puget Lobe pushing south into the Puget Lowland and the Juan de Fuca Lobe pushing west to the Pacific Ocean	Olympic National Forest	Mt. Zion-Little Quilcene River Valley Lat: 47°58′00″ Long: 123°00′30″	Fraser	Long, GGEOPW
Terminal Position of Alpine Glacier	A short glacier two miles long sourced in two cirques high on the east side of Mt. Townsend descended the Little Quilcene River valley and reached 2,700 ft altitude;	Olympic National Forest	Little Quilcene River Valley Lat: 47°52′58″ Long: 122°01′37″	Vashon	Long, SSVCIOM

What	Description	Where	Location	Age	Source
	the terminal position of the glacier was just below the junction of Forest Roads No. 2812 and 2812B, where till containing faceted and striated basalt and sandstone clasts of pebble to boulder size is exposed				
Alpine Outwash Terrace and U-Shaped Valley	A flat-topped terrace segment representing outwash debris is 50 ft above the present river grade on the north valley wall 100 yards below the terminal position of the glacier from above; the uppermost 10 ft is compact and hard due to the concentration of clay minerals in the upper few feet and the valley above the terrace is U-shaped	Olympic National Forest	Little Quilcene River Valley Lat: 47°47′30″ Long: 122°52′00″	Vashon	Long, SSVCIOM
Moraine	A well-formed arcuate moraine lies within half a mile of the northeastern cirque's headwall at a 5,000 ft altitude on Mt. Townsend	Olympic National Forest	Mt. Townsend-Little Quilcene River Valley Lat: 47°52′14″ Long: 123°03′03″	Royal	Long, GGEOPW & NNOMW
Glacial Lake	The retreat of the Puget Lobe led to the formation of Glacial Lake Hood, a long water body that occupied the Hood Canal trough and discharged to Case Inlet at North Bay by a channel across the gravel plain at the head of the northeastern arm of Hood Canal; the outlet channel is 60 ft deep and at the highest point lies 220 ft above sea level, which indicates the surface altitude of the lake; deltas were built into the lake by the Olympic streams		Hood Canal-Puget Sound	Vashon	Long, SSVCIOM
Moraines	Valley glaciers from Copper and Silver Creeks joined and deposited a terminal moraine on the east wall of the Dungeness River valley; 2 lateral moraines are along the ridge between the creeks	Olympic National Forest	Silver and Copper Creeks-Dungeness River Valley Lat: 47°53′57″ Long: 123°06′35″	Evans Creek Stade	Long, GNNOP
Alpine Till	0.5 miles beyond Silver Creek bridge on the upper road switchback a cutbank 25 ft high has alpine till	Olympic National Forest	Silver Creek-Dungeness River Valley Lat: 47°53′30″	Evans Creek Stade	Long, GNNOP

What	Description	Where	Location	Age	Source
	overlying slope wash; granite boulders on top of the till are from continental ice		Long: 123°06′00″		
Basalt Boulders	Boulders at 2,800 ft at Silver Creek bridge from the terminal position of pre-Vashon glaciers	Olympic National Forest	Silver Creek-Dungeness River Valley Lat: 47°53′30″ Long: 123°06′00″	Pre-Vashon Stade	Long, GNNOP
Former Glacial Lake	Behind moraine from Silver and Copper Creeks a landslide exposed ~25 ft of horizontally bedded sand and silt from water ponded behind the moraine	Olympic National Forest	Silver and Copper Creeks-Dungeness River Valley Lat: 47°53′30″ Long: 123°06′00″	Evans Creek Stade	Long, GNNOP
Alpine Outwash	Readvance of alpine glaciers left outwash in an alpine lake from lowland ice which existed at 3,250 ft inside the mouths of Silver and Copper Creeks	Olympic National Forest	Silver and Copper Creeks-Dungeness River Valley Lat: 47°53′30″ Long: 123°06′00″		Long, GNNOP
Paired Terraces	Terraces represent the outwash from Copper and Silver Creeks that was deposited in the lake dammed in the Dungeness Valley by the ice sheet	Olympic National Forest	Dungeness River Valley Lat: 47°53′30″ Long: 123°06′00″		Long, GNNOP
Moraine	Moraine in Silver Creek valley at 3,700 ft	Olympic National Forest	Silver Creek-Dungeness River Valley Lat: 47°52′30″ Long: 123°04′51″		Long, GNNOP
End Moraine	Ridge segment of an end moraine lies at the west valley wall of the Dungeness River just below the mouth of Royal Creek; crest is 600 ft above river and roadcuts exist in it	Olympic National Forest	Dungeness River Valley Lat: 47°52′42″ Long: 123°08′03″	Evans Creek Stade	Long, GNNOP
Glacial Extent	Dungeness Glacier likely flowed another mile or so downvalley from previous deposit as below Silver Creek the valley narrows and does not have features of alpine glaciers	Olympic National Forest	Dungeness River Valley Lat: 47°52′30″ Long: 123°09′00″		Long, GNNOP
Alpine Till and Glacio-lacustrine Sediments	A mudslide one mile above and on the east side of Royal Creek exposed alpine till overlying glaciolacustrine sediments; the lacustrine and till layers are ~25 ft thick	Olympic National Park	Dungeness River Valley Lat: 47°53′30″ Long: 123°11′30″		Long, GNNOP
Bouldery Outwash Valley	The outwash train has been channeled by the river into long ridges up to 10 ft high	Olympic National Park	Dungeness River Valley Lat: 47°53′30″		Long, GNNOP

What	Description	Where	Location	Age	Source
Train	occurs below the previous deposit and extends to mouth of Royal Creek		Long: 123°11′30″		
Moraine	Royal Lake, off of Royal Creek, is dammed by a moraine at the south end	Olympic National Park	Royal Creek-Dungeness River Valley Lat: 47°46′30″ Long: 123°12′00″		Long, GNNOP
Moraine	Moraine from a late readvance or standstill of the Dungeness glacier in Home Creek valley is 2 miles downstream from the head of the valley	Olympic National Forest/ Park	Home Creek-Dungeness River Valley Lat: 47°42′30″ Long: 123°09′30″		Long, GNNOP
Alpine Ice Extent	In the Dungeness River the alpine glacier seems to have extended at least as far as the lower part of the valley, but the extent of glaciation has been obscured by an overlap of Vashon continental drift	Olympic National Forest	Dungeness River Valley Lat: 47°54′15″ Long: 123°06′25″	Evans Creek	Long, SSVCIOM
Glacial Erratics	Granite erratics on Mt. Zion up to 3,550 ft elevation	Olympic National Forest	Mt. Zion-Dungeness River Valley Lat: 47°55′30″ Long: 123°00′30″	Vashon	Long, GGNOP
Glacial Erratics in the Dungeness River Valley	a. Bon Jon Pass; 3,200 ft b. South end of Mt. Zion Ridge; 3,450 ft c. East side of Gold Creek on Mt. Zion trail; 3,400 ft d. North end of Mt. Zion ridge; 3,550 ft e. Mid-section of Sleepy Hollow Creek on west wall; 3,200 ft f. Ridge of Maynard Peak between Skookum and Cougar Creeks; 3,550 ft g. Dungeness River at Mueller Creek; 2,500 ft h. Camp Tony on Gray Wolf River; 1,800 ft i. Upper Slab Camp Creek near Deer Ridge; 3,550 ft	Olympic National Forest	Dungeness River Valley Lat: 47°48′30″ Long: 123°08′30″		Long, GNNOP
Till, Outwash, and Erratics	Upper Gold Creek valley has thick sandy gravel till and outwash with smoothed rock bosses	Olympic National Forest	Gold Creek-Dungeness River Valley Lat: 47°54′30″-47°57′00″ Long:123°00′30″-123°03′00″	Vashon	Long, GNNOP
Granite-bearing Continental	Extends upvalley in the Dungeness as far as Mueller Creek at bridge across river;	Olympic National Forest	Mueller Creek-Dungeness River Valley	Vashon	Long, GNNOP

What	Description	Where	Location	Age	Source
Drift	Marks terminal position of ice sheet in valley		Lat: 47°52′30″ Long: 123°08′00″		
Bedded Silts and Clays	Bedded silts and clays underlie the drift at Mueller Creek and was deposited by a glacial lake dammed in the Dungeness Valley by the ice sheet	Olympic National Forest	Mueller Creek-Dungeness River Valley Lat: 47°52′30″ Long: 123°08′00″	Vashon	Long, GNNOP
Granitic Stones	Scattered, iceberg rafted stones were deposited by a lake inside mouth of Royal Creek Valley to an altitude of 3,150 ft; a single boulder lies in the river valley above Royal Creek at 2,850 ft	Olympic National Forest & Olympic National Park	Mueller Creek to maximum altitude in Royal Creek Valley-Dungeness River Valley Lat: 47°52′30″ Long: 123°08′00″ - 123°10′30″	Vashon	Long, GNNOP
Granite Erratics	Granite was found as float to a height of 3,350 ft on the east valley wall of Royal Creek opposite of Tyler Peak; indicates that the surface of the Dungeness glacial lake was near 3,400 ft	Olympic National Forest & Olympic National Park	Royal Creek-Dungeness River Valley Lat: 47°52′30″ Long: 123°09′00″	Vashon	Long, GNNOP
Terminal Moraine	A terminal moraine lies 1.5 miles below the cirque headwall for Royal Glacier in Royal Basin at an altitude of 5,050 ft; vegetation changes on both sides of the moraine as well as the soil with a wet meadow below the ice limit and drier, terrain behind it; bouldery lateral moraines descend to the terminal and Royal Lake is dammed at the southern end by it	Olympic National Park	Royal Creek-Dungeness River Valley Lat: 47°49′51″ Long: 123°12′34″	Royal	Long, NNOMW
Terminal Moraine	A terminal moraine composed of angular basalt blocks up to 20 ft in diameter lies 2 miles downstream from the valley head at an altitude of 3,900 ft	Olympic National Forest/ Park	Home Creek-Dungeness River Valley Lat: 47°48′00″ Long: 123°09′33″	Royal	Long, NNOMW
Morainal Deposit	Sleepy Hollow Creek on the north side of Mt. Townsend has a hummocky morainal deposit at its head; drainage is mainly subsurface and the creek issues from the toe of the deposit at 4,700 ft	Olympic National Forest	Sleepy Hollow Creek-Dungeness River Valley Lat: 47°52′53″ Long: 123°04′51″	Royal	Long, NNOMW
Moraines	A moraine composed of huge mafic volcanic blocks and rubble dams Home Lake at an altitude of 5,300 ft and	Olympic National Forest/ Park	Home Creek-Dungeness River Valley Lat: 47°46′18″	Constance	Long, NNOMW

What	Description	Where	Location	Age	Source
	lies along the base of the west wall of the Mt. Constance massif; this wall also has 5-7 long, sinuous ridges of debris that connect with arcuate moraines-these morainal ridges are superimposed and rise to heights of 250 ft, are a mile in length, and lie up to 2,000 ft beyond the valley wall		Long: 123°09′48″		
Moraines	At the downvalley end of Home Creek the long parallel moraines from above form morainal loops and lie at an elevation of 4,100 ft; a second moraine loop hits the first and this moraine comes from a cirque between the Mt. Constance massif and Warrior Peak	Olympic National Forest/ Park	Home Creek-Dungeness River Valley Lat: 47°47′14″ Long: 123°09′06″	Constance	Long, NNOMW
Lateral Moraine	Royal Glacier deposited a continuous moraine along its northwest side and it is composed of volcanic boulders and a little slate; in places it is covered by a thick turf; up to 7 short recessional moraine loops descend from the inside of the lateral moraine with the lowest at an altitude of 5,400 ft	Olympic National Park	Royal Creek-Dungeness River Valley Lat: 47°49′03″ Long: 123°13′12″	Constance	Long, NNOMW
Moraines	Two moraines lie close together in front of Surprise Glacier in Upper Royal Basin and support sparse vegetation	Olympic National Park	Royal Creek-Dungeness River Valley Lat: 47°49′35″ Long: 123°13′16″	Constance	Long, NNOMW
Moraine	A moraine deposit lies at an altitude of 5,750 ft about 1,500 ft from the cirque headwall that is the source of Copper Creek	Olympic National Park	Copper Creek-Dungeness River Valley Lat: 47°49′58″ Long: 123°07′24″	Constance	Long, NNOMW
Moraine	A moraine lies on the lip of a high cirque on the northwest side of Iron Mountain near the source of Copper Creek at an altitude of 5,950 ft	Olympic National Park	Copper Creek-Dungeness River Valley Lat: 47°49′46″ Long: 123°06′44″	Constance	Long, NNOMW
Moraine	A moraine lies at an altitude of 5,600 ft on the north side of Buckhorn Mountain and a second one is seen in a cirque half a mile north of Buckhorn Pass	Olympic National Park	Copper Creek-Dungeness River Valley Lat: 47°49′53″ Long: 123°06′52″	Constance	Long, NNOMW
Moraine	A large moraine lies at 5,750	Olympic	Royal Creek-	Deception	Long,

What	Description	Where	Location	Age	Source
	ft and consists of highly unstable rubble before the base of Royal Glacier; at least 20 closely spaced recessional moraines 2-5 ft high lie behind the outermost moraine and these contain glacial fluting 1-3 ft high and were overridden after they were built	National Park	Dungeness River Valley Lat: 47°49′20″ Long: 123°13′08″		NNOMW
Moraines	Two prominent moraines 40-50 ft high lie 350 and 500 ft outside of the large moraine above and have a little soil in which patches of turf and a few conifers are growing	Olympic National Park	Royal Creek-Dungeness River Valley Lat: 47°49′18″ Long: 123°12′34″ Lat: 47°49′16″ Long: 123°12′35″	Deception	Long, NNOMW
Moraine	Surprise Glacier in Upper Royal Basin is bordered on the north and east by a fresh moraine with unstable slopes and lies at an altitude of 6,250 ft	Olympic National Park	Royal Creek-Dungeness River Valley Lat: 47°49′38″ Long: 123°13′33″	Deception	Long, NNOMW
End Moraine	An end moraine lies on the north side of Mt. Fricaba at an altitude of 6,200 ft	Olympic National Forest	Dungeness River Valley Lat: 47°48′54″ Long: 123°12′06″	Deception	Long, NNOMW
Glacial Erratics	Granite erratics up to 3,850 ft elevation	Olympic National Park	Blue Mountain-Cameron Creek-Gray Wolf River Valley Lat: 47°57′00″ Long: 123°15′00″	Vashon	Long, GGNOP
Bedded Continental Glacial Deposits	Borrow pit at Slab Camp on lower Gray Wolf River, altitude 2,600 ft, has unconsolidated sediments 30 ft thick according to a seismic survey	Olympic National Forest	Slab Camp-Gray Wolf River Valley Lat: 47°57′00″ Long: 123°10′30″	Vashon	Long, GNNOP
Granite Erratics	Erratics found up to a height of 3,550 ft along Deer Ridge Trail 900 ft above Slab Camp	Olympic National Forest	Deer Ridge Trail-Gray Wolf River Valley Lat: 47°57′30″ Long: 123°10′30″	Vashon	Long, GNNOP
Erratics	Many erratics are in lower Gray Wolf River valley with a 20 foot granite boulder by the foot bridge 4 miles above the junction with the Dungeness River	Olympic National Forest	Gray Wolf River Valley Lat: 47°46′00″ Long: 123°07′00″	Vashon	Long, GNNOP
Continental Drift	Ned Hill Ridge was a barrier to the ice sheet and barely overrun with drift exposed at 3,100 ft 2 miles south of Slab Camp	Olympic National Forest	Ned Hill Ridge-Gray Wolf River Valley Lat: 47°46′00″ Long: 123°08′30″	Vashon	Long, GNNOP

What	Description	Where	Location	Age	Source
Continental Drift Body	At Camp Tony opposite of Slab Camp Creek mouth stands a ridge of drift 1,750 ft high; composed of pebbles and cobbles of native and exotic rock types in a fine-grained matrix	Olympic National Forest	Gray Wolf River Valley Lat: 47°46′00″ Long: 123°08′30″	Vashon	Long, GNNOP
Iceberg-rafted Granite Boulders	Many boulders as high as 3,175 ft on the south side of Blue Mountain along the Three Forks-Deer Park Trail	Olympic National Park	Blue Mountain-Gray Wolf River Valley Lat: 47°57′30″ Long: 123°15′00″	Vashon	Long, GNNOP
Iceberg-rafted Granite Boulders	Cameron Creek valley has the farthest upvalley boulders at 2,850 ft, 2 miles above Three Forks	Olympic National Park	Cameron Creek-Gray Wolf River Valley Lat: 47°55′00″ Long: 123°15′00″	Vashon	Long, GNNOP
Iceberg-rafted Granite Boulders	In Upper Gray Wolf River valley, boulders were found 3 miles south of Three Forks	Olympic National Park	Gray Wolf River Valley Lat: 47°55′00″ Long: 123°15′00″	Vashon	Long, GNNOP
Continental Drift	Abundant drift with exotic stones is exposed in cutbanks up to 3,200 ft along Deer Park- Blue Mountain Road (below 12 mile post)	Olympic National Park	Gray Wolf River Valley Lat: 47°57′30″ Long: 123°15′00″	Vashon	Long, GNNOP
Granite Erratics	Northwest ridge of Blue Mountain has granite boulders 6 ft in diameter up to an altitude of 3,850 ft	Olympic National Park	Blue Mountain-Gray Wolf River Valley Lat: 47°57′30″ Long: 123°15′00″	Vashon	Long, GNNOP
Terminal Moraine	Terminal moraine of Gray Wolf Glacier lies 2 miles south of Three Forks and 7 miles from the cirque basin at the head of the valley; crest at 3,000 ft and base beside river at 2,800 ft; length is 0.25 miles	Olympic National Park	Gray Wolf River Valley Lat: 47°53′05″ Long: 123°14′36″		Long, GNNOP
Basalt Boulders	Deposit of large basalt boulders 1 mile upstream of the moraine on Gray Wolf River	Olympic National Park	Gray Wolf River Valley Lat: 47°54′00″ Long: 123°15′00″		Long, GNNOP
Granite Erratics	Granite erratics on the east valley wall behind the moraine are from icebergs in a glacial lake dammed by continental ice	Olympic National Park	Gray Wolf River Valley Lat: 47°54′00″ Long: 123°15′00″	Vashon	Long, GNNOP
Till and Terminal Position of Glacier	Hills of till and basalt boulders mark the terminal position of a glacier at 4,400 ft in Upper Gray Wolf River valley	Olympic National Park	Gray Wolf River Valley Lat: 47°50′26″ Long: 123°16′06″		Long, GNNOP
End Moraine	End moraine in valley to the north of the Gray Wolf glacier at 4,800 ft altitude	Olympic National Park	Gray Wolf River Valley Lat: 47°50′00″		Long, GNNOP

What	Description	Where	Location	Age	Source
			Long: 123°16′07″		
End Moraine	End moraine in valley from short tributary to Gray Wolf River at 800 ft above the river 4 miles south of Three Forks, just east of Camp Ellis	Olympic National Park	Gray Wolf River Valley Lat: 47°52′51″ Long: 123°14′13″		Long, GNNOP
Lateral Moraine	Lateral moraine on the southeast wall of Cameron Creek valley, 700 ft above river, 4 miles above Three Forks; composed of huge, angular blocks of massive basalt and breccia which indicate the glacier flowed through the only short trough composed of basalt in the area; the moraine segment is 0.25 miles long; it descends in altitude from 4,100-3,900 ft or roughly 800 ft/mile	Olympic National Park	Cameron Creek-Gray Wolf River Valley Lat: 47°52′40″ Long: 123°18′38″	Vashon	Long, GNNOP and Long, SSVCIOM
Moraine	Heavy concentration of basalt boulders between 3,100-3,300 ft one mile farther down from previous deposit represent an old alpine moraine from the glacier at a cirque that was ~6.5 miles in length	Olympic National Park	Cameron Creek-Gray Wolf River Valley Lat: 47°53′23″ Long: 123°17′48″	Vashon	Long, GNNOP and Long, SSVCIOM
Terminal Moraine	Terminal moraine from Cameron Glacier composed of till and no basalt at 3,500 ft 4 miles from valley head (1.5 miles from previous moraine); 1,000 ft long, rises 200 ft between upper and lower ends; it is only found on the northwest side of Cameron Creek and consists of loose angular slate and sandstone rubble-no basalt	Olympic National Park	Cameron Creek-Gray Wolf River Valley Lat: 47°52′29″ Long: 123°18′56″		Long, GNNOP
End Moraine	End moraine deposited by Cameron Glacier 2 miles from cirque headwalls and 3.5 miles upvalley from the previous moraine	Olympic National Park	Gray Wolf River Valley Lat: 47°50′55″ Long: 123°21′20″		Long, GNNOP
Moraine	Large basalt boulders and till hills mark the most extensive Neoglacial advance of Deception Glacier on the northwest side of Mt. Deception at an altitude of 4,400 ft; below the moraine the stream enters a slot-like gorge cut 30-50 ft into the	Olympic National Park	Mt. Deception-Gray Wolf River Valley Lat: 47°50′26″ Long: 123°16′06″	Royal	Long, NNOMW

What	Description	Where	Location	Age	Source
	bedrock while above the moraine the stream is flowing on glacial drift				
Moraines	Needles Glacier lies in a cirque at the head of the next valley north of Deception Glacier and has deposited a moraine that is bouldery and composed of basalt eroded from The Needles; the outermost moraine lies at 4,800 ft	Olympic National Park	The Needles-Gray Wolf River Valley Lat: 47°50′50″ Long: 123°15′26″	Royal	Long, NNOMW
Moraines	A prominent, densely vegetated moraine 40 ft high lies along the west side of the upland at the westernmost branch of Cameron Creek with a second well-defined moraine inside the first; the moraine is about 1,500 ft from the base of the valley wall, 1 mile long, consists of angular boulders and rubble of sandstone and slate, and it is covered with thick turf and mature conifers	Olympic National Park	Cameron Creek-Gray Wolf River Valley Lat: 47°50′30″ Long: 123°22′08″	Royal	Long, NNOMW
End Moraines	End moraine segments mark the southeast margin of the glacier at Cameron Creek at 5,100 ft in altitude and a continuous morainal ridge marks the northwest side; the end moraine encloses areas of bare, striated sandstone bedrock and near-polish; two arcuate moraines are located near the upper Cameron shelter	Olympic National Park	Cameron Creek-Gray Wolf River Valley Lat: 47°50′36″ Long: 123°21′31″	Royal	Long, NNOMW
Moraines	Three other high cirques lie at the head of Cameron Creek and contain moraines that lie at the cirque thresholds, have thick turf, and support trees; the southwest facing cirque moraine has an altitude of 5,700 ft, in the north facing cirque an altitude of 5,300 ft, and in the northwest facing cirque an altitude of 5,200 ft	Olympic National Park	Cameron Creek-Gray Wolf River Valley Cirque #1 Lat: 47°50′52″ Long: 123°22′14″ Cirque #2 Lat: 47°50′30″ Long: 123°22′09″ Cirque #3 Lat: 47°50′37″ Long: 123°21′02″	Royal	Long, NNOMW
Moraine	A moraine lies just south of Cameron Pass at the head of the Lost River with a crestal altitude of 5,400 ft and dense	Olympic National Park	Cameron Creek-Gray Wolf River Valley Lat: 47°49′05″ Long: 123°20′40″	Royal	Long, NNOMW

What	Description	Where	Location	Age	Source
	vegetative cover				
Glacial Troughs	Four glacial troughs indent the southeast wall of Grand Creek between Moose and Grand Lakes; they face northwest and the trough mouths hang 300-600 ft above the valley floor with mouth heights increasing progressively from the southwest to the northeast	Olympic National Park	Cameron Creek-Gray Wolf River Valley Lat: 47°54′00″ Long: 123°20′30″	Royal	Long, NNOMW
End Moraine	A bouldery drift body fronted by a complete end moraine occupies the trough above Grand Lake; drift covers the floor behind the moraine; it lies at an altitude of 5,350 ft and composed of huge, angular sandstone blocks with almost no fine material; have lichens and a small cluster of trees	Olympic National Park	Grand Creek-Gray Wolf River Valley Lat: 47°53′07″ Long: 123°20′30″	Royal	Long, NNOMW
End Moraine	An end moraine lies one mile northwest of Grand Lake at an altitude of 5,400 ft on the threshold of a large, east facing cirque on the west wall of Grand Valley; it has a thick turf cover	Olympic National Park	Grand Creek-Gray Wolf River Valley Lat: 47°53′47″ Long: 123°21′17″	Royal	Long, NNOMW
Terminal Moraine	The terminal moraine lies at an altitude of 5,650 ft in Grand Creek, consists of micaceous sandstone, and has abundant striated stones	Olympic National Park	Grand Creek-Cameron Creek-Gray Wolf River Valley Lat: 47°52′21″ Long: 123°21′31″	Constance	Long, NNOMW
Moraine	Deception Glacier has a bouldery moraine at an altitude of 4,750 ft deposited about 1 mile in front of it	Olympic National Park	Mt. Deception-Gray Wolf River Valley Lat: 47°49′52″ Long: 123°15′36″	Constance	Long, NNOMW
Arcuate Moraines	A belt of arcuate moraines cross the valley floor, have stable, sparsely vegetated slopes, and lie in front of Needles Glacier at an altitude of 5,250 ft	Olympic National Park	The Needles-Gray Wolf River Valley Lat: 47°50′42″ Long: 123°14′58″	Constance	Long, NNOMW
Terminal Moraine	A terminal moraine lies at 4,700 ft and was deposited by Cameron Glacier, it is bouldery and supports vegetation over 30% of its surface	Olympic National Park	Cameron Creek-Gray Wolf River Valley Lat: 47°50′44″ Long: 123°21′32″	Constance	Long, NNOMW
Moraines	Many bouldery recessional moraines lie behind the moraine listed above and lie at an altitude of 5,450 ft	Olympic National Park	Cameron Creek-Gray Wolf River Valley Lat: 47°50′17″ Long: 123°21′21″	Constance	Long, NNOMW

What	Description	Where	Location	Age	Source
End Moraines	A fresh, sharp-crested end moraine with no vegetation lies before Deception Glacier at an altitude of 6,000 ft; a smaller moraine lies behind the outermost moraine and 2 recessional moraines lie at the present glacier terminus	Olympic National Park	Mt. Deception-Gray Wolf River Valley Lat: 47°49′28″ Long: 123°14′34″	Deception	Long, NNOMW
Terminal Moraine	On the lip of the cirque where Needles Glacier is located, a massive, unbreached, double-crested terminal moraine 200 ft high and composed of unstable basalt debris lies at an altitude of 6,000 ft; it has many low recessional moraines behind it	Olympic National Park	The Needles-Gray Wolf River Valley Lat: 47°50′21″ Long: 123°14′19″	Deception	Long, NNOMW
Moraine	Walkinshaw Glacier lies in a cirque on the north side of Mt. Walkinshaw and a multiple-crested moraine with barren, unstable slopes lies at an altitude of 6,500 ft in front of it	Olympic National Park	Mt. Walkinshaw-Gray Wolf River Valley Lat: 47°51′11″ Long: 123°14′07″	Deception	Long, NNOMW
Morainic Loops	The glacier at the head of the westernmost branch of Cameron Creek has 10-12 morainic loops 1-3 ft high that are bare of vegetation and mark the different stands of the glacier; they lie at an altitude of 5,800 ft	Olympic National Park	Cameron Creek-Gray Wolf River Valley Lat: 47°49′46″ Long: 123°21′07″	Deception	Long, NNOMW
End Moraines	End moraines extend slightly more than a mile beyond the modern glacier margins; these are fresh with only scattered plants and conifer seedlings: Royal Glacier-5,750 ft Mystery Glacier-5,750 ft Surprise Glacier-6,250 ft Needles Glacier-6,000 ft Deception Glacier-6,000 ft Walkinshaw Glacier-6,500 ft Debris Glacier-5,300 ft Constance Glacier-5,200 ft Warrior Peak-6,100 ft and 5,750 ft Upper Charlia Lake-6,300 ft Mount Fricaba-6,200 ft West of Home Lake-5,800ft East of Home Lake-5,750 ft Mount Clark-6,700 ft	Olympic National Park		Holocene	Long, GNNOP

What	Description	Where	Location	Age	Source
	Mount Walkinshaw-6,200 ft Northwest of Mount Constance-6,200 ft				
Former Glacial Extent	The Juan de Fuca Lobe of the Cordilleran Ice Sheet advanced: (a) 11 miles into the Dungeness River Valley (b) 5 miles into the Gray Wolf River Valley (c) terminated in a deep glacial lake ponded in the Elwha River Valley (d) reached within one mile of Forks	Olympic National Forest			Long, GGNOP
Granite Erratics	Highest granite boulders are at 3,300 ft on north wall of Morse Creek along Hurricane Ridge Road 2.3 miles above Lookout Rock	Olympic National Park	Morse Creek Valley Lat: 48°00′30″ Long: 123°22′30″	Vashon	Long, GNNOP
Ice-Limit and Highest Granite Boulder	Lake Angeles Trail passes above ice limit at 3,750 ft with the highest boulder at 3,675 ft by Halfway Rock	Olympic National Park	Morse Creek Valley Lat: 48°00′00″ Long: 123°28′30″	Vashon	Long, GNNOP
Granite Boulders	Wildcat Mountain was overridden by ice with boulders found at the top	Olympic National Park	Wildcat Mountain-Elwha River Valley Lat: 48°09′30″ Long: 123°29′00″	Vashon	Long, GNNOP
Granite Boulders	Ice reached as high as 3,600 ft in the South Branch Little River valley	Olympic National Park	South Branch Little River-Elwha River Valley Lat: 48°09′30″ Long: 123°29′00″	Vashon	Long, GNNOP
Granite Erratics	Granite erratics are found 10 miles into the valley along the abandoned Hurricane Ridge Road up to an altitude of 3,225 ft	Olympic National Park	Elwha River Valley Lat: 48°04′00″ Long: 123°33′30″	Vashon	Long, GNNOP
Granite Boulders	Opposite the mouth of Lillian River, boulders were found on Long Ridge at a maximum altitude of 3,125 ft	Olympic National Park	Elwha River Valley Lat: 48°04′30″ Long: 123°31′30″	Vashon	Long, GNNOP
Erratics	In Boulder Creek valley, erratics are found at 2,475 ft 1 mile above Olympic Hot Springs by the Appleton Pass Trail	Olympic National Park	Boulder Creek-Elwha River Valley Lat: 47°57′30″ Long: 123°41′00″	Vashon	Long, GNNOP
Moraine	Olympic Hot Springs and Boulder Campground are on an old alpine terminal moraine; has granite stones on surfaces so it predates the damming of the Elwha valley	Olympic National Park	Olympic Hot Springs-Elwha River Valley Lat: 47°58′33″ Long: 123°41′25″		Long, GNNOP

What	Description	Where	Location	Age	Source
	by the Juan de Fuca Lobe				
Moraines	Three moraines were located at the source of the Lillian River with the outer most moraine lying at an altitude of 5,225 ft and damming a wet meadow; it has abundant vegetation; the innermost moraines are very fresh, are covered by grass and a few trees, are unstable, and lie at elevations of 5,450 ft	Olympic National Park	Lillian River-Elwha River Valley Moraine #1 Lat: 47°51′47″ Long: 123°23′08″ Moraine #2 Lat: 47°51′37″ Long: 123°23′10″	Constance	Long, NNOMW
Granite Erratics	The distribution of granite erratics on the northern Olympic front westward from Lake Angeles to Snider Peak strongly indicate that Vashon ice filled the Lake Crescent defile and made contact with ice moving up the Sol Duc River valley	Olympic National Park	Lake Crescent Lat: 48°06′00″ Long: 123°48′30″	Vashon	Long, SSVCIOM
Vashon Ice Sheet Extent	The ice sheet overrode The Foothills ridge, which is 3 miles south of Port Angeles; the crest lies between 2,400-2,650 ft in altitude; it pushed southward 3 miles up the South Branch of the Little River at least as high as 2,250 ft; Pyramid Mountain lies between 3,000-3,100 ft in altitude and was overridden by ice as the summit is lower than the highest granite erratics on the peaks between it and Mt. Muller	Olympic National Park and Federal Lands	Lake Crescent Area Pyramid Mountain Lat: 48°07′30″ Long: 123°49′00″ The Foothills Lat: 48°05′30″ Long: 123°26′00″	Vashon	Long, SSVCIOM
Granite Erratics	Fresh granite erratics are found in the lake defile and westward beyond Barnes Creek to Fairholm; erratics at the west end of the lake indicates that Vashon ice occupied all of the defile; road cuts on the north side of Lake Crescent, a mile from the west end of the lake, expose up to 75 ft of gravel containing fresh, well-rounded granite pebbles and cobbles	Olympic National Park	Lake Crescent Area Lat: 48°06′00″ Long: 123°48′30″	Vashon	Long, SSVCIOM
Granite Erratics	Granite erratics are found in road cuts and on the surface up to an altitude of 3,150 ft	Olympic National Park	Lake Crescent Area Lat: 48°06′00″ Long: 123°48′30″	Vashon	Long, SSVCIOM

What	Description	Where	Location	Age	Source
	at a point 5 miles west of Pyramid Mountain; ice undoubtedly spilled through the 2,500 ft saddle just west of the mountain and into the Lake Crescent defile; granite is also found along the Pyramid Mountain-Snider Peak ridge at the crest which varies in altitude from 2,500-3,750 ft		Pyramid Mountain Lat: 48°07′30″ Long: 123°49′00″		
Granite Erratics and Drift	Granite erratics are found on: a. near the summit of Ellis Mountain, 2,673 ft, suggesting it was overrun b. at the highest point on Deadmans Hill, just over 2,500 ft, suggesting it was overrun c. a large body of unconsolidated drift nearly fills the Snider Creek valley and has a surface altitude of 1,100 ft; 150 ft higher a granite boulder is by the North Point Road just above the Snider Work Center	Olympic National Park/ Olympic National Forest	Lake Crescent Area Snider Peak Lat: 48°03′00″ Long: 124°07′00″ Pyramid Mountain Lat: 48°07′30″ Long: 123°49′00″	Vashon	Long, SSVCIOM
Alpine Lateral Moraine	An alpine lateral moraine just over 1.5 miles in length is located near the mouth of Barnes Creek; the crest descends from an altitude of 1,300 ft near Barnes Creek to ~800 ft near Aurora Creek and may extend below the surface of Lake Crescent; the west end of the moraine lies ~8 miles from cirques at the head of Barnes Creek; the presence of granite erratics on lower Aurora Creek means the moraine is younger than the Vashon Ice Sheet maximum	Olympic National Forest	Barnes Creek-Lake Crescent Lat: 48°03′23″ Long: 123°48′01″	Vashon	Long, SSVCIOM
Alpine Till	An alpine till is visible in cutbanks along road No. 2931A between Goodman and Tom Creeks in the lower Sol Duc River valley; the till is composed of locally derived sedimentary and volcanic rocks, is unsorted, and contains debris ranging in size from clay to boulders	Olympic National Forest	Between Tom and Goodman Creeks-Sol Duc River Valley Lat: 48°04′30″ Long: 123°57′00″ Tom Creek Lat: 48°02′30″ Long: 123°56′30″	Evans Creek	Long, SSVCIOM

What	Description	Where	Location	Age	Source
	several feet in diameter; slopewash five feet thick overlies the till; contains numerous well-striated and polished stones		Goodman Creek Lat: 48°05′00″ Long: 123°55′30″		
Alpine Till	An alpine till similar to the one above is exposed in road cutbanks in lower Goodman and Tom Creeks between altitudes of 1,500-1,750 ft	Olympic National Forest	Tom and Goodman Creeks-Sol Duc River Valley Lat: 48°04′30″ Long: 123°57′00″	Evans Creek	Long, SSVCIOM
Alpine Till	Near Snider Creek, till is exposed in cutbanks along the lower part of the road to North Point; it is compact, dark brown, contains striated basaltic stones, and was deposited by an alpine glacier that descended the Sol Duc River valley	Olympic National Forest	Tom and Goodman Creeks-Sol Duc River Valley Lat: 48°01′30″ Long: 124°07′30″	Evans Creek	Long, SSVCIOM
Glacial Erratics	Granite erratics up to 2,750 ft elevation	Olympic National Forest	Snider Mountain-Sol Duc River Valley Lat: 48°05′10″ Long: 124°07′30″	Vashon	Long, GGNOP
Continental Ice Drift and Till	On the north end of Calawah Ridge, road cuts along Forest Road No. 306 reveal abundant Vashon drift with many well-striated basalt and greywacke stones in addition to many granite boulders; the till occurs up to a minimum height of 1,350 ft	Olympic National Forest	Calawah Ridge-Sol Duc Valley Lat: 48°00′00″ Long: 124°19′30″	Vashon	Long, SSVCIOM
Kettles	At maximum extent the continental ice sheet blocked the Sol Duc valley and filled the broad embayment between Calawah Ridge and Bigler Mountain; kettles are found in the terminal zone of a glacier and occur on the floor of the embayment; one kettle is 75 ft deep	Olympic National Forest	Calawah Ridge-Sol Duc River Valley Lat: 48°00′00″ Long: 124°19′30″ Bigler Mountain Lat: 48°04′00″ Long: 124°07′30″	Vashon	Long, SSVCIOM
Outwash Terraces	A thick outwash plain covers the floor of the mile wide Kugel-Bonidu Creek embayment; a broad gravel terrace at 1,020 ft along the east side of the embayment marks the original surface of the outwash body; a broad second terrace lies at 965 ft; a third terrace lies at 930 ft and was carved by glacial streams; its scarp sweeps into	Olympic National Forest	Kugel Creek-Sol Duc River Valley Lat: 48°06′30″ Long: 124°06′30″	Vashon	Long, SSVCIOM

What	Description	Where	Location	Age	Source
	the embayment in a near perfect arc of curvature which is convex to the stream; the glacial streams also carved a 2 mile long sweeping terrace scarp 75-100 ft high completely across the mouth of the embayment in the upper Sol Duc valley				
Continental Drift	Continental glacial deposits are exposed in road cuts (roads 2903 and 2903H) on the east branch of upper Bockman Creek and drift occurs to an altitude of 1,100 ft; many stones are striated and granite is abundant; more drift occurs near the end of road 2903F (Shuwah Road) up to 1,250 ft in altitude and a solid 6 ft granite boulder is in the creek bed at 1,125 ft	Olympic National Forest/ Federal Lands	Bockman Creek-Sol Duc River Valley Lat: 48°05′00″ Long: 124°19′30″	Vashon	Long, SSVCIOM
Hills of Continental Drift	Just south of Lake Pleasant in the area drained by Bockman, Shuwah, and Maxfield Creeks are many low hills which grade from rounded form into long narrow ridges with the long axis paralleling the south side of the lower Sol Duc valley; some hills are chiefly composed of bedrock and others of drift, but it is difficult to distinguish as the exposures of drift are few and the vegetation is dense	Olympic National Forest	Lake Pleasant-Sol Duc River Valley Lat: 48°07′00″ Long: 124°19′30″	Vashon	Long, SSVCIOM
Glacial Lake	A body of laminated clay and silt about 5 acres in extent and up to 25 ft thick is exposed in road cuts and slumps along road 2903F; it is from a small lake with a surface altitude of ~1,100 ft and apparently dammed at the head of the short valley by the glacier; similar lake fines are seen at 1,125 ft at the head of the west branch of Bockman Creek	Olympic National Forest/ Federal Lands	Bockman Creek-Sol Duc River Valley Lat: 48°05′00″ Long: 124°19′30″	Vashon	Long, SSVCIOM
Continental Drift	Continental drift is present at the mouth of Tassel Creek valley near the south end of	Olympic National Forest/	Tassel Creek-Sol Duc River Valley Lat: 47°58′00″	Vashon	Long, SSVCIOM

What	Description	Where	Location	Age	Source
	Calawah Ridge; the drift is exposed in a road cut at an altitude of 725 ft and a gully slightly lower in elevation; composed of many rounded and striated stones some of which are granitic	Private Land	Long: 124°23′30″		
Continental Ice Margin	Between the head of Bockman Creek at the north end of Calawah Ridge and Forks Prairie at the southern end, the Vashon ice margin lowered 525 ft in a distance of only 5 miles toward the southwest	Olympic National Forest	Calawah Ridge-Sol Duc River Valley Lat: 48°00′00″ Long: 124°19′30″	Vashon	Long, SSVCIOM
Outwash Sediments	Forks Prairie debouches into the Quillayute-Sol Duc-Bogachiel River valley which has an average width of 2.5 miles; the valley extends west 12 miles from Forks to the Pacific Ocean at LaPush and it is filled with thick Pleistocene outwash sediments that came from both continental and local alpine ice	Federal Land	Forks Prairie-Sol Duc River Valley Lat: 47°57′00″ Long: 124°23′30″	Vashon	Long, SSVCIOM
Outwash Terrace	For 8 miles along the north side of the Quillayute River valley, a steep gravel terrace scarp rises 100 ft above the valley floor; the scarp was cut by the glacial stream from the recessional meltwater channel; the sediment composing the terrace is exposed by the Quillayute Road in the vicinity of Quillayute Prairie and is comprised of pebble to small boulder sized sandy gravel of sandstone, basalt, and some foreign stones overlain by windblown sediments up to 10 ft thick	Federal Land	Forks Prairie-Sol Duc River Valley Lat: 47°57′00″ Long: 124°23′30″	Vashon	Long, SSVCIOM
Alpine End Moraine	On the southwest side of the Sol Duc River, road No. 303 rises over the crest of an end moraine from a late Fraser alpine glacial advance at a 1,375 ft altitude		Sol Duc River Valley Lat: 48°01′45″ Long: 123°57′47″	Vashon	Long, SSVCIOM
Alpine Till and Striations	A mile and a half up the road from the above moraine a borrow pit exposes till and		Sol Duc River Valley Lat: 47°56′30″ Long: 124°32′00″	Vashon	Long, SSVCIOM

What	Description	Where	Location	Age	Source
	glacially abraded bedrock; the abraded sandstone bedrock have striations that parallel the axial valley; stones have smoothed and well-striated surfaces				
Alpine Outwash Terrace	Outwash terrace deposits are in contact with the terminal moraine from the above two features; an extensive gravel terrace is on the southwest side of the river from the moraine to the mouth of Goodman Creek at an altitude of 1,225 ft and is up to 200 ft above the present river; exposures in the terrace are made by road cutbanks and a large borrow pit; a coarsening of the gravel from bottom to top is observed in the borrow pit		Sol Duc River Valley Lat: 47°56′30″ Long: 124°32′00″	Vashon	Long, SSVCIOM
Terraced Outwash	A large body of outwash lies at the mouth of the Sol Duc valley; two terrace levels were cut in front of the outwash, the upper surfaces slope with the fall of the large glacial stream by which the scarp fronts have been eroded and these present two re-entrants with large curvature and arc carved by the lateral planning of a large stream in the upper valley where no river exists today; the radius of curvature indicates a large volume of water which could only have come from the Lake Crescent defile; the upper terrace lies at 1,160 ft, the lower at 1,080 ft, and the valley floor at 1,020 ft		Sol Duc River Valley Lat: 47°56′30″ Long: 124°32′00″	Vashon	Long, SSVCIOM
Outwash	The large outwash body at the mouth of Camp Creek, 2 miles west of the Sol Duc valley mouth, was also truncated by west-flowing glacial streams like the terraces from above		Sol Duc River Valley Lat: 47°56′30″ Long: 124°32′00″	Vashon	Long, SSVCIOM
Terraced Outwash	The terraced outwash at the mouth of the Sol Duc River valley is exposed in a borrow		Sol Duc River Valley Lat: 47°56′30″ Long: 124°32′00″	Vashon	Long, SSVCIOM

What	Description	Where	Location	Age	Source
	pit and consists of gravel, sand, and large, angular basaltic boulders; in places the outwash is stratified in courses of foreset beds that dip southward in to the Sol Duc valley; very little granite and metamorphic rock types and the terrace surface lies at 1,275 ft altitude, ~325 ft above the Sol Duc River and 275 ft above the bedrock				
Terrace Scarps	Long, high terrace scarps with regular arcs of curvature sweep both sides of the upper Sol Duc valley indicating that the glacial streams that carved them were about 1 mile wide and up to 100 ft deep		Sol Duc River Valley Lat: 47°56′30″ Long: 124°32′00″	Vashon	Long, SSVCIOM
Terraced Outwash	Against the north valley wall at Littleton, road cuts reveal granite-bearing terraced outwash whose upper surface lies at an altitude of 1,130 ft, ~135 ft above the valley floor		Sol Duc River Valley Lat: 47°56′30″ Long: 124°32′00″	Vashon	Long, SSVCIOM
Recessional Meltwater Channel	When the ice sheet terminated against the south side of the Sol Duc River valley meltwater flowed south down the valley of the North Fork of the Calawah River and southeast across Grindstone Pass at 900 ft in elevation; the channel is 700 ft deep and a mile long and it leaves the west embayment and transects the ridge extending southwest from Bigler Mountain; it is floored with outwash gravel	Olympic National Forest	Grindstone Pass-Bogachiel River Valley Lat: 48°03′00″ Long: 124°09′00″	Vashon	Long, SSVCIOM
Granite Erratic	On the north bank of the Calawah River just south of Tassel Creek a sandstone cored hill covered with thin drift 150 ft high has a 5 ft angular granite erratic near the top thus showing that the glacier must have pushed a short distance onto the prairie as the average height of the prairie is ~150 ft below the crest of the hill		Calawah River-Bogachiel River Valley Lat: 47°56′30″ Long: 124°22′00″	Vashon	Long, SSVCIOM

What	Description	Where	Location	Age	Source
Terminal Zone of Continental Ice Sheet-Hummocks and Closed Depressions	The terminal zone of the ice sheet is preserved along the north bank of the Calawah River between the river and the hill where drift at least 150 ft thick has an irregular surface marked by hummocks and closed depressions		Calawah River-Bogachiel River Valley Lat: 47°56′30″ Long: 124°22′00″	Vashon	Long, SSVCIOM
Till and Alpine Ice Extent	Camp Creek on the Sol Duc River is separated from the upper mile and a half section of the North Fork of the Calawah River valley by a broad saddle whose floor is 200 ft above the river; the river makes a right angle turn at the saddle and road cutbanks on the west side of the saddle expose alpine till with striated stones; glacially abraded sandstone bedrock is observed in the saddle; above the saddle the valley is U-shaped and a little way below the saddle the valley is V-shaped	Olympic National Forest	North Fork of the Calawah River-Bogachiel River Valley Lat: 48°01′36″ Long: 124°01′48″	Evans Creek	Long, SSVCIOM
Alpine and Continental Till	Sediments exposed in road cuts in the North Fork of the Calawah River valley include pebbly silt and fine sand up to 30 ft thick underlain by cobble to small boulder gravel 25 ft or more thick with small granitic pebbles; sharp, angular pebbles are contained in the silt-sand unit; the underlying gravels were from a short valley glacier that occupied the valley while the fine sediments are from a glacial lake that was dammed in the valley by the continental ice sheet as indicated by the presence of granite	Olympic National Forest	North Fork of the Calawah River-Bogachiel River Valley Lat: 48°02′00″ Long: 124°12′00″	Vashon	Long, SSVCIOM
Outwash Terrace	A large outwash terrace segment lies in the North Fork Calawah River meltwater drainage channel at the southeast base of Bigler Mountain; it is composed of local basalt and sandstone with minor	Olympic National Forest	Bigler Mountain-North Fork of the Calawah River-Bogachiel River Valley Lat: 48°04′00″ Long: 124°07′30″	Vashon	Long, SSVCIOM

What	Description	Where	Location	Age	Source
	amounts of granite and other northern stones; the surface lies at 925 ft or 75 ft above the river grade; the frontal scarp is convex outward as if carved by glacial streams rounding the valley curve from north to west				
Embay-ment	Along the west side of Bigler Mountain a wide embayment leads south into the North Fork Calawah River glacial drainage channel-no terrace scarp is present	Olympic National Forest	Bigler Mountain-North Fork of the Calawah River-Bogachiel River Valley Lat: 48°04′00″ Long: 124°07′30″	Vashon	Long, SSVCIOM
Recessional Meltwater Channel	The North Fork of the Calawah River has a stream too small to have carved the valley and it marks the former course of a large glacial river across an easily eroded sandstone and shale terrain; the valley walls are spurless and the valley is broad and nearly straight; the water flowed southwestward out of the Sol Duc River valley with the head marked by the two embayments previously mentioned; the gravel-floored channel is 12 miles long and the slope is ~35 ft/mile	Olympic National Forest	North Fork of the Calawah River-Bogachiel River Valley Lat: 48°02′00″ Long: 124°12′00″	Vashon	Long, SSVCIOM
Recessional Meltwater Channel	On the northwestern peninsula meltwater from Vashon continental ice reached the Pacific Ocean via the North Fork of the Calawah River recessional meltwater channel; the channel is 1,500 ft deep and 12 miles long; it leads southwestward across the foothills out of the mid-Sol Duc valley and discharged meltwater across Forks Prairie and through the Quillayute valley to the Pacific Ocean at LaPush	Olympic National Forest	North Fork Calawah River-Bogachiel River Valley Lat: 47°57′00″ Long: 124°19′00″	Vashon	Long, SSVCIOM
Alpine Glacier Length	The glacier on the Sitkum River reached the east end of Forks Prairie, was 14-15 miles long, and terminated at an altitude between 300-400	Federal Land	Forks Prairie-Sitkum River-South Fork Calawah River-Bogachiel River Valley	Salmon Springs or Evans Creek	Long, SSVCIOM and Long,

What	Description	Where	Location	Age	Source
	ft; traces of the alpine glacier are cirques, hanging tributary valleys, truncated spurs, and U-shaped valleys; cirque floor altitudes lie a little below 2,000 ft and a few short tributary valleys from the Rugged Ridge joined the glacier		Lat: 47°57′49″ Long: 124°20′10″		GSRVN OPW
Alpine Till	On the drainage divide between the Sitkum, South Fork of the Calawah, and the Bogachiel Rivers till is exposed and its distribution indicates that valley glaciers in the drainage basins of these rivers were confluent across low places in the divide; a lobe of the Bogachiel glacier flowed north through mile-wide Indian Pass and joined the South Fork Calawah glacier, which reached the Sitkum River through a 1,000 ft high gap in the west end of Rugged Ridge	Olympic National Forest	Sitkum River-South Fork Calawah River-Bogachiel River Valley Lat: 47°55′30″ Long: 124°14′30″	Salmon Springs or Evans Creek	Long, SSVCIOM and Long, GSRVN OPW
Alpine Till	Road cuts along Forest Road No. 2828 that leads from the Sitkum River to the west end of Rugged Ridge expose till that consists of weathered, compact, poorly sorted stones of pebble to boulder size in a clay-silt matrix; most stones are moderately rounded, some striae are visible on basalt and greywacke clasts; the till occurs up to an altitude of 1350 ft to points 350 ft above the gap and 700 ft above the Sitkum Valley floor	Olympic National Forest	Rugged Ridge-Sitkum River-South Fork Calawah River-Bogachiel River Valley Lat: 47°54′00″ Long: 124°06′30″	Salmon Springs or Evans Creek	Long, SSVCIOM and Long, GSRVN OPW
Alpine Till	West of Rugged Ridge an alpine till similar to the one above is exposed in road cutbanks at several localities along the south side of the Sitkum-South Fork Calawah valley; the exposures decrease in altitude from ~1,100 ft at the upstream point to 475 ft at the downstream point 1.75 miles	Olympic National Forest	Sitkum River-South Fork Calawah River-Bogachiel River Valley Lat: 47°55′30″ Long: 124°14′30″	Salmon Springs or Evans Creek	Long, SSVCIOM and Long, GSRVN OPW

What	Description	Where	Location	Age	Source
	below the mouth of Hyas Creek				
Alpine Terminal Moraine	The glacier on the Sitkum River deposited a terminal moraine just above the mouth of the North Fork of the Sitkum River; the crest of the moraine lies at 875 ft elevation and rises from 350-375 ft above the river grade; the river cut a wide breach in the moraine which has been partially filled in by outwash; Forest Road No. 300 swings around the end of the moraine and high cutbanks expose drift composed of coarse-grained arkosic sandstone, basalt debris, and fine-grained hard greywacke; sediments are moderately rounded, pebble-boulder size, has sand and clay lenses, shows deformation in places, and stones have smooth surfaces with fine scratches	Olympic National Forest	North Fork Sitkum River-Sitkum River-South Fork Calawah River-Bogachiel River Valley Lat: 47°56′36″ Long: 124°08′59″	Evans Creek or Vashon	Long, SSVCIOM and Long, GSRVNOPW
Alpine Outwash Terrace	A large outwash terrace segment lies across the narrow rock gorge of the North Fork Sitkum River on the north side of the Sitkum River 300 yards below the moraine from above; it's 75 ft thick, 1,000 ft across, the surface is 350 ft above the river, and the North Fork has removed the adjacent outwash and cut through the terrace and up to 100 ft down into the underlying bedrock so the terrace is no longer in contact with the moraine	Olympic National Forest	North Fork Sitkum River-Sitkum River-South Fork Calawah River-Bogachiel River Valley Lat: 47°54′30″ Long: 124°09′00″	Evans Creek or Vashon	Long, SSVCIOM and Long, GSRVNOPW
Alpine Terminal Moraine	A terminal moraine from a younger advance is 0.5 miles upstream from the moraine listed above; the glacier was approximately 7 miles long and terminated at an altitude close to 850 ft; the moraine is a set of four closely spaced, densely forested, rounded ridges with crests 225 ft above river grade;	Olympic National Forest	North Fork Sitkum River-Sitkum River-South Fork Calawah River-Bogachiel River Valley Lat: 47°56′48″ Long: 124°08′23″	Vashon	Long, SSVCIOM and Long, GSRVNOPW

What	Description	Where	Location	Age	Source
	uprooted trees expose drift that mainly consists of light sandstone rocks from pebble-small boulders in a sandy matrix; the majority of stones are rounded				
Alpine Alluvial Terraces	Alluvial terraces produced by dissection of an outwash valley train are traced in connection with the youngest moraine from above; a mile below the mouth of the North Fork Sitkum River a slump reveals an alluvial fill 30 ft thick underlying the terrace surface; the bedrock floor on which the deposit rests is 50-60 ft above the present river level; the gravel is slightly weathered; a second terrace lies 25 ft below the surface of the younger terrace near the mouth of the North Fork where the Sitkum River swings laterally	Olympic National Forest	North Fork Sitkum River-Sitkum River-South Fork Calawah River-Bogachiel River Valley Lat: 47°54′30″ Long: 124°09′00″	Vashon	Long, SSVCIOM and Long, GSRVNOPW
Alluvial Fans	Much sediment was deposited by the river and tributaries along the upper Sitkum River during deglaciation; numerous alluvial fans and a thick flood plain were constructed on the valley bottom; a large alluvial fan is located at the mouth of Vast Creek	Olympic National Forest	Sitkum River-South Fork Calawah River-Bogachiel River Valley Lat: 47°55′30″ Long: 124°14′30″	Vashon	Long, GSRVNOPW
Till	On the crest of the ridge between the two forks of the Humptulips and two miles east of the junction of the rivers an ancient till is exposed in a borrow pit; most stones in the upper 8 ft of the till are extremely weathered; a few striated stones are observed; the till caps the ridge and lies at an altitude between 800-850 ft		Humptulips River Valley Lat: 47°04′30″ Long: 124°03′30″	Pre-Wisor Stuck	Long, GHRDBSOPW
Recessional Meltwater Channel	Meltwater from the glacier flowed in an overall south direction across three 150-250 ft passes to the Middle and East Forks of the Hoquiam River and the Wishka River		Humptulips River Valley Lat: 47°04′30″ Long: 124°03′30″	Pre-Wiscor Stuck	Long, GHRDBSOPW

What	Description	Where	Location	Age	Source
Till, Outwash, and Lacustrine Sediments	Moore (1965) observed a till on Donkey Creek Road described in the second listing; he did not interpret it and Long has reinvestigated it; the old weathered till is on Donkey Creek Road about 2.25 miles northeast of U.S. Highway 101 and is known as measured section A; a 160 ft section of till is exposed along the north valley wall of the West Fork Humptulips River; the upper section is till with pebble to large boulder stones and numerous smooth, faceted, striated stones; the middle section consists of pebble-cobble gravel in a sand matrix, poorly sorted, poorly stratified, firmly consolidated, but less compact than the till; the lower unit consists of laminated to thick-bedded silt and clay and contains peat, woody fragments, and sand and gravel lenses; the lower unit is expansive and occurs upstream for six miles and represents deposits in a large lake dammed in the valley by glacial drift with a surface level of 350 ft; the middle unit represents advance outwash deposited by the Quinault piedmont lobe and the glacier in the West Fork which was covered by till when the glacier overrode it; the lower unit's lake must have existed for a long amount of time as vegetation had re-established itself		West Fork of the Humptulips River-Humptulips River Valley Lat: 47°15′00″ Long: 123°53′15″	Older Wisc or Salmon Springs	Long, GHRDB SOPW
Former Glacial Extent	A broad piedmont ice lobe was formed on the lowland beyond the southwest mountain front and was fed mainly by glaciers in the Queets, Sams, and Quinault River valleys; the ice lobe extended south to Humptulips, spread east into the Humptulips embayment,		West Fork of the Humptulips River-Humptulips River Valley Lat: 47°15′00″ Long: 123°53′15″	Older Wisc or Salmon Springs	Long, GHRDB SOPW

What	Description	Where	Location	Age	Source
	and joined ice descending the West Fork valley				
Till	An old till is exposed in road cutbanks and logged areas and has weathering parameters similar to the Donkey Creek till described above; it is widespread in the lower reaches of the West and East Forks of the Humptulips River		West/East Fork of the Humptulips River-Humptulips River Valley Lat: 47°15′00″ Long: 123°53′15″	Older Wisc or Salmon Springs	Long, GHRDB SOPW
Till	A similar old till is exposed in road cutbanks on the west side of the Wishka-East Fork Humptulips drainage divide and on the crest of the divide up to ~1,700 ft which indicates that the Wynoochee alpine glacier crossed the divide and joined the Humptulips ice; Carson (1970) mapped this till on the east side as Mobray Drift of Salmon Springs age		East Fork of the Humptulips River-Humptulips River Valley Lat: 47°15′00″ Long: 123°53′15″	Older Wisc or Salmon Springs	Long, GHRDB SOPW
Outwash Plain	An extensive outwash plain along the lower East Fork of the Humptulips River is graded to the outermost Quinault piedmont lobe drift border that lies at the Humptulips hamlet		East Fork of the Humptulips River-Humptulips River Valley Lat: 47°15′00″ Long: 123°53′15″	Older Wisc or Salmon Springs	Long, GHRDB SOPW
Till	The western-most exposure of Mobray till lies at the north end of Cougar Mountain in a road cut at an altitude of 1,050 ft; till also of this type occurs above Fraser outwash on the East Fork of the Humptulips River between the mouths of Rock and Webfoot Creeks in road cut exposures up to a minimum altitude of 850 ft; a lobe of the West Fork Humptulips glacier must have filled the 1.5 mile wide low hilly area between the West and East forks south of Donkey Creek and joined East Fork ice		Cougar Mountain-East Fork of the Humptulips River-Humptulips River Valley Lat: 47°18′00″ Long: 123°45′00″	Older Wisc or Salmon Springs	Long, GHRDB SOPW
Till	The West Fork glacier overrode the broad 1,200 ft col at the head of Chester Creek and surrounded	Olympic National Forest	Chester Creek-West Fork of the Humptulips River-Humptulips River	Older Wisc or Salmon	Long, GHRDB SOPW

What	Description	Where	Location	Age	Source
	Chester Ridge; at the head of Chester Creek the upper limit of older till lies near 1,300 ft and at Chester Ridge Lookout till is found up to 1,250 ft or barely 100 ft below the lookout point		Valley Lat: 47°23′00″ Long: 123°48′00″	Springs	
Till	On the north side of Burnt Hill, road cutbanks expose 25 ft of compact older till that extends up to 950 ft altitude and a similar till occurs as high as 950 ft along the road to Burnt Hill Lookout which, at 1,258 ft, was not overrun by ice		Burnt Hill-West Fork of the Humptulips River-Humptulips River Valley Lat: 47°17′30″ Long: 123°51′45″	Older Wisc or Salmon Springs	Long, GHRDB SOPW
Till	Till occurs up to 800 ft in cutbanks along the north end of the Furlough Creek Road 3.5 miles southeast of Burnt Hill indicating that the West Fork glacier flowed through the road col south of Rainbow Creek and merged with ice on the East Fork		Burnt Hill-West Fork of the Humptulips River-Humptulips River Valley Lat: 47°17′30″ Long: 123°51′45″	Older Wisc or Salmon Springs	Long, GHRDB SOPW
Drift	Deeply oxidized reddish-brown drift overlain by up to 3 ft of silty soil probably of eolian origin extends eastward from the base of Burnt Hill into the West Fork valley; opposite the mouth of Rainbow Creek the drift rises above intermediate terraces and forms the highest terrace level along the river here		Burnt Hill-West Fork of the Humptulips River-Humptulips River Valley Lat: 47°17′30″ Long: 123°51′45″	Older Wisc or Salmon Springs	Long, GHRDB SOPW
Morainal Segment and Till	A probable morainal segment lies on the west side of the East Fork Humptulips River a mile downstream from measured section B; a very compact, deeply oxidized till is overlain by a younger, fresher till containing striated and faceted stones at this place; the bottom till may represent older Wisc. till overridden by younger Wisc. ice		East Fork of the Humptulips River-Humptulips River Valley Lat: 47°15′00″ Long: 123°53′15″	Older Wisc or Salmon Springs	Long, GHRDB SOPW
Till and Ice Extent	Grisdale ice filled the low 825 ft col in the drainage divide west of Falls Creek and merged with East Fork Humptulips ice; the upper		East Fork of the Humptulips River-Humptulips River Valley Lat: 47°15′00″	Inter-mediate Wisc or Evans	Long, GHRDB SOPW

What	Description	Where	Location	Age	Source
	limit of Grisdale till is near the top of the divide separating the East Fork and Wishka Rivers; road cuts on the east side of the divide expose Grisdale till with many striated stones and a 6 foot basalt boulder; Mobray drift is incorporated into the till; it occurs up to 1,250 ft		Long: 123°53′15″	Creek	
Former Glacial Extent	During the maximum Intermediate Wisc. (or Evans Creek) advance the southern limit of the East Fork glacier was 1.5 miles southwest of the 825 ft col in the drainage divide and the minimum elevation of the ice was near 550 ft		East Fork of the Humptulips River-Humptulips River Valley Lat: 47°15′00″ Long: 123°53′15″	Inter-mediate Wisc or Evans Creek	Long, GHRDB SOPW
Morainal Segments	There are at least five morainal segments on the east side of the East Fork Humptulips River lying between the 825 ft col and the bridge crossing the East Fork; the crest of the highest moraine reaches 850 ft; the South Boundary Road and logging skid roads have exposed till in cutbanks in the moraines		East Fork of the Humptulips River-Humptulips River Valley Lat: 47°24′17″ Long: 123°41′58″ Lat: 47°20′04″ Long: 123°43′12″	Inter-mediate Wisc or Evans Creek	Long, GHRDB SOPW
Outwash	Outwash extends southwest from the outermost moraine and abundant gravel up to ~650 ft between the mouths of Rock and Webfoot Creeks may be graded to the moraine; the outwash is compact, yellow-brown, and oxidized to a depth of 3-4 ft		Rock and Webfoot Creeks-East Fork of the Humptulips River-Humptulips River Valley Lat: 47°18′00″ Long: 123°47′30″	Inter-mediate Wisc or Evans Creek	Long, GHRDB SOPW
Lateral Moraine	A two mile long ridge crest in the dense forest is probably a lateral moraine on the east side of the valley; Rainbow Creek flows along the outer base of the moraine; it rises from ~400 ft to 750 ft at a point where a cut through a topographic high on road No. 2302 exposes till	Olympic National Forest	Rainbow Creek-West Fork of the Humptulips River-Humptulips River Valley Lat: 47°19′53″ Long: 123°49′13″	Inter-mediate Wisc or Evans Creek	Long, GHRDB SOPW
Outwash and Till	Half a mile west of the moraine from above, a gravel pit exposes drift consisting of	Olympic National Forest	Rainbow Creek-West Fork of the Humptulips River-	Inter-mediate Wisc	Long, GHRDB SOPW

What	Description	Where	Location	Age	Source
	alternating layers of till and outwash; the outwash is compact and is located between two very compact lodgement tills which suggests a fluctuating ice margin; basalt till stones are firm and striated		Humptulips River Valley Lat: 47°18′30″ Long: 123°49′00″	or Evans Creek	
Outwash and Soils	Outwash gravels lie between the lateral moraine and the base of the Humptulips Ridge; at an altitude of 635 ft one mile north of the Humptulips Work Center outwash gravels are overlain by 2-3 ft brown soils of probable eolian deposition	Olympic National Forest	Rainbow Creek-West Fork of the Humptulips River-Humptulips River Valley Lat: 47°18′30″ Long: 123°49′00″	Inter-mediate Wisc or Evans Creek	Long, GHRDB SOPW
Moraines and Terrace	A high terrace on the west side of the West Fork valley between Newbury and Grouse Creeks can be graded to a moraine at the mouth of Grouse Creek; the moraine was built by the West Fork alpine glacier following its retreat from it max position at the mouth of Rainbow Creek; a short lateral moraine characterized by hills and ridges up to 50 ft high extends 1 mile upstream to near the mouth of Phillips Creek; till in the moraine consists of moderately rounded stones, many are striated; the river is turned southward by the moraine from its easterly course and flows about a mile along the outside base of the moraine	Olympic National Forest	Newbury and Grouse Creeks-West Fork of the Humptulips River-Humptulips River Valley Lat: 47°21′16″ Long: 123°48′42″	Inter-mediate Wisc or Evans Creek	Long, GHRDB SOPW
End Moraine	Another moraine lies at the mouth of Phillips Creek and its crest reaches 800 ft	Olympic National Forest	Phillips Creek-West Fork of the Humptulips River-Humptulips River Valley Lat: 47°22′57″ Long: 123°47′51″	Inter-mediate Wisc or Evans Creek	Long, GHRDB SOPW
Former Glacial Lake	Behind the second moraine listed above are exposures up to 10 ft thick of laminated silts and clays in road cuts just north of the West Fork rock gorge indicating that a lake having a surface	Olympic National Forest	Phillips Creek-West Fork of the Humptulips River-Humptulips River Valley Lat: 47°23′00″ Long: 123°48′00″	Inter-mediate Wisc or Evans Creek	Long, GHRDB SOPW

What	Description	Where	Location	Age	Source
	elevation of ~625 ft was dammed by the inner moraine				
Bedrock Gorge Depth	The depth of the West Fork of the Humptulips River gorge from the center of the bridge is 160 ft, all of which is postglacial cutting beneath the base of the moraine		West Fork of the Humptulips River-Humptulips River Valley Lat: 47°15′00″ Long: 123°53′15″	Inter-mediate Wisc or Evans Creek	Long, GHRDB SOPW
Measured Section of Glacial Sediments	The younger Wisconsin drift was examined in a high river bank on the east side of the upper East Fork Humptulips River and known as measured section B; at the top is (5) 25 ft of fresh, compact till with numerous smoothed, faceted, and striated pebble-boulder size stones; underlying this is (4) 60 ft of pebble-cobble sand gravel with horizontal stratification; this is underlain by (3) 75 ft of pebble-cobble sandy gravel inclined in layers dipping downvalley; underlying this are pre-Wisc. interglacial sediments starting with (2) 15 ft of laminated to thick bedded clay, silt, and fine sand with peat, woody fragments, and small logs followed by (1) 15 ft of gray unoxidized gravel that is horizontally stratified; the lacustrine sediments of (2) are probably the equivalent of those from West Fork Humptulips River and the surface level would have been at ~890 ft; the logs have a radiocarbon age of 37600±2000 years B.P.		East Fork of the Humptulips River-Humptulips River Valley Lat: 47°15′00″ Long: 123°53′15″	Youn-ger Wisc or Vashon	Long, GHRDB SOPW
Outwash	(3) from above is composed of sandy gravel delta foreset beds exposed to ~965 ft elevation; as they are inclined downvalley they were deposited by the axial stream, not a tributary; they represent advance outwash built up during the readvance of the East Fork glacier and		East Fork of the Humptulips River-Humptulips River Valley Lat: 47°15′00″ Long: 123°53′15″	Youn-ger Wisc or Vashon	Long, GHRDB SOPW

What	Description	Where	Location	Age	Source
	are deltaic sediments deposited in water dammed by the outer Vashon moraine which lies 1 mile downstream from here				
Terrace	The high terrace of the upper East Fork is composed of (4) from above; the horizontal gravel beds are in part topsets representing material laid down in horizontal layers on top of a growing delta and in part advance glacial outwash built up after the moraine dammed lake filled with sediments		East Fork of the Humptulips River-Humptulips River Valley Lat: 47°15′00″ Long: 123°53′15″	Younger Wisc or Vashon	Long, GHRDB SOPW
Alpine Terminal Morainal Segment	The till of (5) from above forms an alpine terminal morainal segment on top of the terrace surface; there are three short arcuate morainal ridges that rise ~1,075 ft at the base of the east wall; two road cuts expose 5 ft of fresh gray till composed of greywacke and basalt; across the terrace surface the morainal segments are barely more than 3 ft high and are hidden in the low brush		East Fork of the Humptulips River-Humptulips River Valley Lat: 47°15′00″ Long: 123°53′15″	Younger Wisc or Vashon	Long, GHRDB SOPW
Moraine	An outer moraine of Vashon age was deposited by a glacier ~7.5 miles long that reached a minimum altitude of 800 ft; the morainal segment on the west side of the river curves toward the river and its crest lies between 950-1,100 ft		East Fork of the Humptulips River-Humptulips River Valley Lat: 47°26′06″ Long: 123°40′33″	Younger Wisc or Vashon	Long, GHRDB SOPW
Morainal Segment	A morainal segment lies on the upper West Fork of the Humptulips River; it lies on the east side of the valley and was exposed by a road along its crest which lies at 750 ft altitude; on the opposite side of the valley along the side of Chester Ridge, the moraine rises to higher levels and fills the broad 850 ft saddle there; in the saddle the main West Fork road cuts through the moraine and exposes till		West Fork of the Humptulips River-Humptulips River Valley Lat: 47°24′41″ Long: 123°46′41″	Younger Wisc or Vashon	Long, GHRDB SOPW

What	Description	Where	Location	Age	Source
Outwash	The sublobe of the glacier in the 850 ft saddle fed outwash into Chester Creek and this outwash reached the West Fork of the Humptulips River		West Fork of the Humptulips River-Humptulips River Valley Lat: 47°15′00″ Long: 123°53′15″	Youn-ger Wisc or Vashon	Long, GHRDB SOPW
Floodplain	Much sediment was deposited by the river and its tributaries during the last glaciation and constructed a thick floodplain; during Holocene time aggradation ceased and the floodplain was abandoned and the river began downcutting		Humptulips River Valley Lat: 47°04′30″ Long: 124°03′30″	Holocene	Long, GHRDB SOPW
Alluvial Fans	Numerous alluvial fans developed in response to the large amount of sediment present in the river valley as described above; they are located in the upper East and West Fork valley bottoms; the fans are deeply trenched by small side streams and in places have cut down through the fans and a few tens of feet into the underlying bedrock		Humptulips River Valley Lat: 47°04′30″ Long: 124°03′30″	Holocene	Long, GHRDB SOPW
Terraces	The river has exposed 200 ft of valley fill in steep margining bluffs leaving unpaired terraces along the valley walls; at a few places landslides have dropped from the valley walls and lie on the terraces		Humptulips River Valley Lat: 47°04′30″ Long: 124°03′30″	Holocene	Long, GHRDB SOPW

4.3 REFERENCES OF DEPOSITS FROM OTHER AUTHORS BY WILLIAM LONG

What	Description	Where	Location	Age	Source
Recessional Meltwater Channel	The Bingham Creek channel extends from Vance Creek over Windy Siding to the East Fork of the Satsop River; the retreating ice of the Vashon glacier allowed the 600 ft col at Windy Siding to be used as an outlet to the glacial lake that formed along Vance Creek		South Fork of the Skokomish River Valley	Vashon	Carson (1970)
Recessional Meltwater Channel, Moraines, Kettles	The Winter Creek channel begins at the 450 ft col 3 miles east of Windy Siding and was near the southwest margin of the glacier; thick moraine deposits at the mouth of the channel are irregular in frontal outline and the surface is pocked with kettles, many of which contain ponds; kettles also occur opposite the mouth of the channel in thick drift deposits and water flowed out through the Skokomish valley; steep bluffs in the drift mark the course of the channel		South Fork of the Skokomish River Valley	Vashon	Carson (1970)
Basaltic Till	The North Fork Skokomish glacier may have overridden Dow Mountain and flowed out into the Puget Lobe and it left Olympic basaltic till (and an absence of granites) on the mountain above 1,900 ft	Olympic National Forest	North Fork Skokomish Glacier	Admiralty (Salmon Springs?)	Todd (1939)
Moraine	Granitic stones were found within less than a mile of old Lake Cushman, but none along the lakeward slope; the valley of the North Fork was dammed by a moraine deposit of the Puget Lobe which crowded up the river valley and held back the local glacier; deposits have		Lake Cushman-North Fork Skokomish River Valley	Vashon	Bretz (1913)

What	Description	Where	Location	Age	Source
	moraine topography close to the lake, but there are no traces of Puget glacial stones except where a stream enters from the Puget drift plain				
Piedmont Glacier	Found evidence of an Olympic piedmont glacier in Puget Sound before the last Puget Lobe invaded; Olympic till overlies weathered Admiralty drift and is overlain by Vashon Puget drift; till contains sandstones, basalts, and a few granitic stones from previous Puget lobe advances	Olympic National Forest	Hamma Hamma River		Bretz (1913)
Puget and Alpine Glaciers Coalesced	Puget ice flowing up the Hamma Hamma River coalesced with the alpine glacier noting that granite bearing till is not found farther upvalley than one-half mile	Olympic National Forest	Hamma Hamma River		Todd (1939)
Terminal Moraine	Terminal moraine 3 miles in from the mouth of the Hamma Hamma River (at Cabin Creek) and terraces which are graded to and in contact with the moraine; if the gradient maintained by the tops of the terrace are extended to the mouth of the Hamma Hamma River they reach a point 300 ft above sea level which matches the height of the delta observed there and suggests the delta and terraces are part of the same surface	Olympic National Forest	Hamma Hamma River Lat: 47°35′43″ Long: 123°07′34″	Late-Vashon	Todd (1939)
End Moraine	An Olympic end moraine half a mile west of Camp Collins and four miles into the valley; terrace gravels extend downstream from the moraine and were deposited after the retreat of the Vashon Puget ice	Olympic National Forest	Duckabush River Lat: 47°41′04″ Long: 123°01′35″		Frisken (1965)
Granite Stones as Floats in Glacial Lakes	Grainitic stones occurred as float 4.5 miles up the Duckabush valley and 5.5 miles up the Dosewallips		Dosewallips and Duckabush Rivers	Vashon	Frisken (1965)

What	Description	Where	Location	Age	Source
	valley from Hood Canal indicating that glacial lakes were ponded in the valleys by the Puget Lobe and the glaciers were restricted in extent				
Olympic Till	Olympic till under the Brinnon delta and along the shore of the Hood Canal for a short distance north of the mouth of the valley indicate that Olympic ice spread beyond the mountain front before the arrival of the last Puget Lobe		Dosewallips River		Bretz (1913)
Olympic Till	Four miles east of the mouth of the Dosewallips River along the southern tip of the Toandas Peninsula stratified, loose Olympic gravels were overlain by Vashon Puget till; the thickness and widespread occurrence indicate it is a portion of the outwash plain from the Dosewallips glacier when it terminated in the Hood Canal		Dosewallips River		Frisken (1965)
End Moraine	Probable end moraine lying at 650 ft crosses the Dosewallips valley 8 miles above the valley mouth at the mouth of Stony Brook; it is hummocky and boulder strewn with boulders up to 20 ft in diameter and appears as a ridge crossing the river; alluvial sediments extend downstream from Stony Brook for ~3 miles	Olympic National Forest	Dosewallips River Lat: 47°43′51″ Long: 123°05′14″	Vashon	Frisken (1965)
Lacustrine Sediments	Evidence for two advances of the Puget Lobe into the Dosewallips River Valley as there are two Vashon till sheets separated by 20-50 ft of lacustrine sediments		Dosewallips River Valley		Frisken (1965)
Two Vashon Advances of Puget Ice	Found evidence for two advances of Vashon Puget ice in the lower Dosewallips River valley		Lower Dosewallips River Valley	Vashon	Frisken (1965)

What	Description	Where	Location	Age	Source
	in the form of two till sheets separated by 20-50 ft of lacustrine sand, silt, and clay				
Glacial Lakes	When the Puget Lobe was in retreat, ice-carved valleys were exposed and these became large glacial lakes; Lake Russell formed when the ice retreated from the southern most arm of Puget Sound (Budd Inlet) and at its maximum was more extensive than the part of Puget Sound lying south of Everett; drainage from the lake used the Black Lake outlet south into the Chehalis River; a later readvance destroyed this lake and closed the Black Lake outlet, but a new lake with a different level and outlet formed along the eastern portion of the lowland; a second retreat gave rise to Later Lake Russell and the Black Lake outlet was once again used		Southern Puget Sound-Chehalis River	Vashon	Bretz (1913)
Continental Ice Sheet Till	The continental ice sheet must have covered the area north of Snider Peak to an altitude of at least 2,750 ft as abundant till containing granitic and other northern stones occur that high half a mile east of Snider Peak; the till lies on ridge crests and is exposed in road cutbanks	Olympic National Forest	Sol Duc Valley	Vashon	Gower (1960)
Till	A deeply weathered till crops out in a roadcut along U. S. Highway 101 at an altitude of 225 ft about 2 miles south of Humptulips; the stones are decomposed to a depth of at least 6 feet and a less weathered gravel overlies the till		Humptulips River Valley	Pre-Wisc or Stuck	Crandell (1964)
Till	An old weathered till on Donkey Creek Road about 2.25 miles northeast of U.		Humptulips River Valley	Older Wisc or	Moore (1965)

What	Description	Where	Location	Age	Source
	S. Highway 101 was designated as the type section for the till; this is the oldest till he observed; 30 ft of compact, weathered till caps a 130 ft section of stratified, semi-consolidated sand, silt, clay, and gravel			Salmon Springs	
Drift	A unit was mapped extending southeast from near the Humptulips Work Center across the broad 700 ft col to the East Fork as being underlain by Chow Chow or younger Wisconsin outwash; however, the meltwater would have had to flow through the col, which is 200 ft higher than intermediate terraces in the adjacent West Fork, and it has a degree of weathering that is too old for Chow Chow drift, so it should be associated with older Wisconsin piedmont ice		Humptulips River Valley	Older Wisc or Salmon Springs	Moore (1965)
Former Glacier Extent	During the Salmon Springs glaciation, the Wynoochee alpine glacier advanced south 10-11 miles beyond the mountain front and deposited Mobray Drift; glaciers were 500 ft thicker than during the Fraser Glaciation when glaciers advanced to within 6 miles of the Mobray glacier limit and deposited Grisdale Drift; Mobray till is commonly incorporated into the Grisdale till particularly near the Fraser alpine drift border		Humptulips River Valley	Older Wisc or Salmon Springs and Inter-mediate Wisc. or Evans Creek	Moore (1965)

4.4 FIGURES

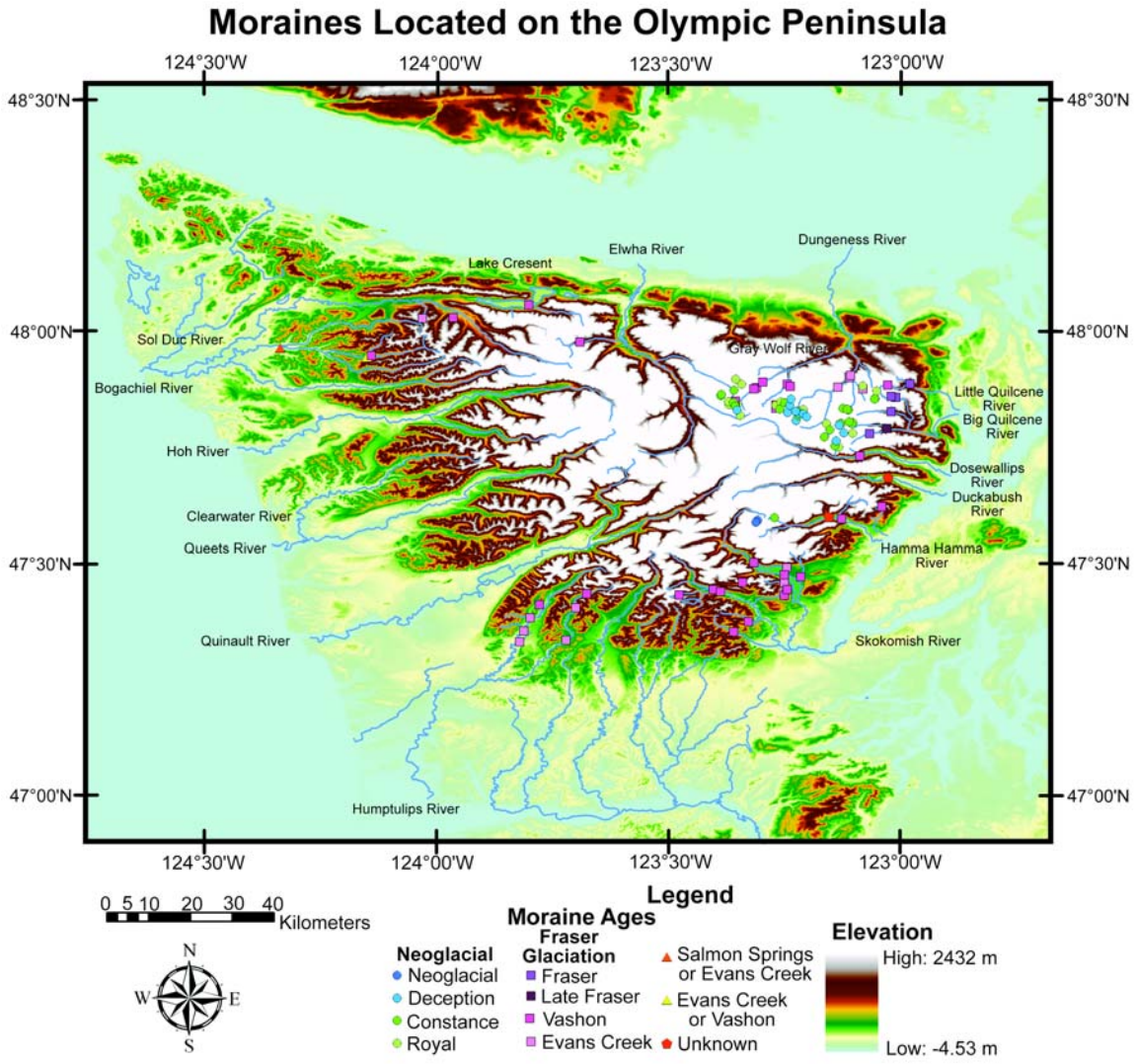

Figure 4.1. Location of the moraines listed in the tables in this chapter. The moraines are separated according to their ages. Further information on the ages can be found on page 121. A few moraines are of unknown age or could not be specified more closely and are listed as to what possible glaciation or stade they are from.

CHAPTER 5: SUMMARY AND FUTURE WORK

5.1 HYPOTHESES AND MOTIVATION

The interaction of climate, tectonics, and erosion in the Olympic Mountains of Washington State is investigated to see the influence of glaciers. The focus of this work is on the relationships between climate, glacial extent, and the spatial patterns of glacial erosion and rock uplift. The tectonic setting of an accretionary wedge dictates an average large-scale topographic form (Dahlen, 1984). There are strong and persistent spatial gradients in precipitation across the peninsula. The Olympic Mountains are thought to be in steady-state in which the spatially variable erosion and rock uplift patterns have been maintained in a close balance over several million years (Brandon et al., 1998; Pazzaglia and Brandon, 2001). The spatial variability in rock uplift rates cannot be explained by variability in fluvial erosion rates (Tomkin et al., 2003).

Glaciers are powerful agents of erosion that have long been present on the peninsula: could glacial erosion explain the observed pattern of rock uplift rates? A numerical model of glacial flow, ICE Cascade, is used to investigate this hypothesis through two research questions. Firstly, can the glacial extent of the LGM be modeled with ICE Cascade? Secondly, does glacial erosion based on sliding produce a pattern that matches the observed pattern of rock uplift rates? ICE Cascade is used to reproduce glaciers that are consistent with paleoclimate and geomorphic evidence constraining glacial extent and climatic conditions during the late Quaternary. The spatial distribution of glacial erosion produced by the numerical model is compared with the observed pattern of long-term exhumation.

The glacial record for the northern and eastern sides of the Olympic Mountains is poorly constrained. This lack of information makes it impossible to determine how the climatic variability across the range has influenced the topographic and tectonic development. The record of recent glaciations and glacial landforms on the Olympic Peninsula is examined and the spatial variability in the timing and extent of glaciers across the range is compared with the modern climatic gradients. Lichenometry is used to date moraines at the base of Royal Glacier on Mount Deception. Equilibrium line altitudes (ELAs) of the reconstructed glaciers are estimated and compared to ELAs for

Blue Glacier in the western Olympics to illustrate the impact of the precipitation gradients on glacier extent. A compendium of glacial deposits observed throughout the peninsula is also summarized so a broader picture of the glacial extent can be developed. The culmination of work in these three areas allows for a greater understanding of how climate, erosion, and tectonics interact on the Olympic Peninsula.

5.2 RESULTS

The numerical model, ICE Cascade, can reproduce the observed LGM ice extent based on dated geomorphic landforms in river valleys on the western side of the Olympic Mountains. The model requires summer temperatures of 7.0-8.0°C and a precipitation fraction of 0.4-0.8 to accurately simulate the ice extent. These precipitation and temperature ranges are consistent with paleoclimate estimates.

The glacial erosion calculated by ICE Cascade is based on a sliding law in which erosion is proportional to sliding velocity raised to the power l, with a canonical value of 1. The glacial erosion pattern predicted by ICE Cascade resembles the observed rock uplift pattern: erosion rates increase from the coast towards the center of the range. Modeled glacial erosion rates are predicted to be the fastest in the Hoh River Valley, where measured rock uplift rates are also the fastest. Erosion is highest in the valleys, which is expected, so the glacial erosion rule overdeepens the valleys. Significant local erosion through valley-wall slope failure is required to prevent unrealistic ridge-valley relief from being produced.

When the glacial erosion is examined on a valley scale, the predicted glacial erosion rates are significantly faster than the observed rock uplift rates. Since the Olympics are in a steady state, the total erosion rates must equal the rock uplift rates over timescales resolvable by thermochronology and geomorphology. This study assumes that glacial erosion is the dominant process of erosion and that it perfectly matches rock uplift rates. This assumption allows for calibration of the sliding law and interpretation of the constants in terms of their physical implications. With l held at one and K_g allowed to vary, the best fit between modeled glacial erosion and observed uplift occurs for a K_g on the order of 10^{-5} in three separate river valleys. This value lies within the range of observed values for K_g (Humphrey and Raymond, 1994). When both K_g and l are allowed

to vary, the overall best fitting cases with the lowest misfit between the uplift and erosion are found. For the Hoh River Valley, the best fitting case occurs when K_g is 2.691e-4 and l is 0.4. The Quinault River has its best fitting case when K_g is 9.245e-4 and l is 0.1. The Queets River has its best fitting case when K_g is 6.2375e-4 and l is 0. The two cases with low values for l imply that the ice sliding erosion rule may be inaccurate and that glacial erosion rates may be successfully predicted by the duration of ice cover rather than the details of ice flow. It is possible that glacial erosion is strongly influenced by processes other than sliding, perhaps including the presence of subglacial water. In addition uncertainties and limited spatial resolution of the uplift data may influence the fitted parameters. Finally, erosional processes in addition to glaciers have certainly played a role and are neglected in this analysis. Overall, the sliding based glacial erosion model is plausible, especially since with l fixed at one, three independent valleys provide a similar and physically reasonable value for K_g.

The lichenometric investigation into the neoglacial history of the Olympic Mountains resulted in the formation of a regional growth curve for the Pacific Northwest. This curve was applied to four moraines that lie at the base of Royal Glacier on Mount Deception, on the eastern side of the Olympic Mountains, and they were found to date from 1839, 1895, 1963, and younger than 1963. These dates constrain the glacial recession history of Royal Glacier.

Glaciers were reconstructed from the dated moraines and ELAs were estimated. The average ELA of Royal Glacier over the past 200 years is 1774 m. In comparison, the ELA of Blue Glacier over the same time period is 1688 m. These ELAs are used to construct an ELA gradient across the Olympic Peninsula. The slope of this climate gradient is similar to both Porter's (1964) and Spicer's (1986) modern climate gradients, while it differs greatly from Porter's (1964) Pleistocene climate gradient. This implies a change in the climate in the Pleistocene as compared to the current climate.

5.3 FUTURE WORK

There is an opportunity for much additional work to be conducted in the Olympic Mountains of Washington State. As there is no detailed glacial history for the eastern Olympic Mountains, a compendium of glacial deposits observed in the northern and

eastern sides of the range was developed. However, the majority of the deposits are not verified or dated. A map of all of the glacial deposits, especially the geomorphic landforms, with the corresponding dates would be an invaluable tool for further research. This would require researchers to physically map and examine the deposits and landforms in each of the valleys and peaks in the Olympic Mountains. Dating of the deposits through techniques like lichenometry, dendrochronology, and radiocarbon dating would allow for a more detailed and well-defined glacial history to be developed. This history could be employed in numerical models, including ICE Cascade, to evaluate the spatial and temporal variability in glacial erosion rates, to constrain the ice extent at the LGM, by projects that are comparing the western and eastern sides of the range, or in climatic comparisons, for example.

A numerical model that includes a more complete description of glacial erosion than just the glacial sliding erosion rule might more effectively model the glacial erosion on the Olympic Peninsula. The total erosion rate in ICE Cascade does not include the effects that entrained debris within the ice will have on the rates of erosion. Local processes must occur which erode the ridges and transport the material to the glaciers where it is incorporated into the ice. This entrained material can protect the bed from further erosion and is analogous to the armoring of the bed in a fluvial system (Bennett and Glassner, 1996). It can also provide tools to erode the bed. Including all of these processes in the numerical model could more accurately describe the erosion that has occurred in the Olympic Mountains. In addition, the numerical model could also include the effects of the continental ice sheet if the glacial history was better constrained. The ice sheet had the ability to interact with the alpine ice and change the amounts of glacial erosion. There could also be changes in the climate due to the presence of the ice sheet and these factors could be included in the numerical model to make it more accurate for the Olympic Peninsula.

The observed rock uplift pattern is not well constrained in two of the three rivers on the western side of the Olympic Peninsula. Few points were sampled in these regions and the contours are not well constrained. If more data was sampled throughout the peninsula, but especially in these two valleys, the uplift pattern could be much better

constrained. This new uplift pattern could improve the correlation with the glacial erosion.

Future work could also focus on the orographic precipitation pattern. If the precipitation pattern was more detailed and well-constrained, a more accurate determination of the precipitation changes over time and the effects of precipitation on glacial extent and the various ELAs of glaciers in the Olympics could be discovered. By examining the paleo-ELAs for all of the glaciers within the mountains, the precipitation pattern at the time of the last glacial maximum could be constrained. The climate changes discovered by this work could also help us to learn about what is currently happening and what may happen in the future with glacial extent in this range. Our climate is currently changing in new ways with the full impacts having yet to be seen.

REFERENCES

Allen, Sandra M., and Smith, Dan J., 2007, Late Holocene glacial activity of Bridge Glacier, British Columbia Coast Mountains: Canadian Journal of Earth Sciences, Vol. 44, pgs. 1753-1773.

Alley, R. B., Lawson, D. E., Larson, G. J., Evenson, E. B., and Baker, G. S., 2003, Stabilizing feedbacks in glacier-bed erosion: Nature, Vol. 424, pgs. 758-760.

Anders, A. M., Roe G. H., Durran, D. R., Minder, J. R., 2007, Small-scale Spatial Gradients in Climatological Precipitation of the Olympic Peninsula: Journal of Hydrometeorology, Vol. 8, No. 5, pgs. 1068-1081.

Armstrong, Richard, 2004, Lichens, Lichenometry and Global Warming: Microbiologist, pgs. 32-35.

Batt, Geoffrey E., Brandon, Mark T., Farley, Kenneth A., and Roden-Tice, Mary, 2001: Tectonic synthesis of the Olympic Mountains segment of the Cascadia wedge, using two-dimensional thermal and kinematic modeling of thermochronological ages: Journal of Geophysical Research, Vol. 106, No. B11, pgs. 26,731-26,746.

Benedict, James B., 1991, Experiments on Lichen Growth II, Effects of a Seasonal Snow Cover: Arctic and Alpine Research, Vol. 23, No. 2, pgs. 189-199.

Benedict, James B., 1990, Lichen Mortality Due to Late-Lying Snow: Results of a Transplant Study: Arctic and Alpine Research, Vol. 22, No. 1, pgs. 81-89.

Benn, Douglas I., and Evans, David J. A., 1998, Glaciers and Glaciation: Great Britain, The Bath Press, Bath, pgs. 74-90.

Bennett, M. R., and Glassner, N. F., 1996, Glacial Geology Ice Sheets and Landforms: John Wiley, Hoboken, New Jersey, 364 pgs.

Bindschadler, Robert, 1983, The importance of pressurized subglacial water in separation and sliding at the glacier bed: Journal of Glaciology, Vol. 29, No. 101, pgs. 3-18.

Brandon, M. T., 2004, The Cascadia subduction wedge: the role of accretion, uplift, and erosion: in: van der Pluijm, B. A., and Marshak, S., 2004, Earth Structure: An Introduction to Structural Geology and Tectonics (Leo A. W. Wiegman (ed.)): WCB/McGraw Hill Press, 2nd Ed., pgs. 566-574.

Brandon, Mark T., Roden-Tice, Mary K., and Garver, John I., 1998, Late Cenozoic exhumation of the Cascadia accretionary wedge in the Olympc Mountains, northwest Washington State: GSA Bulletin, Vol. 110, No. 8, pgs. 985-1009.

Braun, Jean, Zwartz, Dan, and Tomkin, Jonathan H., 1999, A new surface-processes model combining glacial and fluvial erosion: Annals of Glaciology, Vol. 28, pgs. 282-290.

Bretz, J. H., 1913, Glaciation of the Puget Sound Region: Washington Geological Survey Bulletin, No. 8, 244 pgs.

Budd, W. F., Keage, P. L., and Blundy, N. A., 1979, Empirical studies of ice sliding: Journal of Glaciology, Vol. 23, No. 89, pgs. 157-170.

Bull, W. B., 1996, Dating San Andreas fault earthquakes with lichenometry: Geology, Vol. 24, No. 2, pgs. 111-114.

Bull, W. B., and Brandon, M. T., 1998, Lichen dating of earthquake-generated rockfall events, Southern Alps, New Zealand: Geological Society of America Bulletin, Vol. 110, No. 1, pgs. 60-84.

Burbank, D. W., 1981, A Chronology of Late Holocene Glacial Fluctuations on Mount Rainier, Washington: Arctic and Alpine Research, Vol. 13, No. 4, pgs. 369-386.

Burbank, D. W., 1982, Correlations of Climate, Mass Balances, and Glacial Fluctuations at Mount Rainier, Washington, U.S.A., Since 1850: Arctic and Alpine Research, Vol. 14, No. 2, pgs. 137-148.

Carson, R. J., III, 1970, Quaternary geology of the south-central Olympic Peninsula, Washington: Unpublished Ph.D. thesis, University of Washington, 67 pages.

Conway, H., Rasmussen, L. A., and Marshall, H.-P., 1999, Annual Mass Balance of Blue Glacier, USA: 1955-97: Geografiska Annaler, Vol. 81 A, No. 4, pgs. 509-520.

Crandell, D. R., 1964, Pleistocene glaciations of the southwestern Olympic Peninsula, Washington: U. S. Geological Survey Professional Paper 501-B, pgs. 135-139.

Crandell, Dwight R., 1965, The Glacial History of Western Washington and Oregon: in: Wright, H. E., Jr. and Frey, D. G., 1965, The Quaternary of the United States: Princeton University Press, pgs. 341-353.

Dahlen, F. A., 1984, Noncohesive Critical Coulomb Wedges: An Exact Solution: American Geophysical Union, Vol. 89, No. B12, pgs. 10,125-10,133.

DePriest, Paula, 1994, What is a lichen?: Smithsonian Institution, http://botany.si.edu/lichens/

Drewry, D., 1986, Glacial Geologic Processes: Edward Arnold, London, 281 pgs.

Frisken, J. G., 1965, Pleistocene glaciation of the Brinnon area, east-central Olympic Peninsula, Washington: Unpublished M. S. Thesis, University of Washington, 75 pgs.

Garcia, Antonio F., 1996, Active Tectonic Deformation and Late Pleistocene and Holocene Geomorphic and Soil Profile Evolution in the Dosewallips River Drainage Basin, Olympic Mountains, Western Washington State: Master of Science Thesis, University of New Mexico, 43 pgs.

Gower, H. D., 1960, Geology of the Pysht Quadrangle, Washington: U. S. Geological Survey Quadrangle Map GQ-129.

Harbor, J. M., 1992a, Application of a general sliding law to simulating flow in a glacier cross section: Journal of Glaciology, Vol. 38, pgs. 182-190.

Harbor, J. M., 1992b, Numerical modeling of the development of U-shaped valleys by glacial erosion: Geological Society of America Bulletin, Vol. 104, pgs. 1364-1375.

Harbor, J. M., Hallet, B., and Raymond, C. F., 1988, A numerical model of landform development by glacial erosion: Nature, Vol. 333, pgs. 347-349.

Hallet, B., 1979, A theoretical model of glacial abrasion: Journal of Glaciology, Vol. 17., pgs. 209-222.

Hallet, B., 1996, Glacial quarrying: A simple theoretical model: Annals of Glaciology, Vol. 22, pgs. 1-8.

Hallet, B., Hunter, I., and Bogen, J., 1996, Rates of erosion and sediment evacuation by glaciers: A review of field data and their implications: Global Planetary Change, Vol. 12, pgs. 213-235.

Harper, J. T., 1993, Glacier Terminus Fluctuations on Mount Baker, Washington, U.S.A., 1940-1990, and Climatic Variations: Arctic and Alpine Research, Vol. 25, No. 4, pgs. 332-340.

Heusser, Calvin J., 1957, Variations of Blue, Hoh, and White Glaciers in recent centuries: Arctic, Vol. 10, pgs. 139-150.

Heusser, Calvin J., 1972, Palynology and Phytogeographical Significance of a Late-Pleistocene Refugium Near Kalaloch, Washington: Quaternary Research, Vol. 2, pgs. 189-201.

Heusser, Calvin J., 1974, Quaternary Vegetation, Climate, and Glaciation of the Hoh River Valley, Washington: Geological Society of America Bulletin, Vol. 85, pgs. 1547-1560.

Heusser, C. J., Heusser, L. E., and Peteet, D. M., 1999, Humptulips revisited: a revised interpretation of Quaternary vegetation and climate of western Washington, USA: Palaeogeography, Palaeoclimatology, Palaeoecology, Vol. 150, pgs. 191-221.

Hilley, G. E., and Strecker, M., 2004, Steady state erosion of critical Coulomb wedges with applications to Taiwan and the Himalaya: Journal of Geophysical Research, Vol. 19, 17 pgs.

Hooke, Roger LeB., 2005, Principles of Glacier Mechanics, 2nd Ed.: United Kingdom, University Press, Cambridge, pgs. 17-41.

Howard, A. D., and Kerby, G., 1983, Channel changes in badlands: Geological Society of America Bulletin, Vol. 94, pgs. 13,971-13,986.

Humphrey, N. F., and Raymond, C. F., 1994, Hydrology, erosion and sediment production in a surging glacier: Variegated Glacier, Alaska, 1982-1983: Journal of Glaciology, Vol. 40, pgs. 539-552.

Hutter, K., 1983, Theoretical Glaciology: Springer, New York, 510 pgs.

Innes, J. L., 1984, The Optimal Sample Size in Lichenometric Studies: Arctic Alpine Research, Vol. 16, No. 2, pgs. 233-244.

Innes, J. L., 1985a, An Examination of Some Factors Affecting the Largest Lichens on a Substrate: Arctic Alpine Research, Vol. 17, No. 1, pgs. 99-106.

Innes, J. L., 1985b, Moisture Availability and Lichen Growth: The Effects of Snow Cover and Streams on Lichenometric Measurements: Arctic Alpine Research, Vol. 17, No. 4, pgs. 417-424.

Iverson, N. R., 1991, Potential effects of subglacial water-pressure fluctuations on quarrying: Journal of Glaciology, Vol. 37, pgs. 27-36.

Kerr, Andrew, 1993, Topography, climate and ice masses: a review: Terra Nova, Vol. 5, pgs. 332-342.

Knap, Wouter H., Oerlemans, Johannes, and Cadee, Martin, 1996, Climate sensitivity of the ice cap of King George Island, South Shetland Islands, Antarctica: Annals of Glaciology, Vol. 23, pgs. 154-159.

Knight, Peter G., 1999, Glaciers: Great Britain, Martins the Printers Ltd., Berwick upon Tweed, pgs. 23-38.

Koons, P. O., Norris, R. J., Craw, D., and Cooper, A. F., 2003, Influence of exhumation on the structural evolution of transpressional plate boundaries; an example from the Southern Alps, New Zealand: Geology, Vol. 31, pgs. 3-6.

Kuhlemann, J., Rohling, E. J., Krumrei, I., Kubik, P., Ivy-Ochs, S., and Kucera, M., 2008, Regional synthesis of Mediterranean atmospheric circulation during the Last Glacial Maximum: Science, Vol. 321, pgs. 1338-1340.

Larocque, S. J., and Smith, D. J., 2004, Calibrated *Rhizocarpon* spp. Growth Curve for the Mount Waddington Area, British Columbia Coast Mountains, Canada: Arctic, Antarctic, and Alpine Research, Vol. 36, No. 4, pgs. 407-418.

Leonard, Eric M., 1984, Late Pleistocene Equilibrium-Line Altitudes and Modern Snow Accumulation Patterns, San Juan Mountains, Colorado, U.S.A.: Arctic and Alpine Research, Vol. 16, No. 1, pgs. 65-76.

Leonard, Eric M., 1989, Climate Change in the Colorado Rocky Mountains: Estimates Based on Modern Climate at Late Pleistocene Equilibrium Lines: Arctic and Alpine Research, Vol. 21, No. 3, pgs. 245-255.

Lewis, Dave H., and Smith, Dan J., 2004, Little Ice Age glacial activity in Strathcona Provincial Park, Vancouver Island, British Columbia, Canada: Canadian Journal of Earth Sciences, Vol. 41, pgs. 285-297.

Lliboutry, L. A., 1994, Monolithologic erosion of hard beds by temperate glaciers: Journal of Glaciology, Vol. 40, pgs. 433-450.

Long, William A., Glacial Geology of the Eastern Olympic Peninsula, Washington: Unpublished Report, on file at Olympic National Park, Port Angeles, Washington, and Olympic National Forest, Olympia, Washington.

Long, William, Glacial Geology of the Northern Olympic Peninsula: Unpublished Report, on file at Olympic National Park, Port Angeles, Washington, and Olympic National Forest, Olympia, Washington.

Long, William A., Glacial Geology of the Southeastern Olympic Peninsula, Washington: Unpublished Report, on file at Olympic National Park, Port Angeles, Washington, and Olympic National Forest, Olympia, Washington.

Long, William A., Glaciation of the Sitkum River Valley, Northwestern Olympic Peninsula, Washington: Unpublished Report on file at Olympic National Park, Port Angeles, Washington, and Olympic National Forest, Olympia, Washington.

Long, William A., Glaciations in the Humptulips River Drainage Basin, Southwestern Olympic Peninsula, Washington: Unpublished Report on file at Olympic National Park, Port Angeles, Washington, and Olympic National Forest, Olympia, Washington.

Long, William A., Neoglaciation in the Northeastern Olympic Mountains, Washington: Unpublished Report, on file at Olympic National Park, Port Angeles, Washington, and Olympic National Forest, Olympia, Washington.

Long, William A., 1975, Salmon Springs and Vashon Continental Ice in the Olympic Mountains and Relation of Vashon Continental to Fraser Olympic Ice: Unpublished Report, on file at Olympic National Park, Port Angeles, Washington, and Olympic National Forest, Olympia, Washington.

Lillquist, K., and Walker, K., 2006, Historical Glacier and Climate Fluctuations at Mount Hood, Oregon: Arctic and Antarctic Alpine Research, Vol. 38, No. 3, pgs. 399-412.

Minder, J. R., Durran, D. R., Roe, G. H., Anders, A. M., 2008, The climatology of small-scale orographic precipitation over the Olympic Mountains: Patterns and processes: Quarterly Journal of the Royal Meteorological Society, Vol. 134, pgs. 817-839.

Montgomery, David R., Balco, Greg, and Willett, Sean D., 2001, Climate, tectonics, and the morphology of the Andes: Geology, Vol. 29, No. 7, pgs. 579-582.

Moore, J. L., 1965, Surficial geology of the southwestern Olympic Peninsula: Unpublished M. S. thesis, University of Washington, 63 pgs.

Muller, Greg, 2006, Lichenometry and Environmental History: Environmental History, Vol. 11, pgs. 604-609.

National Oceanic and Atmospheric Administration, 2007, NNDC Climate Data Online: National Oceanic and Atmospherc Administration, <http://www7.ncdc.noaa.gov/CDO/cdo>.

Oerlemans, J., 1984, Numerical experiments of large scale glacial erosion: Zeitschrift fur Gletscherkunde und Glazialgeologie, Vol. 20, pgs. 107-126.

O'Neal, M. A., Schoenenberger, K. R., 2003, A *Rhizocarpon geographicum* growth curve for the Cascade Range of Washington and northern Oregon, USA: Quaternary Research, Vol. 60, pgs. 233-241.

Osipov, Eduard Yu., 2004, Equilibrium-line altitudes on reconstructed LGM glaciers of the northwest Barguzinsky Ridge, Northern Baikal, Russia: Palaeogeography, Palaeoclimatology, Palaeoecology, Vol. 209, pgs. 219-226.

Paterson, W.S.B., 1994, The Physics of Glaciers, 3rd Ed.: Great Britain, Redwood Books, Trowbridge, pgs. 26-52.

Pazzaglia, Frank J., and Brandon, Mark T., 2001, A Fluvial Record of Long-Term Steady-State Uplift and Erosion Across the Cascadia Forearc High, Western Washington State: American Journal of Science, Vol. 301, pgs. 385-431.

Porter, Stephen C., 1964, Composite Pleistocene Snow Line of the Olympic Mountains and Cascade Range, Washington: Geological Society of America, Vol. 75, pgs. 477-482.

Porter, Steven, 1981, Lichenometric Studies in the Cascade Range of Washington: Establishment of *Rhizocarpon Geographicum* Growth Curves at Mount Rainier: Arctic and Alpine Research, Vol. 13, No. 1, pgs. 11-23.

Porter, Stephen C., 2001, Snowline depression in the tropics during the Last Glaciation: Quaternary Science Reviews, Vol. 20, pgs. 1067-1091.

Porter, Stephen C., and Swanson, Terry W., 1998, Radiocarbon Age Constraints on Rates of Advance and Retreat of the Puget Lobe of the Cordilleran Ice Sheet during the Last Glaciation: Quaternary Research, Vol. 50, pgs. 205-213.

Ramage, Joan M., Smith, Jacqueline A., Rodbell, Donald T., and Seltzer, Geoffrey O., 2005, Comparing reconstructed Pleistocene equilibrium-line altitudes in the tropical Andes of central Peru: Journal of Quaternary Science, Vol. 20, pgs. 777-788.

Rasmussen, L. A., and Conway, H., 2001, Estimating South Cascade Glacier (Washington, U.S.A.) mass balance from a distant radiosonde and comparison with Blue Glacier: Journal of Glaciology, Vol. 47, No. 159, pgs. 579-588.

Ritter, Dale F., Kochel, R. Craig, and Miller, Jerry R., 2002, Process Geomorphology: United States of America, Waveland Press, Inc., Long Grove, IL, pgs. 297-357.

Roe, G. H., Stolar, D. S., and Willett, S. D., 2006, Response of a steady-state critical wedge orogen to changes in climate and tectonic forcing: Special Paper-Geological Society of America, Vol. 398, pgs. 227-239.

Shapiro, S. S., Wilk, M. B., 1965, An analysis of variance test for normality (complete samples): Biometrika, Vol. 52, No. ¾, pgs. 591-611.

Spicer, Richard C., 1986, Glaciers in the Olympic Mountains, Washington: Present Distribution and Recent Variations: Master of Science Thesis, University of Washington, 158 pgs.

Spicer, Richard C., 1989, Recent Variations of Blue Glacier, Olympic Mountains, Washington, U.S.A.: Arctic and Alpine Research, Vol. 21, No. 1, pgs. 1-21.

Stansell, Nathan D., Polissar, Pratigya J., and Abbott, Mark B., 2007, Last glacial maximum equilibrium-line altitude and paleo-temperature reconstructions for the Cordillera de Merida, Venezuelan Andes: Quaternary Research, Vol. 67, pgs. 115-127.

Stolar, D. B., Willett, S. D., and Roe, G. R., 2006, Climate and tectonic forcing of a critical orogen: in: Tectonics, climate, and landscape evolution: Geological Society of America Special Paper, 398, pgs. 241-250.

Thackray, Glenn, 1996, Glaciation and Neotectonic Deformation on the Western Olympic Peninsula, Washington: Doctoral Dissertation, University of Washington, 139 pgs.

Thackray, Glenn D., 2001, Extensive Early and Middle Wisconsin Glaciation on the Western Olympic Peninsula, Washington, and the Variability of Pacific Moisture Delivery to the Northwestern United States: Quaternary Research, Vol. 55, pgs. 257-270.

Thorson, Robert M., 1980, Ice-Sheet Glaciation of the Puget Lowland, Washington, during the Vashon Stade (Late Pleistocene): Quaternary Research, Vol. 13, pgs. 303-321.

Todd, M. R., 1939, The glaciation of the Hamma Hamma valley and its relation to the glacial history of the Puget Sound Basin: Unpublished M. S. Thesis, University of Washington, 48 pgs.

Tomkin, Jonathan H., 2007, Coupling glacial erosion and tectonics at active orogens: A numerical modeling study: Journal of Geophysical Research, Vol. 112, 14 pgs.

Tomkin, Jonathan H., and Braun, Jean, 2002, The influence of alpine glaciation on the relief of tectonically active mountain belts: American Journal of Science, Vol. 302, pgs. 169-190.

Tomkin, Jonathan H., and Roe, Gerard H., 2007, Climate and tectonic controls on glaciated critical-taper orogens: Earth and Planetary Science Letters, Vol. 262, pgs. 385-397.

Tomkin, Jonathan H., Brandon, Mark T., Pazzaglia, Frank J., Barbour, Jonathan R., and Willett, Sean D., 2003, Quantitative testing of bedrock incision models for the Clearwater River, NW Washington State: Journal of Geophysical Research, Vol. 108, No. B6, 19 pgs.

Tucker, G. E., and Bras, R. L., 2000, A stochastic approach to modeling the role of rainfall variability in drainage basin evolution: Water Resources Research, Vol. 36, pgs. 1953-1964.

United States Geological Survey, 2007, The National Map Seamless Server: United States Geological Survey, <http://seamless.usgs.gov>.

Waitt, Richard B., Jr., and Thorson, Robert M., 1983, The Cordilleran Ice Sheet in Washington, Idaho, and Montana: in: Wright, H. E., Jr., (ed.), 1983, Late-Quaternary Environments of the United States, Volume 1: The Late Pleistocene (Stephen C. Porter (ed.)): University of Minnesota Press, 407 pgs., Chp. 3, pgs. 53-70.

Wegmann, Karl W., and Pazzaglia, Frank J., 2002, Holocene strath terraces, climate change, and active tectonics: The Clearwater River basin, Olympic Peninsula, Washington State: GSA Bulletin, Vol. 114, No. 6, pgs. 731-744.

Whipple, K. X., and Meade, B. J., 2004, Controls on the strength of coupling among climate, erosion, and deformation in two-sided, frictional orogenic wedges at steady state: Journal of Geophysical Research, Vol. 109, 24 pgs.

Willett, S. D., 1999, Orogeny and orography: the effects of erosion on the structure of mountain belts: Journal of Geophysical Research, Vol. 104, pgs. 28957-28981.

Willett, S. D., and Brandon, M. T., 2002, On steady states in mountain belts: Geology, Vol. 30, pgs. 175-178.

Zeitler, P. K., Koons, P. O., Bishop, M. P., Chamberlain, C. P., Craw, D., Edwards, M. A., Hamidullah, S., Jan, M. Q., Khan, M. A., Khattak, M. U. K., Kidd, W. S. F., Mackie, R. L., Meltzer, A. S., Park, S. K., Pecher, A., Poage, M. A., Sarker, G., Schneider, D. A., Seeber, L., and Shroder, J. F., 2001, Crustal reworking at Nanga Parbat, Pakistan: Metamorphic consequences of thermal-mechanical coupling facilitated by erosion, Vol. 20, No. 5, pgs. 712-728.

APPENDIX A: SUMMARY OF CODES AND PROCESSES FOR TRANSFORMING THE ICE CASCADE DATA

A.1 ICE CASCADE CODES, DATA, AND METHODS FOR RUNNING

ICE Cascade produces data in the form of output files that contain multiple columns of data. The main output files used in this study are: long_DENUD.out, long_glac.out, long_erosion.out, long_topo.out, long_ice_locat.out, long_temps.out, and ice_time_data.out. The summary of the relevant data contained in each file is located in Table A.1. The data is specified in each file by the x and y coordinates of the value.

To conduct multiple runs at a single time and have all of the files saved with names based on the climatic properties specified, a perl file was written to allow for batches of runs to be accomplished (see file at the end of the appendix). The perl file allows for the temperature, precipitation, and ablation values to be specified for a group of runs. It then creates an overall folder that contains a data folder that has folders for each individual run with the run properties listed in the title of each folder. It also creates a batch file that lists all of the runs contained in the overall folder. The file names are as follows: T16.0ac1.5pc0.4, where T and the following number (16.0) represent the maximum temperature from the temperature equation used in ICE Cascade, ac and the following number (1.5) represent the ablation constant, and pc and the following number (0.4) represent the precipitation constant. This base file naming system makes it easier to identify each model run and provides an easy access system for later processing of the data.

To run the model for an individual run (or a batch of runs), the variables for each run must first be specified. The time length of the run (either 10,000 or 100,000 years) and the temperature and precipitation equations need to be set in ICE Cascade. Following this, the precipitation constant, ablation constant, and temperature need to be specified in the perl file. The model can then be run by running the perl file for a batch of runs. When the model finishes, the perl file saves the data in the corresponding run folder.

ICE Cascade Output Files and the Corresponding Data	
File Name	**Data**
long_DENUD.out	Total denudation summed for each timestep over the entire run
long_erosion.out	Glacial erosion at each timestep
	Total erosion at each timestep
long_topo.out	Topographic height at each timestep
	Ice thickness at each timestep
	Topographic height plus the ice thickness at each timestep
	Precipitation at each timestep
long_glac.out	Mass balance change for each timestep
	Ice thickness change for each timestep
	Sliding velocity for each timestep
long_ice_locat.out	The locations of ice at each timestep
long_temps.out	Surface temperature at each timestep
ice_time_data.out	Number of nodes with ice
	Average ice thickness
	The individual timesteps in the model run

Table A.1. The output files produced by ICE Cascade. The data contained within these files and used in data interpretation is contained in the second column.

A.2 MATLAB CODES AND METHODS

To process the data and turn it into a usable form, codes were developed in Matlab that allow for the data to be turned into visible formats via figures. The codes make the images seen in Chapter 2 and are included at the end of the appendix. To run each set of codes for a batch of runs, codes were written to read in the batch folders and make figures for each individual run:

```
%Get the names of datasets to process
directory_name=input('Location of data folders: ','s');
base_file_name_list=textread(strcat(directory_name,'/',input('File of base names
      of data to process (batch log file): ','s')),'%s');

%Begin loop to process all files
for entry=1:size(base_file_name_list)

%Get the base file name from the list
base_file_name=strcat(directory_name,'/',base_file_name_list{entry},'/',base_file
      _name_list{entry});
```

```
%Load the data, using the base name
longice_loc_temp=load(strcat(base_file_name,'_long_ice_locat.out'),'-ascii');
longerosion_temp=load(strcat(base_file_name,'_long_erosion.out'),'-ascii');
longtopo_temp=load(strcat(base_file_name,'_long_topo.out'),'-ascii');
longglac_temp=load(strcat(base_file_name,'_long_glac.out'),'-ascii');
longdenud_temp=load(strcat(base_file_name,'_long_DENUD.out'),'-ascii');
longtemps_temp=load(strcat(base_file_name,'_long_temps.out'),'-ascii');
```

By supplying the folder location and the base file name to Matlab, Matlab will automatically find all of the data from that batch, run the Matlab codes, and save the images produced in the folder with the corresponding data. The code is written so the data does not have to be saved in any particular directory – Matlab finds the data.

The Matlab codes have been developed to plot the topography, precipitation, ice thickness, ice locations, temperature, uplift, and erosion for each of the timesteps. These codes allow for the data to be turned into an interpretable form and for the data to be compared with each other and other runs. The codes relevant to Chapter 2 are included here. The codes that follow have the names and purposes listed below and are located in the same order:

ice_batch.pl – For running ICE Cascade

Ice_extent_plots_batch.m – Climate Sensitivity Analysis

metric_temp_aloss_pc_3.m – Climate Sensitivity Analysis

plotting.m – Climate Sensitivity Analysis

Ice_Thickness_with_timesteps.m – Glacial Erosion

Sliding_Velocity.m – Glacial Erosion

Temperature_with_timesteps.m – Glacial Erosion

Timestep_images_part1_topoicelocat.m – Glacial Erosion

Timestep_images_part4denud.m – Glacial Erosion

Timestep_images_part5denudcont.m – Glacial Erosion

Timestep_images_part6xsections.m – Glacial Erosion

Timestep_images_part7newdenudstuff.m – Glacial Erosion

Timestep_images_part8newdenud2.m – Glacial Erosion

Uplift_newcoords.m – Glacial Erosion

Uplift_Contours.m – Glacial Erosion

Ice_Duration.m – Glacial Erosion

upliftandicecover.m – Glacial Erosion

Hoh_River_Profile_Kg.m – Glacial Erosion

Misfit_Uplift.m – Glacial Erosion

Part1.m – Glacial Erosion

Part2.m – Glacial Erosion

The river profile and misfit/best fitting case files are set up for the Hoh River currently, but they can be adapted to fit the other two rivers, the Queets and the Quinault, by changing the name Hoh to the desired river. In addition, other pertinent information, for example the number of nodes or coordinates of the profile, need to be changed and the data for these other rivers is located in Part2.m. The codes are annotated to aid in the understanding of what each section or step is supposed to accomplish and to explain the order and purpose of each step.

A.3 MATLAB AND ICE CASCADE CODES

ice_batch.pl

```
#! /usr/bin/perl

# A script for running batches of runs of ICE.
# Sea level temperature, aloss constant, and precipitation constant may
be varied. Precipitation may also be set to be spatially constant.
#
#
# Geoffrey Poore
# June 20, 2008
# Jessica Hellwig (additional changes)


# Set whether precipitation is constant in space.
# If it is constant in space, then the precipitation constants will be
used as the precipitation in m/yr rather than multiplied by the
spatially variable precipitation.  Also, ``pc'' is replaced ``pconst''
in the base file name to designate this.
$precip_is_const_in_space=0;
# Make sure the value of precip_is_const_in_space is acceptable
if ($precip_is_const_in_space!=0 && $precip_is_const_in_space!=1) {
    die("Precipitation has not been properly set to be/not be constant
in space!\nSet the value of precip_is_const_in_space to 0 or 1.\n");
}


# Put all the values to be used in the batch in arrays

@seaLevelTempSet=("16.0");
#@seaLevelTempSet=("7.2");
#@seaLevelTempSet=("6.0","6.2","6.4","6.5","6.6","6.8");
#@seaLevelTempSet=("8.5");
#@seaLevelTempSet=("7.0","7.2","7.4","7.5","7.6","7.8","8.0","8.2","8.4
","8.5");
#@seaLevelTempSet=("6.0","6.2","6.4","6.5","6.6","6.8","7.0","7.2","7.4
","7.5");
#@seaLevelTempSet=("7.0","7.5","8.0","8.5","9.0","9.5","10.0","10.5","1
1.0","11.5","12.0","12.5","13.0","13.5","14.0","14.5","15.0");
#@seaLevelTempSet=("4.0","4.5","5.0","5.5","6.0","6.5");
#@seaLevelTempSet=("7.0");
#@seaLevelTempSet=("4.0","4.5","5.0","5.5","6.0","6.5","7.0","7.5","8.0
","8.5","9.0","9.5","10.0","10.5","11.0","11.5","12.0","12.5","13.0","1
3.5","14.0","14.5","15.0");
#@seaLevelTempSet=("4.0","4.5","5.0","5.5","6.0","6.5","7.0","7.5","8.0
","8.5","9.0","9.5","10.0","10.5","11.0","11.5","12.0","12.5","13.0","1
3.5","14.0","14.5","15.0");
#@seaLevelTempSet=("6.0");
@alossConstSet=("1.5");
#@alossConstSet=("0.5","1.0","1.5","2.0","2.5");
#@alossConstSet=("1.5");
#@precipConstSet=("0.8");
#@precipConstSet=("0.4");
@precipConstSet=("0.5");
#@precipConstSet=("0.6");
#@precipConstSet=("0.7","0.8");
```

```
#@precipConstSet=("0.2","0.3","0.4","0.5","0.6","0.7","0.8");
#@precipConstSet=("0.2","0.3","0.4","0.5","0.6");
#@precipConstSet=("1.5");
#@precipConstSet=("0.25","0.50","0.75");
#@precipConstSet=("0.25","0.5","1","2","3","4");
#@precipConstSet=("0.5","0.8");

# Calculate the number of runs to do
$totalRuns=($#seaLevelTempSet+1)*($#alossConstSet+1)*($#precipConstSet+
1);
$currentRun=0;

# Open a "log" file for the batch, in which the base file names are
listed
# This log file can serve as the input for batch processing data in
Matlab
$currentTime=`date`;
chomp($currentTime);
$currentTime=~s/ /_/g;
$currentTime=~s/://g;
open(LOG_FILE, "> data/ICE_batch_" . $currentTime . ".txt");

# Do one run for each set of parameters
foreach $seaLevelTemp (@seaLevelTempSet) {
foreach $alossConst (@alossConstSet) {
foreach $precipConst (@precipConstSet) {

# Get the base file name for the next run
# Use ``pconst'' rather than ``pc'' in the name if precip is const in
space
# See if a directory with that name exists -- if so, die to prevent
overwrite
$baseFileName="T" . $seaLevelTemp . "ac" . $alossConst . "pc" .
$precipConst;
if ($precip_is_const_in_space) {
  $baseFileName=~s/pc/pconst/;
}
$dirName="data/" . $baseFileName;
if (-d $dirName) {die ("Directory $baseFileName already exists.
Exiting.\n");}

# Print the current run number
$currentRun++;
print "Starting run $currentRun of $totalRuns\n";

# Edit surface_temperature.f90 for the sea level temperature
####Comment out so that New temp model is used
#open(TEMP_FILE, "surface_temperature.f90") || die("Cannot open
surface_temperature.f90!");
#@temp=<TEMP_FILE>;
#close(TEMP_FILE);
#for ($i=0; $i<=$#temp; $i++) {
#    if ($temp[$i]!~/!/ && $temp[$i]=~/temps=/) {
#        $temp[$i]=~s/=\d+\.*\d*d*\d*-/=$seaLevelTemp-/;
#        $i=$#temp+1;
#    }
#}
```

```
#open(TEMP_FILE, "> surface_temperature.f90") || die("Cannot open
surface_temperature.f90!");
#print TEMP_FILE @temp;
#close(TEMP_FILE);

# Edit precipitation_rate.f90 for the precipitation constant and the
aloss constant
open(PRECIP_FILE, "precipitation_rate.f90") || die("Cannot open
precipition_rate.f90!");
@precip=<PRECIP_FILE>;
close(PRECIP_FILE);
for ($i=0; $i<=$#precip; $i++) {
    if ($precip[$i]!~/!/ &&
$precip[$i]=~/a\(i,j\)=preciprate_spatial\(i,j\)/) {
        if ($precip_is_const_in_space==0) {

$precip[$i]=~s/\*\d+\.*\d*d*\d*\+*\d*\.*\d*/\*$precipConst/;
        }
      else {

$precip[$i]=~s/\*\d+\.*\d*d*\d*\+*\d*\.*\d*/\*0+$precipConst/;
        }
    }
    if ($precip[$i]!~/!/ && $precip[$i]=~/aloss\(i,j\)=/) {
        $precip[$i]=~s/\*\d+\.*\d*d*\d*/\*$alossConst/;
        $i=$#precip+1;
    }
}
open(PRECIP_FILE, "> precipitation_rate.f90") || die("Cannot open
precipitation_rate.f90!");
print PRECIP_FILE @precip;
close(PRECIP_FILE);


# Compile
system("pgf90 -c ICE.f90");
system("pgf90 -c precipitation_rate.f90");
system("pgf90 -c surface_temperature.f90");
system("pgf90 -c init.f90");
system("pgf90 -c effective_diffusivity.f90");
system("pgf90 -c velocity.f90");
system("pgf90 -c update_height.f90");
system("make ICE");

# Run
system("./ICE");

# Make a directory for the data, and move the data, renaming it to
reflect the runs
system("mkdir data/" . $baseFileName);
@outFileList=("DENUD.out", "erosion.out", "glac.out",
"ice_locations.out", "info1.out", "time.out", "topo.out",
"ice_time_data.out",  "progress.out", "long_DENUD.out",
"long_ice_locat.out", "long_topo.out", "long_erosion.out",
"long_glac.out", "long_temps.out", "temps.out", "temps_time_data.out");
```

```
#@outFileList=("DENUD.out", "erosion.out", "glac.out",
"ice_locations.out", "info1.out", "time.out", "topo.out",
"ice_time_data.out", "ice_loc_over_time.out");
foreach $outFile (@outFileList) {
    system("mv " . $outFile . " data/" . $baseFileName . "/" .
$baseFileName . "_" . $outFile);
}

# Save base file name to the log file
print LOG_FILE $baseFileName . "\r\n";

# End the foreach loops
}
}
}

close LOG_FILE;
```

Ice_extent_plots_batch.m

```
%M file for creating images out of the outputs from the model as a
precursor to plotting the metric

%Get the names of datasets to process
directory_name=input('Location of data folders: ','s');
base_file_name_list=textread(strcat(directory_name,'/',input('File of
      base names of data to process (batch log file): ','s')),'%s');

%Begin loop to process all files
for entry=1:size(base_file_name_list)

%Get the base file name from the list
base_file_name=strcat(directory_name,'/',base_file_name_list{entry},'/
      ',base_file_name_list{entry});

%Load the ice locations and topo data, using the base name
ice_loc_temp=load(strcat(base_file_name,'_ice_locations.out'),'-
      ascii');
topo_temp=load(strcat(base_file_name,'_topo.out'),'-ascii');
ice_time_temp=load(strcat(base_file_name,'_ice_time_data.out'),'-
      ascii');
glac_temp=load(strcat(base_file_name,'_glac.out'),'-ascii');
erosion_temp=load(strcat(base_file_name,'_erosion.out'),'-ascii');

%I. Reshape topo_output to be a 165*165 grid and plot it
t_temp=reshape(topo_temp(:,3),165,165);

figure;
ph=pcolor(t_temp);
hold on;
set(ph,'linestyle','none');
colorbar;

%II. Plot current ice extent on the topography
x=[84;84;84;85;84;85;85;85;86;86;86;88;87;87;87;87;86;86;86;86;85;85;
      85;85;85;85;86;86;86;86;87;88;89;90;90;90;90;90;89;89;89;90;90;93
      ;93;93;93;92;92;92;92;89;89;89;87;87;87;89;88;88;88;88;88;88;88;8
      9;89;89;89;88;87;87;87;87;87;86;86;86;86;85;85;85;84;85;85;85;84;
      84;84;84;83;84;83;83;84;83;83;84;84;84;85;85;85;85;85;83;83;83;83
      ;83;83;79;79;79;79;79;79;78;78;78;77;77;76;77;76;77;77;78;78;78;7
      9;78;77;77;76;77;77;77;77;78;78;77;77;77;79;79;78;79;79;79;80;80;
      80;80;80;80;80;81;81;81;80;80;80;79;79;80;80;80;78;78;78;78;79;78
      ;79;78;79;79;79;79;79;79;80;80;80;79;83;83;83;83;83;82;82;82;8
      2;82;83;84;83;84;83;83;83;82;82;82;81;81;81;82;80;81;81;80;80;79;
      80;80;81;80;81;81;82;81;82;82;82;82;82;82;82;82;81;81;82;80;104;1
      05;108;108;109;109;124;123;123;122;122;105;106;106;106;108;108;10
      8;109;109;109;112;112;113;109;109;109;108;108;108;108;108;107;107
      ;107;107;107;107;107;108;108;107;108;107;107;108;107;107;115;115;
      115;116;116;116;115;115;116;116;117;117;118;118;118;118;117;117;1
      16];

y=[105;105;105;106;105;105;105;105;106;106;106;105;104;105;104;105;105;
      105;105;104;105;105;105;105;104;104;104;104;104;104;102;102;102;1
      02;101;99;99;98;96;96;96;96;99;82;82;83;83;83;83;83;83;88;87;88;8
```

```
      9;89;88;90;91;91;90;90;91;94;94;94;94;94;94;94;94;94;94;94;94;94;
      94;95;94;94;94;94;94;94;95;95;94;94;94;94;94;94;94;93;94;93;93;93
      ;93;93;93;93;93;93;93;97;97;97;96;95;96;96;96;95;95;96;95;96;95;9
      6;96;95;95;94;94;94;95;95;94;94;94;95;94;94;93;93;89;90;90;89;90;
      89;89;89;91;91;91;90;91;91;91;92;92;92;93;92;92;92;93;93;93;93;93
      ;92;92;92;93;93;93;93;94;94;94;94;94;93;93;93;93;93;94;94;94;94;9
      4;94;93;92;92;91;91;91;92;92;92;92;94;95;96;95;95;94;94;93;93;93;
      92;92;93;94;94;94;94;95;95;95;95;95;96;96;96;95;96;97;97;97;96;95
      ;95;94;94;93;93;93;95;95;95;100;100;97;97;97;97;92;91;78;78;78;76
      ;75;76;76;77;77;81;81;81;81;82;82;82;87;86;86;85;84;84;84;84;85;8
      5;85;85;85;87;86;86;85;86;86;87;87;86;86;87;100;100;98;98;97;97;9
      7;96;96;96;96;96;96;95;94;95;94;94;95];

i=1:304;

glacialmap_current=zeros(304,2);
glacialmap_current (x(i),y(i))=1;

figure;
ph=pcolor(t_temp);
hold on;
set(ph,'linestyle','none');
colorbar;
plot(x,y,'k*');

%III. Plot new model ice locations on current ice and topography
figure;
ph=pcolor(t_temp);
hold on;
set(ph,'linestyle','none');
colorbar;
plot(x,y,'k*');
if (size(ice_loc_temp,1)>0)
    plot(ice_loc_temp(:,1),ice_loc_temp(:,2),'mx');
end
lgmxy=load('lgmxy.txt','-ascii');
saveas(ph,strcat(base_file_name,'_ice_locations.png'));

%IV. Plot average ice thickness as a function of time
figure;
ph=plot(ice_time_temp(:,1),ice_time_temp(:,2));
xlabel('Time (yr)');
ylabel('Average Ice Thickness (m) (sum(h)/nx*ny))');
title('Average Ice Thickness vs. Time');
saveas(ph,strcat(base_file_name,'_ice_thickness_vs_time.png'));

%V. Plot number of nodes containing ice as a function of time
figure;
ph=plot(ice_time_temp(:,1),ice_time_temp(:,3));
xlabel('Time (yr)');
ylabel('Number of nodes containing ice');
title('Number of nodes containing ice vs. Time');
saveas(ph,strcat(base_file_name,'_ice_nodes_vs_time.png'));

%VI. Plot velocity
```

```
figure;
ph=pcolor(reshape(glac_temp(:,6),165,165));
hold on;
set(ph,'linestyle','none');
colorbar;
contour(t_temp,5,'k');
saveas(ph,strcat(base_file_name,'_velocity.png'));

%VI.i. Plot velocity with cutoff of 100
figure;
ph=pcolor(min(reshape(glac_temp(:,6),165,165),100));
hold on;
set(ph,'linestyle','none');
colorbar;
contour(t_temp,5,'k');
saveas(ph,strcat(base_file_name,'_velocity_cutoff100.png'));

%VI.ii. Plot velocity with cutoff of 1000
figure;
ph=pcolor(min(reshape(glac_temp(:,6),165,165),1000));
hold on;
set(ph,'linestyle','none');
colorbar;
contour(t_temp,5,'k');
saveas(ph,strcat(base_file_name,'_velocity_cutoff1000.png'));

%VII. Plot new model ice locations on current ice and topography, with
lgm deposit locations
figure;
ph=pcolor(t_temp);
hold on;
set(ph,'linestyle','none');
colorbar;
plot(x,y,'k*');
if (size(ice_loc_temp,1)>0)
    plot(ice_loc_temp(:,1),ice_loc_temp(:,2),'mx');
end
lgmxy=load('lgmxy.txt','-ascii');
plot(lgmxy(:,1),lgmxy(:,2),'rs');
saveas(ph,strcat(base_file_name,'_ice_locations+lgm.png'));

%VIII. Plot erosion
figure;
erosion_glac_temp=reshape(erosion_temp(:,5),165,165);
ph=pcolor(erosion_glac_temp);
hold on;
set(ph,'linestyle','none');
colorbar;
contour(t_temp,5,'k');
saveas(ph,strcat(base_file_name,'_erosion.png'));

%CLEANUP
close all;
end;
```

metric_temp_aloss_pc_3.m

```
%M file for plotting the metric for a matrix of temperature, aloss, and
%precipitation constant values.

%Revised 20090219 to include the Clearwater, and make some minor
additional changes to increase efficiency/simplicity.

%Load the LGM ice locations, and the topography, from .txt files
load('lgmxy.txt','-ascii');
t_temp=reshape(load('new_topo_line.txt','-ascii'),165,165);

%Set up a name, an index, and a deposit for each river
%Names of rivers corresponding to deposits
%!!!!!!!!!!  NOTE:  If another river is ever added, be careful to make
sure that the metric selection option works correctly. Currently, it is
easy to disable the Clearwater because it is last. Things wouldn't be
so simple if there were two rivers that might be disabled.
use_clearwater='string';
while (~strcmp(use_clearwater,'y') && ~strcmp(use_clearwater,'n'))
    use_clearwater=input('Use Clearwater? (y,n)  ','s');
end
if (strcmp(use_clearwater,'n'))
    river_names=strvcat(' Hoh River',' Queets River',' Quinault
River');
else
    river_names=strvcat(' Hoh River',' Queets River',' Quinault
River',' Clearwater River');
end
hoh_index=1;
queets_index=2;
quinault_index=3;
clearwater_index=4;

%Deposit locations to use for the metric, from the LGM ice locations
data
depositxy=[38,95;44,68;64,54;60,88];

%Start building a structure to hold all info
clear rivers;
for index=1:size(river_names,1)
    rivers(index).name=river_names(index,:);
    rivers(index).depositxy=depositxy(index,:);
end

%Points through which the metric should go
%Note that points upstream and downstream are not distinguished; this
is done using the x coordinate of the deposit, which assumes that
upstream points always have a larger x coordinate and downstream points
always have a smaller x coordinate. This should always be true, given
the geometry.  Note that each x value should be used only for a single
point; otherwise,  the plotting function isn't happy and leaves gaps.
rivers(hoh_index).points=[1,60;depositxy(hoh_index,:);59,97];
rivers(queets_index).points=[1,57;depositxy(queets_index,:);63,78];
rivers(quinault_index).points=[1,25;depositxy(quinault_index,:);75,64];
if (strcmp(use_clearwater,'y'))
```

```
rivers(clearwater_index).points=[1,57;36,68;37,75;39,78;48,80;53,86;dep
ositxy(clearwater_index,:);63,88];
end

%Using the points above, get the coordinates of all points that are to
be used as part of the metric.
%Loop through rivers
for river_index=1:size(rivers,2)
    %Loop through points, except for the last point, which is taken
      care of by looking ahead
    path_index=1;
    for points_index=1:size(rivers(river_index).points,1)-1
        %Get the coordinates of the current and next points
        current_point=rivers(river_index).points(points_index,:);
        next_point=rivers(river_index).points(points_index+1,:);
        %Calculate the slope between the points, and return an error if
        %slope is infinite
        slope=(next_point(1,2)-current_point(1,2))/(next_point(1,1)-
            current_point(1,1));
        if (isinf(slope))
            error('The points used gave an infinite slope!');
        end
        %Go through all x values between the points, calculate the
            corresponding y values using the slope, and add the
            coordinates of these locations to the path that is used to
            measure the metric.
        %Don't use that last x value because that will be incorporated
            when taking the next point.
        for x=current_point(1,1):next_point(1,1)-1
            rivers(river_index).path(path_index,:)=[x,round((x-
                  current_point(1,1))*slope+current_point(1,2))];
            path_index=path_index+1;
        end
        %If evaluating the last pair of points, add in the coordinates
            of the last point (the next_point isn't added normally,
            because it will be the current_point on the next loop).
        if points_index==size(rivers(river_index).points,1)-1
            rivers(river_index).path(path_index,:)=next_point;
            path_index=path_index+1;
        end
    end
end

%Make a figure showing all LGM deposits, and the lines that will be
used to measure the metric
a=[38;44;64];
b=[95;68;54];

figure;
ph=pcolor(t_temp);
hold on;
set(ph,'linestyle','none');
%plot(lgmxy(:,1),lgmxy(:,2),'ms');
plot(a,b,'ms');
for river_index=1:size(rivers,2)
```

```
plot(rivers(river_index).path(:,1),rivers(river_index).path(:,2),'r')

plot(rivers(river_index).depositxy(:,1),rivers(river_index).depositxy(:
      ,2),'wx')
end
title('Lines used in metric, with LGM deposits');
ah=gca;
set(ah,'YTick',[1 117]);
set(ah,'YTickLabel',{'47 N','48 N'});
set(ah,'XTick',[14 86]);
set(ah,'XTickLabel',{'124 W','123 W'});

%Determine if the user wants to continue using this metric
do_metric='';
while (~strcmp(do_metric,'y') && ~strcmp(do_metric,'n'))
    do_metric=input('Metric lines are plotted. Continue with this
metric? (y/n)  ','s');
end
if (strcmp(do_metric,'n'))
    close all;
    return;
end
close all;

%Get the location of data to apply the metric to
directory_name=input('Location of data folders: ','s');
base_file_name_list=textread(strcat(directory_name,'/',input('File of
      base names of data to process (batch log file): ','s')),'%s');

%Using the batch log file, figure out the step sizes for temperature,
%aloss, and precipitation constant
%Start by putting the first values into the T, aloss, pc axis vectors
clear temperature_axis aloss_axis pc_axis;
entry=1;
temperature=regexprep(base_file_name_list{entry},'T','');
temperature=regexprep(temperature,'ac.*','');
temperature=str2double(temperature);
aloss=regexprep(base_file_name_list{entry},'T.*ac','');
aloss=regexprep(aloss,'pc.*','');
aloss=str2double(aloss);
pc=regexprep(base_file_name_list{entry},'T.*pc','');
pc=str2double(pc);
temperature_axis(1)=temperature;
aloss_axis(1)=aloss;
pc_axis(1)=pc;

%Note that index of for loop starts with two, because 1 has already
been used
for entry=2:size(base_file_name_list,1)
    %Get the temperature, aloss, and precip constant values for the
      current simulation
    temperature=regexprep(base_file_name_list{entry},'T','');
    temperature=regexprep(temperature,'ac.*','');
    temperature=str2double(temperature);
    aloss=regexprep(base_file_name_list{entry},'T.*ac','');
```

```
    aloss=regexprep(aloss,'pc.*','');
    aloss=str2double(aloss);
    pc=regexprep(base_file_name_list{entry},'T.*pc','');
    pc=str2double(pc);
    temperature_resolved=0;
    for index=1:size(temperature_axis,2)
        if (temperature==temperature_axis(index))
            temperature_resolved=1;
            break;
        end
    end
    if (temperature_resolved==0)
        temperature_axis(size(temperature_axis,2)+1)=temperature;
    end
    aloss_resolved=0;
    for index=1:size(aloss_axis,2)
        if (aloss==aloss_axis(index))
            aloss_resolved=1;
            break;
        end
    end
    if (aloss_resolved==0)
        aloss_axis(size(aloss_axis,2)+1)=aloss;
    end
    pc_resolved=0;
    for index=1:size(pc_axis,2)
        if (pc==pc_axis(index))
            pc_resolved=1;
            break;
        end
    end
    if (pc_resolved==0)
        pc_axis(size(pc_axis,2)+1)=pc;
    end
end

%Sort the axes
temperature_axis=sort(temperature_axis);
aloss_axis=sort(aloss_axis);
pc_axis=sort(pc_axis);

%Allocate space for the metric, now that we know the number of T,
      aloss, and pc values that we're looking at
combined_metric=zeros(size(temperature_axis,2),size(aloss_axis,2),size(
      pc_axis,2));
individual_metric=zeros(size(temperature_axis,2),size(aloss_axis,2),siz
      e(pc_axis,2),size(depositxy,1));
metric_flags=zeros(size(temperature_axis,2),size(aloss_axis,2),size(pc_
      axis,2),size(depositxy,1));

%Begin loop to process all files
for entry=1:size(base_file_name_list,1)
    %Get the temperature, aloss, and values
    temperature=regexprep(base_file_name_list{entry},'T','');
    temperature=regexprep(temperature,'ac.*','');
    temperature=str2double(temperature);
```

```
aloss=regexprep(base_file_name_list{entry},'T.*ac','');
aloss=regexprep(aloss,'pc.*','');
aloss=str2double(aloss);
pc=regexprep(base_file_name_list{entry},'T.*pc','');
pc=str2double(pc);
%Now figure out which coordinates these values correspond to, using
  the corresponding axes
for index=1:size(temperature_axis,2)
    if (temperature==temperature_axis(index))
        temperature=index;
        break;
    end
end
for index=1:size(aloss_axis,2)
    if (aloss==aloss_axis(index))
        aloss=index;
        break;
    end
end
for index=1:size(pc_axis,2)
    if (pc==pc_axis(index))
        pc=index;
        break;
    end
end

%Get the base file name from the list
  base_file_name=strcat(directory_name,'/',base_file_name_list{entr
        y},'/',base_file_name_list{entry});
%Load the ice locations.
ice_loc_temp=load(strcat(base_file_name,'_ice_locations.out'),'-
  ascii');
topo_temp=load(strcat(base_file_name,'_topo.out'),'-ascii');

%Make a matrix of ice thicknesses
h_temp=reshape(topo_temp(:,5),165,165);

%Loop through each river basin, measuring the metric for each basin
%Loop rivers
for river_index=1:size(rivers,2)
    resolved=0;
    %Loop through path, with x going from small to large
    for path_index=1:size(rivers(river_index).path,1)
        %If there is ice
        if (h_temp(rivers(river_index).path(path_index,2),rivers
              (river_index).path(path_index,1))>0)
            %Get the sign of the metric--downstream (-) or upstream
              (+)
            if (rivers(river_index).path(path_index,1)<rivers
              (river_index).depositxy(1,1))
                metric_sign=-1;
            else
                metric_sign=1;
            end
            %Calculate the metric, measuring distance along the
              path
```

```
                if (metric_sign==-1)
                    while rivers(river_index).path(path_index,1)<rivers
                        (river_index).depositxy(1,1)

                        individual_metric(temperature,aloss,pc,river_in
                              dex)=individual_metric(temperature,aloss,
                              pc,river_index)+metric_sign*sqrt((rivers(
                              river_index).path(path_index,1)-rivers
                              (river_index).path(path_index+1,1))^2+(ri
                              vers(river_index).path(path_index,2)river
                              s(river_index).path(path_index+1,2))^2);
                        path_index=path_index+1;
                    end
                else
                    while rivers(river_index).path(path_index,1)>rivers
                        (river_index).depositxy(1,1)

                        individual_metric(temperature,aloss,pc,river_in
                              dex)=individual_metric(temperature,aloss,
                              pc,river_index)+metric_sign*sqrt((rivers(
                              river_index).path(path_index,1)-rivers
                              (river_index).path(path_index-1,1))^2+(ri
                              vers(river_index).path(path_index,2)-rive
                              rs(river_index).path(path_index-1,2))^2);
                        path_index=path_index-1;
                    end
                end
                %Set resolved as true
                resolved=1;
                break;
            end
        end
        %Account for no ice on path, or no ice at all
        if (resolved==0)
            %If there is ice
            if (size(ice_loc_temp,1)>0)

                  individual_metric(temperature,aloss,pc,river_index)=m
                        in(sqrt((ice_loc_temp(:,1)-rivers(river_index)
                        .depositxy(1,1)).^2+(ice_loc_temp(:,2)-
                        rivers(river_index).depositxy(1,2)).^2));
            %If there isn't ice, use a constant, high value
            else

                  individual_metric(temperature,aloss,pc,river_index)=
                        165/2;
            end
            %Flag the metric as having used an alternate calculation
                  method
            metric_flags(temperature,aloss,pc,river_index)=1;
        end
    end

strcat('Calculation:',num2str(entry),'/',num2str(size(base_file_name_li
      st,1)))
end
```

```
%Calculate combined metric from individual metrics
%Use a root-mean-square method
for river_index=1:size(rivers,2)

combined_metric=combined_metric+reshape(individual_metric(:,:,:,river_i
      ndex).^2,size(individual_metric,1),size(individual_metric,2),size
      (individual_metric,3));
end
combined_metric=combined_metric/size(rivers,2);
combined_metric=combined_metric.^0.5;

save(strcat(directory_name,'_metrics'),'temperature_axis','aloss_axis',
      'pc_axis','individual_metric','combined_metric','metric_flags');

%OLD PLOTTING STUFF -- likely doesn't work anymore, but could be
adapted
% %Plot results for combined metric
% figure;
% ph=pcolor(aloss_axis,temperature_axis,combined_metric);
% hold on;
% set(ph,'linestyle','none');
% plot_title='Combined RMS metric for the';
% colorbar;
% for deposit=1:size(depositxy,1)
%     if (deposit~=size(depositxy,1) && deposit~=size(depositxy,1)-1)
%         plot_title=strcat(plot_title,river_names(deposit,:),',');
%     elseif (deposit==size(depositxy,1)-1)
%         plot_title=strcat(plot_title,river_names(deposit,:),', and');
%     else
%         plot_title=strcat(plot_title,river_names(deposit,:));
%     end
% end
% title(plot_title);
% saveas(ph,strcat(directory_name,'/combined_metric.png'));
%
% %Plot results for individual metrics
% for deposit=1:size(depositxy,1)
%     figure;
%     ph=pcolor(aloss_axis,temperature_axis,reshape(individual_metric(d
          eposit,:,:),size(individual_metric,2),size(individual_metri
          c,3)));
%     hold on;
%     set(ph,'linestyle','none');
%     plot_title=strcat('Individual metric for the',river_names
          (deposit,:));
%     title(plot_title);
%     colorbar;
%     file_name=strcat('individual_metric',river_names(deposit,:),
          '.png');
%     file_name=strrep(file_name,' ','_');
%     saveas(ph,strcat(directory_name,'/',file_name));
% end
```

plotting.m

```
%Visualizer for metric with contours and cut along the aloss values

%we need to load results.mat file - this file is made by
metric_temp_aloss_pc.m - put the name in the first coding line and
specify the dimensions the file has (i(temperature), j(aloss),
k(precipitation constant))
%Also, respecify the second "for i=..." for the number of aloss and set
contour interval start, stop, and spacing. Also, make sure the
directory is set to the one in which the data files are for the
results.mat file being run.

%note results.mat was named 07(06-07-
      14)2008_1ka_T_ac_pc_matrixmetrics.mat; i=1:23, j=1:5, k=1:4;
      spacing of 2, start 4, end 20
%note results_2.mat was named Sensitivity_Results_T_6.0-
      7.5_a_1.5_pc_0.2-0.6.mat i=1:10, j=1:1, k=1:5; spacing of 0.5
%note results_3.mat was named Sensitivity_Results_T_6.0-
      7.5_a_1.5_pc_0.2-0.6_metrics.mat; i=1:10, j=1:1, k=1:5; spacing
      of 0.5, start 4, end 20
%results_2-11-2009.mat was from Sensitivity_Tests_T_6.0-
      8.5_a_1.5_pc_0.2-0.8_metrics.mat; i=1:16, j=1:1, k=1:7

load results_3-13-2009.mat

for i=1:16
    for j = 1
        for k = 1:7
            new_metric(i,k,j) = combined_metric(i,j,k);
        end
    end
end

[temperatures,precip_fraction] = meshgrid(temperature_axis,pc_axis);
temperatures = temperatures';
precip_fraction = precip_fraction';
for i=1
    contour_lines_start = 4;
    contour_lines_stop = 20;
    contour_lines =
[round(contour_lines_start):0.5:contour_lines_stop];
    figure
    %title(eval(num2str(aloss_axis(i))))
    contour(temperatures,precip_fraction,new_metric(:,:,i),
      contour_lines)
    colorbar;
    hold on;
    plot(temperatures, precip_fraction,'k*')
    plot(5,0.33,'rs')
end
```

Ice_Thickness_with_timesteps.m

```
%M-file for plotting ice thickness, timesteps included

%==========
%Get the names of datasets to process
directory_name=input('Location of data folders: ','s');
base_file_name_list=textread(strcat(directory_name,'/',input('File of
      base names of data to process (batch log file): ','s')),'%s');

%Begin loop to process all files
for entry=1:size(base_file_name_list)

%Get the base file name from the list
base_file_name=strcat(directory_name,'/',base_file_name_list{entry},'/'
      ,base_file_name_list{entry});

%Load the ice locations and topo data, using the base name
topo_temp=load(strcat(base_file_name,'_topo.out'),'-ascii');
longtopo_temp=load(strcat(base_file_name,'_long_topo.out'),'-ascii');
ice_time_temp=load(strcat(base_file_name,'_ice_time_data.out'),'-
      ascii');
%==========

%=====================================================
%Plot the basic file of topo
%=====================================================
%I. Reshape topo_output to be a 165*165 grid and plot it
t_temp=reshape(topo_temp(:,3),165,165);

figure;
ph=pcolor(t_temp);
hold on;
set(ph,'linestyle','none');
colorbar;

%==========
%Create the colorbar to use in the plots (this is based off of the
%default 'jet' but adds gray to the bottom or 0 value)
%==========
map=[0.5,0.5,0.5;0,0,0.625;0,0,0.6875;0,0,0.75;0,0,0.8125;0,0,0.875;0,0
      ,0.9375;0,0,1;0,0.0625,1;0,0.125,1;0,0.1875,1;0,0.25,1;0,0.3125,1
      ;0,0.375,1;0,0.4375,1;0,0.5,1;0,0.5625,1;0,0.625,1;0,0.6875,1;0,0
      .75,1;0,0.8125,1;0,0.875,1;0,0.9375,1;0,1,1;0.0625,1,0.9375;0.125
      ,1,0.875;0.1875,1,0.8125;0.25,1,0.75;0.3125,1,0.6875;0.375,1,0.62
      5;0.4375,1,0.5625;0.5,1,0.5;0.5625,1,0.4375;0.625,1,0.375;0.6875,
      1,0.3125;0.75,1,0.25;0.8125,1,0.1875;0.875,1,0.125;0.9375,1,0.062
      5;1,1,0;1,0.9375,0;1,0.875,0;1,0.8125,0;1,0.75,0;1,0.6875,0;1,0.6
      25,0;1,0.5625,0;1,0.5,0;1,0.4375,0;1,0.375,0;1,0.3125,0;1,0.25,0;
      1,0.1875,0;1,0.125,0;1,0.0625,0;1,0,0;0.9375,0,0;0.875,0,0;0.8125
      ,0,0;0.75,0,0;0.6875,0,0;0.625,0,0;0.5625,0,0;0.5,0,0;];

%==========
%Set colorbar for ice thickness plots
%==========
ice_thick_min=min(min(longtopo_temp(:,5)))
```

```
ice_thick_max=max(max(longtopo_temp(:,5)))

%==========
%Plot the ice thickness as a map
%==========
topo_general=reshape(topo_temp(:,5),165,165);

figure;
ph=pcolor(topo_general);
hold on;
set(ph,'linestyle','none');
title('Ice Thickness');
%colormap Winter
colorbar;
saveas(ph,strcat(base_file_name,'_icethick.png'));

%====================================
%Plot the average ice thickness and nodes against time
%====================================
%Plot average ice thickness as a function of time
figure;
ph=plot(ice_time_temp(:,1),ice_time_temp(:,2));
xlabel('Time (yr)');
ylabel('Average Ice Thickness (m) (sum(h)/nx*ny))');
title('Average Ice Thickness vs. Time');
saveas(ph,strcat(base_file_name,'_ice_thickness_vs_time.png'));

%Plot number of nodes containing ice as a function of time
figure;
ph=plot(ice_time_temp(:,1),ice_time_temp(:,3));
xlabel('Time (yr)');
ylabel('Number of nodes containing ice');
title('Number of nodes containing ice vs. Time');
saveas(ph,strcat(base_file_name,'_ice_nodes_vs_time.png'));

%====================================================
%Plot the ice thickness over timesteps; first cut long files into
%timesteps
%====================================================
%I. Cut the long_temps file into each of the timestep pieces
filesize1 = size (longtopo_temp);
a = filesize1(1,1);
aa = a/27225;
x=1;
for n = 1:aa
    SS_str = [ 'SS_topo', int2str(n), '=longtopo_temp(x:x+27224,:);'];
    eval(SS_str);
    x = x+27225;
end

%Set up the topo to be plotted as contours
topotopo_ss1=reshape(SS_topo1(:,3),165,165);
topotopo_ss2=reshape(SS_topo2(:,3),165,165);
topotopo_ss3=reshape(SS_topo3(:,3),165,165);
topotopo_ss4=reshape(SS_topo4(:,3),165,165);
topotopo_ss5=reshape(SS_topo5(:,3),165,165);
```

```
topotopo_ss6=reshape(SS_topo6(:,3),165,165);
topotopo_ss7=reshape(SS_topo7(:,3),165,165);
topotopo_ss8=reshape(SS_topo8(:,3),165,165);
topotopo_ss9=reshape(SS_topo9(:,3),165,165);
topotopo_ss10=reshape(SS_topo10(:,3),165,165);

%=====================================================================
%I. Reshape ice_thickness to be a 165*165 grid and plot it
%=====================================================================
topo_ss1=reshape(SS_topo1(:,5),165,165);

figure;
ph=pcolor(topo_ss1);
hold on;
set(ph,'linestyle','none');
colorbar;
colormap(map);
caxis([ice_thick_min ice_thick_max]);
contour(topotopo_ss1,5,'k');
title('Ice Thickness at 1000 yrs');
ah=gca;
set(ah,'YTick',[1 117]);
set(ah,'YTickLabel',{'47 N','48 N'});
set(ah,'XTick',[14 86]);
set(ah,'XTickLabel',{'124 W','123 W'});
saveas(ph,strcat(base_file_name,'_icethick1kyr.png'));

topo_ss2=reshape(SS_topo2(:,5),165,165);

figure;
ph=pcolor(topo_ss2);
hold on;
set(ph,'linestyle','none');
colorbar;
colormap(map);
caxis([ice_thick_min ice_thick_max]);
contour(topotopo_ss2,5,'k');
title('Ice Thickness at 2000 yrs');
ah=gca;
set(ah,'YTick',[1 117]);
set(ah,'YTickLabel',{'47 N','48 N'});
set(ah,'XTick',[14 86]);
set(ah,'XTickLabel',{'124 W','123 W'});
saveas(ph,strcat(base_file_name,'_icethick2kyr.png'));

topo_ss3=reshape(SS_topo3(:,5),165,165);

figure;
ph=pcolor(topo_ss3);
hold on;
set(ph,'linestyle','none');
colorbar;
colormap(map);
caxis([ice_thick_min ice_thick_max]);
contour(topotopo_ss3,5,'k');
title('Ice Thickness at 3000 yrs');
```

```
ah=gca;
set(ah,'YTick',[1 117]);
set(ah,'YTickLabel',{'47 N','48 N'});
set(ah,'XTick',[14 86]);
set(ah,'XTickLabel',{'124 W','123 W'});
saveas(ph,strcat(base_file_name,'_icethick3kyr.png'));

topo_ss4=reshape(SS_topo4(:,5),165,165);

figure;
ph=pcolor(topo_ss4);
hold on;
set(ph,'linestyle','none');
colorbar;
colormap(map);
caxis([ice_thick_min ice_thick_max]);
contour(topotopo_ss4,5,'k');
title('Ice Thickness at 4000 yrs');
ah=gca;
set(ah,'YTick',[1 117]);
set(ah,'YTickLabel',{'47 N','48 N'});
set(ah,'XTick',[14 86]);
set(ah,'XTickLabel',{'124 W','123 W'});
saveas(ph,strcat(base_file_name,'_icethick4kyr.png'));

topo_ss5=reshape(SS_topo5(:,5),165,165);

figure;
ph=pcolor(topo_ss5);
hold on;
set(ph,'linestyle','none');
colorbar;
colormap(map);
caxis([ice_thick_min ice_thick_max]);
contour(topotopo_ss5,5,'k');
title('Ice Thickness at 5000 yrs');
ah=gca;
set(ah,'YTick',[1 117]);
set(ah,'YTickLabel',{'47 N','48 N'});
set(ah,'XTick',[14 86]);
set(ah,'XTickLabel',{'124 W','123 W'});
saveas(ph,strcat(base_file_name,'_icethick5kyr.png'));

topo_ss6=reshape(SS_topo6(:,5),165,165);

figure;
ph=pcolor(topo_ss6);
hold on;
set(ph,'linestyle','none');
colorbar;
colormap(map);
caxis([ice_thick_min ice_thick_max]);
contour(topotopo_ss6,5,'k');
title('Ice Thickness at 6000 yrs');
ah=gca;
set(ah,'YTick',[1 117]);
```

```
set(ah,'YTickLabel',{'47 N','48 N'});
set(ah,'XTick',[14 86]);
set(ah,'XTickLabel',{'124 W','123 W'});
saveas(ph,strcat(base_file_name,'_icethick6kyr.png'));

topo_ss7=reshape(SS_topo7(:,5),165,165);

figure;
ph=pcolor(topo_ss7);
hold on;
set(ph,'linestyle','none');
colorbar;
colormap(map);
caxis([ice_thick_min ice_thick_max]);
contour(topotopo_ss7,5,'k');
title('Ice Thickness at 7000 yrs');
ah=gca;
set(ah,'YTick',[1 117]);
set(ah,'YTickLabel',{'47 N','48 N'});
set(ah,'XTick',[14 86]);
set(ah,'XTickLabel',{'124 W','123 W'});
saveas(ph,strcat(base_file_name,'_icethick7kyr.png'));

topo_ss8=reshape(SS_topo8(:,5),165,165);

figure;
ph=pcolor(topo_ss8);
hold on;
set(ph,'linestyle','none');
colorbar;
colormap(map);
caxis([ice_thick_min ice_thick_max]);
contour(topotopo_ss8,5,'k');
title('Ice Thickness at 8000 yrs');
ah=gca;
set(ah,'YTick',[1 117]);
set(ah,'YTickLabel',{'47 N','48 N'});
set(ah,'XTick',[14 86]);
set(ah,'XTickLabel',{'124 W','123 W'});
saveas(ph,strcat(base_file_name,'_icethick8kyr.png'));

topo_ss9=reshape(SS_topo9(:,5),165,165);

figure;
ph=pcolor(topo_ss9);
hold on;
set(ph,'linestyle','none');
colorbar;
colormap(map);
caxis([ice_thick_min ice_thick_max]);
contour(topotopo_ss9,5,'k');
title('Ice Thickness at 9000 yrs');
ah=gca;
set(ah,'YTick',[1 117]);
set(ah,'YTickLabel',{'47 N','48 N'});
set(ah,'XTick',[14 86]);
```

```
set(ah,'XTickLabel',{'124 W','123 W'});
saveas(ph,strcat(base_file_name,'_icethick9kyr.png'));

topo_ss10=reshape(SS_topo10(:,5),165,165);

figure;
ph=pcolor(topo_ss10);
hold on;
set(ph,'linestyle','none');
colorbar;
colormap(map);
caxis([ice_thick_min ice_thick_max]);
contour(topotopo_ss10,5,'k');
title('Ice Thickness at 10000 yrs');
ah=gca;
set(ah,'YTick',[1 117]);
set(ah,'YTickLabel',{'47 N','48 N'});
set(ah,'XTick',[14 86]);
set(ah,'XTickLabel',{'124 W','123 W'});
saveas(ph,strcat(base_file_name,'_icethick10kyr.png'));

%=========================================================
%Clean-up
%=========================================================
clear topo_temp longtopo_temp ice_time_temp t_temp ice_thick_min
clear ice_thick_max topo_general filesize1 a aa x n SS_str topo_ss1
clear SS_topo1 topo_ss2 SS_topo2 topo_ss3 SS_topo3 topo_ss4 SS_topo4
clear topo_ss5 SS_topo5 topo_ss6 SS_topo6 topo_ss7 SS_topo7 topo_ss8
clear SS_topo8 topo_ss9 SS_topo9 topo_ss10 SS_topo10 topotopo_ss1
clear topotopo_ss2 topotopo_ss3 topotopo_ss4 topotopo_ss5 topotopo_ss6
clear topotopo_ss7 topotopo_ss8 topotopo_ss9 topotopo_ss10

close all;
end;
```

Sliding_Velocity.m

```
%File for plotting the velocity (column 6 of long_glac.out
%'sqrt(u(i,j)**2+v(i,j)**2)') and sliding (column 5 of long_glac.out)

%==========
%Get the names of datasets to process
directory_name=input('Location of data folders: ','s');
base_file_name_list=textread(strcat(directory_name,'/',input('File of
      base names of data to process (batch log file): ','s')),'%s');

%Begin loop to process all files
for entry=1:size(base_file_name_list)

%Get the base file name from the list
base_file_name=strcat(directory_name,'/',base_file_name_list{entry},'/'
      ,base_file_name_list{entry});

%Load the ice locations and topo data, using the base name
longtopo_temp=load(strcat(base_file_name,'_long_topo.out'),'-ascii');
longglac_temp=load(strcat(base_file_name,'_long_glac.out'),'-ascii');
%==========

%==========
%Create the colorbar to use in the plots (this is based off of the
%default 'jet' but adds gray to the bottom or 0 value)
%==========
map=[0.5,0.5,0.5;0,0,0.625;0,0,0.6875;0,0,0.75;0,0,0.8125;0,0,0.875;0,0
      ,0.9375;0,0,1;0,0.0625,1;0,0.125,1;0,0.1875,1;0,0.25,1;0,0.3125,1
      ;0,0.375,1;0,0.4375,1;0,0.5,1;0,0.5625,1;0,0.625,1;0,0.6875,1;0,0
      .75,1;0,0.8125,1;0,0.875,1;0,0.9375,1;0,1,1;0.0625,1,0.9375;0.125
      ,1,0.875;0.1875,1,0.8125;0.25,1,0.75;0.3125,1,0.6875;0.375,1,0.62
      5;0.4375,1,0.5625;0.5,1,0.5;0.5625,1,0.4375;0.625,1,0.375;0.6875,
      1,0.3125;0.75,1,0.25;0.8125,1,0.1875;0.875,1,0.125;0.9375,1,0.062
      5;1,1,0;1,0.9375,0;1,0.875,0;1,0.8125,0;1,0.75,0;1,0.6875,0;1,0.6
      25,0;1,0.5625,0;1,0.5,0;1,0.4375,0;1,0.375,0;1,0.3125,0;1,0.25,0;
      1,0.1875,0;1,0.125,0;1,0.0625,0;1,0,0;0.9375,0,0;0.875,0,0;0.8125
      ,0,0;0.75,0,0;0.6875,0,0;0.625,0,0;0.5625,0,0;0.5,0,0;];

%=========
%Set colorbar for ice thickness plots
%=========
sliding_min=min(min(longglac_temp(:,5)))
sliding_max=max(max(longglac_temp(:,5)))

velocity_min=min(min(longglac_temp(:,6)))
velocity_max=max(max(longglac_temp(:,6)))

%==========
%Cut the long files so the data can be plotted
%==========
%Cut the long_topo file into each of the timestep pieces
filesize1 = size (longtopo_temp);
a = filesize1(1,1);
aa = a/27225;
x=1;
```

```
for n = 1:aa
    SS_str = [ 'SS_topo', int2str(n), '=longtopo_temp(x:x+27224,:);'];
    eval(SS_str);
    x = x+27225;
end

%Cut the long_glac file into each of the timestep pieces
filesize2 = size (longglac_temp);
a = filesize2(1,1);
aa = a/27225;
x=1;
for n = 1:aa
    SS_str = [ 'SS_glac', int2str(n), '=longglac_temp(x:x+27224,:);'];
    eval(SS_str);
    x = x+27225;
end

%==========
%Reshape files for the columns of data that are needed
%==========
topo_ss1=reshape(SS_topo1(:,3),165,165);
topo_ss2=reshape(SS_topo2(:,3),165,165);
topo_ss3=reshape(SS_topo3(:,3),165,165);
topo_ss4=reshape(SS_topo4(:,3),165,165);
topo_ss5=reshape(SS_topo5(:,3),165,165);
topo_ss6=reshape(SS_topo6(:,3),165,165);
topo_ss7=reshape(SS_topo7(:,3),165,165);
topo_ss8=reshape(SS_topo8(:,3),165,165);
topo_ss9=reshape(SS_topo9(:,3),165,165);
topo_ss10=reshape(SS_topo10(:,3),165,165);

sliding_ss1=reshape(SS_glac1(:,5),165,165);
sliding_ss2=reshape(SS_glac2(:,5),165,165);
sliding_ss3=reshape(SS_glac3(:,5),165,165);
sliding_ss4=reshape(SS_glac4(:,5),165,165);
sliding_ss5=reshape(SS_glac5(:,5),165,165);
sliding_ss6=reshape(SS_glac6(:,5),165,165);
sliding_ss7=reshape(SS_glac7(:,5),165,165);
sliding_ss8=reshape(SS_glac8(:,5),165,165);
sliding_ss9=reshape(SS_glac9(:,5),165,165);
sliding_ss10=reshape(SS_glac10(:,5),165,165);

sqrtvelocity_ss1=reshape(SS_glac1(:,6),165,165);
sqrtvelocity_ss2=reshape(SS_glac2(:,6),165,165);
sqrtvelocity_ss3=reshape(SS_glac3(:,6),165,165);
sqrtvelocity_ss4=reshape(SS_glac4(:,6),165,165);
sqrtvelocity_ss5=reshape(SS_glac5(:,6),165,165);
sqrtvelocity_ss6=reshape(SS_glac6(:,6),165,165);
sqrtvelocity_ss7=reshape(SS_glac7(:,6),165,165);
sqrtvelocity_ss8=reshape(SS_glac8(:,6),165,165);
sqrtvelocity_ss9=reshape(SS_glac9(:,6),165,165);
sqrtvelocity_ss10=reshape(SS_glac10(:,6),165,165);

%==========
%VI. Plot Sliding
%==========
```

```
figure;
ph=pcolor(sliding_ss1);
hold on;
set(ph,'linestyle','none');
colorbar;
colormap(map);
caxis([sliding_min sliding_max]);
contour(topo_ss1,5,'k');
title('Sliding at 1000 yr');
saveas(ph,strcat(base_file_name,'_velocitysliding1kyr.png'));

figure;
ph=pcolor(sliding_ss2);
hold on;
set(ph,'linestyle','none');
colorbar;
colormap(map);
caxis([sliding_min sliding_max]);
contour(topo_ss2,5,'k');
title('Sliding at 2000 yr');
saveas(ph,strcat(base_file_name,'_velocitysliding2kyr.png'));

figure;
ph=pcolor(sliding_ss3);
hold on;
set(ph,'linestyle','none');
colorbar;
colormap(map);
caxis([sliding_min sliding_max]);
contour(topo_ss3,5,'k');
title('Sliding at 3000 yr');
saveas(ph,strcat(base_file_name,'_velocitysliding3kyr.png'));

figure;
ph=pcolor(sliding_ss4);
hold on;
set(ph,'linestyle','none');
colorbar;
colormap(map);
caxis([sliding_min sliding_max]);
contour(topo_ss4,5,'k');
title('Sliding at 4000 yr');
saveas(ph,strcat(base_file_name,'_velocitysliding4kyr.png'));

figure;
ph=pcolor(sliding_ss5);
hold on;
set(ph,'linestyle','none');
colorbar;
colormap(map);
caxis([sliding_min sliding_max]);
contour(topo_ss5,5,'k');
title('Sliding at 5000 yr');
saveas(ph,strcat(base_file_name,'_velocitysliding5kyr.png'));

figure;
```

```
ph=pcolor(sliding_ss6);
hold on;
set(ph,'linestyle','none');
colorbar;
colormap(map);
caxis([sliding_min sliding_max]);
contour(topo_ss6,5,'k');
title('Sliding at 6000 yr');
saveas(ph,strcat(base_file_name,'_velocitysliding6kyr.png'));

figure;
ph=pcolor(sliding_ss7);
hold on;
set(ph,'linestyle','none');
colorbar;
colormap(map);
caxis([sliding_min sliding_max]);
contour(topo_ss7,5,'k');
title('Sliding at 7000 yr');
saveas(ph,strcat(base_file_name,'_velocitysliding7kyr.png'));

figure;
ph=pcolor(sliding_ss8);
hold on;
set(ph,'linestyle','none');
colorbar;
colormap(map);
caxis([sliding_min sliding_max]);
contour(topo_ss8,5,'k');
title('Sliding at 8000 yr');
saveas(ph,strcat(base_file_name,'_velocitysliding8kyr.png'));

figure;
ph=pcolor(sliding_ss9);
hold on;
set(ph,'linestyle','none');
colorbar;
colormap(map);
caxis([sliding_min sliding_max]);
contour(topo_ss9,5,'k');
title('Sliding at 9000 yr');
saveas(ph,strcat(base_file_name,'_velocitysliding9kyr.png'));

figure;
ph=pcolor(sliding_ss10);
hold on;
set(ph,'linestyle','none');
colorbar;
colormap(map);
caxis([sliding_min sliding_max]);
contour(topo_ss10,5,'k');
title('Sliding at 10000 yr');
ah=gca;
set(ah,'YTick',[1 117]);
set(ah,'YTickLabel',{'47 N','48 N'});
set(ah,'XTick',[14 86]);
```

```
set(ah,'XTickLabel',{'124 W','123 W'});
saveas(ph,strcat(base_file_name,'_velocitysliding10kyr.png'));

%==========
%Plot the sqrt velocity
%==========
figure;
ph=pcolor(sqrtvelocity_ss1);
hold on;
set(ph,'linestyle','none');
colorbar;
colormap(map);
caxis([velocity_min velocity_max]);
contour(topo_ss1,5,'k');
title('Velocity at 1000 yr');
saveas(ph,strcat(base_file_name,'_velocity1kyr.png'));

figure;
ph=pcolor(sqrtvelocity_ss2);
hold on;
set(ph,'linestyle','none');
colorbar;
colormap(map);
caxis([velocity_min velocity_max]);
contour(topo_ss2,5,'k');
title('Velocity at 2000 yr');
saveas(ph,strcat(base_file_name,'_velocity2kyr.png'));

figure;
ph=pcolor(sqrtvelocity_ss3);
hold on;
set(ph,'linestyle','none');
colorbar;
colormap(map);
caxis([velocity_min velocity_max]);
contour(topo_ss3,5,'k');
title('Velocity at 3000 yr');
saveas(ph,strcat(base_file_name,'_velocity3kyr.png'));

figure;
ph=pcolor(sqrtvelocity_ss4);
hold on;
set(ph,'linestyle','none');
colorbar;
colormap(map);
caxis([velocity_min velocity_max]);
contour(topo_ss4,5,'k');
title('Velocity at 4000 yr');
saveas(ph,strcat(base_file_name,'_velocity4kyr.png'));

figure;
ph=pcolor(sqrtvelocity_ss5);
hold on;
set(ph,'linestyle','none');
colorbar;
colormap(map);
```

```
caxis([velocity_min velocity_max]);
contour(topo_ss5,5,'k');
title('Velocity at 5000 yr');
saveas(ph,strcat(base_file_name,'_velocity5kyr.png'));

figure;
ph=pcolor(sqrtvelocity_ss6);
hold on;
set(ph,'linestyle','none');
colorbar;
colormap(map);
caxis([velocity_min velocity_max]);
contour(topo_ss6,5,'k');
title('Velocity at 6000 yr');
saveas(ph,strcat(base_file_name,'_velocity6kyr.png'));

figure;
ph=pcolor(sqrtvelocity_ss7);
hold on;
set(ph,'linestyle','none');
colorbar;
colormap(map);
caxis([velocity_min velocity_max]);
contour(topo_ss7,5,'k');
title('Velocity at 7000 yr');
saveas(ph,strcat(base_file_name,'_velocity7kyr.png'));

figure;
ph=pcolor(sqrtvelocity_ss8);
hold on;
set(ph,'linestyle','none');
colorbar;
colormap(map);
caxis([velocity_min velocity_max]);
contour(topo_ss8,5,'k');
title('Velocity at 8000 yr');
saveas(ph,strcat(base_file_name,'_velocity8kyr.png'));

figure;
ph=pcolor(sqrtvelocity_ss9);
hold on;
set(ph,'linestyle','none');
colorbar;
colormap(map);
caxis([velocity_min velocity_max]);
contour(topo_ss9,5,'k');
title('Velocity at 9000 yr');
saveas(ph,strcat(base_file_name,'_velocity9kyr.png'));

figure;
ph=pcolor(sqrtvelocity_ss10);
hold on;
set(ph,'linestyle','none');
colorbar;
colormap(map);
caxis([velocity_min velocity_max]);
```

```
contour(topo_ss10,5,'k');
title('Velocity at 10000 yr');
saveas(ph,strcat(base_file_name,'_velocity10kyr.png'));

%==========
%Clean-up
%==========
clear longtopo_temp longglac_temp filesize1 a aa x n SS_str
clear filesize2 a aa x n SS_str topo_ss1 topo_ss2 topo_ss3
clear topo_ss4 topo_ss5 topo_ss6 topo_ss7 topo_ss8 topo_ss9
clear topo_ss10 sliding_ss1 sliding_ss2 sliding_ss3 sliding_ss4
clear sliding_ss5 sliding_ss6 sliding_ss7 sliding_ss8 sliding_ss
clear sliding_ss10 sqrtvelocity_ss1 sqrtvelocity_ss2
clear sqrtvelocity_ss3 sqrtvelocity_ss4 sqrtvelocity_ss5
clear sqrtvelocity_ss6 sqrtvelocity_ss7 sqrtvelocity_ss8
clear sqrtvelocity_ss9 sqrtvelocity_ss10 SS_topo1 SS_topo2 SS_topo3
clear SS_topo4 SS_topo5 SS_topo6 SS_topo7 SS_topo8 SS_topo9
clear SS_topo10 SS_glac1 SS_glac2 SS_glac3 SS_glac4 SS_glac5
clear SS_glac6 SS_glac7 SS_glac8 SS_glac9 SS_glac10

close all;
end;
```

Temperature_with_timesteps.m

```
%File for plotting the temperature, timesteps included

%==========
%Get the names of datasets to process
directory_name=input('Location of data folders: ','s');
base_file_name_list=textread(strcat(directory_name,'/',input('File of
      base names of data to process (batch log file): ','s')),'%s');

%Begin loop to process all files
for entry=1:size(base_file_name_list)

%Get the base file name from the list
base_file_name=strcat(directory_name,'/',base_file_name_list{entry},'/'
      ,base_file_name_list{entry});

%Load the ice locations and topo data, using the base name
topo_temp=load(strcat(base_file_name,'_topo.out'),'-ascii');
temps_temp=load(strcat(base_file_name,'_temps.out'),'-ascii');
longtemps_temp=load(strcat(base_file_name,'_long_temps.out'),'-ascii');
temps_time_temp=load(strcat(base_file_name,'_temps_time_data.out'),'-
      ascii');
%==========

%=====================================================
%Plot the basic file of topo
%=====================================================
%I. Reshape topo_output to be a 165*165 grid and plot it
t_temp=reshape(topo_temp(:,3),165,165);

figure;
ph=pcolor(t_temp);
hold on;
set(ph,'linestyle','none');
colorbar;

%==========
%Set colorbar for temperature plots
%==========
temps_min=min(min(longtemps_temp(:,3)))
temps_max=max(max(longtemps_temp(:,3)))

%===================
%Plot the temperature as a map
%===================
temps=reshape(temps_temp(:,3),165,165);

figure;
ph=pcolor(temps);
hold on;
set(ph,'linestyle','none');
title('Temperature');
colorbar;
saveas(ph,strcat(base_file_name,'_temps.png'));
```

```
%====================================
%Plot the average temperature and sea level temperature against time
%====================================
%Plot the average temperature against time
figure;
ph=plot(temps_time_temp(:,2),temps_time_temp(:,3));
xlabel('Time (yr)');
ylabel('Average Temperature');
title('Average Temperature vs. Time');
saveas(ph,strcat(base_file_name,'_avgtemps_vs_time.png'));

%Plot the temp at sea level over time
%tempsSL=[7.2,8.08,8.96,9.84,10.72,11.6,12.48,13.36,14.24,15.12,16];
%time=[0,10000,20000,30000,40000,50000,60000,70000,80000,90000,100000];

SLTemps=[0 16
    1000 15.2
    2000 14.4
    3000 13.6
    4000 12.8
    5000 12
    6000 11.2
    7000 10.4
    8000 9.6
    9000 8.8
   10000 8.0];

figure;
ph=plot(SLTemps(:,1),SLTemps(:,2));
xlabel('Time (yr)');
ylabel('Temperature At Sea Level (C)');
title('Temperature At Sea Level vs. Time');
saveas(ph,strcat(base_file_name,'_tempsatSL_vs_time.png'));

%====================================================
%Plot the temperature over timesteps; first cut the long files into
%timesteps
%====================================================
%I. Cut the long_temps file into each of the timestep pieces
filesize1 = size (longtemps_temp);
a = filesize1(1,1);
aa = a/27225;
x=1;
for n = 1:aa
    SS_str = [ 'SS_temps', int2str(n),'=longtemps_temp(x:x+27224,:);'];
    eval(SS_str);
    x = x+27225;
end

%=================================================================
%I. Reshape the output to be a 165*165 grid and plot it
%=================================================================
temps_ss1=reshape(SS_temps1(:,3),165,165);
```

```
figure;
ph=pcolor(temps_ss1);
hold on;
set(ph,'linestyle','none');
colorbar;
caxis('manual');
caxis([temps_min temps_max]);
title('Temperature at 1000 yrs');
saveas(ph,strcat(base_file_name,'_temps1kyr.png'));

temps_ss2=reshape(SS_temps2(:,3),165,165);

figure;
ph=pcolor(temps_ss2);
hold on;
set(ph,'linestyle','none');
colorbar;
caxis('manual');
caxis([temps_min temps_max]);
title('Temperature at 2000 yrs');
saveas(ph,strcat(base_file_name,'_temps2kyr.png'));

temps_ss3=reshape(SS_temps3(:,3),165,165);

figure;
ph=pcolor(temps_ss3);
hold on;
set(ph,'linestyle','none');
colorbar;
caxis('manual');
caxis([temps_min temps_max]);
title('Temperature at 3000 yrs');
saveas(ph,strcat(base_file_name,'_temps3kyr.png'));

temps_ss4=reshape(SS_temps4(:,3),165,165);

figure;
ph=pcolor(temps_ss4);
hold on;
set(ph,'linestyle','none');
colorbar;
caxis('manual');
caxis([temps_min temps_max]);
title('Temperature at 4000 yrs');
saveas(ph,strcat(base_file_name,'_temps4kyr.png'));

temps_ss5=reshape(SS_temps5(:,3),165,165);

figure;
ph=pcolor(temps_ss5);
hold on;
set(ph,'linestyle','none');
colorbar;
caxis('manual');
caxis([temps_min temps_max]);
```

```
title('Temperature at 5000 yrs');
saveas(ph,strcat(base_file_name,'_temps5kyr.png'));

temps_ss6=reshape(SS_temps6(:,3),165,165);

figure;
ph=pcolor(temps_ss6);
hold on;
set(ph,'linestyle','none');
colorbar;
caxis('manual');
caxis([temps_min temps_max]);
title('Temperature at 6000 yrs');
saveas(ph,strcat(base_file_name,'_temps6kyr.png'));

temps_ss7=reshape(SS_temps7(:,3),165,165);

figure;
ph=pcolor(temps_ss7);
hold on;
set(ph,'linestyle','none');
colorbar;
caxis('manual');
caxis([temps_min temps_max]);
title('Temperature at 7000 yrs');
saveas(ph,strcat(base_file_name,'_temps7kyr.png'));

temps_ss8=reshape(SS_temps8(:,3),165,165);

figure;
ph=pcolor(temps_ss8);
hold on;
set(ph,'linestyle','none');
colorbar;
caxis('manual');
caxis([temps_min temps_max]);
title('Temperature at 8000 yrs');
saveas(ph,strcat(base_file_name,'_temps8kyr.png'));

temps_ss9=reshape(SS_temps9(:,3),165,165);

figure;
ph=pcolor(temps_ss9);
hold on;
set(ph,'linestyle','none');
colorbar;
caxis('manual');
caxis([temps_min temps_max]);
title('Temperature at 9000 yrs');
saveas(ph,strcat(base_file_name,'_temps9kyr.png'));

temps_ss10=reshape(SS_temps10(:,3),165,165);

figure;
ph=pcolor(temps_ss10);
```

```
hold on;
set(ph,'linestyle','none');
colorbar;
caxis('manual');
caxis([temps_min temps_max]);
title('Temperature at 10000 yrs');
saveas(ph,strcat(base_file_name,'_temps10kyr.png'));

%=========================================================
%Clean-up
%=========================================================
clear topo_temp temps_temp temps_time_temp longtemps_temp t_temp
clear glacialmap_current lgmxy x y temps temps_time_temp
clear temps_time_temp filesize1 a aa x n SS_str temps_ss1 SS_temps1
clear temps_ss2 SS_temps2 temps_ss3 SS_temps3 temps_ss4 SS_temps4
clear temps_ss5 SS_temps5 temps_ss6 SS_temps6 temps_ss7 SS_temps7
clear temps_ss8 SS_temps8 temps_ss9 SS_temps9 temps_ss10 SS_temps10

close all;
end;
```

Timestep_images_part1_topoicelocat.m

```
%File for creating images from long files
%Part 1-Topography and Ice Locations

%==========
%Get the names of datasets to process
directory_name=input('Location of data folders: ','s');
base_file_name_list=textread(strcat(directory_name,'/',input('File of
      base names of data to process (batch log file): ','s')),'%s');

%Begin loop to process all files
for entry=1:size(base_file_name_list)

%Get the base file name from the list
base_file_name=strcat(directory_name,'/',base_file_name_list{entry},'/'
      ,base_file_name_list{entry});

%Load the ice locations and topo data, using the base name
longice_loc_temp=load(strcat(base_file_name,'_long_ice_locat.out'),'-
      ascii');
longerosion_temp=load(strcat(base_file_name,'_long_erosion.out'),'-
      ascii');
longtopo_temp=load(strcat(base_file_name,'_long_topo.out'),'-ascii');
longglac_temp=load(strcat(base_file_name,'_long_glac.out'),'-ascii');
longdenud_temp=load(strcat(base_file_name,'_long_DENUD.out'),'-ascii');
%==========

%=====================================================
%Cut the long files into the timesteps
%=====================================================
%Cut the long_topo file into each of the timestep pieces
filesize1 = size (longtopo_temp);
a = filesize1(1,1);
aa = a/27225;
x=1;
for n = 1:aa
    SS_str = ['SS_topo',int2str(n),'=longtopo_temp(x:x+27224,:);'];
    eval(SS_str);
    x = x+27225;
end

%Cut the long_erosion file into each of the timestep pieces
filesize2 = size (longerosion_temp);
a = filesize2(1,1);
aa = a/27225;
x=1;
for n = 1:aa
    SS_str=['SS_erosion',int2str(n),'=longerosion_temp(x:x+27224,:);'];
    eval(SS_str);
    x = x+27225;
end

%Cut the long_DENUD file into each of the timestep pieces
filesize3 = size (longdenud_temp);
a = filesize3(1,1);
```

```
aa = a/27225;
x = 1;
for n = 1:aa
    SS_str = ['SS_denud',int2str(n),'=longdenud_temp(x:x+27224,:);'];
    eval(SS_str);
    x = x+27225;
end

%Record the breaks in the ice locations by looking it up in the actual
file and recording it in the parentheses (start at the end)
%SS_iceloc1=longice_loc_temp(1:1000,:);
%SS_iceloc2=longice_loc_temp(1001:2168,:);
SS_iceloc3=longice_loc_temp(1:4,:);
SS_iceloc4=longice_loc_temp(5:25,:);
SS_iceloc5=longice_loc_temp(26:160,:);
SS_iceloc6=longice_loc_temp(161:1144,:);
SS_iceloc7=longice_loc_temp(1145:3451,:);
SS_iceloc8=longice_loc_temp(3452:6679,:);
SS_iceloc9=longice_loc_temp(6680:10537,:);
SS_iceloc10=longice_loc_temp(10538:15305,:);

%SS_iceloc1=longice_loc_temp(1:4078,:);
%SS_iceloc2=longice_loc_temp(4079:7545,:);
%SS_iceloc3=longice_loc_temp(7546:10566,:);
%SS_iceloc4=longice_loc_temp(10567:13122,:);
%SS_iceloc5=longice_loc_temp(13123:15188,:);
%SS_iceloc6=longice_loc_temp(15189:16901,:);
%SS_iceloc7=longice_loc_temp(16902:18482,:);
%SS_iceloc8=longice_loc_temp(18483:19959,:);
%SS_iceloc9=longice_loc_temp(19960:21336,:);
%SS_iceloc10=longice_loc_temp(21337:22587,:);

%====================================================================
%I. Reshape the topography output to be a 165*165 grid and plot it
%====================================================================
topo_ss1=reshape(SS_topo1(:,3),165,165);
figure;
ph=pcolor(topo_ss1);
hold on;
set(ph,'linestyle','none');
colorbar;
title('Topography at 1000 yrs');
saveas(ph,strcat(base_file_name,'_topo1kyr.png'));

topo_ss2=reshape(SS_topo2(:,3),165,165);
figure;
ph=pcolor(topo_ss2);
hold on;
set(ph,'linestyle','none');
colorbar;
title('Topography at 2000 yrs');
%saveas(ph,strcat(base_file_name,'_topo2kyr.png'));

topo_ss3=reshape(SS_topo3(:,3),165,165);
figure;
ph=pcolor(topo_ss3);
```

```
hold on;
set(ph,'linestyle','none');
colorbar;
title('Topography at 3000 yrs');
%saveas(ph,strcat(base_file_name,'_topo3kyr.png'));

topo_ss4=reshape(SS_topo4(:,3),165,165);
figure;
ph=pcolor(topo_ss4);
hold on;
set(ph,'linestyle','none');
colorbar;
title('Topography at 4000 yrs');
%saveas(ph,strcat(base_file_name,'_topo4kyr.png'));

topo_ss5=reshape(SS_topo5(:,3),165,165);
figure;
ph=pcolor(topo_ss5);
hold on;
set(ph,'linestyle','none');
colorbar;
title('Topography at 5000 yrs');
%saveas(ph,strcat(base_file_name,'_topo5kyr.png'));

topo_ss6=reshape(SS_topo6(:,3),165,165);
figure;
ph=pcolor(topo_ss6);
hold on;
set(ph,'linestyle','none');
colorbar;
title('Topography at 6000 yrs');
%saveas(ph,strcat(base_file_name,'_topo6kyr.png'));

topo_ss7=reshape(SS_topo7(:,3),165,165);
figure;
ph=pcolor(topo_ss7);
hold on;
set(ph,'linestyle','none');
colorbar;
title('Topography at 7000 yrs');
%saveas(ph,strcat(base_file_name,'_topo7kyr.png'));

topo_ss8=reshape(SS_topo8(:,3),165,165);
figure;
ph=pcolor(topo_ss8);
hold on;
set(ph,'linestyle','none');
colorbar;
title('Topography at 8000 yrs');
%saveas(ph,strcat(base_file_name,'_topo8kyr.png'));

topo_ss9=reshape(SS_topo9(:,3),165,165);
figure;
ph=pcolor(topo_ss9);
hold on;
set(ph,'linestyle','none');
```

```
colorbar;
title('Topography at 9000 yrs');
%saveas(ph,strcat(base_file_name,'_topo9kyr.png'));

topo_ss10=reshape(SS_topo10(:,3),165,165);
figure;
ph=pcolor(topo_ss10);
hold on;
set(ph,'linestyle','none');
colorbar;
title('Topography at 10000 yrs');
ah=gca;
set(ah,'YTick',[1 117]);
set(ah,'YTickLabel',{'47 N','48 N'});
set(ah,'XTick',[14 86]);
set(ah,'XTickLabel',{'124 W','123 W'});
%contour(new_topo,5,'-k');
saveas(ph,strcat(base_file_name,'_topo10kyr.tif'));

%For Plotting Precipitation
topo_min=min(min(longtopo_temp(:,6)))
topo_max=max(max(longtopo_temp(:,6)))

topo_ss11=reshape(SS_topo10(:,6),165,165);
figure;
ph=pcolor(topo_ss11);
hold on;
set(ph,'linestyle','none');
colorbar;
colormap;
caxis([topo_min topo_max]);
contour(topo_ss10,5,'-k');
title('Precipitation at 10000 yrs');
ah=gca;
set(ah,'YTick',[1 117]);
set(ah,'YTickLabel',{'47 N','48 N'});
set(ah,'XTick',[14 86]);
set(ah,'XTickLabel',{'124 W','123 W'});
saveas(ph,strcat(base_file_name,'_precip10kyr.tif'));

%==========
%II. Plot current ice extent on the topography
%==========
x=[84;84;84;85;84;85;85;85;86;86;86;88;87;87;87;87;86;86;86;86;85;85;85
    ;85;85;85;86;86;86;86;87;88;89;90;90;90;90;90;89;89;89;90;90;93;93;
    93;93;92;92;92;92;89;89;89;87;87;87;89;88;88;88;88;88;88;88;89;89;
    89;89;88;87;87;87;87;87;86;86;86;86;85;85;85;84;85;85;85;84;84;84;
    84;83;84;83;83;84;83;83;84;84;84;85;85;85;85;85;83;83;83;83;83;83;
    79;79;79;79;79;79;78;78;78;77;77;76;77;76;77;77;78;78;78;79;78;77;
    77;76;77;77;77;77;78;78;77;77;77;79;79;78;79;79;79;80;80;80;80;80;
    80;80;81;81;81;80;80;80;79;79;80;80;80;78;78;78;78;79;78;79;78;79;
    79;79;79;79;79;79;80;80;80;79;83;83;83;83;83;82;82;82;82;82;83;84;
    83;84;83;83;83;82;82;82;81;81;81;82;80;81;81;80;80;79;80;80;81;80;
    81;81;82;81;82;82;82;82;82;82;82;82;81;81;82;80;104;105;108;108;
    109;109;124;123;123;122;122;105;106;106;106;108;108;108;109;109;
    109;112;112;113;109;109;109;108;108;108;108;108;107;107;107;107;
```

```
    107;107;107;108;108;107;108;107;107;108;107;107;115;115;115;116;
    116;116;115;115;116;116;117;117;118;118;118;118;117;117;116];

y=[105;105;105;106;105;105;105;105;106;106;106;105;104;105;104;105;105;
   105;105;104;105;105;105;105;104;104;104;104;104;104;102;102;102;102;
   101;99;99;98;96;96;96;96;99;82;82;83;83;83;83;83;88;87;88;89;89;
   88;90;91;91;90;90;91;94;94;94;94;94;94;94;94;94;94;94;94;94;95;
   94;94;94;94;94;94;95;95;94;94;94;94;94;94;94;93;94;93;93;93;93;93;
   93;93;93;93;93;97;97;97;96;95;96;96;96;95;95;96;95;96;95;96;96;95;
   95;94;94;94;95;95;94;94;94;95;94;94;93;93;89;90;90;89;90;89;89;89;
   91;91;91;90;91;91;91;92;92;92;93;92;92;92;93;93;93;93;93;92;92;92;
   93;93;93;93;94;94;94;94;94;93;93;93;93;93;94;94;94;94;94;94;93;92;
   92;91;91;91;92;92;92;92;94;95;96;95;95;94;94;93;93;93;92;92;93;94;
   94;94;94;95;95;95;95;95;96;96;96;95;96;97;97;97;96;95;95;94;94;93;
   93;93;95;95;95;100;100;97;97;97;97;92;91;78;78;78;76;75;76;76;77;
   77;81;81;81;81;82;82;82;87;86;86;85;84;84;84;84;85;85;85;85;85;87;
   86;86;85;86;86;87;87;86;86;87;100;100;98;98;97;97;97;96;96;96;96;
   96;96;95;94;95;94;94;95];

i=1:304;

glacialmap_current=zeros(304,2);
glacialmap_current (x(i), y(i))=1;

figure;
ph=pcolor(topo_ss1);
hold on;
set(ph,'linestyle','none');
colorbar;
plot(x,y,'k*');
title('Current Ice Extent');

%Locations of LGM Deposits used in the Climate Sensitivity Analysis
a=[62;38;44;64];
b=[88;95;68;54];

x_1=[38;44;64];
y_1=[95;68;54];

%Plot current ice and LGM Deposits
figure;
ph=pcolor(topo_ss1);
hold on;
set(ph,'linestyle','none');
colorbar;
%plot(x,y,'k*');
%lgmxy=load('lgmxy.txt','-ascii');
%plot(lgmxy(:,1),lgmxy(:,2),'rs');
plot(x_1,y_1,'rs');
%lgmxy2=[38,95;44,68;64,54;60,88]
%plot(lgmxy2(:,1),lgmxy2(:,2),'rs');
plot(a,b,'wx');
ah=gca;
set(ah,'YTick',[1 117]);
set(ah,'YTickLabel',{'47 N','48 N'});
set(ah,'XTick',[14 86]);
```

```
set(ah,'XTickLabel',{'124 W','123 W'});
title('Current ice and LGM Deposits');
saveas(ph,strcat(base_file_name,'_currenticeLGM.tif'));

%III. Plot new model ice locations on current ice and topography, with
lgm deposit locations
figure;
ph=pcolor(topo_ss1);
hold on;
set(ph,'linestyle','none');
colorbar;
%plot(x,y,'k*');
%if (size(SS_iceloc1,1)>0)
%    plot(SS_iceloc1(:,1),SS_iceloc1(:,2),'mx');
%end
%lgmxy=load('lgmxy.txt','-ascii');
%plot(lgmxy(:,1),lgmxy(:,2),'rs');
lgmxy2=[38,95;44,68;64,54;60,88];
plot(lgmxy2(:,1),lgmxy2(:,2),'ws');
title('Ice Extent for 1000 yrs');
ah=gca;
set(ah,'YTick',[1 117]);
set(ah,'YTickLabel',{'47 N','48 N'});
set(ah,'XTick',[14 86]);
set(ah,'XTickLabel',{'124 W','123 W'});
saveas(ph,strcat(base_file_name,'_ice_locations+lgm1kyr.png'));

figure;
ph=pcolor(topo_ss2);
hold on;
set(ph,'linestyle','none');
colorbar;
%plot(x,y,'k*');
%if (size(SS_iceloc2,1)>0)
%    plot(SS_iceloc2(:,1),SS_iceloc2(:,2),'mx');
%end
%lgmxy=load('lgmxy.txt','-ascii');
%plot(lgmxy(:,1),lgmxy(:,2),'rs');
lgmxy2=[38,95;44,68;64,54;60,88];
plot(lgmxy2(:,1),lgmxy2(:,2),'ws');
title('Ice Extent for 2000 yrs');
ah=gca;
set(ah,'YTick',[1 117]);
set(ah,'YTickLabel',{'47 N','48 N'});
set(ah,'XTick',[14 86]);
set(ah,'XTickLabel',{'124 W','123 W'});
saveas(ph,strcat(base_file_name,'_ice_locations+lgm2kyr.png'));

figure;
ph=pcolor(topo_ss3);
hold on;
set(ph,'linestyle','none');
colorbar;
%plot(x,y,'k*');
if (size(SS_iceloc3,1)>0)
    plot(SS_iceloc3(:,1),SS_iceloc3(:,2),'mx');
```

```
end
%lgmxy=load('lgmxy.txt','-ascii');
%plot(lgmxy(:,1),lgmxy(:,2),'rs');
lgmxy2=[38,95;44,68;64,54;60,88];
plot(lgmxy2(:,1),lgmxy2(:,2),'ws');
title('Ice Extent for 3000 yrs');
ah=gca;
set(ah,'YTick',[1 117]);
set(ah,'YTickLabel',{'47 N','48 N'});
set(ah,'XTick',[14 86]);
set(ah,'XTickLabel',{'124 W','123 W'});
saveas(ph,strcat(base_file_name,'_ice_locations+lgm3kyr.png'));

figure;
ph=pcolor(topo_ss4);
hold on;
set(ph,'linestyle','none');
colorbar;
%plot(x,y,'k*');
if (size(SS_iceloc4,1)>0)
    plot(SS_iceloc4(:,1),SS_iceloc4(:,2),'mx');
end
%lgmxy=load('lgmxy.txt','-ascii');
%plot(lgmxy(:,1),lgmxy(:,2),'rs');
lgmxy2=[38,95;44,68;64,54;60,88];
plot(lgmxy2(:,1),lgmxy2(:,2),'ws');
title('Ice Extent for 4000 yrs');
ah=gca;
set(ah,'YTick',[1 117]);
set(ah,'YTickLabel',{'47 N','48 N'});
set(ah,'XTick',[14 86]);
set(ah,'XTickLabel',{'124 W','123 W'});
saveas(ph,strcat(base_file_name,'_ice_locations+lgm4kyr.png'));

figure;
ph=pcolor(topo_ss5);
hold on;
set(ph,'linestyle','none');
colorbar;
%plot(x,y,'k*');
if (size(SS_iceloc5,1)>0)
    plot(SS_iceloc5(:,1),SS_iceloc5(:,2),'mx');
end
%lgmxy=load('lgmxy.txt','-ascii');
%plot(lgmxy(:,1),lgmxy(:,2),'rs');
lgmxy2=[38,95;44,68;64,54;60,88];
plot(lgmxy2(:,1),lgmxy2(:,2),'ws');
title('Ice Extent for 5000 yrs');
ah=gca;
set(ah,'YTick',[1 117]);
set(ah,'YTickLabel',{'47 N','48 N'});
set(ah,'XTick',[14 86]);
set(ah,'XTickLabel',{'124 W','123 W'});
saveas(ph,strcat(base_file_name,'_ice_locations+lgm5kyr.png'));

figure;
```

```
ph=pcolor(topo_ss6);
hold on;
set(ph,'linestyle','none');
colorbar;
%plot(x,y,'k*');
if (size(SS_iceloc6,1)>0)
    plot(SS_iceloc6(:,1),SS_iceloc6(:,2),'mx');
end
%lgmxy=load('lgmxy.txt','-ascii');
%plot(lgmxy(:,1),lgmxy(:,2),'rs');
lgmxy2=[38,95;44,68;64,54;60,88];
plot(lgmxy2(:,1),lgmxy2(:,2),'ws');
title('Ice Extent for 6000 yrs');
ah=gca;
set(ah,'YTick',[1 117]);
set(ah,'YTickLabel',{'47 N','48 N'});
set(ah,'XTick',[14 86]);
set(ah,'XTickLabel',{'124 W','123 W'});
saveas(ph,strcat(base_file_name,'_ice_locations+lgm6kyr.png'));

figure;
ph=pcolor(topo_ss7);
hold on;
set(ph,'linestyle','none');
colorbar;
%plot(x,y,'k*');
if (size(SS_iceloc7,1)>0)
    plot(SS_iceloc7(:,1),SS_iceloc7(:,2),'mx');
end
%lgmxy=load('lgmxy.txt','-ascii');
%plot(lgmxy(:,1),lgmxy(:,2),'rs');
lgmxy2=[38,95;44,68;64,54;60,88];
plot(lgmxy2(:,1),lgmxy2(:,2),'ws');
title('Ice Extent for 7000 yrs');
ah=gca;
set(ah,'YTick',[1 117]);
set(ah,'YTickLabel',{'47 N','48 N'});
set(ah,'XTick',[14 86]);
set(ah,'XTickLabel',{'124 W','123 W'});
saveas(ph,strcat(base_file_name,'_ice_locations+lgm7kyr.png'));

figure;
ph=pcolor(topo_ss8);
hold on;
set(ph,'linestyle','none');
colorbar;
%plot(x,y,'k*');
if (size(SS_iceloc8,1)>0)
    plot(SS_iceloc8(:,1),SS_iceloc8(:,2),'mx');
end
%lgmxy=load('lgmxy.txt','-ascii');
%plot(lgmxy(:,1),lgmxy(:,2),'rs');
lgmxy2=[38,95;44,68;64,54;60,88];
plot(lgmxy2(:,1),lgmxy2(:,2),'ws');
title('Ice Extent for 8000 yrs');
ah=gca;
```

```
set(ah,'YTick',[1 117]);
set(ah,'YTickLabel',{'47 N','48 N'});
set(ah,'XTick',[14 86]);
set(ah,'XTickLabel',{'124 W','123 W'});
saveas(ph,strcat(base_file_name,'_ice_locations+lgm8kyr.png'));

figure;
ph=pcolor(topo_ss9);
hold on;
set(ph,'linestyle','none');
colorbar;
%plot(x,y,'k*');
if (size(SS_iceloc9,1)>0)
    plot(SS_iceloc9(:,1),SS_iceloc9(:,2),'mx');
end
%lgmxy=load('lgmxy.txt','-ascii');
%plot(lgmxy(:,1),lgmxy(:,2),'rs');
lgmxy2=[38,95;44,68;64,54;60,88];
plot(lgmxy2(:,1),lgmxy2(:,2),'ws');
title('Ice Extent for 9000 yrs');
ah=gca;
set(ah,'YTick',[1 117]);
set(ah,'YTickLabel',{'47 N','48 N'});
set(ah,'XTick',[14 86]);
set(ah,'XTickLabel',{'124 W','123 W'});
saveas(ph,strcat(base_file_name,'_ice_locations+lgm9kyr.png'));

figure;
ph=pcolor(topo_ss10);
hold on;
set(ph,'linestyle','none');
colorbar;
%plot(x,y,'k*');
if (size(SS_iceloc10,1)>0)
    plot(SS_iceloc10(:,1),SS_iceloc10(:,2),'mx');
end
%lgmxy=load('lgmxy.txt','-ascii');
%plot(lgmxy(:,1),lgmxy(:,2),'rs');
lgmxy2=[38,95;44,68;64,54;60,88]
plot(lgmxy2(:,1),lgmxy2(:,2),'ws');
title('Ice Extent for 10000 yrs');
ah=gca;
set(ah,'YTick',[1 117]);
set(ah,'YTickLabel',{'47 N','48 N'});
set(ah,'XTick',[14 86]);
set(ah,'XTickLabel',{'124 W','123 W'});
%contour(new_topo,5,'-k');
saveas(ph,strcat(base_file_name,'_ice_locations+lgm10kyr.png'));

%============================================================
%Clean-up
%============================================================
clear topo_ss1 topo_ss2 topo_ss3 topo_ss4 topo_ss5 topo_ss6 topo_ss7
clear topo_ss8 topo_ss9 topo_ss10 SS_topo1  SS_topo2 SS_topo3 SS_topo4
clear SS_topo5 SS_topo6 SS_topo7 SS_topo8 SS_topo9 SS_topo10
```

```
clear glacialmap_current lgmxy n x a aa filesize1 filesize2 filesize3
clear SS_iceloc1 SS_iceloc2 SS_iceloc3 SS_iceloc4 SS_iceloc5 SS_iceloc6
clear SS_iceloc7 SS_iceloc8 SS_iceloc9 SS_iceloc10

close all;
end;
```

Timestep_images_part4denud.m

```
%File for creating images from long files
%Part 4-Denududation file plotting

%==========
%Get the names of datasets to process
directory_name=input('Location of data folders: ','s');
base_file_name_list=textread(strcat(directory_name,'/',input('File of
      base names of data to process (batch log file): ','s')),'%s');

%Begin loop to process all files
for entry=1:size(base_file_name_list)

%Get the base file name from the list
base_file_name=strcat(directory_name,'/',base_file_name_list{entry},'/'
      ,base_file_name_list{entry});

%Load the ice locations and topo data, using the base name
ice_loc_temp=load(strcat(base_file_name,'_ice_locations.out'),'-
      ascii');
longerosion_temp=load(strcat(base_file_name,'_long_erosion.out'),'-
      ascii');
longtopo_temp=load(strcat(base_file_name,'_long_topo.out'),'-ascii');
longglac_temp=load(strcat(base_file_name,'_long_glac.out'),'-ascii');
longdenud_temp=load(strcat(base_file_name,'_long_DENUD.out'),'-ascii');
%==========

%Cut the long_DENUD file into each of the timestep pieces
filesize3 = size (longdenud_temp);
a = filesize3(1,1);
aa = a/27225;
x = 1;
for n = 1:aa
    SS_str = ['SS_denud',int2str(n),'=longdenud_temp(x:x+27224,:);'];
    eval(SS_str);
    x = x+27225;
end

%==========
%Create the colorbar to use in the plots (this is based off of the
%default 'jet' but adds gray to the bottom or 0 value)
%==========
map=[0.5,0.5,0.5;0,0,0.625;0,0,0.6875;0,0,0.75;0,0,0.8125;0,0,0.875;0,0
      ,0.9375;0,0,1;0,0.0625,1;0,0.125,1;0,0.1875,1;0,0.25,1;0,0.3125,1
      ;0,0.375,1;0,0.4375,1;0,0.5,1;0,0.5625,1;0,0.625,1;0,0.6875,1;0,0
      .75,1;0,0.8125,1;0,0.875,1;0,0.9375,1;0,1,1;0.0625,1,0.9375;0.125
      ,1,0.875;0.1875,1,0.8125;0.25,1,0.75;0.3125,1,0.6875;0.375,1,0.62
      5;0.4375,1,0.5625;0.5,1,0.5;0.5625,1,0.4375;0.625,1,0.375;0.6875,
      1,0.3125;0.75,1,0.25;0.8125,1,0.1875;0.875,1,0.125;0.9375,1,0.062
      5;1,1,0;1,0.9375,0;1,0.875,0;1,0.8125,0;1,0.75,0;1,0.6875,0;1,0.6
      25,0;1,0.5625,0;1,0.5,0;1,0.4375,0;1,0.375,0;1,0.3125,0;1,0.25,0;
      1,0.1875,0;1,0.125,0;1,0.0625,0;1,0,0;0.9375,0,0;0.875,0,0;0.8125
      ,0,0;0.75,0,0;0.6875,0,0;0.625,0,0;0.5625,0,0;0.5,0,0;];

%=========
```

```
%Set colorbar for ice thickness plots
%=========
denud_min=min(min(longdenud_temp(:,3)))
denud_max=max(max(longdenud_temp(:,3)))

%=====================================================================
%Plot the total glacial erosion from DENUD file with the uplift
%=====================================================================
d_temp_ss1=reshape(SS_denud1(:,3),165,165);

figure;
ph=pcolor(d_temp_ss1);
hold on;
set(ph,'linestyle','none');
colorbar;
colormap(map);
caxis([denud_min denud_max]);
title('Denudation (m) 1000yr');
saveas(ph,strcat(base_file_name,'_denudtotal1kyr.png'));

d_temp_ss2=reshape(SS_denud2(:,3),165,165);

figure;
ph=pcolor(d_temp_ss2);
hold on;
set(ph,'linestyle','none');
colorbar;
colormap(map);
caxis([denud_min denud_max]);
title('Denudation m 2000yr');
saveas(ph,strcat(base_file_name,'_denudtotal2kyr.png'));

d_temp_ss3=reshape(SS_denud3(:,3),165,165);

figure;
ph=pcolor(d_temp_ss3);
hold on;
set(ph,'linestyle','none');
colorbar;
colormap(map);
caxis([denud_min denud_max]);
title('Denudation m 3000yr');
saveas(ph,strcat(base_file_name,'_denudtotal3kyr.png'));

d_temp_ss4=reshape(SS_denud4(:,3),165,165);

figure;
ph=pcolor(d_temp_ss4);
hold on;
set(ph,'linestyle','none');
colorbar;
colormap(map);
caxis([denud_min denud_max]);
title('Denudation m 4000yr');
saveas(ph,strcat(base_file_name,'_denudtotal4kyr.png'));
```

```
d_temp_ss5=reshape(SS_denud5(:,3),165,165);

figure;
ph=pcolor(d_temp_ss5);
hold on;
set(ph,'linestyle','none');
colorbar;
colormap(map);
caxis([denud_min denud_max]);
title('Denudation m 5000yr');
saveas(ph,strcat(base_file_name,'_denudtotal5kyr.png'));

d_temp_ss6=reshape(SS_denud6(:,3),165,165);

figure;
ph=pcolor(d_temp_ss6);
hold on;
set(ph,'linestyle','none');
colorbar;
colormap(map);
caxis([denud_min denud_max]);
title('Denudation m 6000yr');
saveas(ph,strcat(base_file_name,'_denudtotal6kyr.png'));

d_temp_ss7=reshape(SS_denud7(:,3),165,165);

figure;
ph=pcolor(d_temp_ss7);
hold on;
set(ph,'linestyle','none');
colorbar;
colormap(map);
caxis([denud_min denud_max]);
title('Denudation m 7000yr');
saveas(ph,strcat(base_file_name,'_denudtotal7kyr.png'));

d_temp_ss8=reshape(SS_denud8(:,3),165,165);

figure;
ph=pcolor(d_temp_ss8);
hold on;
set(ph,'linestyle','none');
colorbar;
colormap(map);
caxis([denud_min denud_max]);
title('Denudation m 8000yr');
saveas(ph,strcat(base_file_name,'_denudtotal8kyr.png'));

d_temp_ss9=reshape(SS_denud9(:,3),165,165);

figure;
ph=pcolor(d_temp_ss9);
hold on;
set(ph,'linestyle','none');
```

```
colorbar;
colormap(map);
caxis([denud_min denud_max]);
title('Denudation m 9000yr');
saveas(ph,strcat(base_file_name,'_denudtotal9kyr.png'));

d_temp_ss10=reshape(SS_denud10(:,3),165,165);

figure;
ph=pcolor(d_temp_ss10);
hold on;
set(ph,'linestyle','none');
colorbar;
colormap(map);
caxis([denud_min denud_max]);
ah=gca;
set(ah,'YTick',[1 117]);
set(ah,'YTickLabel',{'47 N','48 N'});
set(ah,'XTick',[14 86]);
set(ah,'XTickLabel',{'124 W','123 W'});
contour(new_topo,5,'-k');
title('Denudation m 10000yr');
saveas(ph,strcat(base_file_name,'_denudtotal10kyr.png'));

%=================================================
%Plot uplift which will be used to compare with erosion
%=================================================
%I. Make uplift a 165x165 grid
new_uplift=uplift(1:165,1:165);

%II. Plot uplift-full and unchanged
figure;
ph=pcolor(new_uplift);
hold on;
set(ph,'linestyle','none');
colorbar;
title('Uplift in the Olympic Mountains')
saveas(ph,strcat(base_file_name,'_uplift.png'));

%III. PLot the contoured uplift
figure;
ph=pcolor(uplift_contours);
hold on;
set(ph,'linestyle','none');
colorbar;
title('Uplift From Brandon et al. 1998');
saveas(ph,strcat(base_file_name,'_upliftcontours.png'));

%=========================================
%Rotation of figure for Uplift and Glacial Erosion Correlation
%=========================================
%First, make matrices X and Y that are your cartesian co-ordinate grid
%I think your grid is 160 by 160 not 512 by 512.
[X,Y] = meshgrid([1:1:165],[1:1:165]);
```

```
%convert your cartesian co-ordinates to polar co-ordinates
[THETA,R] = cart2pol(X,Y);

%set your angle to be equal to the angle of the transect from
horizontal in
%radians (and won't be pi)
angle = 24*pi/180;

%adjust the theta grid to do the rotation
THETA_ROT = THETA-angle;

%figure out the new cartesian co-ordinates of the rotated grid
[X_ROT,Y_ROT] = pol2cart(THETA_ROT,R);

%figure out how big the new grid is
bigx = max(max(X_ROT));
bigy = max(max(Y_ROT));
smx = min(min(X_ROT));
smy = min(min(Y_ROT));

%make new vectors of new X and Y coordinates
XI = [smx:1:bigx];
YI = [smy:1:bigy]';

%Interpolate the topography to the new grid - newtopo(newerosion_rot)
will be your rotated topography (or rotated erosion rates) and
topo(erosion_glac_temp) is the old grid. First try leaving off the
{'QJ','Pp'} part - this was the fudging deal - but you might need it in
the end.  I'd rotate your topography first just as a check because this
is going to be easy to see if it went correctly.
new_uplift_rot = griddata(X_ROT,Y_ROT,new_uplift,XI,YI,'linear');
new_contour_uplift_rot=griddata(X_ROT,Y_ROT,uplift_contours,XI,YI,
      'linear');
newdenud_rot_ss1 = griddata(X_ROT,Y_ROT,d_temp_ss1,XI,YI,'linear');
newdenud_rot_ss2 = griddata(X_ROT,Y_ROT,d_temp_ss2,XI,YI,'linear');
newdenud_rot_ss3 = griddata(X_ROT,Y_ROT,d_temp_ss3,XI,YI,'linear');
newdenud_rot_ss4 = griddata(X_ROT,Y_ROT,d_temp_ss4,XI,YI,'linear');
newdenud_rot_ss5 = griddata(X_ROT,Y_ROT,d_temp_ss5,XI,YI,'linear');
newdenud_rot_ss6 = griddata(X_ROT,Y_ROT,d_temp_ss6,XI,YI,'linear');
newdenud_rot_ss7 = griddata(X_ROT,Y_ROT,d_temp_ss7,XI,YI,'linear');
newdenud_rot_ss8 = griddata(X_ROT,Y_ROT,d_temp_ss8,XI,YI,'linear');
newdenud_rot_ss9 = griddata(X_ROT,Y_ROT,d_temp_ss9,XI,YI,'linear');
newdenud_rot_ss10 = griddata(X_ROT,Y_ROT,d_temp_ss10,XI,YI,'linear');

%note, this "griddata" step could take a while - shouldn't be forever,
but definitely could be minutes - so don't get alarmed if matlab chugs
on it a while.

b=isnan(newdenud_rot_ss1);
newdenud_rot_ss1(b)=0;

b=isnan(newdenud_rot_ss2);
newdenud_rot_ss2(b)=0;

b=isnan(newdenud_rot_ss3);
```

```
newdenud_rot_ss3(b)=0;

b=isnan(newdenud_rot_ss4);
newdenud_rot_ss4(b)=0;

b=isnan(newdenud_rot_ss5);
newdenud_rot_ss5(b)=0;

b=isnan(newdenud_rot_ss6);
newdenud_rot_ss6(b)=0;

b=isnan(newdenud_rot_ss7);
newdenud_rot_ss7(b)=0;

b=isnan(newdenud_rot_ss8);
newdenud_rot_ss8(b)=0;

b=isnan(newdenud_rot_ss9);
newdenud_rot_ss9(b)=0;

b=isnan(newdenud_rot_ss10);
newdenud_rot_ss10(b)=0;

b=isnan(new_contour_uplift_rot);
new_contour_uplift_rot(b)=0;

b=isnan(new_uplift_rot);
new_uplift_rot(b)=0;

%==========
%Plot denud with rotation and trimmed
%==========
figure;
ph=pcolor(newdenud_rot_ss1);
hold on;
set(ph,'linestyle','none');
colorbar;
colormap(map);
caxis([denud_min denud_max]);
title('Rotated DENUD Glacial Erosion 1000yr');
saveas(ph,strcat(base_file_name,'_denudglacerosion_rotated1kyr.png'));

figure;
ph=pcolor(newdenud_rot_ss2);
hold on;
set(ph,'linestyle','none');
colorbar;
colormap(map);
caxis([denud_min denud_max]);
title('Rotated DENUD Glacial Erosion 2000yr');
saveas(ph,strcat(base_file_name,'_denudglacerosion_rotated2kyr.png'));

figure;
ph=pcolor(newdenud_rot_ss3);
```

```
hold on;
set(ph,'linestyle','none');
colorbar;
colormap(map);
caxis([denud_min denud_max]);
title('Rotated DENUD Glacial Erosion 3000yr');
saveas(ph,strcat(base_file_name,'_denudglacerosion_rotated3kyr.png'));

figure;
ph=pcolor(newdenud_rot_ss4);
hold on;
set(ph,'linestyle','none');
colorbar;
colormap(map);
caxis([denud_min denud_max]);
title('Rotated DENUD Glacial Erosion 4000yr');
saveas(ph,strcat(base_file_name,'_denudglacerosion_rotated4kyr.png'));

figure;
ph=pcolor(newdenud_rot_ss5);
hold on;
set(ph,'linestyle','none');
colorbar;
colormap(map);
caxis([denud_min denud_max]);
title('Rotated DENUD Glacial Erosion 5000yr');
saveas(ph,strcat(base_file_name,'_denudglacerosion_rotated5kyr.png'));

figure;
ph=pcolor(newdenud_rot_ss6);
hold on;
set(ph,'linestyle','none');
colorbar;
colormap(map);
caxis([denud_min denud_max]);
title('Rotated DENUD Glacial Erosion 6000yr');
saveas(ph,strcat(base_file_name,'_denudglacerosion_rotated6kyr.png'));

figure;
ph=pcolor(newdenud_rot_ss7);
hold on;
set(ph,'linestyle','none');
colorbar;
colormap(map);
caxis([denud_min denud_max]);
title('Rotated DENUD Glacial Erosion 7000yr');
saveas(ph,strcat(base_file_name,'_denudglacerosion_rotated7kyr.png'));

figure;
ph=pcolor(newdenud_rot_ss8);
hold on;
set(ph,'linestyle','none');
colorbar;
colormap(map);
caxis([denud_min denud_max]);
title('Rotated DENUD Glacial Erosion 8000yr');
```

```
saveas(ph,strcat(base_file_name,'_denudglacerosion_rotated8kyr.png'));

figure;
ph=pcolor(newdenud_rot_ss9);
hold on;
set(ph,'linestyle','none');
colorbar;
colormap(map);
caxis([denud_min denud_max]);
title('Rotated DENUD Glacial Erosion 9000yr');
saveas(ph,strcat(base_file_name,'_denudglacerosion_rotated9kyr.png'));

figure;
ph=pcolor(newdenud_rot_ss10);
hold on;
set(ph,'linestyle','none');
colorbar;
colormap(map);
caxis([denud_min denud_max]);
title('Rotated DENUD Glacial Erosion 10000yr');
saveas(ph,strcat(base_file_name,'_denudglacerosion_rotated10kyr.png'));

%==========
%Trim the rotated figure down
%==========
newdenud_glac_ss1=newdenud_rot_ss1(60:180,60:180);
figure;
ph=pcolor(newdenud_glac_ss1);
hold on;
set(ph,'linestyle','none');
colorbar;
colormap(map);
caxis([denud_min denud_max]);
title('Rotated DENUD Glacial Erosion 2 1000yr');
saveas(ph,strcat(base_file_name,'_denudglacerosion_rotated21kyr.png'));

newdenud_glac_ss2=newdenud_rot_ss2(60:180,60:180);
figure;
ph=pcolor(newdenud_glac_ss2);
hold on;
set(ph,'linestyle','none');
colorbar;
colormap(map);
caxis([denud_min denud_max]);
title('Rotated DENUD Glacial Erosion 2 2000yr');
saveas(ph,strcat(base_file_name,'_denudglacerosion_rotated22kyr.png'));

newdenud_glac_ss3=newdenud_rot_ss3(60:180,60:180);
figure;
ph=pcolor(newdenud_glac_ss3);
hold on;
set(ph,'linestyle','none');
colorbar;
colormap(map);
caxis([denud_min denud_max]);
title('Rotated DENUD Glacial Erosion 2 3000yr');
```

```
saveas(ph,strcat(base_file_name,'_denudglacerosion_rotated23kyr.png'));

newdenud_glac_ss4=newdenud_rot_ss4(60:180,60:180);
figure;
ph=pcolor(newdenud_glac_ss4);
hold on;
set(ph,'linestyle','none');
colorbar;
colormap(map);
caxis([denud_min denud_max]);
title('Rotated DENUD Glacial Erosion 2 4000yr');
saveas(ph,strcat(base_file_name,'_denudglacerosion_rotated24kyr.png'));

newdenud_glac_ss5=newdenud_rot_ss5(60:180,60:180);
figure;
ph=pcolor(newdenud_glac_ss5);
hold on;
set(ph,'linestyle','none');
colorbar;
colormap(map);
caxis([denud_min denud_max]);
title('Rotated DENUD Glacial Erosion 2 5000yr');
saveas(ph,strcat(base_file_name,'_denudglacerosion_rotated25kyr.png'));

newdenud_glac_ss6=newdenud_rot_ss6(60:180,60:180);
figure;
ph=pcolor(newdenud_glac_ss6);
hold on;
set(ph,'linestyle','none');
colorbar;
colormap(map);
caxis([denud_min denud_max]);
title('Rotated DENUD Glacial Erosion 2 6000yr');
saveas(ph,strcat(base_file_name,'_denudglacerosion_rotated26kyr.png'));

newdenud_glac_ss7=newdenud_rot_ss7(60:180,60:180);
figure;
ph=pcolor(newdenud_glac_ss7);
hold on;
set(ph,'linestyle','none');
colorbar;
colormap(map);
caxis([denud_min denud_max]);
title('Rotated DENUD Glacial Erosion 2 7000yr');
saveas(ph,strcat(base_file_name,'_denudglacerosion_rotated27kyr.png'));

newdenud_glac_ss8=newdenud_rot_ss8(60:180,60:180);
figure;
ph=pcolor(newdenud_glac_ss8);
hold on;
set(ph,'linestyle','none');
colorbar;
colormap(map);
caxis([denud_min denud_max]);
title('Rotated DENUD Glacial Erosion 2 8000yr');
saveas(ph,strcat(base_file_name,'_denudglacerosion_rotated28kyr.png'));
```

```
newdenud_glac_ss9=newdenud_rot_ss9(60:180,60:180);
figure;
ph=pcolor(newdenud_glac_ss9);
hold on;
set(ph,'linestyle','none');
colorbar;
colormap(map);
caxis([denud_min denud_max]);
title('Rotated DENUD Glacial Erosion 2 9000yr');
saveas(ph,strcat(base_file_name,'_denudglacerosion_rotated29kyr.png'));

newdenud_glac_ss10=newdenud_rot_ss10(60:180,60:180);
figure;
ph=pcolor(newdenud_glac_ss10);
hold on;
set(ph,'linestyle','none');
colorbar;
colormap(map);
caxis([denud_min denud_max]);
title('Rotated DENUD Glacial Erosion 2 10000yr');
saveas(ph,strcat(base_file_name,'_denudglacerosion_rotated210kyr.png'))
;

new_uplift_trim=new_uplift_rot(60:180,60:180);
figure;
ph=pcolor(new_uplift_trim);
hold on;
set(ph,'linestyle','none');
colorbar;
colormap(map);
caxis([glacerosion_min glacerosion_max]);
title('Rotated Uplift 2');
saveas(ph,strcat(base_file_name,'_uplift_rotated2.png'));

new_contour_uplift_trim=new_contour_uplift_rot(60:180,60:180);
figure;
ph=pcolor(new_contour_uplift_trim);
hold on;
set(ph,'linestyle','none');
colorbar;
colormap(map);
caxis([glacerosion_min glacerosion_max]);
title('Rotated Uplift 2');
saveas(ph,strcat(base_file_name,'_uplift_rotated2.png'));

%Plot the denud as a rate
newdenud_glacrate_ss1=newdenud_rot_ss1(60:180,60:180)*1000/1000;
newdenud_glacrate_ss2=newdenud_rot_ss2(60:180,60:180)*1000/2000;
newdenud_glacrate_ss3=newdenud_rot_ss3(60:180,60:180)*1000/3000;
newdenud_glacrate_ss4=newdenud_rot_ss4(60:180,60:180)*1000/4000;
newdenud_glacrate_ss5=newdenud_rot_ss5(60:180,60:180)*1000/5000;
newdenud_glacrate_ss6=newdenud_rot_ss6(60:180,60:180)*1000/6000;
newdenud_glacrate_ss7=newdenud_rot_ss7(60:180,60:180)*1000/7000;
newdenud_glacrate_ss8=newdenud_rot_ss8(60:180,60:180)*1000/8000;
newdenud_glacrate_ss9=newdenud_rot_ss9(60:180,60:180)*1000/9000;
```

```
newdenud_glacrate_ss10=newdenud_rot_ss10(60:180,60:180)*1000/10000;

rate_min=min(min(newdenud_glacrate_ss10))
rate_max=max(max(newdenud_glacrate_ss10))

figure;
ph=pcolor(newdenud_glacrate_ss1);
hold on;
set(ph,'linestyle','none');
colorbar;
colormap(map);
caxis([rate_min rate_max]);
title('Rotated DENUD Glacial Erosion Rate 2 1000yr');
saveas(ph,strcat(base_file_name,'_denud_rot2rate1kyr.png'));

figure;
ph=pcolor(newdenud_glacrate_ss2);
hold on;
set(ph,'linestyle','none');
colorbar;
colormap(map);
caxis([rate_min rate_max]);
title('Rotated DENUD Glacial Erosion Rate 2 2000yr');
saveas(ph,strcat(base_file_name,'_denud_rot2rate2kyr.png'));

figure;
ph=pcolor(newdenud_glacrate_ss3);
hold on;
set(ph,'linestyle','none');
colorbar;
colormap(map);
caxis([rate_min rate_max]);
title('Rotated DENUD Glacial Erosion 2 Rate 3000yr');
saveas(ph,strcat(base_file_name,'_denud_rot2rate3kyr.png'));

figure;
ph=pcolor(newdenud_glacrate_ss4);
hold on;
set(ph,'linestyle','none');
colorbar;
colormap(map);
caxis([rate_min rate_max]);
title('Rotated DENUD Glacial Erosion Rate 2 4000yr');
saveas(ph,strcat(base_file_name,'_denud_rot2rate4kyr.png'));

figure;
ph=pcolor(newdenud_glacrate_ss5);
hold on;
set(ph,'linestyle','none');
colorbar;
colormap(map);
caxis([rate_min rate_max]);
title('Rotated DENUD Glacial Erosion Rate 2 5000yr');
saveas(ph,strcat(base_file_name,'_denud_rot2rate5kyr.png'));
```

```
figure;
ph=pcolor(newdenud_glacrate_ss6);
hold on;
set(ph,'linestyle','none');
colorbar;
colormap(map);
caxis([rate_min rate_max]);
title('Rotated DENUD Glacial Erosion Rate 2 6000yr');
saveas(ph,strcat(base_file_name,'_denud_rot2rate6kyr.png'));

figure;
ph=pcolor(newdenud_glacrate_ss7);
hold on;
set(ph,'linestyle','none');
colorbar;
colormap(map);
caxis([rate_min rate_max]);
title('Rotated DENUD Glacial Erosion Rate 2 7000yr');
saveas(ph,strcat(base_file_name,'_denud_rot2rate7kyr.png'));

figure;
ph=pcolor(newdenud_glacrate_ss8);
hold on;
set(ph,'linestyle','none');
colorbar;
colormap(map);
caxis([rate_min rate_max]);
title('Rotated DENUD Glacial Erosion Rate 2 8000yr');
saveas(ph,strcat(base_file_name,'_denud_rot2rate8kyr.png'));

figure;
ph=pcolor(newdenud_glacrate_ss9);
hold on;
set(ph,'linestyle','none');
colorbar;
colormap(map);
caxis([rate_min rate_max]);
title('Rotated DENUD Glacial Erosion Rate 2 9000yr');
saveas(ph,strcat(base_file_name,'_denud_rot2rate9kyr.png'));

figure;
ph=pcolor(newdenud_glacrate_ss10);
hold on;
set(ph,'linestyle','none');
colorbar;
colormap(map);
caxis([rate_min rate_max]);
title('Rotated DENUD Glacial Erosion Rate 2 10000yr');
saveas(ph,strcat(base_file_name,'_denud_rotyr.png'));

%=========================================================
%Clean-up
%=========================================================
clear d_temp_ss1 SS_denud1 d_temp_ss2 SS_denud2 d_temp_ss3 SS_denud3
clear d_temp_ss4 SS_denud4 d_temp_ss5 SS_denud5 d_temp_ss6 SS_denud6
clear d_temp_ss7 SS_denud7 d_temp_ss8 SS_denud8 d_temp_ss9 SS_denud9
```

```
clear d_temp_ss10 SS_denud10 b

close all;
end;
```

Timestep_images_part5denudcont.m

```
%File for creating images from long files
%Part 5-denud trimmed

%==========
%Get the names of datasets to process
directory_name=input('Location of data folders: ','s');
base_file_name_list=textread(strcat(directory_name,'/',input('File of
      base names of data to process (batch log file): ','s')),'%s');

%Begin loop to process all files
for entry=1:size(base_file_name_list)

%Get the base file name from the list
base_file_name=strcat(directory_name,'/',base_file_name_list{entry},'/'
      ,base_file_name_list{entry});

%Load the ice locations and topo data, using the base name
ice_loc_temp=load(strcat(base_file_name,'_ice_locations.out'),'-
      ascii');
longerosion_temp=load(strcat(base_file_name,'_long_erosion.out'),'-
      ascii');
longtopo_temp=load(strcat(base_file_name,'_long_topo.out'),'-ascii');
longglac_temp=load(strcat(base_file_name,'_long_glac.out'),'-ascii');
longdenud_temp=load(strcat(base_file_name,'_long_DENUD.out'),'-ascii');
%==========

%=====================================================================
%Plot the total summed columns of denud continued
%==========
%Now look at smaller ranges of erosion
for k=1:120
    newdenud_glac_total_ss1(k)=sum(newdenud_glac_ss1(:,k))/120;
end

for k=1:120
    newdenud_glac_26to90_ss1(k)=sum(newdenud_glac_ss1(26:90,k))/64;
end

for k=1:120
    newdenud_glac_30to83_ss1(k)=sum(newdenud_glac_ss1(30:83,k))/53;
end

for k=1:120
    newdenud_glac_48to59_ss1(k)=sum(newdenud_glac_ss1(48:59,k))/11;
end



for k=1:120
    newdenud_glac_total_ss2(k)=sum(newdenud_glac_ss2(:,k))/120;
end

for k=1:120
    newdenud_glac_26to90_ss2(k)=sum(newdenud_glac_ss2(26:90,k))/64;
```

```
end

for k=1:120
    newdenud_glac_30to83_ss2(k)=sum(newdenud_glac_ss2(30:83,k))/53;
end

for k=1:120
    newdenud_glac_48to59_ss2(k)=sum(newdenud_glac_ss2(48:59,k))/11;
end


for k=1:120
    newdenud_glac_total_ss3(k)=sum(newdenud_glac_ss3(:,k))/120;
end

for k=1:120
    newdenud_glac_26to90_ss3(k)=sum(newdenud_glac_ss3(26:90,k))/64;
end

for k=1:120
    newdenud_glac_30to83_ss3(k)=sum(newdenud_glac_ss3(30:83,k))/53;
end

for k=1:120
    newdenud_glac_48to59_ss3(k)=sum(newdenud_glac_ss3(48:59,k))/11;
end


for k=1:120
    newdenud_glac_total_ss4(k)=sum(newdenud_glac_ss4(:,k))/120;
end

for k=1:120
    newdenud_glac_26to90_ss4(k)=sum(newdenud_glac_ss4(26:90,k))/64;
end

for k=1:120
    newdenud_glac_30to83_ss4(k)=sum(newdenud_glac_ss4(30:83,k))/53;
end

for k=1:120
    newdenud_glac_48to59_ss4(k)=sum(newdenud_glac_ss4(48:59,k))/11;
end


for k=1:120
    newdenud_glac_total_ss5(k)=sum(newdenud_glac_ss5(:,k))/120;
end

for k=1:120
    newdenud_glac_26to90_ss5(k)=sum(newdenud_glac_ss5(26:90,k))/64;
end

for k=1:120
```

```
    newdenud_glac_30to83_ss5(k)=sum(newdenud_glac_ss5(30:83,k))/53;
end

for k=1:120
    newdenud_glac_48to59_ss5(k)=sum(newdenud_glac_ss5(48:59,k))/11;
end


for k=1:120
    newdenud_glac_total_ss6(k)=sum(newdenud_glac_ss6(:,k))/120;
end

for k=1:120
    newdenud_glac_26to90_ss6(k)=sum(newdenud_glac_ss6(26:90,k))/64;
end

for k=1:120
    newdenud_glac_30to83_ss6(k)=sum(newdenud_glac_ss6(30:83,k))/53;
end

for k=1:120
    newdenud_glac_48to59_ss6(k)=sum(newdenud_glac_ss6(48:59,k))/11;
end


for k=1:120
    newdenud_glac_total_ss7(k)=sum(newdenud_glac_ss7(:,k))/120;
end

for k=1:120
    newdenud_glac_26to90_ss7(k)=sum(newdenud_glac_ss7(26:90,k))/64;
end

for k=1:120
    newdenud_glac_30to83_ss7(k)=sum(newdenud_glac_ss7(30:83,k))/53;
end

for k=1:120
    newdenud_glac_48to59_ss7(k)=sum(newdenud_glac_ss7(48:59,k))/11;
end


for k=1:120
    newdenud_glac_total_ss8(k)=sum(newdenud_glac_ss8(:,k))/120;
end

for k=1:120
    newdenud_glac_26to90_ss8(k)=sum(newdenud_glac_ss8(26:90,k))/64;
end

for k=1:120
    newdenud_glac_30to83_ss8(k)=sum(newdenud_glac_ss8(30:83,k))/53;
end
```

```
for k=1:120
    newdenud_glac_48to59_ss8(k)=sum(newdenud_glac_ss8(48:59,k))/11;
end


for k=1:120
    newdenud_glac_total_ss9(k)=sum(newdenud_glac_ss9(:,k))/120;
end

for k=1:120
    newdenud_glac_26to90_ss9(k)=sum(newdenud_glac_ss9(26:90,k))/64;
end

for k=1:120
    newdenud_glac_30to83_ss9(k)=sum(newdenud_glac_ss9(30:83,k))/53;
end

for k=1:120
    newdenud_glac_48to59_ss9(k)=sum(newdenud_glac_ss9(48:59,k))/11;
end


for k=1:120
    newdenud_glac_total_ss10(k)=sum(newdenud_glac_ss10(:,k))/120;
end

for k=1:120
    newdenud_glac_26to90_ss10(k)=sum(newdenud_glac_ss10(26:90,k))/64;
end

for k=1:120
    newdenud_glac_30to83_ss10(k)=sum(newdenud_glac_ss10(30:83,k))/53;
end

for k=1:120
    newdenud_glac_48to59_ss10(k)=sum(newdenud_glac_ss10(48:59,k))/11;
end

%3. Plot the uplift so it matches the erosion from above
%First add up all of the columns to get total amount of erosion along
each column of the matrix
for k=1:120
    new_uplift_total(k)=sum(new_uplift_trim(:,k))/120;
end

for k=1:120
    new_contour_uplift_total(k)=sum(new_contour_uplift_trim(:,k))/120;
end

%Now look at smaller ranges of uplift
for k=1:120
    new_uplift_26to90(k)=sum(new_uplift_trim(26:90,k))/64;
end
```

```
for k=1:120
    new_uplift_30to83(k)=sum(new_uplift_trim(30:83,k))/53;
end

for k=1:120
    new_uplift_48to59(k)=sum(new_uplift_trim(48:59,k))/11;
end


for k=1:120
 new_contour_uplift_26to90(k)=sum(new_contour_uplift_trim(26:90,k))/64;
end

for k=1:120
 new_contour_uplift_30to83(k)=sum(new_contour_uplift_trim(30:83,k))/53;
end

for k=1:120
 new_contour_uplift_48to59(k)=sum(new_contour_uplift_trim(48:59,k))/11;
end

%============================================================
%Clean-up
%============================================================
clear newdenud_rot_ss10 newdenud_rot_ss1 newdenud_rot_ss2
clear newdenud_rot_ss3 newdenud_rot_ss4 newdenud_rot_ss5
clear newdenud_rot_ss6 newdenud_rot_ss7 newdenud_rot_ss8
clear newdenud_rot_ss9 clear newdenud_glac_ss1 newdenud_glac_ss2
clear newdenud_glac_ss3 newdenud_glac_ss4 newdenud_glac_ss5
clear newdenud_glac_ss6 newdenud_glac_ss7 newdenud_glac_ss8
clear newdenud_glac_ss9 newdenud_glac_ss10

close all;
end;
```

Timestep_images_part6xsections.m

```
%File for creating images from long files
%Part 6-Denud as cross-sections against uplift

%==========
%Get the names of datasets to process
directory_name=input('Location of data folders: ','s');
base_file_name_list=textread(strcat(directory_name,'/',input('File of
      base names of data to process (batch log file): ','s')),'%s');

%Begin loop to process all files
for entry=1:size(base_file_name_list)

%Get the base file name from the list
base_file_name=strcat(directory_name,'/',base_file_name_list{entry},'/'
      ,base_file_name_list{entry});

%Load the ice locations and topo data, using the base name
ice_loc_temp=load(strcat(base_file_name,'_ice_locations.out'),'-
      ascii');
longerosion_temp=load(strcat(base_file_name,'_long_erosion.out'),'-
      ascii');
longtopo_temp=load(strcat(base_file_name,'_long_topo.out'),'-ascii');
longglac_temp=load(strcat(base_file_name,'_long_glac.out'),'-ascii');
longdenud_temp=load(strcat(base_file_name,'_long_DENUD.out'),'-ascii');
%==========

%=====================================================
%Plot lines for where transects are for each of the smaller ranges of
%erosion/uplift on figures for reference
%=====================================================
figure;
ph=pcolor(newdenud_rot_ss10);
hold on;
set(ph,'linestyle','none');
colorbar;
title('Location of Transects of the Glacial Erosion');
plot(1:217,85,'-r.');
plot(1:217,145,'-r.');
plot(1:217,105,'-y.');
plot(1:217,120,'-y.');
saveas(ph,strcat(base_file_name,'_glaceros_transectlocat_large.png'));

figure;
ph=pcolor(newdenud_glac_ss10);
hold on;
set(ph,'linestyle','none');
colorbar;
title('Location of Transects of the Glacial Erosion');
plot(1:120,30,'-r.');
plot(1:120,83,'-r.');
plot(1:120,26,'-g.');
plot(1:120,90,'-g.');
plot(1:120,48,'-y.');
plot(1:120,59,'-y.');
```

```
saveas(ph,strcat(base_file_name,'_glacero_transectlocat_small.png'));

%============================================================
%Plot A-A' line on the glacial erosion with Mt. Olympus marked by white
%star
%============================================================
figure;
ph=pcolor(newdenud_rot_ss10);
hold on;
set(ph,'linestyle','none');
colorbar;
plot(1:217,122,'-r.');
plot(112,122,'w*');
title('Location of Uplift Line from Brandon and Bull with Mt. Olympus
      marked by white star');
saveas(ph,strcat(base_file_name,'_glacerosion_lineforAtoAprm.png'));

%============================================================
%Plot Uplift and glacial erosion together
%==========
figure;
ph=plot(1:k,(newdenud_glac_26to90_ss1)*1000/1000);
hold on;
plot(1:k,(new_uplift_26to90),'g-');
title('Uplift and DENUD Glacial Erosion from 26 to 90 1000yr');
xlabel('Horizontal Distance');
ylabel('Average Uplift or Erosion Rate (mm/yr)');
saveas(ph,strcat(base_file_name,'_upliftdenudglacerosion_26to901kyr.png
      '));

figure;
ph=plot(1:k,(newdenud_glac_30to83_ss1)*1000/1000);
hold on;
plot(1:k,(new_uplift_30to83),'g-');
title('Uplift and DENUD Glacial Erosion from 30 to 83 1000yr');
xlabel('Horizontal Distance');
ylabel('Average Uplift or Erosion Rate (mm/yr)');
saveas(ph,strcat(base_file_name,'_upliftdenudglacerosion_30to831kyr.png
      '));

figure;
ph=plot(1:k,(newdenud_glac_48to59_ss1)*1000/1000);
hold on;
plot(1:k,(new_uplift_48to59),'g-');
title('Uplift and DENUD Glacial Erosion from 48 to 59 1000yr');
xlabel('Horizontal Distance');
ylabel('Average Uplift or Erosion Rate (mm/yr)');
saveas(ph,strcat(base_file_name,'_upliftdenudglacerosion_48to591kyr.png
      '));

figure;
ph=plot(1:k,(newdenud_glac_total_ss1)*1000/1000);
hold on;
plot(1:k,(new_uplift_total),'g-');
title('Uplift and DENUD Glacial Erosion from 60 to 180 (total)
1000yr');
```

```
xlabel('Horizontal Distance');
ylabel('AAverage Uplift or Erosion Rate (mm/yr)');
saveas(ph,strcat(base_file_name,'_upliftdenudglacerosion_60to180total1k
      yr.png'));


figure;
ph=plot(1:k,(newdenud_glac_26to90_ss2)*1000/2000);
hold on;
plot(1:k,(new_uplift_26to90),'g-');
title('Uplift and DENUD Glacial Erosion from 26 to 90 2000yr');
xlabel('Horizontal Distance');
ylabel('Average Uplift or Erosion Rate (mm/yr)');
saveas(ph,strcat(base_file_name,'_upliftdenudglacerosion_26to902kyr.png
      '));

figure;
ph=plot(1:k,(newdenud_glac_30to83_ss2)*1000/2000);
hold on;
plot(1:k,(new_uplift_30to83),'g-');
title('Uplift and DENUD Glacial Erosion from 30 to 83 2000yr');
xlabel('Horizontal Distance');
ylabel('Average Uplift or Erosion Rate (mm/yr)');
saveas(ph,strcat(base_file_name,'_upliftdenudglacerosion_30to832kyr.png
      '));

figure;
ph=plot(1:k,(newdenud_glac_48to59_ss2)*1000/2000);
hold on;
plot(1:k,(new_uplift_48to59),'g-');
title('Uplift and DENUD Glacial Erosion from 48 to 59 2000yr');
xlabel('Horizontal Distance');
ylabel('Average Uplift or Erosion Rate (mm/yr)');
saveas(ph,strcat(base_file_name,'_upliftdenudglacerosion_48to592kyr.png
      '));

figure;
ph=plot(1:k,(newdenud_glac_total_ss2)*1000/2000);
hold on;
plot(1:k,(new_uplift_total),'g-');
title('Uplift and DENUD Glacial Erosion from 60 to 180 (total)
2000yr');
xlabel('Horizontal Distance');
ylabel('AAverage Uplift or Erosion Rate (mm/yr)');
saveas(ph,strcat(base_file_name,'_upliftdenudglacerosion_60to180total2k
      yr.png'));


figure;
ph=plot(1:k,(newdenud_glac_26to90_ss3)*1000/3000);
hold on;
plot(1:k,(new_uplift_26to90),'g-');
title('Uplift and DENUD Glacial Erosion from 26 to 90 3000yr');
xlabel('Horizontal Distance');
ylabel('Average Uplift or Erosion Rate (mm/yr)');
```

```
saveas(ph,strcat(base_file_name,'_upliftdenudglacerosion_26to903kyr.png
      '));

figure;
ph=plot(1:k,(newdenud_glac_30to83_ss3)*1000/3000);
hold on;
plot(1:k,(new_uplift_30to83),'g-');
title('Uplift and DENUD Glacial Erosion from 30 to 83 3000yr');
xlabel('Horizontal Distance');
ylabel('Average Uplift or Erosion Rate (mm/yr)');
saveas(ph,strcat(base_file_name,'_upliftdenudglacerosion_30to833kyr.png
      '));

figure;
ph=plot(1:k,(newdenud_glac_48to59_ss3)*1000/3000);
hold on;
plot(1:k,(new_uplift_48to59),'g-');
title('Uplift and DENUD Glacial Erosion from 48 to 59 3000yr');
xlabel('Horizontal Distance');
ylabel('Average Uplift or Erosion Rate (mm/yr)');
saveas(ph,strcat(base_file_name,'_upliftdenudglacerosion_48to593kyr.png
      '));

figure;
ph=plot(1:k,(newdenud_glac_total_ss3)*1000/3000);
hold on;
plot(1:k,(new_uplift_total),'g-');
title('Uplift and DENUD Glacial Erosion from 60 to 180 (total)
3000yr');
xlabel('Horizontal Distance');
ylabel('AAverage Uplift or Erosion Rate (mm/yr)');
saveas(ph,strcat(base_file_name,'_upliftdenudglacerosion_60to180total3k
     yr.png'));


figure;
ph=plot(1:k,(newdenud_glac_26to90_ss4)*1000/4000);
hold on;
plot(1:k,(new_uplift_26to90),'g-');
title('Uplift and DENUD Glacial Erosion from 26 to 90 4000yr');
xlabel('Horizontal Distance');
ylabel('Average Uplift or Erosion Rate (mm/yr)');
saveas(ph,strcat(base_file_name,'_upliftdenudglacerosion_26to904kyr.png
      '));

figure;
ph=plot(1:k,(newdenud_glac_30to83_ss4)*1000/4000);
hold on;
plot(1:k,(new_uplift_30to83),'g-');
title('Uplift and DENUD Glacial Erosion from 30 to 83 4000yr');
xlabel('Horizontal Distance');
ylabel('Average Uplift or Erosion Rate (mm/yr)');
saveas(ph,strcat(base_file_name,'_upliftdenudglacerosion_30to834kyr.png
      '));
```

```
figure;
ph=plot(1:k,(newdenud_glac_48to59_ss4)*1000/4000);
hold on;
plot(1:k,(new_uplift_48to59),'g-');
title('Uplift and DENUD Glacial Erosion from 48 to 59 4000yr');
xlabel('Horizontal Distance');
ylabel('Average Uplift or Erosion Rate (mm/yr)');
saveas(ph,strcat(base_file_name,'_upliftdenudglacerosion_48to594kyr.png
      '));

figure;
ph=plot(1:k,(newdenud_glac_total_ss4)*1000/4000);
hold on;
plot(1:k,(new_uplift_total),'g-');
title('Uplift and DENUD Glacial Erosion from 60 to 180 (total)
4000yr');
xlabel('Horizontal Distance');
ylabel('AAverage Uplift or Erosion Rate (mm/yr)');
saveas(ph,strcat(base_file_name,'_upliftdenudglacerosion_60to180total4k
      yr.png'));


figure;
ph=plot(1:k,(newdenud_glac_26to90_ss5)*1000/5000);
hold on;
plot(1:k,(new_uplift_26to90),'g-');
title('Uplift and DENUD Glacial Erosion from 26 to 90 5000yr');
xlabel('Horizontal Distance');
ylabel('Average Uplift or Erosion Rate (mm/yr)');
saveas(ph,strcat(base_file_name,'_upliftdenudglacerosion_26to905kyr.png
      '));

figure;
ph=plot(1:k,(newdenud_glac_30to83_ss5)*1000/5000);
hold on;
plot(1:k,(new_uplift_30to83),'g-');
title('Uplift and DENUD Glacial Erosion from 30 to 83 5000yr');
xlabel('Horizontal Distance');
ylabel('Average Uplift or Erosion Rate (mm/yr)');
saveas(ph,strcat(base_file_name,'_upliftdenudglacerosion_30to835kyr.png
      '));

figure;
ph=plot(1:k,(newdenud_glac_48to59_ss5)*1000/5000);
hold on;
plot(1:k,(new_uplift_48to59),'g-');
title('Uplift and DENUD Glacial Erosion from 48 to 59 5000yr');
xlabel('Horizontal Distance');
ylabel('Average Uplift or Erosion Rate (mm/yr)');
saveas(ph,strcat(base_file_name,'_upliftdenudglacerosion_48to595kyr.png
      '));

figure;
ph=plot(1:k,(newdenud_glac_total_ss5)*1000/5000);
hold on;
plot(1:k,(new_uplift_total),'g-');
```

```
title('Uplift and DENUD Glacial Erosion from 60 to 180 (total)
5000yr');
xlabel('Horizontal Distance');
ylabel('AAverage Uplift or Erosion Rate (mm/yr)');
saveas(ph,strcat(base_file_name,'_upliftdenudglacerosion_60to180total5k
      yr.png'));


figure;
ph=plot(1:k,(newdenud_glac_26to90_ss6)*1000/6000);
hold on;
plot(1:k,(new_uplift_26to90),'g-');
title('Uplift and DENUD Glacial Erosion from 26 to 90 6000yr');
xlabel('Horizontal Distance');
ylabel('Average Uplift or Erosion Rate (mm/yr)');
saveas(ph,strcat(base_file_name,'_upliftdenudglacerosion_26to906kyr.png
      '));

figure;
ph=plot(1:k,(newdenud_glac_30to83_ss6)*1000/6000);
hold on;
plot(1:k,(new_uplift_30to83),'g-');
title('Uplift and DENUD Glacial Erosion from 30 to 83 6000yr');
xlabel('Horizontal Distance');
ylabel('Average Uplift or Erosion Rate (mm/yr)');
saveas(ph,strcat(base_file_name,'_upliftdenudglacerosion_30to836kyr.png
      '));

figure;
ph=plot(1:k,(newdenud_glac_48to59_ss6)*1000/6000);
hold on;
plot(1:k,(new_uplift_48to59),'g-');
title('Uplift and DENUD Glacial Erosion from 48 to 59 6000yr');
xlabel('Horizontal Distance');
ylabel('Average Uplift or Erosion Rate (mm/yr)');
saveas(ph,strcat(base_file_name,'_upliftdenudglacerosion_48to596kyr.png
      '));

figure;
ph=plot(1:k,(newdenud_glac_total_ss6)*1000/6000);
hold on;
plot(1:k,(new_uplift_total),'g-');
title('Uplift and DENUD Glacial Erosion from 60 to 180 (total)
      6000yr');
xlabel('Horizontal Distance');
ylabel('AAverage Uplift or Erosion Rate (mm/yr)');
saveas(ph,strcat(base_file_name,'_upliftdenudglacerosion_60to180total6k
      yr.png'));


figure;
ph=plot(1:k,(newdenud_glac_26to90_ss7)*1000/7000);
hold on;
plot(1:k,(new_uplift_26to90),'g-');
title('Uplift and DENUD Glacial Erosion from 26 to 90 7000yr');
```

```
xlabel('Horizontal Distance');
ylabel('Average Uplift or Erosion Rate (mm/yr)');
saveas(ph,strcat(base_file_name,'_upliftdenudglacerosion_26to907kyr.png
      '));

figure;
ph=plot(1:k,(newdenud_glac_30to83_ss7)*1000/7000);
hold on;
plot(1:k,(new_uplift_30to83),'g-');
title('Uplift and DENUD Glacial Erosion from 30 to 83 7000yr');
xlabel('Horizontal Distance');
ylabel('Average Uplift or Erosion Rate (mm/yr)');
saveas(ph,strcat(base_file_name,'_upliftdenudglacerosion_30to837kyr.png
      '));

figure;
ph=plot(1:k,(newdenud_glac_48to59_ss7)*1000/7000);
hold on;
plot(1:k,(new_uplift_48to59),'g-');
title('Uplift and DENUD Glacial Erosion from 48 to 59 7000yr');
xlabel('Horizontal Distance');
ylabel('Average Uplift or Erosion Rate (mm/yr)');
saveas(ph,strcat(base_file_name,'_upliftdenudglacerosion_48to597kyr.png
      '));

figure;
ph=plot(1:k,(newdenud_glac_total_ss7)*1000/7000);
hold on;
plot(1:k,(new_uplift_total),'g-');
title('Uplift and DENUD Glacial Erosion from 60 to 180 (total)
7000yr');
xlabel('Horizontal Distance');
ylabel('AAverage Uplift or Erosion Rate (mm/yr)');
saveas(ph,strcat(base_file_name,'_upliftdenudglacerosion_60to180total7k
     yr.png'));


figure;
ph=plot(1:k,(newdenud_glac_26to90_ss8)*1000/8000);
hold on;
plot(1:k,(new_uplift_26to90),'g-');
title('Uplift and DENUD Glacial Erosion from 26 to 90 8000yr');
xlabel('Horizontal Distance');
ylabel('Average Uplift or Erosion Rate (mm/yr)');
saveas(ph,strcat(base_file_name,'_upliftdenudglacerosion_26to908kyr.png
      '));

figure;
ph=plot(1:k,(newdenud_glac_30to83_ss8)*1000/8000);
hold on;
plot(1:k,(new_uplift_30to83),'g-');
title('Uplift and DENUD Glacial Erosion from 30 to 83 8000yr');
xlabel('Horizontal Distance');
ylabel('Average Uplift or Erosion Rate (mm/yr)');
saveas(ph,strcat(base_file_name,'_upliftdenudglacerosion_30to838kyr.png
      '));
```

```
figure;
ph=plot(1:k,(newdenud_glac_48to59_ss8)*1000/8000);
hold on;
plot(1:k,(new_uplift_48to59),'g-');
title('Uplift and DENUD Glacial Erosion from 48 to 59 8000yr');
xlabel('Horizontal Distance');
ylabel('Average Uplift or Erosion Rate (mm/yr)');
saveas(ph,strcat(base_file_name,'_upliftdenudglacerosion_48to598kyr.png
      '));

figure;
ph=plot(1:k,(newdenud_glac_total_ss8)*1000/8000);
hold on;
plot(1:k,(new_uplift_total),'g-');
title('Uplift and DENUD Glacial Erosion from 60 to 180 (total)
8000yr');
xlabel('Horizontal Distance');
ylabel('AAverage Uplift or Erosion Rate (mm/yr)');
saveas(ph,strcat(base_file_name,'_upliftdenudglacerosion_60to180total8k
      yr.png'));


figure;
ph=plot(1:k,(newdenud_glac_26to90_ss9)*1000/9000);
hold on;
plot(1:k,(new_uplift_26to90),'g-');
title('Uplift and DENUD Glacial Erosion from 26 to 90 9000yr');
xlabel('Horizontal Distance');
ylabel('Average Uplift or Erosion Rate (mm/yr)');
saveas(ph,strcat(base_file_name,'_upliftdenudglacerosion_26to909kyr.png
      '));

figure;
ph=plot(1:k,(newdenud_glac_30to83_ss9)*1000/9000);
hold on;
plot(1:k,(new_uplift_30to83),'g-');
title('Uplift and DENUD Glacial Erosion from 30 to 83 9000yr');
xlabel('Horizontal Distance');
ylabel('Average Uplift or Erosion Rate (mm/yr)');
saveas(ph,strcat(base_file_name,'_upliftdenudglacerosion_30to839kyr.png
      '));

figure;
ph=plot(1:k,(newdenud_glac_48to59_ss9)*1000/9000);
hold on;
plot(1:k,(new_uplift_48to59),'g-');
title('Uplift and DENUD Glacial Erosion from 48 to 59 9000yr');
xlabel('Horizontal Distance');
ylabel('Average Uplift or Erosion Rate (mm/yr)');
saveas(ph,strcat(base_file_name,'_upliftdenudglacerosion_48to599kyr.png
      '));

figure;
ph=plot(1:k,(newdenud_glac_total_ss9)*1000/9000);
```

```
hold on;
plot(1:k,(new_uplift_total),'g-');
title('Uplift and DENUD Glacial Erosion from 60 to 180 (total)
      9000yr');
xlabel('Horizontal Distance');
ylabel('AAverage Uplift or Erosion Rate (mm/yr)');
saveas(ph,strcat(base_file_name,'_upliftdenudglacerosion_60to180total9k
      yr.png'));


figure;
ph=plot(1:k,(newdenud_glac_26to90_ss10)*1000/10000);
hold on;
plot(1:k,(new_uplift_26to90),'g-');
title('Uplift and DENUD Glacial Erosion from 26 to 90 10000yr');
xlabel('Horizontal Distance');
ylabel('Average Uplift or Erosion Rate (mm/yr)');
saveas(ph,strcat(base_file_name,'_upliftdenudglacerosion_26to9010kyr.pn
      g'));

figure;
ph=plot(1:k,(newdenud_glac_30to83_ss10)*1000/10000);
hold on;
plot(1:k,(new_uplift_30to83),'g-');
title('Uplift and DENUD Glacial Erosion from 30 to 83 10000yr');
xlabel('Horizontal Distance');
ylabel('Average Uplift or Erosion Rate (mm/yr)');
saveas(ph,strcat(base_file_name,'_upliftdenudglacerosion_30to8310kyr.pn
      g'));

figure;
ph=plot(1:k,(newdenud_glac_48to59_ss10)*1000/10000);
hold on;
plot(1:k,(new_uplift_48to59),'g-');
title('Uplift and DENUD Glacial Erosion from 48 to 59 10000yr');
xlabel('Horizontal Distance');
ylabel('Average Uplift or Erosion Rate (mm/yr)');
saveas(ph,strcat(base_file_name,'_upliftdenudglacerosion_48to5910kyr.pn
      g'));

figure;
ph=plot(1:k,(newdenud_glac_total_ss10)*1000/10000);
hold on;
plot(1:k,(new_uplift_total),'g-');
title('Uplift and DENUD Glacial Erosion from 60 to 180 (total)
      10000yr');
xlabel('Horizontal Distance');
ylabel('Average Uplift or Erosion Rate (mm/yr)');
saveas(ph,strcat(base_file_name,'_upliftdenudglacerosion_60to180total10
      kyr.png'));

%=========================================================
%Clean-up
%=========================================================
clear newdenud_glac_total_ss1 newdenud_glac_total_ss2
clear newdenud_glac_total_ss3 newdenud_glac_total_ss4
```

```
clear newdenud_glac_total_ss5 newdenud_glac_total_ss6
clear newdenud_glac_total_ss7 newdenud_glac_total_ss8
clear newdenud_glac_total_ss0 newdenud_glac_total_ss10
clear newdenud_glac_26to90_ss1 newdenud_glac_26to90_ss2
clear newdenud_glac_26to90_ss3 newdenud_glac_26to90_ss4
clear newdenud_glac_26to90_ss5 newdenud_glac_26to90_ss6
clear newdenud_glac_26to90_ss7 newdenud_glac_26to90_ss8
clear newdenud_glac_26to90_ss9 newdenud_glac_26to90_ss10
clear newdenud_glac_30to83_ss1 newdenud_glac_30to83_ss2
clear newdenud_glac_30to83_ss3 newdenud_glac_30to83_ss4
clear newdenud_glac_30to83_ss5 newdenud_glac_30to83_ss6
clear newdenud_glac_30to83_ss7 newdenud_glac_30to83_ss8
clear newdenud_glac_30to83_ss9 newdenud_glac_30to83_ss10
clear newdenud_glac_48to59_ss1 newdenud_glac_48to59_ss2
clear newdenud_glac_48to59_ss3 newdenud_glac_48to59_ss4
clear newdenud_glac_48to59_ss5 newdenud_glac_48to59_ss6
clear newdenud_glac_48to59_ss7 newdenud_glac_48to59_ss8
clear newdenud_glac_48to59_ss9 newdenud_glac_48to59_ss10
clear X Y THETA R angle THETA_ROT X_ROT Y_ROT bigx bigy smx smy XI YI

close all;
end;
```

Timestep_images_part7newdenudstuff.m

```
%File for creating images from long files
%Part 6-Denud as cross-sections against uplift

%==========
%Get the names of datasets to process
directory_name=input('Location of data folders: ','s');
base_file_name_list=textread(strcat(directory_name,'/',input('File of
      base names of data to process (batch log file): ','s')),'%s');

%Begin loop to process all files
for entry=1:size(base_file_name_list)

%Get the base file name from the list
base_file_name=strcat(directory_name,'/',base_file_name_list{entry},'/'
      ,base_file_name_list{entry});
%==========

%=================================================================
%Create columns of denud erosion for each valley and a smaller total
%==========
for k=1:120
   newdenud_glac_10to97total_ss1(k)=sum(newdenud_glac_ss1(10:97,k))/87;
end

for k=1:120
    newdenud_glac_66to83hoh_ss1(k)=sum(newdenud_glac_ss1(66:83,k))/17;
end

for k=1:120
  newdenud_glac_48to59queets_ss1(k)=sum(newdenud_glac_ss1(48:59,k))/11;
end

for k=1:120
 newdenud_glac_31to40quinault_ss1(k)=sum(newdenud_glac_ss1(31:40,k))/9;
end



for k=1:120
   newdenud_glac_10to97total_ss2(k)=sum(newdenud_glac_ss2(10:97,k))/87;
end

for k=1:120
    newdenud_glac_66to83hoh_ss2(k)=sum(newdenud_glac_ss2(66:83,k))/17;
end

for k=1:120
  newdenud_glac_48to59queets_ss2(k)=sum(newdenud_glac_ss2(48:59,k))/11;
end

for k=1:120
 newdenud_glac_31to40quinault_ss2(k)=sum(newdenud_glac_ss2(31:40,k))/9;
end
```

```
for k=1:120
   newdenud_glac_10to97total_ss3(k)=sum(newdenud_glac_ss3(10:97,k))/87;
end

for k=1:120
    newdenud_glac_66to83hoh_ss3(k)=sum(newdenud_glac_ss3(66:83,k))/17;
end

for k=1:120
  newdenud_glac_48to59queets_ss3(k)=sum(newdenud_glac_ss3(48:59,k))/11;
end

for k=1:120
 newdenud_glac_31to40quinault_ss3(k)=sum(newdenud_glac_ss3(31:40,k))/9;
end


for k=1:120
   newdenud_glac_10to97total_ss4(k)=sum(newdenud_glac_ss4(10:97,k))/87;
end

for k=1:120
    newdenud_glac_66to83hoh_ss4(k)=sum(newdenud_glac_ss4(66:83,k))/17;
end

for k=1:120
  newdenud_glac_48to59queets_ss4(k)=sum(newdenud_glac_ss4(48:59,k))/11;
end

for k=1:120
 newdenud_glac_31to40quinault_ss4(k)=sum(newdenud_glac_ss4(31:40,k))/9;
end


for k=1:120
   newdenud_glac_10to97total_ss5(k)=sum(newdenud_glac_ss5(10:97,k))/87;
end

for k=1:120
    newdenud_glac_66to83hoh_ss5(k)=sum(newdenud_glac_ss5(66:83,k))/17;
end

for k=1:120
  newdenud_glac_48to59queets_ss5(k)=sum(newdenud_glac_ss5(48:59,k))/11;
end

for k=1:120
 newdenud_glac_31to40quinault_ss5(k)=sum(newdenud_glac_ss5(31:40,k))/9;
end


for k=1:120
   newdenud_glac_10to97total_ss6(k)=sum(newdenud_glac_ss6(10:97,k))/87;
```

```
end

for k=1:120
    newdenud_glac_66to83hoh_ss6(k)=sum(newdenud_glac_ss6(66:83,k))/17;
end

for k=1:120
  newdenud_glac_48to59queets_ss6(k)=sum(newdenud_glac_ss6(48:59,k))/11;
end

for k=1:120
 newdenud_glac_31to40quinault_ss6(k)=sum(newdenud_glac_ss6(31:40,k))/9;
end


for k=1:120
   newdenud_glac_10to97total_ss7(k)=sum(newdenud_glac_ss7(10:97,k))/87;
end

for k=1:120
    newdenud_glac_66to83hoh_ss7(k)=sum(newdenud_glac_ss7(66:83,k))/17;
end

for k=1:120
  newdenud_glac_48to59queets_ss7(k)=sum(newdenud_glac_ss7(48:59,k))/11;
end

for k=1:120
 newdenud_glac_31to40quinault_ss7(k)=sum(newdenud_glac_ss7(31:40,k))/9;
end


for k=1:120
   newdenud_glac_10to97total_ss8(k)=sum(newdenud_glac_ss8(10:97,k))/87;
end

for k=1:120
    newdenud_glac_66to83hoh_ss8(k)=sum(newdenud_glac_ss8(66:83,k))/17;
end

for k=1:120
  newdenud_glac_48to59queets_ss8(k)=sum(newdenud_glac_ss8(48:59,k))/11;
end

for k=1:120
 newdenud_glac_31to40quinault_ss8(k)=sum(newdenud_glac_ss8(31:40,k))/9;
end


for k=1:120
   newdenud_glac_10to97total_ss9(k)=sum(newdenud_glac_ss9(10:97,k))/87;
end

for k=1:120
```

```
    newdenud_glac_66to83hoh_ss9(k)=sum(newdenud_glac_ss9(66:83,k))/17;
end

for k=1:120
  newdenud_glac_48to59queets_ss9(k)=sum(newdenud_glac_ss9(48:59,k))/11;
end

for k=1:120
 newdenud_glac_31to40quinault_ss9(k)=sum(newdenud_glac_ss9(31:40,k))/9;
end


for k=1:120
 newdenud_glac_10to97total_ss10(k)=sum(newdenud_glac_ss10(10:97,k))/87;
end

for k=1:120
   newdenud_glac_66to83hoh_ss10(k)=sum(newdenud_glac_ss10(66:83,k))/17;
end

for k=1:120
newdenud_glac_48to59queets_ss10(k)=sum(newdenud_glac_ss10(48:59,k))/11;
end

for k=1:120
newdenud_glac_31to40quinault_ss10(k)=sum(newdenud_glac_ss10(31:40,k))/9
;
end

%Create uplift this way too
for k=1:120
    new_uplift_66to83hoh(k)=sum(new_uplift_trim(66:83,k))/17;
end

for k=1:120
    new_uplift_10to97total(k)=sum(new_uplift_trim(10:97,k))/87;
end


for k=1:120
new_contour_uplift_66to83hoh(k)=sum(new_contour_uplift_trim(66:83,k))/1
7;
end

for k=1:120
new_contour_uplift_10to97total(k)=sum(new_contour_uplift_trim(10:97,k))
/87;
end

%=====================================================
%Plot lines for where transects are for each of the smaller ranges of
%erosion/uplift on figures for reference
%=====================================================
figure;
```

```
ph=pcolor(newdenud_glac_ss10);
hold on;
set(ph,'linestyle','none');
colorbar;
title('Location of Transects of the Glacial Erosion');
plot(1:120,10,'-r.');
plot(1:120,97,'-r.');
plot(1:120,66,'-g.');
plot(1:120,83,'-g.');
plot(1:120,48,'-m.');
plot(1:120,59,'-m.');
plot(1:120,31,'-c.');
plot(1:120,40,'-c.');
saveas(ph,strcat(base_file_name,'_glacero_transectlocat_smallvalleys.pn
      g'));

%==========
%Determine the max an min values for each valley
%==========
denudtotal_min=min(min(newdenud_glac_10to97total_ss10))
denudtotal_max=max(max(newdenud_glac_10to97total_ss10))

denudhoh_min=min(min(newdenud_glac_66to83hoh_ss10))
denudhoh_max=max(max(newdenud_glac_66to83hoh_ss10))

denudqueets_min=min(min(newdenud_glac_48to59queets_ss10))
denudqueets_max=max(max(newdenud_glac_48to59queets_ss10))

denudquinault_min=min(min(newdenud_glac_31to40quinault_ss10))
denudquinault_max=max(max(newdenud_glac_31to40quinault_ss10))

%=========================================================
%Clean-up
%=========================================================
close all;
end;
```

Timestep_images_part8newdenud2.m

```
%File for creating images from long files
%Part 8-Denud as cross-sections against uplift, but for valleys

%==========
%Get the names of datasets to process
directory_name=input('Location of data folders: ','s');
base_file_name_list=textread(strcat(directory_name,'/',input('File of
      base names of data to process (batch log file): ','s')),'%s');

%Begin loop to process all files
for entry=1:size(base_file_name_list)

%Get the base file name from the list
base_file_name=strcat(directory_name,'/',base_file_name_list{entry},'/'
      ,base_file_name_list{entry});

%============================================================
%Plot Uplift and glacial erosion together
%============================================================
%==========
%Plot the denud erosion in the Hoh Valley with uplift
%==========
figure;
ph=plot(((newdenud_glac_66to83hoh_ss1(:,1:65))*1000/1000),'g-');
hold on;
plot((new_uplift_66to83hoh(:,1:65)),'b-');
plot(x1_new,y1,'b--');
title('Uplift and DENUD Glacial Erosion in Hoh 1000yr');
xlabel('Horizontal Distance');
ylabel('Average Uplift or Erosion Rate (mm/yr)');
legend('Hoh','Uplift','Uplift from Brandon et
      al.','Location','NorthWest');
legend('boxoff');
saveas(ph,strcat(base_file_name,'_denuduplift_hoh1kyr.png'));

figure;
ph=plot(((newdenud_glac_66to83hoh_ss2(:,1:65))*1000/2000),'g-');
hold on;
plot((new_uplift_66to83hoh(:,1:65)),'b-');
plot(x1_new,y1,'b--');
title('Uplift and DENUD Glacial Erosion in Hoh 2000yr');
label('Horizontal Distance');
ylabel('Average Uplift or Erosion Rate (mm/yr)');
legend('Hoh','Uplift','Uplift from Brandon et
      al.','Location','NorthWest');
legend('boxoff');
saveas(ph,strcat(base_file_name,'_denuduplift_hoh2kyr.png'));

figure;
ph=plot(((newdenud_glac_66to83hoh_ss3(:,1:65))*1000/3000),'g-');
hold on;
plot((new_uplift_66to83hoh(:,1:65)),'b-');
plot(x1_new,y1,'b--');
title('Uplift and DENUD Glacial Erosion in Hoh 3000yr');
```

```
xlabel('Horizontal Distance');
ylabel('Average Uplift or Erosion Rate (mm/yr)');
legend('Hoh','Uplift','Uplift from Brandon et
      al.','Location','NorthWest');
legend('boxoff');
saveas(ph,strcat(base_file_name,'_denuduplift_hoh3kyr.png'));

figure;
ph=plot(((newdenud_glac_66to83hoh_ss4(:,1:65))*1000/4000),'g-');
hold on;
plot((new_uplift_66to83hoh(:,1:65)),'b-');
plot(x1_new,y1,'b--');
title('Uplift and DENUD Glacial Erosion in Hoh 4000yr');
xlabel('Horizontal Distance');
ylabel('Average Uplift or Erosion Rate (mm/yr)');
legend('Hoh','Uplift','Uplift from Brandon et
      al.','Location','NorthWest');
legend('boxoff');
saveas(ph,strcat(base_file_name,'_denuduplift_hoh4kyr.png'));

figure;
ph=plot(((newdenud_glac_66to83hoh_ss5(:,1:65))*1000/5000),'g-');
hold on;
plot((new_uplift_66to83hoh(:,1:65)),'b-');
plot(x1_new,y1,'b--');
title('Uplift and DENUD Glacial Erosion in Hoh 5000yr');
xlabel('Horizontal Distance');
ylabel('Average Uplift or Erosion Rate (mm/yr)');
legend('Hoh','Uplift','Uplift from Brandon et
      al.','Location','NorthWest');
legend('boxoff');
saveas(ph,strcat(base_file_name,'_denuduplift_hoh5kyr.png'));

figure;
ph=plot(((newdenud_glac_66to83hoh_ss6(:,1:65))*1000/6000),'g-');
hold on;
plot((new_uplift_66to83hoh(:,1:65)),'b-');
plot(x1_new,y1,'b--');
title('Uplift and DENUD Glacial Erosion in Hoh 6000yr');
xlabel('Horizontal Distance');
ylabel('Average Uplift or Erosion Rate (mm/yr)');
legend('Hoh','Uplift','Uplift from Brandon et
      al.','Location','NorthWest');
legend('boxoff');
saveas(ph,strcat(base_file_name,'_denuduplift_hoh6kyr.png'));

figure;
ph=plot(((newdenud_glac_66to83hoh_ss7(:,1:65))*1000/7000),'g-');
hold on;
plot((new_uplift_66to83hoh(:,1:65)),'b-');
plot(x1_new,y1,'b--');
title('Uplift and DENUD Glacial Erosion in Hoh 7000yr');
xlabel('Horizontal Distance');
ylabel('Average Uplift or Erosion Rate (mm/yr)');
legend('Hoh','Uplift','Uplift from Brandon et
      al.','Location','NorthWest');
```

```
legend('boxoff');
saveas(ph,strcat(base_file_name,'_denuduplift_hoh7kyr.png'));

figure;
ph=plot(((newdenud_glac_66to83hoh_ss8(:,1:65))*1000/8000),'g-');
hold on;
plot((new_uplift_66to83hoh(:,1:65)),'b-');
plot(x1_new,y1,'b--');
title('Uplift and DENUD Glacial Erosion in Hoh 8000yr');
xlabel('Horizontal Distance');
ylabel('Average Uplift or Erosion Rate (mm/yr)');
legend('Hoh','Uplift','Uplift from Brandon et
      al.','Location','NorthWest');
legend('boxoff');
saveas(ph,strcat(base_file_name,'_denuduplift_hoh8kyr.png'));

figure;
ph=plot(((newdenud_glac_66to83hoh_ss9(:,1:65))*1000/9000),'g-');
hold on;
plot((new_uplift_66to83hoh(:,1:65)),'b-');
plot(x1_new,y1,'b--');
title('Uplift and DENUD Glacial Erosion in Hoh 9000yr');
xlabel('Horizontal Distance');
ylabel('Average Uplift or Erosion Rate (mm/yr)');
legend('Hoh','Uplift','Uplift from Brandon et
      al.','Location','NorthWest');
legend('boxoff');
saveas(ph,strcat(base_file_name,'_denuduplift_hoh9kyr.png'));

figure;
ph=plot(((newdenud_glac_66to83hoh_ss10(:,1:65))*1000/10000),'g-');
hold on;
plot((new_uplift_66to83hoh(:,1:65)),'b-');
plot((new_contour_uplift_66to83hoh(:,1:65)),'c-');
%plot(x1_new,y1,'b--');
title('Uplift and DENUD Glacial Erosion in Hoh 10000yr');
xlabel('Horizontal Distance');
ylabel('Average Uplift or Erosion Rate (mm/yr)');
legend('Hoh','Uplift','Uplift from Brandon et
      al.','Location','NorthWest');
legend('boxoff');
saveas(ph,strcat(base_file_name,'_denuduplift_hoh10kyr.png'));

%==========
%Plot the valleys denud erosion against each other
%==========
figure;
ph=plot(1:k,((newdenud_glac_10to97total_ss1)*1000/1000),'r-');
hold on;
plot(1:k,((newdenud_glac_66to83hoh_ss1)*1000/1000),'g-');
plot(1:k,((newdenud_glac_48to59queets_ss1)*1000/1000),'m-');
plot(1:k,((newdenud_glac_31to40quinault_ss1)*1000/1000),'c-');
title('DENUD Glacial Erosion for the Hoh, Queets, Quinault, and Total
      1000yr');
xlabel('Horizontal Distance');
ylabel('Average Uplift or Erosion Rate (mm/yr)');
```

```
legend('Total','Hoh','Queets','Quinault','Location','NorthWest');
legend('boxoff');
saveas(ph,strcat(base_file_name,'_denudvalleys_1kyr.png'));

figure;
ph=plot(1:k,((newdenud_glac_10to97total_ss2)*1000/2000),'r-');
hold on;
plot(1:k,((newdenud_glac_66to83hoh_ss2)*1000/2000),'g-');
plot(1:k,((newdenud_glac_48to59queets_ss2)*1000/2000),'m-');
plot(1:k,((newdenud_glac_31to40quinault_ss2)*1000/2000),'c-');
title('DENUD Glacial Erosion for the Hoh, Queets, Quinault, and Total
      2000yr');
xlabel('Horizontal Distance');
ylabel('Average Uplift or Erosion Rate (mm/yr)');
legend('Total','Hoh','Queets','Quinault','Location','NorthWest');
legend('boxoff');
saveas(ph,strcat(base_file_name,'_denudvalleys_2kyr.png'));

figure;
ph=plot(1:k,((newdenud_glac_10to97total_ss3)*1000/3000),'r-');
hold on;
plot(1:k,((newdenud_glac_66to83hoh_ss3)*1000/3000),'g-');
plot(1:k,((newdenud_glac_48to59queets_ss3)*1000/3000),'m-');
plot(1:k,((newdenud_glac_31to40quinault_ss3)*1000/3000),'c-');
title('DENUD Glacial Erosion for the Hoh, Queets, Quinault, and Total
      3000yr');
xlabel('Horizontal Distance');
ylabel('Average Uplift or Erosion Rate (mm/yr)');
legend('Total','Hoh','Queets','Quinault','Location','NorthWest');
legend('boxoff');
saveas(ph,strcat(base_file_name,'_denudvalleys_3kyr.png'));

figure;
ph=plot(1:k,((newdenud_glac_10to97total_ss4)*1000/4000),'r-');
hold on;
plot(1:k,((newdenud_glac_66to83hoh_ss4)*1000/4000),'g-');
plot(1:k,((newdenud_glac_48to59queets_ss4)*1000/4000),'m-');
plot(1:k,((newdenud_glac_31to40quinault_ss4)*1000/4000),'c-');
title('DENUD Glacial Erosion for the Hoh, Queets, Quinault, and Total
      4000yr');
xlabel('Horizontal Distance');
ylabel('Average Uplift or Erosion Rate (mm/yr)');
legend('Total','Hoh','Queets','Quinault','Location','NorthWest');
legend('boxoff');
saveas(ph,strcat(base_file_name,'_denudvalleys_4kyr.png'));

figure;
ph=plot(1:k,((newdenud_glac_10to97total_ss5)*1000/5000),'r-');
hold on;
plot(1:k,((newdenud_glac_66to83hoh_ss5)*1000/5000),'g-');
plot(1:k,((newdenud_glac_48to59queets_ss5)*1000/5000),'m-');
plot(1:k,((newdenud_glac_31to40quinault_ss5)*1000/5000),'c-');
title('DENUD Glacial Erosion for the Hoh, Queets, Quinault, and Total
      5000yr');
xlabel('Horizontal Distance');
ylabel('Average Uplift or Erosion Rate (mm/yr)');
```

```
legend('Total','Hoh','Queets','Quinault','Location','NorthWest');
legend('boxoff');
saveas(ph,strcat(base_file_name,'_denudvalleys_5kyr.png'));

figure;
ph=plot(1:k,((newdenud_glac_10to97total_ss6)*1000/6000),'r-');
hold on;
plot(1:k,((newdenud_glac_66to83hoh_ss6)*1000/6000),'g-');
plot(1:k,((newdenud_glac_48to59queets_ss6)*1000/6000),'m-');
plot(1:k,((newdenud_glac_31to40quinault_ss6)*1000/6000),'c-');
title('DENUD Glacial Erosion for the Hoh, Queets, Quinault, and Total
      6000yr');
xlabel('Horizontal Distance');
ylabel('Average Uplift or Erosion Rate (mm/yr)');
legend('Total','Hoh','Queets','Quinault','Location','NorthWest');
legend('boxoff');
saveas(ph,strcat(base_file_name,'_denudvalleys_6kyr.png'));

figure;
ph=plot(1:k,((newdenud_glac_10to97total_ss7)*1000/7000),'r-');
hold on;
plot(1:k,((newdenud_glac_66to83hoh_ss7)*1000/7000),'g-');
plot(1:k,((newdenud_glac_48to59queets_ss7)*1000/7000),'m-');
plot(1:k,((newdenud_glac_31to40quinault_ss7)*1000/7000),'c-');
title('DENUD Glacial Erosion for the Hoh, Queets, Quinault, and Total
      7000yr');
xlabel('Horizontal Distance');
ylabel('Average Uplift or Erosion Rate (mm/yr)');
legend('Total','Hoh','Queets','Quinault','Location','NorthWest');
legend('boxoff');
saveas(ph,strcat(base_file_name,'_denudvalleys_7kyr.png'));

figure;
ph=plot(1:k,((newdenud_glac_10to97total_ss8)*1000/8000),'r-');
hold on;
plot(1:k,((newdenud_glac_66to83hoh_ss8)*1000/8000),'g-');
plot(1:k,((newdenud_glac_48to59queets_ss8)*1000/8000),'m-');
plot(1:k,((newdenud_glac_31to40quinault_ss8)*1000/8000),'c-');
title('DENUD Glacial Erosion for the Hoh, Queets, Quinault, and Total
      8000yr');
xlabel('Horizontal Distance');
ylabel('Average Uplift or Erosion Rate (mm/yr)');
legend('Total','Hoh','Queets','Quinault','Location','NorthWest');
legend('boxoff');
saveas(ph,strcat(base_file_name,'_denudvalleys_8kyr.png'));

figure;
ph=plot(1:k,((newdenud_glac_10to97total_ss9)*1000/9000),'r-');
hold on;
plot(1:k,((newdenud_glac_66to83hoh_ss9)*1000/9000),'g-');
plot(1:k,((newdenud_glac_48to59queets_ss9)*1000/9000),'m-');
plot(1:k,((newdenud_glac_31to40quinault_ss9)*1000/9000),'c-');
title('DENUD Glacial Erosion for the Hoh, Queets, Quinault, and Total
      9000yr');
xlabel('Horizontal Distance');
ylabel('Average Uplift or Erosion Rate (mm/yr)');
```

```
legend('Total','Hoh','Queets','Quinault','Location','NorthWest');
legend('boxoff');
saveas(ph,strcat(base_file_name,'_denudvalleys_9kyr.png'));

figure;
ph=plot(1:k,((newdenud_glac_10to97total_ss10)*1000/10000),'r-');
hold on;
plot(1:k,((newdenud_glac_66to83hoh_ss10)*1000/10000),'g-');
plot(1:k,((newdenud_glac_48to59queets_ss10)*1000/10000),'m-');
plot(1:k,((newdenud_glac_31to40quinault_ss10)*1000/10000),'c-');
title('DENUD Glacial Erosion for the Hoh, Queets, Quinault, and Total
      10000yr');
xlabel('Horizontal Distance');
ylabel('Average Uplift or Erosion Rate (mm/yr)');
legend('Total','Hoh','Queets','Quinault','Location','NorthWest');
legend('boxoff');
saveas(ph,strcat(base_file_name,'_denudvalleys_10kyr.png'));

%==========
%Plot the valleys' denud erosion against uplift
%==========
figure;
ph=plot(1:k,((newdenud_glac_10to97total_ss1)*1000/1000),'r-');
hold on;
plot(1:k,((newdenud_glac_66to83hoh_ss1)*1000/1000),'g-');
plot(1:k,((newdenud_glac_48to59queets_ss1)*1000/1000),'m-');
plot(1:k,((newdenud_glac_31to40quinault_ss1)*1000/1000),'c-');
plot(1:k,(new_uplift_10to97total),'b-');
title('Uplift and DENUD Glacial Erosion for the Hoh, Queets, Quinault,
      and Total 1000yr');
xlabel('Horizontal Distance');
ylabel('Average Uplift or Erosion Rate (mm/yr)');
legend('Total','Hoh','Queets','Quinault','Uplift','Location','NorthWest
      ');
legend('boxoff');
saveas(ph,strcat(base_file_name,'_denudvalleysuplift_1kyr.png'));

figure;
ph=plot(1:k,((newdenud_glac_10to97total_ss2)*1000/2000),'r-');
hold on;
plot(1:k,((newdenud_glac_66to83hoh_ss2)*1000/2000),'g-');
plot(1:k,((newdenud_glac_48to59queets_ss2)*1000/2000),'m-');
plot(1:k,((newdenud_glac_31to40quinault_ss2)*1000/2000),'c-');
plot(1:k,(new_uplift_10to97total),'b-');
title('Uplift and DENUD Glacial Erosion for the Hoh, Queets, Quinault,
      and Total 2000yr');
xlabel('Horizontal Distance');
ylabel('Average Uplift or Erosion Rate (mm/yr)');
legend('Total','Hoh','Queets','Quinault','Uplift','Location','NorthWest
      ');
legend('boxoff');
saveas(ph,strcat(base_file_name,'_denudvalleysuplift_2kyr.png'));

figure;
ph=plot(1:k,((newdenud_glac_10to97total_ss3)*1000/3000),'r-');
hold on;
```

```
plot(1:k,((newdenud_glac_66to83hoh_ss3)*1000/3000),'g-');
plot(1:k,((newdenud_glac_48to59queets_ss3)*1000/3000),'m-');
plot(1:k,((newdenud_glac_31to40quinault_ss3)*1000/3000),'c-');
plot(1:k,(new_uplift_10to97total),'b-');
title('Uplift and DENUD Glacial Erosion for the Hoh, Queets, Quinault,
      and Total 3000yr');
xlabel('Horizontal Distance');
ylabel('Average Uplift or Erosion Rate (mm/yr)');
legend('Total','Hoh','Queets','Quinault','Uplift','Location','NorthWest
      ');
legend('boxoff');
saveas(ph,strcat(base_file_name,'_denudvalleysuplift_3kyr.png'));

figure;
ph=plot(1:k,((newdenud_glac_10to97total_ss4)*1000/4000),'r-');
hold on;
plot(1:k,((newdenud_glac_66to83hoh_ss4)*1000/4000),'g-');
plot(1:k,((newdenud_glac_48to59queets_ss4)*1000/4000),'m-');
plot(1:k,((newdenud_glac_31to40quinault_ss4)*1000/4000),'c-');
plot(1:k,(new_uplift_10to97total),'b-');
title('Uplift and DENUD Glacial Erosion for the Hoh, Queets, Quinault,
      and Total 4000yr');
xlabel('Horizontal Distance');
ylabel('Average Uplift or Erosion Rate (mm/yr)');
legend('Total','Hoh','Queets','Quinault','Uplift','Location','NorthWest
      ');
legend('boxoff');
saveas(ph,strcat(base_file_name,'_denudvalleysuplift_4kyr.png'));

figure;
ph=plot(1:k,((newdenud_glac_10to97total_ss5)*1000/5000),'r-');
hold on;
plot(1:k,((newdenud_glac_66to83hoh_ss5)*1000/5000),'g-');
plot(1:k,((newdenud_glac_48to59queets_ss5)*1000/5000),'m-');
plot(1:k,((newdenud_glac_31to40quinault_ss5)*1000/5000),'c-');
plot(1:k,(new_uplift_10to97total),'b-');
title('Uplift and DENUD Glacial Erosion for the Hoh, Queets, Quinault,
      and Total 5000yr');
xlabel('Horizontal Distance');
ylabel('Average Uplift or Erosion Rate (mm/yr)');
legend('Total','Hoh','Queets','Quinault','Uplift','Location','NorthWest
      ');
legend('boxoff');
saveas(ph,strcat(base_file_name,'_denudvalleysuplift_5kyr.png'));

figure;
ph=plot(1:k,((newdenud_glac_10to97total_ss6)*1000/6000),'r-');
hold on;
plot(1:k,((newdenud_glac_66to83hoh_ss6)*1000/6000),'g-');
plot(1:k,((newdenud_glac_48to59queets_ss6)*1000/6000),'m-');
plot(1:k,((newdenud_glac_31to40quinault_ss6)*1000/6000),'c-');
plot(1:k,(new_uplift_10to97total),'b-');
title('Uplift and DENUD Glacial Erosion for the Hoh, Queets, Quinault,
      and Total 6000yr');
xlabel('Horizontal Distance');
ylabel('Average Uplift or Erosion Rate (mm/yr)');
```

```
legend('Total','Hoh','Queets','Quinault','Uplift','Location','NorthWest
      ');
legend('boxoff');
saveas(ph,strcat(base_file_name,'_denudvalleysuplift_6kyr.png'));

figure;
ph=plot(1:k,((newdenud_glac_10to97total_ss7)*1000/7000),'r-');
hold on;
plot(1:k,((newdenud_glac_66to83hoh_ss7)*1000/7000),'g-');
plot(1:k,((newdenud_glac_48to59queets_ss7)*1000/7000),'m-');
plot(1:k,((newdenud_glac_31to40quinault_ss7)*1000/7000),'c-');
plot(1:k,(new_uplift_10to97total),'b-');
title('Uplift and DENUD Glacial Erosion for the Hoh, Queets, Quinault,
      and Total 7000yr');
xlabel('Horizontal Distance');
ylabel('Average Uplift or Erosion Rate (mm/yr)');
legend('Total','Hoh','Queets','Quinault','Uplift','Location','NorthWest
      ');
legend('boxoff');
saveas(ph,strcat(base_file_name,'_denudvalleysuplift_7kyr.png'));

figure;
ph=plot(1:k,((newdenud_glac_10to97total_ss8)*1000/8000),'r-');
hold on;
plot(1:k,((newdenud_glac_66to83hoh_ss8)*1000/8000),'g-');
plot(1:k,((newdenud_glac_48to59queets_ss8)*1000/8000),'m-');
plot(1:k,((newdenud_glac_31to40quinault_ss8)*1000/8000),'c-');
plot(1:k,(new_uplift_10to97total),'b-');
title('Uplift and DENUD Glacial Erosion for the Hoh, Queets, Quinault,
      and Total 8000yr');
xlabel('Horizontal Distance');
ylabel('Average Uplift or Erosion Rate (mm/yr)');
legend('Total','Hoh','Queets','Quinault','Uplift','Location','NorthWest
      ');
legend('boxoff');
saveas(ph,strcat(base_file_name,'_denudvalleysuplift_8kyr.png'));

figure;
ph=plot(1:k,((newdenud_glac_10to97total_ss9)*1000/9000),'r-');
hold on;
plot(1:k,((newdenud_glac_66to83hoh_ss9)*1000/9000),'g-');
plot(1:k,((newdenud_glac_48to59queets_ss9)*1000/9000),'m-');
plot(1:k,((newdenud_glac_31to40quinault_ss9)*1000/9000),'c-');
plot(1:k,(new_uplift_10to97total),'b-');
title('Uplift and DENUD Glacial Erosion for the Hoh, Queets, Quinault,
      and Total 9000yr');
xlabel('Horizontal Distance');
ylabel('Average Uplift or Erosion Rate (mm/yr)');
legend('Total','Hoh','Queets','Quinault','Uplift','Location','NorthWest
      ');
legend('boxoff');
saveas(ph,strcat(base_file_name,'_denudvalleysuplift_9kyr.png'));

figure;
ph=plot(1:k,((newdenud_glac_10to97total_ss10)*1000/10000),'r-');
hold on;
```

```
plot(1:k,((newdenud_glac_66to83hoh_ss10)*1000/10000),'g-');
plot(1:k,((newdenud_glac_48to59queets_ss10)*1000/10000),'m-');
plot(1:k,((newdenud_glac_31to40quinault_ss10)*1000/10000),'c-');
plot(1:k,(new_uplift_10to97total),'b-');
title('Uplift and DENUD Glacial Erosion for the Hoh, Queets, Quinault,
      and Total 10000yr');
xlabel('Horizontal Distance');
ylabel('Average Uplift or Erosion Rate (mm/yr)');
legend('Total','Hoh','Queets','Quinault','Uplift','Location','NorthWest
      ');
legend('boxoff');
saveas(ph,strcat(base_file_name,'_denudvalleysuplift_10kyr.png'));

%Plot the above figure but shortened to only the first half with the
%valleys on the western side
figure;
ph=plot(((newdenud_glac_10to97total_ss1(:,1:65))*(3*(10^(-5))/(10^(-
      4)))*1000/1000),'r-');
hold on;
plot(((newdenud_glac_66to83hoh_ss1(:,1:65))*(3*(10^(-5))/(10^(-
      4)))*1000/1000),'g-');
plot(((newdenud_glac_48to59queets_ss1(:,1:65))*(3*(10^(-5))/(10^(-
      4)))*1000/1000),'m-');
plot(((newdenud_glac_31to40quinault_ss1(:,1:65))*(3*(10^(-5))/(10^(-
      4)))*1000/1000),'c-');
plot((new_uplift_10to97total(:,1:65)),'b-');
title('Uplift and DENUD Glacial Erosion for the Hoh, Queets, Quinault,
      and Total 1000yr');
xlabel('Horizontal Distance');
ylabel('Average Uplift or Erosion Rate (mm/yr)');
legend('Total','Hoh','Queets','Quinault','Uplift','Location','NorthWest
      ');
legend('boxoff');
saveas(ph,strcat(base_file_name,'_denudvalleysupliftshort_1kyr.png'));

figure;
ph=plot(((newdenud_glac_10to97total_ss2(:,1:65))*(3*(10^(-5))/(10^(-
      4)))*1000/2000),'r-');
hold on;
plot(((newdenud_glac_66to83hoh_ss2(:,1:65))*(3*(10^(-5))/(10^(-
      4)))*1000/2000),'g-');
plot(((newdenud_glac_48to59queets_ss2(:,1:65))*(3*(10^(-5))/(10^(-
      4)))*1000/2000),'m-');
plot(((newdenud_glac_31to40quinault_ss2(:,1:65))*(3*(10^(-5))/(10^(-
      4)))*1000/2000),'c-');
plot((new_uplift_10to97total(:,1:65)),'b-');
title('Uplift and DENUD Glacial Erosion for the Hoh, Queets, Quinault,
      and Total 2000yr');
xlabel('Horizontal Distance');
ylabel('Average Uplift or Erosion Rate (mm/yr)');
legend('Total','Hoh','Queets','Quinault','Uplift','Location','NorthWest
      ');
legend('boxoff');
saveas(ph,strcat(base_file_name,'_denudvalleysupliftshort_2kyr.png'));

figure;
```

```
ph=plot(((newdenud_glac_10to97total_ss3(:,1:65))*(3*(10^(-5))/(10^(-
      4)))*1000/3000),'r-');
hold on;
plot(((newdenud_glac_66to83hoh_ss3(:,1:65))*(3*(10^(-5))/(10^(-
      4)))*1000/3000),'g-');
plot(((newdenud_glac_48to59queets_ss3(:,1:65))*(3*(10^(-5))/(10^(-
      4)))*1000/3000),'m-');
plot(((newdenud_glac_31to40quinault_ss3(:,1:65))*(3*(10^(-5))/(10^(-
      4)))*1000/3000),'c-');
plot((new_uplift_10to97total(:,1:65)),'b-');
title('Uplift and DENUD Glacial Erosion for the Hoh, Queets, Quinault,
      and Total 3000yr');
xlabel('Horizontal Distance');
ylabel('Average Uplift or Erosion Rate (mm/yr)');
legend('Total','Hoh','Queets','Quinault','Uplift','Location','NorthWest
      ');
legend('boxoff');
saveas(ph,strcat(base_file_name,'_denudvalleysupliftshort_3kyr.png'));

figure;
ph=plot(((newdenud_glac_10to97total_ss4(:,1:65))*(3*(10^(-5))/(10^(-
      4)))*1000/4000),'r-');
hold on;
plot(((newdenud_glac_66to83hoh_ss4(:,1:65))*(3*(10^(-5))/(10^(-
      4)))*1000/4000),'g-');
plot(((newdenud_glac_48to59queets_ss4(:,1:65))*(3*(10^(-5))/(10^(-
      4)))*1000/4000),'m-');
plot(((newdenud_glac_31to40quinault_ss4(:,1:65))*(3*(10^(-5))/(10^(-
      4)))*1000/4000),'c-');
plot((new_uplift_10to97total(:,1:65)),'b-');
title('Uplift and DENUD Glacial Erosion for the Hoh, Queets, Quinault,
      and Total 4000yr');
xlabel('Horizontal Distance');
ylabel('Average Uplift or Erosion Rate (mm/yr)');
legend('Total','Hoh','Queets','Quinault','Uplift','Location','NorthWest
      ');
legend('boxoff');
saveas(ph,strcat(base_file_name,'_denudvalleysupliftshort_4kyr.png'));

figure;
ph=plot(((newdenud_glac_10to97total_ss5(:,1:65))*(3*(10^(-5))/(10^(-
      4)))*1000/5000),'r-');
hold on;
plot(((newdenud_glac_66to83hoh_ss5(:,1:65))*(3*(10^(-5))/(10^(-
      4)))*1000/5000),'g-');
plot(((newdenud_glac_48to59queets_ss5(:,1:65))*(3*(10^(-5))/(10^(-
      4)))*1000/5000),'m-');
plot(((newdenud_glac_31to40quinault_ss5(:,1:65))*(3*(10^(-5))/(10^(-
      4)))*1000/5000),'c-');
plot((new_uplift_10to97total(:,1:65)),'b-');
title('Uplift and DENUD Glacial Erosion for the Hoh, Queets, Quinault,
      and Total 5000yr');
xlabel('Horizontal Distance');
ylabel('Average Uplift or Erosion Rate (mm/yr)');
legend('Total','Hoh','Queets','Quinault','Uplift','Location','NorthWest
      ');
```

```
legend('boxoff');
saveas(ph,strcat(base_file_name,'_denudvalleysupliftshort_5kyr.png'));

figure;
ph=plot(((newdenud_glac_10to97total_ss6(:,1:65))*(3*(10^(-5))/(10^(-
      4)))*1000/6000),'r-');
hold on;
plot(((newdenud_glac_66to83hoh_ss6(:,1:65))*(3*(10^(-5))/(10^(-
      4)))*1000/6000),'g-');
plot(((newdenud_glac_48to59queets_ss6(:,1:65))*(3*(10^(-5))/(10^(-
      4)))*1000/6000),'m-');
plot(((newdenud_glac_31to40quinault_ss6(:,1:65))*(3*(10^(-5))/(10^(-
      4)))*1000/6000),'c-');
plot((new_uplift_10to97total(:,1:65)),'b-');
title('Uplift and DENUD Glacial Erosion for the Hoh, Queets, Quinault,
      and Total 6000yr');
xlabel('Horizontal Distance');
ylabel('Average Uplift or Erosion Rate (mm/yr)');
legend('Total','Hoh','Queets','Quinault','Uplift','Location','NorthWest
      ');
legend('boxoff');
saveas(ph,strcat(base_file_name,'_denudvalleysupliftshort_6kyr.png'));

figure;
ph=plot(((newdenud_glac_10to97total_ss7(:,1:65))*(3*(10^(-5))/(10^(-
      4)))*1000/7000),'r-');
hold on;
plot(((newdenud_glac_66to83hoh_ss7(:,1:65))*(3*(10^(-5))/(10^(-
      4)))*1000/7000),'g-');
plot(((newdenud_glac_48to59queets_ss7(:,1:65))*(3*(10^(-5))/(10^(-
      4)))*1000/7000),'m-');
plot(((newdenud_glac_31to40quinault_ss7(:,1:65))*(3*(10^(-5))/(10^(-
      4)))*1000/7000),'c-');
plot((new_uplift_10to97total(:,1:65)),'b-');
title('Uplift and DENUD Glacial Erosion for the Hoh, Queets, Quinault,
      and Total 7000yr');
xlabel('Horizontal Distance');
ylabel('Average Uplift or Erosion Rate (mm/yr)');
legend('Total','Hoh','Queets','Quinault','Uplift','Location','NorthWest
      ');
legend('boxoff');
saveas(ph,strcat(base_file_name,'_denudvalleysupliftshort_7kyr.png'));

figure;
ph=plot(((newdenud_glac_10to97total_ss8(:,1:65))*(3*(10^(-5))/(10^(-
      4)))*1000/8000),'r-');
hold on;
plot(((newdenud_glac_66to83hoh_ss8(:,1:65))*(3*(10^(-5))/(10^(-
      4)))*1000/8000),'g-');
plot(((newdenud_glac_48to59queets_ss8(:,1:65))*(3*(10^(-5))/(10^(-
      4)))*1000/8000),'m-');
plot(((newdenud_glac_31to40quinault_ss8(:,1:65))*(3*(10^(-5))/(10^(-
      4)))*1000/8000),'c-');
plot((new_uplift_10to97total(:,1:65)),'b-');
title('Uplift and DENUD Glacial Erosion for the Hoh, Queets, Quinault,
      and Total 8000yr');
```

```
xlabel('Horizontal Distance');
ylabel('Average Uplift or Erosion Rate (mm/yr)');
legend('Total','Hoh','Queets','Quinault','Uplift','Location','NorthWest
      ');
legend('boxoff');
saveas(ph,strcat(base_file_name,'_denudvalleysupliftshort_8kyr.png'));

figure;
ph=plot(((newdenud_glac_10to97total_ss9(:,1:65))*(3*(10^(-5))/(10^(-
      4)))*1000/9000),'r-');
hold on;
plot(((newdenud_glac_66to83hoh_ss9(:,1:65))*(3*(10^(-5))/(10^(-
      4)))*1000/9000),'g-');
plot(((newdenud_glac_48to59queets_ss9(:,1:65))*(3*(10^(-5))/(10^(-
      4)))*1000/9000),'m-');
plot(((newdenud_glac_31to40quinault_ss9(:,1:65))*(3*(10^(-5))/(10^(-
      4)))*1000/9000),'c-');
plot((new_uplift_10to97total(:,1:65)),'b-');
title('Uplift and DENUD Glacial Erosion for the Hoh, Queets, Quinault,
      and Total, 9000yr');
xlabel('Horizontal Distance');
ylabel('Average Uplift or Erosion Rate (mm/yr)');
legend('Total','Hoh','Queets','Quinault','Uplift','Location','NorthWest
      ');
legend('boxoff');
saveas(ph,strcat(base_file_name,'_denudvalleysupliftshort_9kyr.png'));

figure;
ph=plot(((newdenud_glac_10to97total_ss10(:,1:65))*1000/10000),'r-');
hold on;
plot(((newdenud_glac_66to83hoh_ss10(:,1:65))*1000/10000),'g-');
plot(((newdenud_glac_48to59queets_ss10(:,1:65))*1000/10000),'m-');
plot(((newdenud_glac_31to40quinault_ss10(:,1:65))*1000/10000),'c-');
plot((new_uplift_10to97total(:,1:65))*(10^(-4))/(10^(-4)),'b-');
plot((new_uplift_10to97total(:,1:65))*(10^(-4))/(10^(-5)),'b--');
plot((new_uplift_10to97total(:,1:65))*(10^(-4))/(2*10^(-5)),'b:');
plot((new_uplift_10to97total(:,1:65))*(10^(-4))/(5*10^(-5)),'b-.');
title('Uplift and DENUD Glacial Erosion for the Hoh, Queets, Quinault,
      and Total, 10000yr');
xlabel('Horizontal Distance');
ylabel('Average Uplift or Erosion Rate (mm/yr)');
legend('Total','Hoh','Queets','Quinault','Uplift,10^{-4}','Uplift,10^{-
      5}','Uplift,2x10^{-5}','Uplift,5x10^{-5}','Location','NorthWest')
legend('boxoff');
saveas(ph,strcat(base_file_name,'_denudvalleysupliftshortnew.png'));
%saveas(ph,strcat(base_file_name,'_denudvalleysupliftshort_10kyr.png'))

figure;
ph=plot(((newdenud_glac_10to97total_ss10(:,1:65))),'g-');
hold on;
plot((new_uplift_10to97total(:,1:65))*10000/1000,'b-');
title('Uplift and DENUD Glacial Erosion for the Total');
xlabel('Horizontal Distance');
ylabel('Average Uplift or Erosion (m)');
legend('Total','Uplift','Location','NorthWest');
legend('boxoff');
```

```
saveas(ph,strcat(base_file_name,'_denudvalleysupliftshortnew.png'));

%==========
%Clean-up
%==========
clear newdenud_glac_66to83hoh_ss1 new_uplift_66to83hoh
clear newdenud_glac_66to83hoh_ss2 newdenud_glac_66to83hoh_ss3
clear newdenud_glac_66to83hoh_ss4 newdenud_glac_66to83hoh_ss5
clear newdenud_glac_66to83hoh_ss6 newdenud_glac_66to83hoh_ss7
clear newdenud_glac_66to83hoh_ss8 newdenud_glac_66to83hoh_ss9
clear newdenud_glac_66to83hoh_ss10 newdenud_glac_10to97total_ss1
clear newdenud_glac_48to59queets_ss1 newdenud_glac_31to40quinault_ss1
clear newdenud_glac_10to97total_ss2 newdenud_glac_48to59queets_ss2
clear newdenud_glac_31to40quinault_ss2 newdenud_glac_10to97total_ss3
clear newdenud_glac_48to59queets_ss3 newdenud_glac_31to40quinault_ss3
clear newdenud_glac_10to97total_ss4 newdenud_glac_48to59queets_ss4
clear newdenud_glac_31to40quinault_ss4 newdenud_glac_10to97total_ss5
clear newdenud_glac_48to59queets_ss5 newdenud_glac_31to40quinault_ss5
clear newdenud_glac_10to97total_ss6 newdenud_glac_48to59queets_ss6
clear newdenud_glac_31to40quinault_ss6 newdenud_glac_10to97total_ss7
clear newdenud_glac_48to59queets_ss7 newdenud_glac_31to40quinault_ss7
clear newdenud_glac_10to97total_ss8 newdenud_glac_48to59queets_ss8
clear newdenud_glac_31to40quinault_ss8 newdenud_glac_10to97total_ss9
clear newdenud_glac_48to59queets_ss9 newdenud_glac_31to40quinault_ss9
clear newdenud_glac_10to97total_ss10 newdenud_glac_48to59queets_ss10
clear newdenud_glac_31to40quinault_ss10 new_uplift_10to97total
clear newdenud_glac_ss1 newdenud_glac_ss2 newdenud_glac_ss3
clear newdenud_glac_ss4 newdenud_glac_ss5 newdenud_glac_ss6
clear newdenud_glac_ss7 newdenud_glac_ss8 newdenud_glac_ss9
clear newdenud_glac_ss10 newdenud_rot_ss10

close all;
end;
```

Uplift_newcoords.m

```
%File for transferring coords from UTM to model for new uplift line
i=1:13;

y=[5277663.154;5282849.758;5285437.949;5287372.96;5289088.911;5292597.8
68;5296089.783;5297805.048;5299553.546;5302192.342;5310070.85;5320480.3
73;5334092.702];

x=[395977.3681;404701.9193;409695.8139;414038.0821;418374.2669;421870.0
891;426858.9535;432045.3354;434647.3906;437257.5213;450002.4727;467872.
2413;489960.7861];

x=(round((x(i)-369000)/1000))+2
y=(round((y(i)-5200000)/1000))

lgm_map=zeros(165,165);
lgm_map(x(i),y(i))=1;

figure;
ph=pcolor(new_topo);
hold on;
set(ph,'linestyle','none');
colorbar;
plot(x,y,'m*');

x1=[0;8.473868766;13.85506934;18.32272446;22.79037957;28.07150798;33.85
944519;39.24064577;42.79475543;45.43531963;60.56530372;81.07648839;106.
8688015]

y1=[0;0.3;0.5;0.7;0.9;1.1;1.45;1.1;0.9;0.7;0.5;0.3;0]

x1_new=(round(x1))

figure;
ph=plot(x1_new,y1,'m-');
hold on;
plot(1:k,(new_uplift_66to83hoh),'b-');
title('Uplift and DENUD Glacial Erosion in Hoh 1000yr');
xlabel('Horizontal Distance');
ylabel('Average Uplift or Erosion Rate (mm/yr)');
legend('Hoh','Uplift','Location','NorthWest');
legend('boxoff');
```

Uplift_Contours.m

```
%File for taking UTM coords and turning them into model coords; used
for taking the uplift contours from Brandon et al. 1998 and creating a
new uplift plot

%Get the names of datasets to process
directory_name=input('Location of data folders: ','s');
base_file_name_list=textread(strcat(directory_name,'/',input('File of
      base names of data to process (batch log file): ','s')),'%s');

%Begin loop to process all files
for entry=1:size(base_file_name_list)

%Get the base file name from the list
base_file_name=strcat(directory_name,'/',base_file_name_list{entry},'/'
      ,base_file_name_list{entry});

%Load the ice locations and topo data, using the base name
topo_temp=load(strcat(base_file_name,'_topo.out'),'-ascii');

%=====================================================
%Plot the basic files of topo
%=====================================================
%I. Reshape topo_output to be a 165*165 grid and plot it
t_temp=reshape(topo_temp(:,3),165,165);

figure;
ph=pcolor(t_temp);
hold on;
set(ph,'linestyle','none');
colorbar;

x_11=[422050.7901;422723.5282;422752.6231;423402.3522;423559.9575;
    424174.6079;424475.5043;424685.2318;425641.0235;425877.1342;
    426763.8955;427107.4909;428135.012;428382.4296;429403.837;
    429274.2368;430463.8037;430673.5391;431446.4456;431461.8379;
    431972.2568;432097.6626;432214.4758];

x_09=[417248.516;417294.2303;417631.7291;417807.8851;419017.1047;
    419066.7095;420125.7901;420507.9899;421608.5406;421680.0487;
    422704.5505;422944.3638;423782.6586;424514.8785;425351.9636;
    426081.9156;426528.063;428095.0018;428047.1499;429355.6726;
    429431.6782;430911.3021;431112.1649;432076.5455;432599.8087;
    433236.1109;433693.3701;434392.91;434693.9688;435006.3359;
    435163.1372;435125.6363;435241.6208];

x_07=[413806.0671;414072.2374;414039.9112;414228.4835;414963.7857;
    415389.7397;415281.6206;416104.7743;416625.7801;416827.2599;
    417539.7343;418734.0432;418969.3276;420506.3156;421214.5654;
    422371.9077;423173.5041;424331.0734;425627.5242;426284.5365;
    428085.2644;428530.9766;430253.9015;430771.2933;432225.4966;
    432814.7352;433906.7738;434657.3293;435688.9609;436393.9812;
    436887.9634;437546.452;437797.8342;438287.5597;438446.5171;

    446552.8042;447018.5497;447984.6858;448436.3607;448955.2879;
```

```
    450202.9947;450225.4864;451869.0064;452087.3878;453532.9439;
    454052.1643;454610.3214;455380.584;455436.6798;455763.3378;
    456530.8838;
    468621.5816;468629.4579;469517.8661;470111.6926;470084.6667;
    470993.6438;471653.8313;472262.9769;472929.8551;473535.4374;
    474500.9705;474804.8111;475581.0331;476079.5865;476558.8364;
    477439.2778;477747.1998;478909.5139;479121.8966;480278.0688;
    480788.8488;481550.2338;481764.6889;482625.6804;483333.4381;
    484194.0069;484901.1383;485665.2953;486370.8643;487053.2418;
    487139.3816;487833.8598;488712.3729];

x_05=[407525.7829;407874.0863;407892.5686;408035.7476;408536.2633;
    408608.6411;409730.7838;409565.3645;410748.9065;410820.1148;
    411004.7793;411508.5974;411757.6497;412576.9573;412501.4615;
    412653.325;412349.305;412791.8417;413184.9485;413018.2164;
    413124.2777;413154.8769;413983.6421;413410.7138;414781.9479;
    414572.9863;416074.3241;415637.4781;416770.0557;416809.0641;
    417760.3606;418735.9071;418079.2394;419620.0011;419646.6822;
    420796.606;421775.971;421507.4996;422852.7753;423175.8462;
    423824.215;424992.676;424745.9092;425962.1254;426709.7358;
    427420.2707;428675.3819;428775.8528;429837.5765;429952.3521;
    430703.5302;431278.4382;432146.6611;431816.5453;433020.2344;
    433791.939;433484.0652;434752.1378;435246.6289;436018.3137;
    436797.9326;437087.1181;438253.5675;438449.0231;439711.9195;
    439709.3435;440965.3797;441855.2573;442620.7501;443706.3398;
    444281.4463;446146.0964;445951.1135;447130.9589;448096.3379;
    449073.8722;448703.8599;449947.2624;450383.2035;451207.3624;
    452371.3587;452262.189;454026.9122;454040.9587;454999.4675;
    455875.4593;455824.951;457142.5999;458113.7621;458106.7845;
    459087.3315;460264.0951;460386.4042;461537.9432;462077.5412;
    462715.406;463764.5595;464577.4865;465153.0226;465657.4811;
    466244.4105;466739.8655;467431.7713;468038.5035;468027.2087;
    468126.2559;468531.6431;469707.6621;470597.2224;471565.7856;
    472866.0798;473321.216;473580.0039;474260.9095;474785.5458;
    474857.3638;475434.3195;475426.9523;475937.9012;476151.7496;
    477213.8157;477515.2138;477607.9702;477782.9857;477691.9376;
    479937.5018;479855.2753;480914.5417;482086.0921;482510.2528;
    483062.0788;484330.4594;484671.8929;485305.0861;486342.8354;
    487066.2381;488015.7095;488436.5318;489688.5827;489904.175;
    491162.9762;491471.0616;492055.2444;492057.6362;492343.9889;
    492541.9629];

x_03=[391457.2119;391601.5589;391669.6645;392395.8828;392808.4103;
    393251.8303;393987.5014;394258.1841;394801.7069;395425.2415;
    395716.4772;396333.7009;397449.8619;397177.6435;398452.1962;
    398241.5677;399163.8003;399590.1989;400165.2077;400986.0387;
    401166.3381;401133.7364;401108.6631;401241.4183;402070.8851;
    402974.9487;402208.4042;403678.8462;404192.6314;403843.7939;
    405472.8024;404900.4005;405459.1694;406460.5677;407535.9529;
    406786.0599;407444.3543;407501.189;408701.5177;407874.0796;
    408444.1329;410059.6117;409202.2853;411220.8893;410361.7193;
    411418.7296;412579.2134;413552.7035;412491.7053;414309.769;
    413562.8012;415352.854;415632.2352;414642.7136;416689.065;
    415812.938;417839.5707;416880.7873;417778.3797;419687.2396;
    419480.3465;421340.142;420485.6686;421880.6674;423482.5716;
    423852.7668;425430.1472;425428.7113;426793.2793;427002.8398;
    428253.3741;428183.4177;429612.4072;430044.7874;431266.8709;
```

```
    431222.2267;432729.0114;432696.6415;433456.7497;434376.319;
    433757.755;433923.8119;434277.1028;434398.6626;434429.1335;
    435833.8026;435496.3803;437388.2741;436576.8392;437854.5235;
    438943.8648;439233.6145;440402.0713;440618.0357;441958.1315;
    441904.2585;444098.8405;443777.3944;445951.1431;445857.2361;
    447705.8956;447734.5017;449169.0826;450210.4745;451318.2538;
    452685.4199;453368.3919;454567.8963;455321.1786;457079.2569;
    457047.495;458055.8557;459520.5213;459327.2657;461079.0298;
    461409.2195;462932.4753;463292.7336;464880.881;465078.4099;
    466862.2963;467219.4107;468349.256;468680.1874;469538.7478;
    470238.8375;471223.8117;471797.7726;472709.239;473259.27;
    474391.7661;475502.4535;475281.8994;476467.8315;477840.1189;
    477752.569;479134.549;480714.6614;480861.3398;482193.8951;
    482517.2781;483770.9802;484271.7473;485248.2812;486122.7114;
    486824.3025;487976.9047;488399.1011;489636.2306;489678.78;
    490761.3396;490904.3408;491843.6065;492075.5942;493025.1634;
    493052.7736;494127.3607;494402.2675;494516.401;494907.1262;
    494895.9925;495093.8142;495392.3425;495491.8164;495591.3422;
    495586.8004];

y_11=[5292530.293;5291502.724;5293684.845;5290911.793;5295420.115;
    5297448.919;5290461.189;5299042.725;5289573.197;5300336.778;
    5300761.993;5289118.061;5300744.775;5289102.174;5300438.12;
    5289818.635;5290822.765;5300131.736;5299249.598;5292265.793;
    5294005.699;5296332.056;5297931.115];

y_09=[5292742.42;5295942.694;5298993.417;5290697.415;5299992.427;
    5289515.734;5288046.071;5301572.128;5303303.108;5286860.818;
    5304743.325;5285970.964;5304874.494;5285950.328;5305144.996;
    5285639.152;5305275.408;5305401.174;5285759.964;5304512.556;
    5286615.982;5303620.797;5287614.192;5302879.442;5288906.119;
    5301556.489;5290202.911;5299942.808;5291937.451;5293534.34;
    5298770.205;5295424.41;5297023.409];

y_07=[5292065.057;5290169.543;5287987.553;5294095.867;5297431.502;
    5299753.369;5285641.216;5301779.921;5303954.979;5283872.969;
    5306269.855;5307707.931;5282533.118;5308556.298;5281483.808;
    5309112.805;5281021.071;5309377.767;5280843.767;5309206.933;
    5280958.237;5309033.124;5281513.819;5308278.349;5282072.496;
    5307381.132;5283071.516;5306050.524;5284360.891;5303848.784;
    5286239.106;5301799.278;5288702.535;5297863.113;5294369.636;

    5280468.252;5277699.857;5275799.864;5282342.422;5274336.479;
    5282181.522;5273307.17;5281731.122;5272418.63;5280990.129;
    5272111.836;5280545.259;5278502.558;5272974.014;5277190.347;
    5274566.002;
    5291654.359;5293109.088;5294268.139;5295283.352;5290046.367;
    5295278.864;5290038.481;5294399.824;5290323.356;5293957.404;
    5290607.204;5292933.442;5291038.901;5292928.036;5290307.543;
    5289722.106;5293212.362;5289280.225;5293934.563;5287966.043;
    5293928.792;5286798.091;5292761.86;5285631.009;5292611.647;
    5284608.252;5292316.378;5284167.983;5292021.874;5289983.633;
    5284891.837;5288090.758;5285761.465];

y_05=[5291870.864;5289100.708;5290264.44;5286915.614;5293746.44;
    5285887.952;5294891.72;5284272.415;5310008.713;5295602.416;
```

```
    5282067.701;5308541.911;5312030.224;5314491.445;5296595.247;
    5306632.824;5280010.211;5302847.611;5315937.322;5304881.211;
    5298913.885;5300950.537;5317089.362;5278684.824;5318241.512;
    5277503.675;5319823.082;5276324.189;5320685.956;5275725.299;
    5321690.311;5321676.415;5275125.376;5322100.405;5274667.024;
    5322520.594;5322798.191;5274059.635;5323074.641;5273746.391;
    5322770.631;5322609.723;5273435.009;5322160.592;5273118.977;
    5321705.54;5320671.226;5273093.36;5319929.465;5272788.103;
    5318900.493;5318020.532;5317137.274;5272329.503;5316690.504;
    5315808.631;5271873.857;5270841.054;5314919.027;5269663.174;
    5313883.346;5268342.211;5312994.513;5266727.373;5312251.645;
    5264822.933;5262336.976;5311647.588;5260283.748;5311047.297;
    5258667.543;5310587.464;5257924.45;5257477.217;5310133.061;
    5310124.335;5256881.394;5309389.3;5257157.9;5308069.123;
    5306895.524;5257724.115;5306009.11;5258146.339;5305274.074;
    5304685.327;5259296.371;5304093.799;5303068.322;5261170.774;
    5302333.985;5302616.642;5263046.068;5302899.001;5265507.853;
    5303327.754;5267533.694;5303752.503;5269125.45;5304327.832;
    5270573.76;5305485.314;5306645.301;5310278.876;5308242.268;
    5272745.316;5311149.116;5311724.668;5275059.842;5312006.176;
    5276649.037;5311270.315;5303704.274;5302828.26;5310972.845;
    5305007.864;5302532.17;5277801.42;5306021.574;5310385.061;
    5307034.709;5309215.765;5307906.104;5302522.655;5278810.678;
    5302805.744;5279093.639;5302511.455;5301489.397;5279666.981;
    5300468.151;5298718.838;5279806.364;5297116.037;5280093.165;
    5295802.568;5281398.706;5295217.725;5282704.729;5294051.207;
    5283720.567;5292739.433;5289974.62;5291720.317;5285610.056;
    5287355.487];

y_03=[5292877.279;5295348.383;5298985.18;5301154.373;5291687.99;
    5305067.521;5307818.845;5290497.126;5309550.203;5311576.187;
    5289743.184;5313160.497;5315468.776;5289134.985;5316906.187;
    5288243.183;5318494.385;5286764.563;5319932.088;5322246.246;
    5327045.206;5325154.087;5323699.324;5285717.578;5328630.403;
    5330215.739;5284828.197;5331513.513;5333105.608;5282763.734;
    5333957.371;5281291.281;5279390.672;5334814.3;5335087.859;
    5276313.661;5274411.587;5271791.664;5334923.594;5270476.257;
    5269157.785;5334611.009;5267254.406;5334156.279;5265781.504;
    5264019.386;5333844.298;5333829.496;5263275.796;5332362.98;
    5262386.821;5330455.887;5329578.633;5262080.057;5328544.625;
    5261190.065;5327218.44;5260010.874;5260725.6;5326901.207;
    5262593.353;5326587.244;5264034.508;5265179.6;5326412.722;
    5265299.066;5326241.646;5265278.738;5326078.559;5265113.359;
    5325914.583;5264953.23;5325461.197;5264057.777;5325150.1;
    5263607.313;5325132.757;5263299.271;5260817.27;5324240.722;
    5252521.403;5258484.296;5254843.216;5256878.642;5250768.069;
    5323787.705;5249010.464;5323188.608;5248416.846;5247821.231;
    5322735.322;5247370.338;5322283.473;5247501.671;5321831.009;
    5247634.298;5321227.855;5247179.614;5321064.613;5247742.023;
    5320902.857;5247725.021;5320889.715;5248430.934;5321162.089;
    5248992.296;5321290.568;5249704.843;5321566.034;5321843.503;
    5251140.887;5321981.781;5322116.76;5252433.865;5321814.983;
    5253729.019;5321802.713;5255026.142;5321354.082;5256615.408;
    5258059.741;5320903.765;5259506.21;5320459.125;5260663.632;
    5319868.968;5262546.238;5319424.619;5264139.293;5318981.148;
    5265731.855;5318534.775;5266600.794;5267759.63;5317361.345;
    5268918.328;5270077.07;5271526.33;5315750.195;5272685.362;
```

```
    5314435.615;5273844.495;5313121.249;5274713.343;5310934.365;
    5275582.452;5309620.904;5276451.878;5308308.282;5277176.875;
    5278338.796;5306705.993;5279064.475;5304813.035;5280808.608;
    5303793.475;5301901.062;5282989.24;5299718.494;5298263.387;
    5285607.251;5288080.074;5293025.955;5294771.584;5296662.593;
    5290698.276];

i=1:452;

x=round((x(i)-369000)/1000)+2;
y=round((y(i)-5200000)/1000);

x_11_rot = round((x_11-369000)./1000)+2;
x_09_rot = round((x_09-369000)./1000)+2;
x_07_rot = round((x_07-369000)./1000)+2;
x_05_rot = round((x_05-369000)./1000)+2;
x_03_rot = round((x_03-369000)./1000)+2;

y_11_rot = round((y_11-5200000)./1000);
y_09_rot = round((y_09-5200000)./1000);
y_07_rot = round((y_07-5200000)./1000);
y_05_rot = round((y_05-5200000)./1000);
y_03_rot = round((y_03-5200000)./1000);

figure;
ph=pcolor(t_temp);
hold on;
set(ph,'linestyle','none');
colorbar;
plot(x,y,'k*');
plot(x_11_rot,y_11_rot,'r*');
plot(x_09_rot,y_09_rot,'y*');
plot(x_07_rot,y_07_rot,'k*');
plot(x_05_rot,y_05_rot,'m*');
plot(x_03_rot,y_03_rot,'w*');
title('Uplift Contours From Brandon et al. 1998');
saveas(ph,strcat(base_file_name,'_uplift_contourlocat2.png'));

contour11 = [x_11_rot, y_11_rot, 1.1*ones(length(x_11_rot),1)];
contour09 = [x_09_rot, y_09_rot, 0.9*ones(length(x_09_rot),1)];
contour07 = [x_07_rot, y_07_rot, 0.7*ones(length(x_07_rot),1)];
contour05 = [x_05_rot, y_05_rot, 0.5*ones(length(x_05_rot),1)];
contour03 = [x_03_rot, y_03_rot, 0.3*ones(length(x_03_rot),1)];

contours = [contour11;contour09;contour07;contour05;contour03];

[XI,YI]=meshgrid((1:1:165),(1:1:165)');

uplift_contours =
      griddata(contours(:,1),contours(:,2),contours(:,3),XI,YI);

figure;
ph=pcolor(uplift_contours);
hold on;
set(ph,'linestyle','none');
```

```
colorbar;
plot(x_11_rot,y_11_rot,'r*');
plot(x_09_rot,y_09_rot,'y*');
plot(x_07_rot,y_07_rot,'k*');
plot(x_05_rot,y_05_rot,'m*');
plot(x_03_rot,y_03_rot,'w*');
title('Uplift From Brandon et al. 1998');
saveas(ph,strcat(base_file_name,'_uplift_contours.png'));

figure;
ph=pcolor(uplift_contours);
hold on;
set(ph,'linestyle','none');
colorbar;
title('Uplift From Brandon et al. 1998');
saveas(ph,strcat(base_file_name,'_uplift_contours2.png'));

%============================================================
%Clean-up
%============================================================
clear directory_name base_file_name_list entry base_file_name topo_temp
clear t_temp x_11 x_09 x_07 x_05 x_03 x y_11 y_09 y_07 y_05 y_03 y i
clear x y x_11_rot x_09_rot x_07_rot x_05_rot x_03_rot y_11_rot
clear y_09_rot y_07_rot y_05_rot y_03_rot contour11 contour09 contour07
clear contour05 contour03 contours XI YI

end;
```

Ice_Duration.m

```
%File for taking the ice thickness and determining how often each cell
is covered by ice

%==========
%Get the names of datasets to process
directory_name=input('Location of data folders: ','s');
base_file_name_list=textread(strcat(directory_name,'/',input('File of
      base names of data to process (batch log file): ','s')),'%s');

%Begin loop to process all files
for entry=1:size(base_file_name_list)

%Get the base file name from the list
base_file_name=strcat(directory_name,'/',base_file_name_list{entry},'/'
      ,base_file_name_list{entry});

%Load the ice locations and topo data, using the base name
longtopo_temp=load(strcat(base_file_name,'_long_topo.out'),'-ascii');
longdenud_temp=load(strcat(base_file_name,'_long_DENUD.out'),'-ascii');
%==========

%=====================================================
%Cut the long files into the timesteps
%=====================================================
%Cut the long_topo file into each of the timestep pieces
filesize1 = size (longtopo_temp);
a = filesize1(1,1);
aa = a/27225;
x=1;
for n = 1:aa
    SS_str = ['SS_topo',int2str(n),'=longtopo_temp(x:x+27224,:);'];
    eval(SS_str);
    x = x+27225;
end

%==========
%Create the colorbar to use in the plots (this is based off of the
default
%'jet' but adds gray to the bottom or 0 value)
%==========
map=[0.5,0.5,0.5;0,0,0.625;0,0,0.6875;0,0,0.75;0,0,0.8125;0,0,0.875;0,0
      ,0.9375;0,0,1;0,0.0625,1;0,0.125,1;0,0.1875,1;0,0.25,1;0,0.3125,1
      ;0,0.375,1;0,0.4375,1;0,0.5,1;0,0.5625,1;0,0.625,1;0,0.6875,1;0,0
      .75,1;0,0.8125,1;0,0.875,1;0,0.9375,1;0,1,1;0.0625,1,0.9375;0.125
      ,1,0.875;0.1875,1,0.8125;0.25,1,0.75;0.3125,1,0.6875;0.375,1,0.62
      5;0.4375,1,0.5625;0.5,1,0.5;0.5625,1,0.4375;0.625,1,0.375;0.6875,
      1,0.3125;0.75,1,0.25;0.8125,1,0.1875;0.875,1,0.125;0.9375,1,0.062
      5;1,1,0;1,0.9375,0;1,0.875,0;1,0.8125,0;1,0.75,0;1,0.6875,0;1,0.6
      25,0;1,0.5625,0;1,0.5,0;1,0.4375,0;1,0.375,0;1,0.3125,0;1,0.25,0;
      1,0.1875,0;1,0.125,0;1,0.0625,0;1,0,0;0.9375,0,0;0.875,0,0;0.8125
      ,0,0;0.75,0,0;0.6875,0,0;0.625,0,0;0.5625,0,0;0.5,0,0;];

%==========
%Set colorbar for ice thickness plots
```

```
%==========
ice_thick_min=min(min(longtopo_temp(:,5)))
ice_thick_max=max(max(longtopo_temp(:,5)))

%=================================================================
%I. Reshape ice_thickness to be a 165*165 grid
%=================================================================
topo_ss1=reshape(SS_topo1(:,5),165,165);
topo_ss2=reshape(SS_topo2(:,5),165,165);
topo_ss3=reshape(SS_topo3(:,5),165,165);
topo_ss4=reshape(SS_topo4(:,5),165,165);
topo_ss5=reshape(SS_topo5(:,5),165,165);
topo_ss6=reshape(SS_topo6(:,5),165,165);
topo_ss7=reshape(SS_topo7(:,5),165,165);
topo_ss8=reshape(SS_topo8(:,5),165,165);
topo_ss9=reshape(SS_topo9(:,5),165,165);
topo_ss10=reshape(SS_topo10(:,5),165,165);

%Determine how often each cell is covered
ice_covered_ss1 = zeros(165,165);
ice_covered_ss2 = zeros(165,165);
ice_covered_ss3 = zeros(165,165);
ice_covered_ss4 = zeros(165,165);
ice_covered_ss5 = zeros(165,165);
ice_covered_ss6 = zeros(165,165);
ice_covered_ss7 = zeros(165,165);
ice_covered_ss8 = zeros(165,165);
ice_covered_ss9 = zeros(165,165);
ice_covered_ss10 = zeros(165,165);

for i=1:165
    for j=1:165
        if topo_ss1(i,j)>0 ice_covered_ss1(i,j)=1;
        end
        if topo_ss2(i,j)>0 ice_covered_ss2(i,j)=1;
        end
        if topo_ss3(i,j)>0 ice_covered_ss3(i,j)=1;
        end
        if topo_ss4(i,j)>0 ice_covered_ss4(i,j)=1;
        end
        if topo_ss5(i,j)>0 ice_covered_ss5(i,j)=1;
        end
        if topo_ss6(i,j)>0 ice_covered_ss6(i,j)=1;
        end
        if topo_ss7(i,j)>0 ice_covered_ss7(i,j)=1;
        end
        if topo_ss8(i,j)>0 ice_covered_ss8(i,j)=1;
        end
        if topo_ss9(i,j)>0 ice_covered_ss9(i,j)=1;
        end
        if topo_ss10(i,j)>0 ice_covered_ss10(i,j)=1;
        end
    end
end

total_ice_covered=ice_covered_ss1+ice_covered_ss2+ice_covered_ss3+ice_c
```

```
      overed_ss4+ice_covered_ss5+ice_covered_ss6+ice_covered_ss7+ice_co
      vered_ss8+ice_covered_ss9+ice_covered_ss10;

figure;
ph=pcolor(total_ice_covered);
hold on;
set(ph,'linestyle','none');
colormap(map);
colorbar;
title('Duration of Ice Coverage');

figure;
ph=contour(total_ice_covered);
colormap(map);
colorbar;
title('Duration of Ice Coverage');

%====================
%Clean-up
%====================
clear directory_name base_file_name_list entry base_file_name
clear longtopo_temp longdenud_temp filesize1 a aa x n SS_str
clear filesize3 ice_thick_min ice_thick_max topo_ss1 topo_ss2
clear topo_ss3 topo_ss4 topo_ss5 topo_ss6 topo_ss7 topo_ss8
clear topo_ss9 topo_ss10 ice_covered_ss1 ice_covered_ss2
clear ice_covered_ss3 ice_covered_ss4 ice_covered_ss5 ice_covered_ss6
clear ice_covered_ss7 ice_covered_ss8 ice_covered_ss9
clear ice_covered_ss10 SS_topo1 SS_topo2 SS_topo3 SS_topo4 SS_topo5
clear SS_topo6 SS_topo7 SS_topo8 SS_topo9 SS_topo10

end;
```

upliftandicecover.m

```
%File for plotting the Uplift Against the Ice Cover
%note - need to have total_ice_covered and uplift_contours

icecover = reshape(total_ice_covered,165*165,1);
upliftvector = reshape(uplift_contours,165*165,1);
index = find(isfinite(upliftvector));
useme(:,1) = icecover(index);
useme(:,2) = upliftvector(index);

for i=1:8,
    use=find(useme(:,1)==i);
   uplift025(i)=quantile(useme(use,2),0.025);
   uplift25(i)=quantile(useme(use,2),.25);
   uplift50(i)=mean(useme(use,2));
   uplift75(i)=quantile(useme(use,2),.75);
   uplift975(i)=quantile(useme(use,2),.975);
end

use_1=find(useme(:,1)==1);
use_2=find(useme(:,1)==2);
use_3=find(useme(:,1)==3);
use_4=find(useme(:,1)==4);
use_5=find(useme(:,1)==5);
use_6=find(useme(:,1)==6);
use_7=find(useme(:,1)==7);
use_8=find(useme(:,1)==8);

figure;
plot(reshape(total_ice_covered,165*165,1),reshape(uplift_contours,165*1
65,1),'*');
title('Ice Duration vs. Uplift From Contours');
xlabel('Ice Duration (kyr)');
ylabel('Uplift (mm/yr)');

figure;
y=hist(icecover,9);
hist(icecover);
%figure(gcf);

figure;
plot(uplift50,[1:1:8],'b*')
hold on;
%plot(uplift025,[1:1:8],'*r');
%plot(uplift975,[1:1:8],'*r');
plot(uplift75,[1:1:8],'*g');
plot(uplift25,[1:1:8],'*g');
title('Average Ice Duration vs. Uplift From Contours with Std. Dev.');
xlabel('Uplift (mm/yr)');
ylabel('Ice Duration (kyr)');

%Get R^2
mean_icecover=mean(useme(:,1));
mean_upliftvector=mean(useme(:,2));
```

```
sum_x=(useme(:,1)-(mean_icecover));
sum_y=(useme(:,2)-(mean_upliftvector));

top=sum(sum_x.*sum_y);
bottom_1=sum((sum_x).^2);
bottom_2=sum((sum_y).^2);

r_squared=(top^2)/(bottom_1*bottom_2);

%=================
%Clean-up
%=================
clear icecover upliftvector index useme i use uplift025 uplift25
clear uplift50 uplift75 uplift975 mean_icecover mean_upliftvector
clear sum_x sum_y top bottom_1 bottom_2
```

Hoh_River_Profile_Kg.m

```
%File for determining the l and Kg values for the Hoh River Profile

%==========
%Get the names of datasets to process
directory_name=input('Location of data folders: ','s');
base_file_name_list=textread(strcat(directory_name,'/',input('File of
      base names of data to process (batch log file): ','s')),'%s');

%Begin loop to process all files
for entry=1:size(base_file_name_list)

%Get the base file name from the list
base_file_name=strcat(directory_name,'/',base_file_name_list{entry},'/'
      ,base_file_name_list{entry});

%Load the ice locations and topo data, using the base name
longice_loc_temp=load(strcat(base_file_name,'_long_ice_locat.out'),'-
      ascii');
longerosion_temp=load(strcat(base_file_name,'_long_erosion.out'),'-
      ascii');
longtopo_temp=load(strcat(base_file_name,'_long_topo.out'),'-ascii');
longglac_temp=load(strcat(base_file_name,'_long_glac.out'),'-ascii');
longdenud_temp=load(strcat(base_file_name,'_long_DENUD.out'),'-ascii');
%==========

%====================================================
%Cut the long files into the timesteps
%====================================================
%Cut the long_topo file into each of the timestep pieces
filesize1 = size (longtopo_temp);
a = filesize1(1,1);
aa = a/27225;
x=1;
for n = 1:aa
    SS_str = ['SS_topo',int2str(n),'=longtopo_temp(x:x+27224,:);'];
    eval(SS_str);
    x = x+27225;
end

%Cut the long_erosion file into each of the timestep pieces
filesize2 = size (longerosion_temp);
a = filesize2(1,1);
aa = a/27225;
x=1;
for n = 1:aa
    SS_str=['SS_erosion',int2str(n),'=longerosion_temp(x:x+27224,:);'];
    eval(SS_str);
    x = x+27225;
end

%Cut the long_DENUD file into each of the timestep pieces
filesize3 = size (longdenud_temp);
a = filesize3(1,1);
aa = a/27225;
```

```
x = 1;
for n = 1:aa
    SS_str = ['SS_denud',int2str(n),'=longdenud_temp(x:x+27224,:);'];
    eval(SS_str);
    x = x+27225;
end

%Cut the long_glac file into each of the timestep pieces
filesize2 = size (longglac_temp);
a = filesize2(1,1);
aa = a/27225;
x=1;
for n = 1:aa
    SS_str = ['SS_glac',int2str(n),'=longglac_temp(x:x+27224,:);'];
    eval(SS_str);
    x = x+27225;
end

%Reshape the files so the necessary data can be used
topo_ss1=reshape(SS_topo1(:,3),165,165);
topo_ss2=reshape(SS_topo2(:,3),165,165);
topo_ss3=reshape(SS_topo3(:,3),165,165);
topo_ss4=reshape(SS_topo4(:,3),165,165);
topo_ss5=reshape(SS_topo5(:,3),165,165);
topo_ss6=reshape(SS_topo6(:,3),165,165);
topo_ss7=reshape(SS_topo7(:,3),165,165);
topo_ss8=reshape(SS_topo8(:,3),165,165);
topo_ss9=reshape(SS_topo9(:,3),165,165);
topo_ss10=reshape(SS_topo10(:,3),165,165);

ice_thick_ss1=reshape(SS_topo1(:,5),165,165);
ice_thick_ss2=reshape(SS_topo2(:,5),165,165);
ice_thick_ss3=reshape(SS_topo3(:,5),165,165);
ice_thick_ss4=reshape(SS_topo4(:,5),165,165);
ice_thick_ss5=reshape(SS_topo5(:,5),165,165);
ice_thick_ss6=reshape(SS_topo6(:,5),165,165);
ice_thick_ss7=reshape(SS_topo7(:,5),165,165);
ice_thick_ss8=reshape(SS_topo8(:,5),165,165);
ice_thick_ss9=reshape(SS_topo9(:,5),165,165);
ice_thick_ss10=reshape(SS_topo10(:,5),165,165);

total_erosion_ss1=reshape(SS_denud1(:,3),165,165);
total_erosion_ss2=reshape(SS_denud2(:,3),165,165);
total_erosion_ss3=reshape(SS_denud3(:,3),165,165);
total_erosion_ss4=reshape(SS_denud4(:,3),165,165);
total_erosion_ss5=reshape(SS_denud5(:,3),165,165);
total_erosion_ss6=reshape(SS_denud6(:,3),165,165);
total_erosion_ss7=reshape(SS_denud7(:,3),165,165);
total_erosion_ss8=reshape(SS_denud8(:,3),165,165);
total_erosion_ss9=reshape(SS_denud9(:,3),165,165);
total_erosion_ss10=reshape(SS_denud10(:,3),165,165);

sliding_ss1=reshape(SS_glac1(:,5),165,165);
sliding_ss2=reshape(SS_glac2(:,5),165,165);
sliding_ss3=reshape(SS_glac3(:,5),165,165);
sliding_ss4=reshape(SS_glac4(:,5),165,165);
```

```
sliding_ss5=reshape(SS_glac5(:,5),165,165);
sliding_ss6=reshape(SS_glac6(:,5),165,165);
sliding_ss7=reshape(SS_glac7(:,5),165,165);
sliding_ss8=reshape(SS_glac8(:,5),165,165);
sliding_ss9=reshape(SS_glac9(:,5),165,165);
sliding_ss10=reshape(SS_glac10(:,5),165,165);


%IIII. Make uplift a 165x165 grid
new_uplift=uplift(1:165,1:165);

%X Distance for Longitudinal Profile
Hoh_longitudinalprofile_x_full=[78.58114405;77.58114405;76.58114405;74.
      58114405;73.58114405;72.16693049;71.16693049;68.93086251;67.51664
      895;66.10243539;64.68822182;63.68822182;60.8597947;59.8597947;55.
      61715401;54.61715401;53.61715401;52.61715401;51.61715401;50.61715
      401;49.20294045;47.20294045;46.20294045;45.20294045;43.20294045;4
      2.20294045;40.78872689;39.78872689;38.78872689;36.55265891;35.138
      44535;33.72423179;32.72423179;30.48816381;29.48816381;27.48816381
      ;26.48816381;25.48816381;24.48816381;20.36505818;19.36505818;18.3
      6505818;17.36505818;15.1289902;14.1289902;11.89292223;8.892922227
      ;7.478708665;6.064495102;3.828427125;2.414213562;1.414213562;0];

%Hoh_longitudinalprofile_x=[60.8597947;59.8597947;55.61715401;
%    54.61715401;53.61715401;52.61715401;51.61715401;50.61715401;
%    49.20294045;47.20294045;46.20294045;45.20294045;43.20294045;
%    42.20294045;40.78872689;39.78872689;38.78872689;36.55265891;
%    35.13844535;33.72423179;32.72423179;30.48816381;29.48816381;
%    27.48816381;26.48816381;25.48816381;24.48816381;20.36505818;
%    19.36505818;18.36505818;17.36505818;15.1289902;14.1289902;
%    11.89292223;8.892922227;7.478708665;6.064495102;3.828427125;
%    2.414213562;1.414213562;0];

%This does not have the outlier
Hoh_longitudinalprofile_x=[60.8597947;59.8597947;55.61715401;
    54.61715401;53.61715401;52.61715401;51.61715401;50.61715401;
    49.20294045;47.20294045;46.20294045;45.20294045;43.20294045;
    42.20294045;40.78872689;39.78872689;38.78872689;36.55265891;
    35.13844535;33.72423179;32.72423179;30.48816381;29.48816381;
    27.48816381;26.48816381;25.48816381;24.48816381;20.36505818;
    19.36505818;18.36505818;17.36505818;15.1289902;14.1289902;
    11.89292223;8.892922227;6.064495102;3.828427125;
    2.414213562;1.414213562;0];

%Coordinates of Profile
%Full has zeros in sliding and uplift still present in it
Hoh_x_full=[89;89;89;89;89;88;88;89;90;91;92;92;94;94;97;97;97;97;97;97
      ;96;96;96;96;96;96;97;97;97;98;99;100;100;102;102;102;102;102;102
      ;103;103;103;103;104;104;103;103;102;101;99;98;97;96];

Hoh_y_full=[22;23;24;26;27;28;29;31;32;33;34;35;37;38;41;42;43;44;45;46
      ;47;49;50;51;53;54;55;56;57;59;60;61;62;63;64;66;67;68;69;73;74;7
      5;76;78;79;81;84;85;86;87;86;86;85];

%THIS INCLUDES THE OUTLIER POINT # IN THE LOWER VALLEY WITH MEASURED
```

```
%UPLIFT 6 AND BIG BIG SLIDING AT TIME 10
%Hoh_x=[94;94;97;97;97;97;97;97;96;96;96;96;96;96;97;97;97;98;99;
%    100;100;102;102;102;102;102;102;103;103;103;103;104;104;103;
%    103;102;101;99;98;97;96];

%Hoh_y=[37;38;41;42;43;44;45;46;47;49;50;51;53;54;55;56;57;59;60;
%    61;62;63;64;66;67;68;69;73;74;75;76;78;79;81;84;85;86;87;86;
%    86;85];

%These do not have the Outlier
Hoh_x=[94;94;97;97;97;97;97;97;96;96;96;96;96;96;97;97;97;98;99;
    100;100;102;102;102;102;102;102;103;103;103;103;104;104;103;
    103;101;99;98;97;96];

Hoh_y=[37;38;41;42;43;44;45;46;47;49;50;51;53;54;55;56;57;59;60;
    61;62;63;64;66;67;68;69;73;74;75;76;78;79;81;84;86;87;86;86;85];


Hoh_topography_10_full=zeros(length(Hoh_x_full),1);
Hoh_uplift_old_10_full=zeros(length(Hoh_x_full),1);
Hoh_uplift_contours_10_full=zeros(length(Hoh_x_full),1);
Hoh_ice_thick_10_full=zeros(length(Hoh_x_full),1);
Hoh_sliding_velocity_10_full=zeros(length(Hoh_x_full),1);
Hoh_total_erosion_10_full=zeros(length(Hoh_x_full),1);

Hoh_topography_10=zeros(length(Hoh_x),1);
Hoh_uplift_old_10=zeros(length(Hoh_x),1);
Hoh_uplift_contours_10=zeros(length(Hoh_x),1);
Hoh_ice_thick_10=zeros(length(Hoh_x),1);
Hoh_sliding_velocity_10=zeros(length(Hoh_x),1);
Hoh_total_erosion_10=zeros(length(Hoh_x),1);


for i=1:length(Hoh_x_full)
    Hoh_topography_10_full(i,1)=topo_ss10(Hoh_x_full(i),Hoh_y_full(i));
end

for i=1:length(Hoh_x_full)
   Hoh_uplift_old_10_full(i,1)=new_uplift(Hoh_x_full(i),Hoh_y_full(i));
end

for i=1:length(Hoh_x_full)
Hoh_uplift_contours_10_full(i,1)=uplift_contours(Hoh_x_full(i),Hoh_y_fu
      ll(i));
end

for i=1:length(Hoh_x_full)
Hoh_ice_thick_10_full(i,1)=ice_thick_ss10(Hoh_x_full(i),Hoh_y_full(i));
end

for i=1:length(Hoh_x_full)
Hoh_sliding_velocity_10_full(i,1)=sliding_ss10(Hoh_x_full(i),Hoh_y_full
      (i));
end
```

```
for i=1:length(Hoh_x_full)
Hoh_total_erosion_10_full(i,1)=total_erosion_ss10(Hoh_x_full(i),Hoh_y_f
      ull(i));
end



for i=1:length(Hoh_x)
       Hoh_topography_10(i,1)=topo_ss10(Hoh_x(i),Hoh_y(i));
end

for i=1:length(Hoh_x)
       Hoh_uplift_old_10(i,1)=new_uplift(Hoh_x(i),Hoh_y(i));
end

for i=1:length(Hoh_x)
       Hoh_uplift_contours_10(i,1)=uplift_contours(Hoh_x(i),Hoh_y(i));
end

for i=1:length(Hoh_x)
       Hoh_ice_thick_10(i,1)=ice_thick_ss10(Hoh_x(i),Hoh_y(i));
end

for i=1:length(Hoh_x)
       Hoh_sliding_velocity_10(i,1)=sliding_ss10(Hoh_x(i),Hoh_y(i));
end

for i=1:length(Hoh_x)
       Hoh_total_erosion_10(i,1)=total_erosion_ss10(Hoh_x(i),Hoh_y(i));
end


b=isnan(Hoh_uplift_contours_10_full);
Hoh_uplift_contours_10_full(b)=0;

%Plot the Profiles together
figure;
ph=plot(Hoh_longitudinalprofile_x_full,Hoh_topography_10_full,'g*-');
hold on;
plot(Hoh_longitudinalprofile_x_full,Hoh_uplift_old_10_full,'c*-');
plot(Hoh_longitudinalprofile_x_full,Hoh_uplift_contours_10_full,'b*-');
plot(Hoh_longitudinalprofile_x_full,Hoh_ice_thick_10_full,'m*-');
plot(Hoh_longitudinalprofile_x_full,Hoh_sliding_velocity_10_full,'r*-
      ');
plot(Hoh_longitudinalprofile_x_full,Hoh_total_erosion_10_full,'y*-');
title('Longitudinal Profile of the Hoh River Full Length');
xlabel('Distance (km)');
legend('Topography','Old Uplift','Uplift from Brandon et al','Ice
Thickness','Sliding Velocity','Total Erosion','Location','NorthEast');
legend('boxoff');
saveas(ph,strcat(base_file_name,'_fullprofile.png'));

figure;
```

```
ph=plot(Hoh_longitudinalprofile_x,Hoh_topography_10,'g*-');
hold on;
plot(Hoh_longitudinalprofile_x,Hoh_uplift_old_10,'c*-');
plot(Hoh_longitudinalprofile_x,Hoh_uplift_contours_10,'b*-');
plot(Hoh_longitudinalprofile_x,Hoh_ice_thick_10,'m*-');
plot(Hoh_longitudinalprofile_x,Hoh_sliding_velocity_10,'r*-');
plot(Hoh_longitudinalprofile_x,Hoh_total_erosion_10,'y*-');
title('Longitudinal Profile of the Hoh River, No Zeros');
xlabel('Distance (km)');
legend('Topography','Old Uplift','Uplift from Brandon et al','Ice
Thickness','Sliding Velocity','Total Erosion','Location','NorthEast');
legend('boxoff');
saveas(ph,strcat(base_file_name,'_shortprofile.png'));


%Turn total erosion into a rate so it can be plotted with uplift
%Hoh_totalerosion_rate_full=Hoh_total_erosion_10_full*1000/10000;
%Hoh_totalerosion_rate=Hoh_total_erosion_10*1000/10000;
Hoh_uplift_meters=(Hoh_uplift_contours_10(:,1)).*10000./1000;


%Plot the Total Erosion, Uplifts, and Sliding Velocity together
figure;
ph=plot(Hoh_longitudinalprofile_x_full,Hoh_uplift_contours_10_full,'b-
      ');
hold on;
plot(Hoh_longitudinalprofile_x_full,Hoh_uplift_old_10_full,'c-');
plot(Hoh_longitudinalprofile_x_full,Hoh_totalerosion_rate_full,'r-');
title('Longitudinal Profile of the Hoh River Full Length');
xlabel('Distance (km)');
ylabel('Average Uplift or Erosion Rate (mm/yr)');
legend('Uplift from Brandon et al','Old Uplift','Total
      Erosion','Location','NorthEast');
legend('boxoff');
saveas(ph,strcat(base_file_name,'_fullupliftsliding.png'));

figure;
ph=plot(Hoh_longitudinalprofile_x,Hoh_uplift_contours_10,'b-');
hold on;
plot(Hoh_longitudinalprofile_x,Hoh_uplift_old_10,'c-');
plot(Hoh_longitudinalprofile_x,Hoh_totalerosion_rate,'r-');
title('Longitudinal Profile of the Hoh River');
xlabel('Distance (km)');
ylabel('Average Uplift or Erosion Rate (mm/yr)');
legend('Uplift from Brandon et al','Old Uplift','Total
      Erosion','Location','NorthEast');
legend('boxoff');
saveas(ph,strcat(base_file_name,'_shortupliftsliding.png'));


%Plot the Erosion Against the Uplift
figure;
ph=plot(Hoh_total_erosion_10,Hoh_uplift_meters,'b*');
title('Erosion Rate vs. Uplift Rate');
xlabel('Erosion Rate');
ylabel('Uplift Rate');
```

```
saveas(ph,strcat(base_file_name,'_erosionvsuplift.png'));

figure;
ph=plot(Hoh_longitudinalprofile_x,Hoh_total_erosion_10,'g*-');
hold on;
plot(Hoh_longitudinalprofile_x,Hoh_uplift_meters,'b-');
title('Erosion Rate and Contoured Uplift');
xlabel('Distance Along the Hoh River (km)');
ylabel('Uplift or Erosion (m)');
legend('Erosion','Uplift','Location','NorthEast');
legend('boxoff');
saveas(ph,strcat(base_file_name,'_erosionvsuplift2.png'));


%Get R^2
mean_Hoh_uplift_meters=mean(Hoh_uplift_meters);
mean_Hoh_total_erosion=mean(Hoh_total_erosion_10);
sum_x=(Hoh_uplift_meters-(mean_Hoh_uplift_meters));
sum_y_erosion=(Hoh_total_erosion_10-(mean_Hoh_total_erosion));
top_erosion=sum(sum_x.*sum_y_erosion);
bottom_1=sum((sum_x).^2);
bottom_2_erosion=sum((sum_y_erosion).^2);
r_squared_erosion=(top_erosion^2)/(bottom_1*bottom_2_erosion);


%Determine kg for the profile
%I. For l=1; Kg=(uplift rate/1000)/total erosion
Hoh_sum_uplift=sum(Hoh_uplift_contours_10(:,1));
Hoh_sum_totalerosion=sum(Hoh_total_erosion_10(:,1));

Kg_l_1=((Hoh_sum_uplift)/1000)/(Hoh_sum_totalerosion);

%Now do for varying l from 0.1-2
%II. Get sliding for each timestep
Hoh_sliding_velocity_1=zeros(length(Hoh_x),1);
Hoh_sliding_velocity_2=zeros(length(Hoh_x),1);
Hoh_sliding_velocity_3=zeros(length(Hoh_x),1);
Hoh_sliding_velocity_4=zeros(length(Hoh_x),1);
Hoh_sliding_velocity_5=zeros(length(Hoh_x),1);
Hoh_sliding_velocity_6=zeros(length(Hoh_x),1);
Hoh_sliding_velocity_7=zeros(length(Hoh_x),1);
Hoh_sliding_velocity_8=zeros(length(Hoh_x),1);
Hoh_sliding_velocity_9=zeros(length(Hoh_x),1);
Hoh_sliding_velocity_10=zeros(length(Hoh_x),1);

%III. Pull the sliding for the profile
for i=1:length(Hoh_x)
       Hoh_sliding_velocity_1(i,1)=sliding_ss1(Hoh_x(i),Hoh_y(i));
end

for i=1:length(Hoh_x)
       Hoh_sliding_velocity_2(i,1)=sliding_ss2(Hoh_x(i),Hoh_y(i));
end

for i=1:length(Hoh_x)
```

```
       Hoh_sliding_velocity_3(i,1)=sliding_ss3(Hoh_x(i),Hoh_y(i));
end

for i=1:length(Hoh_x)
       Hoh_sliding_velocity_4(i,1)=sliding_ss4(Hoh_x(i),Hoh_y(i));
end

for i=1:length(Hoh_x)
       Hoh_sliding_velocity_5(i,1)=sliding_ss5(Hoh_x(i),Hoh_y(i));
end

for i=1:length(Hoh_x)
       Hoh_sliding_velocity_6(i,1)=sliding_ss6(Hoh_x(i),Hoh_y(i));
end

for i=1:length(Hoh_x)
       Hoh_sliding_velocity_7(i,1)=sliding_ss7(Hoh_x(i),Hoh_y(i));
end

for i=1:length(Hoh_x)
       Hoh_sliding_velocity_8(i,1)=sliding_ss8(Hoh_x(i),Hoh_y(i));
end

for i=1:length(Hoh_x)
       Hoh_sliding_velocity_9(i,1)=sliding_ss9(Hoh_x(i),Hoh_y(i));
end

for i=1:length(Hoh_x)
       Hoh_sliding_velocity_10(i,1)=sliding_ss10(Hoh_x(i),Hoh_y(i));
end

%IV. Need total uplift
Hoh_uplift_meters=(Hoh_uplift_contours_10(:,1)).*10000./1000;
Hoh_total_uplift=sum((Hoh_uplift_meters(:,1)));

%V. Now use for loop to calculate for all different values of l
for n=1:20
     l=n/10;
     Kg(n)=Hoh_total_uplift/(sum(1000*((Hoh_sliding_velocity_1).^l +
      (Hoh_sliding_velocity_2).^l + (Hoh_sliding_velocity_3).^l +
      (Hoh_sliding_velocity_4).^l + (Hoh_sliding_velocity_5).^l +
      (Hoh_sliding_velocity_6).^l + (Hoh_sliding_velocity_7).^l +
      (Hoh_sliding_velocity_8).^l + (Hoh_sliding_velocity_9).^l +
      (Hoh_sliding_velocity_10).^l)));
end

Kg_0=Hoh_total_uplift/(sum(1000*((Hoh_sliding_velocity_1).^0 +
      (Hoh_sliding_velocity_2).^0 + (Hoh_sliding_velocity_3).^0 +
      (Hoh_sliding_velocity_4).^0 + (Hoh_sliding_velocity_5).^0 +
      (Hoh_sliding_velocity_6).^0 + (Hoh_sliding_velocity_7).^0 +
      (Hoh_sliding_velocity_8).^0 + (Hoh_sliding_velocity_9).^0 +
      (Hoh_sliding_velocity_10).^0)));

%VI. Now make misfit table
Hoh_sliding_matrix=zeros(20,length(Hoh_x));
```

```
Hoh_predicted_uplift=zeros(length(Hoh_x),20);

for n=0:20;
    l=n/10;
    Hoh_predicted_uplift(:,n)=(((Hoh_sliding_velocity_1).^l +
      (Hoh_sliding_velocity_2).^l + (Hoh_sliding_velocity_3).^l +
      (Hoh_sliding_velocity_4).^l + (Hoh_sliding_velocity_5).^l +
      (Hoh_sliding_velocity_6).^l + (Hoh_sliding_velocity_7).^l +
      (Hoh_sliding_velocity_8).^l + (Hoh_sliding_velocity_9).^l +
      (Hoh_sliding_velocity_10).^l)).*Kg(n).*1000;
end

Hoh_predicted_uplift_0=(((Hoh_sliding_velocity_1).^0 +
      (Hoh_sliding_velocity_2).^0 + (Hoh_sliding_velocity_3).^0 +
      (Hoh_sliding_velocity_4).^0 + (Hoh_sliding_velocity_5).^0 +
      (Hoh_sliding_velocity_6).^0 + (Hoh_sliding_velocity_7).^0 +
      (Hoh_sliding_velocity_8).^0 + (Hoh_sliding_velocity_9).^0 +
      (Hoh_sliding_velocity_10).^0)).*Kg_0.*1000;

Hoh_predicted_uplift_0=(((Hoh_sliding_velocity_1).^0 +
      (Hoh_sliding_velocity_2).^0 + (Hoh_sliding_velocity_3).^0 +
      (Hoh_sliding_velocity_4).^0 + (Hoh_sliding_velocity_5).^0 +
      (Hoh_sliding_velocity_6).^0 + (Hoh_sliding_velocity_7).^0 +
      (Hoh_sliding_velocity_8).^0 + (Hoh_sliding_velocity_9).^0 +
      (Hoh_sliding_velocity_10).^0)).*(6.2375*10^(-4)).*1000;

%VII. Check misfits
m=[0;1;2;3;4;5;6;7;8;9;10;11;12];

figure;
ph=plot(Hoh_uplift_meters,Hoh_predicted_uplift_0,'b*');
hold on;
plot(m,m,'g-');
title('Predicted vs. Total Uplift for l=0');
xlabel('Total Uplift');
ylabel('Predicted Uplift');
legend('Uplift vs. Pred. Uplift','1-1 Line','Location','Best');
legend('boxoff');
saveas(ph,strcat(base_file_name,'_upliftmisfit_l_00.png'));

figure;
ph=plot(Hoh_uplift_meters,Hoh_predicted_uplift(:,1),'b*');
hold on;
plot(m,m,'g-');
title('Predicted vs. Total Uplift for l=0.1');
xlabel('Total Uplift');
ylabel('Predicted Uplift');
legend('Uplift vs. Pred. Uplift','1-1 Line','Location','Best');
legend('boxoff');
saveas(ph,strcat(base_file_name,'_upliftmisfit_l_01.png'));

figure;
ph=plot(Hoh_uplift_meters,Hoh_predicted_uplift(:,2),'b*');
hold on;
plot(m,m,'g-');
```

```
title('Predicted vs. Total Uplift for l=0.2');
xlabel('Total Uplift');
ylabel('Predicted Uplift');
legend('Uplift vs. Pred. Uplift','1-1 Line','Location','Best');
legend('boxoff');
saveas(ph,strcat(base_file_name,'_upliftmisfit_l_02.png'));

figure;
ph=plot(Hoh_uplift_meters,Hoh_predicted_uplift(:,3),'b*');
hold on;
plot(m,m,'g-');
title('Predicted vs. Total Uplift for l=0.3');
xlabel('Total Uplift');
ylabel('Predicted Uplift');
legend('Uplift vs. Pred. Uplift','1-1 Line','Location','Best');
legend('boxoff');
saveas(ph,strcat(base_file_name,'_upliftmisfit_l_03.png'));

figure;
ph=plot(Hoh_uplift_meters,Hoh_predicted_uplift(:,4),'b*');
hold on;
plot(m,m,'g-');
title('Predicted vs. Total Uplift for l=0.4');
xlabel('Total Uplift');
ylabel('Predicted Uplift');
legend('Uplift vs. Pred. Uplift','1-1 Line','Location','Best');
legend('boxoff');
saveas(ph,strcat(base_file_name,'_upliftmisfit_l_04.png'));

figure;
ph=plot(Hoh_uplift_meters,Hoh_predicted_uplift(:,5),'b*');
hold on;
plot(m,m,'g-');
title('Predicted vs. Total Uplift for l=0.5');
xlabel('Total Uplift');
ylabel('Predicted Uplift');
legend('Uplift vs. Pred. Uplift','1-1 Line','Location','Best');
legend('boxoff');
saveas(ph,strcat(base_file_name,'_upliftmisfit_l_05.png'));

figure;
ph=plot(Hoh_uplift_meters,Hoh_predicted_uplift(:,6),'b*');
hold on;
plot(m,m,'g-');
title('Predicted vs. Total Uplift for l=0.6');
xlabel('Total Uplift');
ylabel('Predicted Uplift');
legend('Uplift vs. Pred. Uplift','1-1 Line','Location','Best');
legend('boxoff');
saveas(ph,strcat(base_file_name,'_upliftmisfit_l_06.png'));

figure;
ph=plot(Hoh_uplift_meters,Hoh_predicted_uplift(:,7),'b*');
hold on;
plot(m,m,'g-');
title('Predicted vs. Total Uplift for l=0.7');
```

```
xlabel('Total Uplift');
ylabel('Predicted Uplift');
legend('Uplift vs. Pred. Uplift','1-1 Line','Location','Best');
legend('boxoff');
saveas(ph,strcat(base_file_name,'_upliftmisfit_l_07.png'));

figure;
ph=plot(Hoh_uplift_meters,Hoh_predicted_uplift(:,8),'b*');
hold on;
plot(m,m,'g-');
title('Predicted vs. Total Uplift for l=0.8');
xlabel('Total Uplift');
ylabel('Predicted Uplift');
legend('Uplift vs. Pred. Uplift','1-1 Line','Location','Best');
legend('boxoff');
saveas(ph,strcat(base_file_name,'_upliftmisfit_l_08.png'));

figure;
ph=plot(Hoh_uplift_meters,Hoh_predicted_uplift(:,9),'b*');
hold on;
plot(m,m,'g-');
title('Predicted vs. Total Uplift for l=0.9');
xlabel('Total Uplift');
ylabel('Predicted Uplift');
legend('Uplift vs. Pred. Uplift','1-1 Line','Location','Best');
legend('boxoff');
saveas(ph,strcat(base_file_name,'_upliftmisfit_l_09.png'));

figure;
ph=plot(Hoh_uplift_meters,Hoh_predicted_uplift(:,10),'b*');
hold on;
plot(m,m,'g-');
title('Predicted vs. Total Uplift for l=1.0');
xlabel('Total Uplift');
ylabel('Predicted Uplift');
legend('Uplift vs. Pred. Uplift','1-1 Line','Location','Best');
legend('boxoff');
saveas(ph,strcat(base_file_name,'_upliftmisfit_l_10.png'));

figure;
ph=plot(Hoh_uplift_meters,Hoh_predicted_uplift(:,11),'b*');
hold on;
plot(m,m,'g-');
title('Predicted vs. Total Uplift for l=1.1');
xlabel('Total Uplift');
ylabel('Predicted Uplift');
legend('Uplift vs. Pred. Uplift','1-1 Line','Location','Best');
legend('boxoff');
saveas(ph,strcat(base_file_name,'_upliftmisfit_l_11.png'));

figure;
ph=plot(Hoh_uplift_meters,Hoh_predicted_uplift(:,12),'b*');
hold on;
plot(m,m,'g-');
title('Predicted vs. Total Uplift for l=1.2');
xlabel('Total Uplift');
```

```
ylabel('Predicted Uplift');
legend('Uplift vs. Pred. Uplift','1-1 Line','Location','Best');
legend('boxoff');
saveas(ph,strcat(base_file_name,'_upliftmisfit_l_12.png'));

figure;
ph=plot(Hoh_uplift_meters,Hoh_predicted_uplift(:,13),'b*');
hold on;
plot(m,m,'g-');
title('Predicted vs. Total Uplift for l=1.3');
xlabel('Total Uplift');
ylabel('Predicted Uplift');
legend('Uplift vs. Pred. Uplift','1-1 Line','Location','Best');
legend('boxoff');
saveas(ph,strcat(base_file_name,'_upliftmisfit_l_13.png'));

figure;
ph=plot(Hoh_uplift_meters,Hoh_predicted_uplift(:,14),'b*');
hold on;
plot(m,m,'g-');
title('Predicted vs. Total Uplift for l=1.4');
xlabel('Total Uplift');
ylabel('Predicted Uplift');
legend('Uplift vs. Pred. Uplift','1-1 Line','Location','Best');
legend('boxoff');
saveas(ph,strcat(base_file_name,'_upliftmisfit_l_14.png'));

figure;
ph=plot(Hoh_uplift_meters,Hoh_predicted_uplift(:,15),'b*');
hold on;
plot(m,m,'g-');
title('Predicted vs. Total Uplift for l=1.5');
xlabel('Total Uplift');
ylabel('Predicted Uplift');
legend('Uplift vs. Pred. Uplift','1-1 Line','Location','Best');
legend('boxoff');
saveas(ph,strcat(base_file_name,'_upliftmisfit_l_15.png'));

figure;
ph=plot(Hoh_uplift_meters,Hoh_predicted_uplift(:,16),'b*');
hold on;
plot(m,m,'g-');
title('Predicted vs. Total Uplift for l=1.6');
xlabel('Total Uplift');
ylabel('Predicted Uplift');
legend('Uplift vs. Pred. Uplift','1-1 Line','Location','Best');
legend('boxoff');
saveas(ph,strcat(base_file_name,'_upliftmisfit_l_16.png'));

figure;
ph=plot(Hoh_uplift_meters,Hoh_predicted_uplift(:,17),'b*');
hold on;
plot(m,m,'g-');
title('Predicted vs. Total Uplift for l=1.7');
xlabel('Total Uplift');
ylabel('Predicted Uplift');
```

```
legend('Uplift vs. Pred. Uplift','1-1 Line','Location','Best');
legend('boxoff');
saveas(ph,strcat(base_file_name,'_upliftmisfit_l_17.png'));

figure;
ph=plot(Hoh_uplift_meters,Hoh_predicted_uplift(:,18),'b*');
hold on;
plot(m,m,'g-');
title('Predicted vs. Total Uplift for l=1.8');
xlabel('Total Uplift');
ylabel('Predicted Uplift');
legend('Uplift vs. Pred. Uplift','1-1 Line','Location','Best');
legend('boxoff');
saveas(ph,strcat(base_file_name,'_upliftmisfit_l_18.png'));

figure;
ph=plot(Hoh_uplift_meters,Hoh_predicted_uplift(:,19),'b*');
hold on;
plot(m,m,'g-');
title('Predicted vs. Total Uplift for l=1.9');
xlabel('Total Uplift');
ylabel('Predicted Uplift');
legend('Uplift vs. Pred. Uplift','1-1 Line','Location','Best');
legend('boxoff');
saveas(ph,strcat(base_file_name,'_upliftmisfit_l_19.png'));

figure;
ph=plot(Hoh_uplift_meters,Hoh_predicted_uplift(:,20),'b*');
hold on;
plot(m,m,'g-');
title('Predicted vs. Total Uplift for l=2.0');
xlabel('Total Uplift');
ylabel('Predicted Uplift');
legend('Uplift vs. Pred. Uplift','1-1 Line','Location','Best');
legend('boxoff');
saveas(ph,strcat(base_file_name,'_upliftmisfit_l_20.png'));

%!!!!!!Now do linear fits for each and r-squared values
%Linear fits must be done by hand!!!!!
%Record r-squared values in notebook

%Get R^2
mean_Hoh_uplift_meters=mean(Hoh_uplift_meters);

mean_Hoh_predicted_uplift_00=mean(Hoh_predicted_uplift_0);
mean_Hoh_predicted_uplift_01=mean(Hoh_predicted_uplift(:,1));
mean_Hoh_predicted_uplift_02=mean(Hoh_predicted_uplift(:,2));
mean_Hoh_predicted_uplift_03=mean(Hoh_predicted_uplift(:,3));
mean_Hoh_predicted_uplift_04=mean(Hoh_predicted_uplift(:,4));
mean_Hoh_predicted_uplift_05=mean(Hoh_predicted_uplift(:,5));
mean_Hoh_predicted_uplift_06=mean(Hoh_predicted_uplift(:,6));
mean_Hoh_predicted_uplift_07=mean(Hoh_predicted_uplift(:,7));
mean_Hoh_predicted_uplift_08=mean(Hoh_predicted_uplift(:,8));
mean_Hoh_predicted_uplift_09=mean(Hoh_predicted_uplift(:,9));
mean_Hoh_predicted_uplift_10=mean(Hoh_predicted_uplift(:,10));
mean_Hoh_predicted_uplift_11=mean(Hoh_predicted_uplift(:,11));
```

```
mean_Hoh_predicted_uplift_12=mean(Hoh_predicted_uplift(:,12));
mean_Hoh_predicted_uplift_13=mean(Hoh_predicted_uplift(:,13));
mean_Hoh_predicted_uplift_14=mean(Hoh_predicted_uplift(:,14));
mean_Hoh_predicted_uplift_15=mean(Hoh_predicted_uplift(:,15));
mean_Hoh_predicted_uplift_16=mean(Hoh_predicted_uplift(:,16));
mean_Hoh_predicted_uplift_17=mean(Hoh_predicted_uplift(:,17));
mean_Hoh_predicted_uplift_18=mean(Hoh_predicted_uplift(:,18));
mean_Hoh_predicted_uplift_19=mean(Hoh_predicted_uplift(:,19));
mean_Hoh_predicted_uplift_20=mean(Hoh_predicted_uplift(:,20));

sum_x=(Hoh_uplift_meters-(mean_Hoh_uplift_meters));

sum_y_00=(Hoh_predicted_uplift_0-(mean_Hoh_predicted_uplift_00));
sum_y_01=(Hoh_predicted_uplift(:,1)-(mean_Hoh_predicted_uplift_01));
sum_y_02=(Hoh_predicted_uplift(:,2)-(mean_Hoh_predicted_uplift_02));
sum_y_03=(Hoh_predicted_uplift(:,3)-(mean_Hoh_predicted_uplift_03));
sum_y_04=(Hoh_predicted_uplift(:,4)-(mean_Hoh_predicted_uplift_04));
sum_y_05=(Hoh_predicted_uplift(:,5)-(mean_Hoh_predicted_uplift_05));
sum_y_06=(Hoh_predicted_uplift(:,6)-(mean_Hoh_predicted_uplift_06));
sum_y_07=(Hoh_predicted_uplift(:,7)-(mean_Hoh_predicted_uplift_07));
sum_y_08=(Hoh_predicted_uplift(:,8)-(mean_Hoh_predicted_uplift_08));
sum_y_09=(Hoh_predicted_uplift(:,9)-(mean_Hoh_predicted_uplift_09));
sum_y_10=(Hoh_predicted_uplift(:,10)-(mean_Hoh_predicted_uplift_10));
sum_y_11=(Hoh_predicted_uplift(:,11)-(mean_Hoh_predicted_uplift_11));
sum_y_12=(Hoh_predicted_uplift(:,12)-(mean_Hoh_predicted_uplift_12));
sum_y_13=(Hoh_predicted_uplift(:,13)-(mean_Hoh_predicted_uplift_13));
sum_y_14=(Hoh_predicted_uplift(:,14)-(mean_Hoh_predicted_uplift_14));
sum_y_15=(Hoh_predicted_uplift(:,15)-(mean_Hoh_predicted_uplift_15));
sum_y_16=(Hoh_predicted_uplift(:,16)-(mean_Hoh_predicted_uplift_16));
sum_y_17=(Hoh_predicted_uplift(:,17)-(mean_Hoh_predicted_uplift_17));
sum_y_18=(Hoh_predicted_uplift(:,18)-(mean_Hoh_predicted_uplift_18));
sum_y_19=(Hoh_predicted_uplift(:,19)-(mean_Hoh_predicted_uplift_19));
sum_y_20=(Hoh_predicted_uplift(:,20)-(mean_Hoh_predicted_uplift_20));

top_00=sum(sum_x.*sum_y_00);
top_01=sum(sum_x.*sum_y_01);
top_02=sum(sum_x.*sum_y_02);
top_03=sum(sum_x.*sum_y_03);
top_04=sum(sum_x.*sum_y_04);
top_05=sum(sum_x.*sum_y_05);
top_06=sum(sum_x.*sum_y_06);
top_07=sum(sum_x.*sum_y_07);
top_08=sum(sum_x.*sum_y_08);
top_09=sum(sum_x.*sum_y_09);
top_10=sum(sum_x.*sum_y_10);
top_11=sum(sum_x.*sum_y_11);
top_12=sum(sum_x.*sum_y_12);
top_13=sum(sum_x.*sum_y_13);
top_14=sum(sum_x.*sum_y_14);
top_15=sum(sum_x.*sum_y_15);
top_16=sum(sum_x.*sum_y_16);
top_17=sum(sum_x.*sum_y_17);
top_18=sum(sum_x.*sum_y_18);
top_19=sum(sum_x.*sum_y_19);
top_20=sum(sum_x.*sum_y_20);
```

```
bottom_1=sum((sum_x).^2);

bottom_2_00=sum((sum_y_00).^2);
bottom_2_01=sum((sum_y_01).^2);
bottom_2_02=sum((sum_y_02).^2);
bottom_2_03=sum((sum_y_03).^2);
bottom_2_04=sum((sum_y_04).^2);
bottom_2_05=sum((sum_y_05).^2);
bottom_2_06=sum((sum_y_06).^2);
bottom_2_07=sum((sum_y_07).^2);
bottom_2_08=sum((sum_y_08).^2);
bottom_2_09=sum((sum_y_09).^2);
bottom_2_10=sum((sum_y_10).^2);
bottom_2_11=sum((sum_y_11).^2);
bottom_2_12=sum((sum_y_12).^2);
bottom_2_13=sum((sum_y_13).^2);
bottom_2_14=sum((sum_y_14).^2);
bottom_2_15=sum((sum_y_15).^2);
bottom_2_16=sum((sum_y_16).^2);
bottom_2_17=sum((sum_y_17).^2);
bottom_2_18=sum((sum_y_18).^2);
bottom_2_19=sum((sum_y_19).^2);
bottom_2_20=sum((sum_y_20).^2);

r_squared_00=(top_00^2)/(bottom_1*bottom_2_00);
r_squared_01=(top_01^2)/(bottom_1*bottom_2_01);
r_squared_02=(top_02^2)/(bottom_1*bottom_2_02);
r_squared_03=(top_03^2)/(bottom_1*bottom_2_03);
r_squared_04=(top_04^2)/(bottom_1*bottom_2_04);
r_squared_05=(top_05^2)/(bottom_1*bottom_2_05);
r_squared_06=(top_06^2)/(bottom_1*bottom_2_06);
r_squared_07=(top_07^2)/(bottom_1*bottom_2_07);
r_squared_08=(top_08^2)/(bottom_1*bottom_2_08);
r_squared_09=(top_09^2)/(bottom_1*bottom_2_09);
r_squared_10=(top_10^2)/(bottom_1*bottom_2_10);
r_squared_11=(top_11^2)/(bottom_1*bottom_2_11);
r_squared_12=(top_12^2)/(bottom_1*bottom_2_12);
r_squared_13=(top_13^2)/(bottom_1*bottom_2_13);
r_squared_14=(top_14^2)/(bottom_1*bottom_2_14);
r_squared_15=(top_15^2)/(bottom_1*bottom_2_15);
r_squared_16=(top_16^2)/(bottom_1*bottom_2_16);
r_squared_17=(top_17^2)/(bottom_1*bottom_2_17);
r_squared_18=(top_18^2)/(bottom_1*bottom_2_18);
r_squared_19=(top_19^2)/(bottom_1*bottom_2_19);
r_squared_20=(top_20^2)/(bottom_1*bottom_2_20);

%VIII. On average, how badly is predicted uplift calculated?
for q=1:20
     Hoh_misfit(q)=(sum((Hoh_uplift_meters-
      Hoh_predicted_uplift(:,q)).^2)/(29-2));
end

Hoh_misfit_0=(sum((Hoh_uplift_meters-Hoh_predicted_uplift_0).^2)/(29-
      2));

%IX. Make figure plots
```

```
%Plot Kg versus l
l=[0.1;0.2;0.3;0.4;0.5;0.6;0.7;0.8;0.9;1.0;1.1;1.2;1.3;1.4;1.5;1.6;
    1.7;1.8;1.9;2.0];

figure;
ph=plot(l,Kg,'b*');
hold on;
plot(0,Kg_0,'b*');
title('Kg Against l');
saveas(ph,strcat(base_file_name,'_Kgvsl.png'));

figure;
ph=semilogy(l,Kg,'b*');
hold on;
semilogy(0,Kg_0,'b*');
title('Kg Against l');
xlabel('l');
ylabel('log Kg');
saveas(ph,strcat(base_file_name,'_Kgvslogl.png'));

%Plot uplipft against predicted uplift for the profile
figure;
ph=plot(Hoh_longitudinalprofile_x,Hoh_uplift_meters,'b-');
hold on;
plot(Hoh_longitudinalprofile_x,Hoh_predicted_uplift_0,'r*-');
plot(Hoh_longitudinalprofile_x,Hoh_predicted_uplift(:,10),'g*-');
title('Predicted vs. Total Uplift for l=0');
xlabel('Distance Along the Hoh River (km)');
ylabel('Uplift Over 10,000 yrs (m)');
legend('Uplift','Pred. Uplift l=0','Pred. Uplift
      l=1','Location','NorthEast');
legend('boxoff');
saveas(ph,strcat(base_file_name,'_upliftvspreduplift_l_00.png'));

figure;
ph=plot(Hoh_longitudinalprofile_x,Hoh_uplift_meters,'b-');
hold on;
plot(Hoh_longitudinalprofile_x,Hoh_predicted_uplift(:,1),'r*-');
plot(Hoh_longitudinalprofile_x,Hoh_predicted_uplift(:,10),'g*-');
title('Predicted vs. Total Uplift for l=0.1');
xlabel('Distance Along the Hoh River (km)');
ylabel('Uplift Over 10,000 yrs (m)');
legend('Uplift','Pred. Uplift l=0.1','Pred. Uplift
      l=1','Location','NorthEast');
legend('boxoff');
saveas(ph,strcat(base_file_name,'_upliftvspreduplift_l_01.png'));

figure;
ph=plot(Hoh_longitudinalprofile_x,Hoh_uplift_meters,'b-');
hold on;
plot(Hoh_longitudinalprofile_x,Hoh_predicted_uplift(:,2),'r*-');
plot(Hoh_longitudinalprofile_x,Hoh_predicted_uplift(:,10),'g*-');
title('Predicted vs. Total Uplift for l=0.2');
xlabel('Distance Along the Hoh River (km)');
ylabel('Uplift Over 10,000 yrs (m)');
legend('Uplift','Pred. Uplift l=0.2','Pred. Uplift
```

```
      l=1','Location','NorthEast');
legend('boxoff');
saveas(ph,strcat(base_file_name,'_upliftvspreduplift_l_02.png'));

figure;
ph=plot(Hoh_longitudinalprofile_x,Hoh_uplift_meters,'b-');
hold on;
plot(Hoh_longitudinalprofile_x,Hoh_predicted_uplift(:,3),'r*-');
plot(Hoh_longitudinalprofile_x,Hoh_predicted_uplift(:,10),'g*-');
title('Predicted vs. Total Uplift for l=0.3');
xlabel('Distance Along the Hoh River (km)');
ylabel('Uplift Over 10,000 yrs (m)');
legend('Uplift','Pred. Uplift l=0.3','Pred. Uplift
      l=1','Location','NorthEast');
legend('boxoff');
saveas(ph,strcat(base_file_name,'_upliftvspreduplift_l_03.png'));

figure;
ph=plot(Hoh_longitudinalprofile_x,Hoh_uplift_meters,'b-');
hold on;
plot(Hoh_longitudinalprofile_x,Hoh_predicted_uplift(:,4),'r*-');
plot(Hoh_longitudinalprofile_x,Hoh_predicted_uplift(:,10),'g*-');
title('Predicted vs. Total Uplift for l=0.4');
xlabel('Distance Along the Hoh River (km)');
ylabel('Uplift Over 10,000 yrs (m)');
legend('Uplift','Pred. Uplift l=0.4','Pred. Uplift
      l=1','Location','NorthEast');
legend('boxoff');
saveas(ph,strcat(base_file_name,'_upliftvspreduplift_l_04.png'));

figure;
ph=plot(Hoh_longitudinalprofile_x,Hoh_uplift_meters,'b-');
hold on;
plot(Hoh_longitudinalprofile_x,Hoh_predicted_uplift(:,5),'r*-');
plot(Hoh_longitudinalprofile_x,Hoh_predicted_uplift(:,10),'g*-');
title('Predicted vs. Total Uplift for l=0.5');
xlabel('Distance Along the Hoh River (km)');
ylabel('Uplift Over 10,000 yrs (m)');
legend('Uplift','Pred. Uplift l=0.5','Pred. Uplift
      l=1','Location','NorthEast');
legend('boxoff');
saveas(ph,strcat(base_file_name,'_upliftvspreduplift_l_05.png'));

figure;
ph=plot(Hoh_longitudinalprofile_x,Hoh_uplift_meters,'b-');
hold on;
plot(Hoh_longitudinalprofile_x,Hoh_predicted_uplift(:,6),'r*-');
plot(Hoh_longitudinalprofile_x,Hoh_predicted_uplift(:,10),'g*-');
title('Predicted vs. Total Uplift for l=0.6');
xlabel('Distance Along the Hoh River (km)');
ylabel('Uplift Over 10,000 yrs (m)');
legend('Uplift','Pred. Uplift l=0.6','Pred. Uplift
      l=1','Location','NorthEast');
legend('boxoff');
saveas(ph,strcat(base_file_name,'_upliftvspreduplift_l_06.png'));
```

```
figure;
ph=plot(Hoh_longitudinalprofile_x,Hoh_uplift_meters,'b-');
hold on;
plot(Hoh_longitudinalprofile_x,Hoh_predicted_uplift(:,7),'r*-');
plot(Hoh_longitudinalprofile_x,Hoh_predicted_uplift(:,10),'g*-');
title('Predicted vs. Total Uplift for l=0.7');
xlabel('Distance Along the Hoh River (km)');
ylabel('Uplift Over 10,000 yrs (m)');
legend('Uplift','Pred. Uplift l=0.7','Pred. Uplift
      l=1','Location','NorthEast');
legend('boxoff');
saveas(ph,strcat(base_file_name,'_upliftvspreduplift_l_07.png'));

figure;
ph=plot(Hoh_longitudinalprofile_x,Hoh_uplift_meters,'b-');
hold on;
plot(Hoh_longitudinalprofile_x,Hoh_predicted_uplift(:,8),'r*-');
plot(Hoh_longitudinalprofile_x,Hoh_predicted_uplift(:,10),'g*-');
title('Predicted vs. Total Uplift for l=0.8');
xlabel('Distance Along the Hoh River (km)');
ylabel('Uplift Over 10,000 yrs (m)');
legend('Uplift','Pred. Uplift l=0.8','Pred. Uplift
      l=1','Location','NorthEast');
legend('boxoff');
saveas(ph,strcat(base_file_name,'_upliftvspreduplift_l_08.png'));

figure;
ph=plot(Hoh_longitudinalprofile_x,Hoh_uplift_meters,'b-');
hold on;
plot(Hoh_longitudinalprofile_x,Hoh_predicted_uplift(:,9),'r*-');
plot(Hoh_longitudinalprofile_x,Hoh_predicted_uplift(:,10),'g*-');
title('Predicted vs. Total Uplift for l=0.9');
xlabel('Distance Along the Hoh River (km)');
ylabel('Uplift Over 10,000 yrs (m)');
legend('Uplift','Pred. Uplift l=0.9','Pred. Uplift
      l=1','Location','NorthEast');
legend('boxoff');
saveas(ph,strcat(base_file_name,'_upliftvspreduplift_l_09.png'));

figure;
ph=plot(Hoh_longitudinalprofile_x,Hoh_uplift_meters,'b-');
hold on;
plot(Hoh_longitudinalprofile_x,Hoh_predicted_uplift(:,10),'r*-');
plot(Hoh_longitudinalprofile_x,Hoh_predicted_uplift(:,10),'g*-');
title('Predicted vs. Total Uplift for l=1.0');
xlabel('Distance Along the Hoh River (km)');
ylabel('Uplift Over 10,000 yrs (m)');
legend('Uplift','Pred. Uplift l=1.0','Pred. Uplift
      l=1','Location','NorthEast');
legend('boxoff');
saveas(ph,strcat(base_file_name,'_upliftvspreduplift_l_10.png'));

figure;
ph=plot(Hoh_longitudinalprofile_x,Hoh_uplift_meters,'b-');
hold on;
plot(Hoh_longitudinalprofile_x,Hoh_predicted_uplift(:,11),'r*-');
```

```
plot(Hoh_longitudinalprofile_x,Hoh_predicted_uplift(:,10),'g*-');
title('Predicted vs. Total Uplift for l=1.1');
xlabel('Distance Along the Hoh River (km)');
ylabel('Uplift Over 10,000 yrs (m)');
legend('Uplift','Pred. Uplift l=1.1','Pred. Uplift
      l=1','Location','NorthEast');
legend('boxoff');
saveas(ph,strcat(base_file_name,'_upliftvspreduplift_l_11.png'));

figure;
ph=plot(Hoh_longitudinalprofile_x,Hoh_uplift_meters,'b-');
hold on;
plot(Hoh_longitudinalprofile_x,Hoh_predicted_uplift(:,12),'r*-');
plot(Hoh_longitudinalprofile_x,Hoh_predicted_uplift(:,10),'g*-');
title('Predicted vs. Total Uplift for l=1.2');
xlabel('Distance Along the Hoh River (km)');
ylabel('Uplift Over 10,000 yrs (m)');
legend('Uplift','Pred. Uplift l=1.2','Pred. Uplift
      l=1','Location','NorthEast');
legend('boxoff');
saveas(ph,strcat(base_file_name,'_upliftvspreduplift_l_12.png'));

figure;
ph=plot(Hoh_longitudinalprofile_x,Hoh_uplift_meters,'b-');
hold on;
plot(Hoh_longitudinalprofile_x,Hoh_predicted_uplift(:,13),'r*-');
plot(Hoh_longitudinalprofile_x,Hoh_predicted_uplift(:,10),'g*-');
title('Predicted vs. Total Uplift for l=1.3');
xlabel('Distance Along the Hoh River (km)');
ylabel('Uplift Over 10,000 yrs (m)');
legend('Uplift','Pred. Uplift l=1.3','Pred. Uplift
      l=1','Location','NorthEast');
legend('boxoff');
saveas(ph,strcat(base_file_name,'_upliftvspreduplift_l_13.png'));

figure;
ph=plot(Hoh_longitudinalprofile_x,Hoh_uplift_meters,'b-');
hold on;
plot(Hoh_longitudinalprofile_x,Hoh_predicted_uplift(:,14),'r*-');
plot(Hoh_longitudinalprofile_x,Hoh_predicted_uplift(:,10),'g*-');
title('Predicted vs. Total Uplift for l=1.4');
xlabel('Distance Along the Hoh River (km)');
ylabel('Uplift Over 10,000 yrs (m)');
legend('Uplift','Pred. Uplift l=1.4','Pred. Uplift
      l=1','Location','NorthEast');
legend('boxoff');
saveas(ph,strcat(base_file_name,'_upliftvspreduplift_l_14.png'));

figure;
ph=plot(Hoh_longitudinalprofile_x,Hoh_uplift_meters,'b-');
hold on;
plot(Hoh_longitudinalprofile_x,Hoh_predicted_uplift(:,15),'r*-');
plot(Hoh_longitudinalprofile_x,Hoh_predicted_uplift(:,10),'g*-');
title('Predicted vs. Total Uplift for l=1.5');
xlabel('Distance Along the Hoh River (km)');
ylabel('Uplift Over 10,000 yrs (m)');
```

```
legend('Uplift','Pred. Uplift l=1.5','Pred. Uplift
      l=1','Location','NorthEast');
legend('boxoff');
saveas(ph,strcat(base_file_name,'_upliftvspreduplift_l_15.png'));

figure;
ph=plot(Hoh_longitudinalprofile_x,Hoh_uplift_meters,'b-');
hold on;
plot(Hoh_longitudinalprofile_x,Hoh_predicted_uplift(:,16),'r*-');
plot(Hoh_longitudinalprofile_x,Hoh_predicted_uplift(:,10),'g*-');
title('Predicted vs. Total Uplift for l=1.6');
xlabel('Distance Along the Hoh River (km)');
ylabel('Uplift Over 10,000 yrs (m)');
legend('Uplift','Pred. Uplift l=1.6','Pred. Uplift
      l=1','Location','NorthEast');
legend('boxoff');
saveas(ph,strcat(base_file_name,'_upliftvspreduplift_l_16.png'));

figure;
ph=plot(Hoh_longitudinalprofile_x,Hoh_uplift_meters,'b-');
hold on;
plot(Hoh_longitudinalprofile_x,Hoh_predicted_uplift(:,17),'r*-');
plot(Hoh_longitudinalprofile_x,Hoh_predicted_uplift(:,10),'g*-');
title('Predicted vs. Total Uplift for l=1.7');
xlabel('Distance Along the Hoh River (km)');
ylabel('Uplift Over 10,000 yrs (m)');
legend('Uplift','Pred. Uplift l=1.7','Pred. Uplift
      l=1','Location','NorthEast');
legend('boxoff');
saveas(ph,strcat(base_file_name,'_upliftvspreduplift_l_17.png'));

figure;
ph=plot(Hoh_longitudinalprofile_x,Hoh_uplift_meters,'b-');
hold on;
plot(Hoh_longitudinalprofile_x,Hoh_predicted_uplift(:,18),'r*-');
plot(Hoh_longitudinalprofile_x,Hoh_predicted_uplift(:,10),'g*-');
title('Predicted vs. Total Uplift for l=1.8');
xlabel('Distance Along the Hoh River (km)');
ylabel('Uplift Over 10,000 yrs (m)');
legend('Uplift','Pred. Uplift l=1.8','Pred. Uplift
      l=1','Location','NorthEast');
legend('boxoff');
saveas(ph,strcat(base_file_name,'_upliftvspreduplift_l_18.png'));

figure;
ph=plot(Hoh_longitudinalprofile_x,Hoh_uplift_meters,'b-');
hold on;
plot(Hoh_longitudinalprofile_x,Hoh_predicted_uplift(:,19),'r*-');
plot(Hoh_longitudinalprofile_x,Hoh_predicted_uplift(:,10),'g*-');
title('Predicted vs. Total Uplift for l=1.9');
xlabel('Distance Along the Hoh River (km)');
ylabel('Uplift Over 10,000 yrs (m)');
legend('Uplift','Pred. Uplift l=1.9','Pred. Uplift
      l=1','Location','NorthEast');
legend('boxoff');
saveas(ph,strcat(base_file_name,'_upliftvspreduplift_l_19.png'));
```

```
figure;
ph=plot(Hoh_longitudinalprofile_x,Hoh_uplift_meters,'b-');
hold on;
plot(Hoh_longitudinalprofile_x,Hoh_predicted_uplift(:,20),'r*-');
plot(Hoh_longitudinalprofile_x,Hoh_predicted_uplift(:,10),'g*-');
title('Predicted vs. Total Uplift for l=2.0');
xlabel('Distance Along the Hoh River (km)');
ylabel('Uplift Over 10,000 yrs (m)');
legend('Uplift','Pred. Uplift l=2.0','Pred. Uplift
      l=1','Location','NorthEast');
legend('boxoff');
saveas(ph,strcat(base_file_name,'_upliftvspreduplift_l_20.png'));

%==========
%Clean-up
%==========
clear directory_name base_file_name_list entry base_file_name
clear longice_loc_temp longerosion_temp longtopo_temp longglac_temp
clear longdenud_temp filesize1 filesize3 filesize2 a aa SS_str x
clear topo_ss1 topo_ss2 topo_ss3 topo_ss4 topo_ss5 topo_ss6 topo_ss7
clear topo_ss8 topo_ss9 topo_ss10 ice_thick_ss1 ice_thick_ss2
clear ice_thick_ss3 ice_thick_ss4 ice_thick_ss5 ice_thick_ss6
clear ice_thick_ss7 ice_thick_ss8 ice_thick_ss9 ice_thick_ss10
clear total_erosion_ss1 total_erosion_ss2 total_erosion_ss3
clear total_erosion_ss4 total_erosion_ss5 total_erosion_ss6
clear total_erosion_ss7 total_erosion_ss8 total_erosion_ss9
clear total_erosion_ss10 sliding_ss1 sliding_ss2 sliding_ss3
clear sliding_ss4 sliding_ss5 sliding_ss6 sliding_ss7 sliding_ss8
clear sliding_ss9 sliding_ss10 Hoh_longitudinalprofile_x_full
clear Hoh_longitudinalprofile_x Hoh_x_full Hoh_y_full Hoh_x Hoh_y
clear Hoh_topography_10_full Hoh_uplift_old_10_full
clear Hoh_uplift_contours_10_full Hoh_ice_thick_10_full
clear Hoh_sliding_velocity_10_full Hoh_total_erosion_10_full
clear Hoh_topography_10 Hoh_uplift_old_10 Hoh_uplift_contours_10
clear Hoh_ice_thick_10 Hoh_sliding_velocity_10 Hoh_total_erosion_10
clear Hoh_totalerosion_rate_full Hoh_totalerosion_rate Hoh_sum_uplift
clear Hoh_sum_totalerosion Kg_l_1 Hoh_sliding_velocity_1
clear Hoh_sliding_velocity_2 Hoh_sliding_velocity_3
clear Hoh_sliding_velocity_4 Hoh_sliding_velocity_5
clear Hoh_sliding_velocity_6 Hoh_sliding_velocity_7
clear Hoh_sliding_velocity_8 Hoh_sliding_velocity_9
clear Hoh_sliding_velocity_10 Hoh_total_uplift Hoh_sliding_matrix
clear n m mean_Hoh_uplift_meters mean_Hoh_predicted_uplift_01
clear mean_Hoh_predicted_uplift_02 mean_Hoh_predicted_uplift_03
clear mean_Hoh_predicted_uplift_04 mean_Hoh_predicted_uplift_05
clear mean_Hoh_predicted_uplift_06 mean_Hoh_predicted_uplift_07
clear mean_Hoh_predicted_uplift_08 mean_Hoh_predicted_uplift_09
clear mean_Hoh_predicted_uplift_10 mean_Hoh_predicted_uplift_11
clear mean_Hoh_predicted_uplift_12 mean_Hoh_predicted_uplift_13
clear mean_Hoh_predicted_uplift_14 mean_Hoh_predicted_uplift_15
clear mean_Hoh_predicted_uplift_16 mean_Hoh_predicted_uplift_17
clear mean_Hoh_predicted_uplift_18 mean_Hoh_predicted_uplift_19
clear mean_Hoh_predicted_uplift_20 sum_x sum_y_01 sum_y_02 sum_y_03
clear sum_y_04 sum_y_05 sum_y_06 sum_y_07 sum_y_08 sum_y_09 sum_y_10
clear sum_y_11 sum_y_12 sum_y_13 sum_y_14 sum_y_15 sum_y_16 sum_y_17
```

```
clear sum_y_18 sum_y_19 sum_y_20 top_01 top_02 top_03 top_04 top_05
clear top_06 top_07 top_08 top_09 top_10 top_11 top_12 top_13 top_14
clear top_15 top_16 top_17 top_18 top_19 top_20 bottom_1 bottom_2_01
clear bottom_2_02 bottom_2_03 bottom_2_04 bottom_2_05 bottom_2_06
clear bottom_2_07 bottom_2_08 bottom_2_09 bottom_2_10 bottom_2_11
clear bottom_2_12 bottom_2_13 bottom_2_14 bottom_2_15 bottom_2_16
clear bottom_2_17 bottom_2_18 bottom_2_19 bottom_2_20 bottom_2_00
clear top_00 sum_y_00 mean_Hoh_predicted_uplift_00 S_denud1 SS_denud2
clear SS_denud3 SS_denud4 SS_denud5 SS_denud6 SS_denud7 SS_denud8
clear SS_denud9 SS_denud10 SS_str SS_topo1 SS_topo2 SS_topo3 SS_topo4
clear SS_topo5 SS_topo6 SS_topo7 SS_topo8 SS_topo9 SS_topo10
clear SS_erosion1 SS_erosion2 SS_erosion3 SS_erosion4 SS_erosion5
clear SS_erosion6 SS_erosion7 SS_erosion8 SS_erosion9 SS_erosion10
clear SS_glac1 SS_glac2 SS_glac3 SS_glac4 SS_glac5 SS_glac6 SS_glac7
clear SS_glac8 SS_glac9 SS_glac10 mean_Hoh_total_erosion sum_y_erosion
clear top_erosion bottom_2_erosion

end;
```

Misfit_Uplift.m

```
%File for determining the misfit and best fitting cases for predicted
uplift, uplift, and erosion in each valley (specify the names and
pertinent information first)

function misfit_new=Misfit_Uplift(input)

load fittingqueets
%This contains the uplift, sliding, and erosion from the river profile
kg=input(1);
%l_set=input(2);

%kg=9.245*10^(-4);
l_set=-0.1;

%Get predicted uplift from sliding
%Set l and Kg and n
n=29;

for l=l_set
    sliding = Queets_sliding_velocity_1.^l+Queets_sliding_velocity_2.^l
      +Queets_sliding_velocity_3.^l+Queets_sliding_velocity_4.^l+Queets
      _sliding_velocity_5.^l+Queets_sliding_velocity_6.^l+Queets_slidin
      g_velocity_7.^l+Queets_sliding_velocity_8.^l+Queets_sliding_veloc
      ity_9.^l+Queets_sliding_velocity_10.^l;
end

sliding_2 = 1000*sliding;

Queets_predicted=(kg).*sliding_2;


%average_erosion=sum(Queets_total_erosion_10)/n

average_uplift=sum(Queets_uplift_meters)/n

average_predicted=sum(Queets_predicted)/n


%Now get the error
%sigma=(sum(observed-expected)^2)/(n-m) with m=2 because Kg and l vary

step_1=Queets_predicted-Queets_uplift_meters;
%step_1=Queets_total_erosion_10-Queets_uplift_meters;

step_2=step_1.^2;

q=n-2;

step_3=sum(step_2)/q;

misfit_new=sqrt(step_3)
```

Part1.m

```
%File for determining the data needed for the misfit calculations by
extending the uplift to the edges of the continents

Quinault_pred_uplift_full_10=Quinault_predicted_uplift(:,10);
Quinault_pred_uplift_full_1=Quinault_predicted_uplift(:,1);
Quinault_uplift_full=Quinault_uplift_meters
Quinault_totalerosion_full=Quinault_total_erosion_10
Quinault_pred_uplift_full_0=Quinault_predicted_uplift_0
```

Part2.m

```
%File for plotting the data from the misfit calculations by extending
the uplift to the edges of the continents

%X Distance for Longitudinal Profile
Hoh_longitudinalprofile_x_full=[78.58114405;77.58114405;76.58114405;
      74.58114405;73.58114405;72.16693049;71.16693049;68.93086251;67.51
      664895;66.10243539;64.68822182;63.68822182;60.8597947;59.8597947;
      55.61715401;54.61715401;53.61715401;52.61715401;51.61715401;50.61
      715401;49.20294045;47.20294045;46.20294045;45.20294045;43.2029404
      5;42.20294045;40.78872689;39.78872689;38.78872689;36.55265891;35.
      13844535;33.72423179;32.72423179;30.48816381;29.48816381;27.48816
      381;26.48816381;25.48816381;24.48816381;20.36505818;19.36505818;1
      8.36505818;17.36505818;15.1289902;14.1289902;11.89292223;8.892922
      227;6.064495102;3.828427125;2.414213562;1.414213562;0];

%This does not have the outlier
Hoh_longitudinalprofile_x=[60.8597947;59.8597947;55.61715401;
    54.61715401;53.61715401;52.61715401;51.61715401;50.61715401;
    49.20294045;47.20294045;46.20294045;45.20294045;43.20294045;
    42.20294045;40.78872689;39.78872689;38.78872689;36.55265891;
    35.13844535;33.72423179;32.72423179;30.48816381;29.48816381;
    27.48816381;26.48816381;25.48816381;24.48816381;20.36505818;
    19.36505818;18.36505818;17.36505818;15.1289902;14.1289902;
    11.89292223;8.892922227;6.064495102;3.828427125;
    2.414213562;1.414213562;0];



%Coordinates of Profile
%Full has zeros in sliding and uplift still present in it
Hoh_x_full=[89;89;89;89;89;88;88;89;90;91;92;92;94;94;97;97;97;97;97;
      97;96;96;96;96;96;96;97;97;97;98;99;100;100;102;102;102;102;102;
      102;103;103;103;103;104;104;103;103;102;101;99;98;97;96];

Hoh_y_full=[22;23;24;26;27;28;29;31;32;33;34;35;37;38;41;42;43;44;45;
      46;47;49;50;51;53;54;55;56;57;59;60;61;62;63;64;66;67;68;69;73;
      74;75;76;78;79;81;84;85;86;87;86;86;85];

%These do not have the Outlier
Hoh_x=[94;94;97;97;97;97;97;97;96;96;96;96;96;96;97;97;97;98;99;
    100;100;102;102;102;102;102;102;103;103;103;103;104;104;103;
    103;101;99;98;97;96];

Hoh_y=[37;38;41;42;43;44;45;46;47;49;50;51;53;54;55;56;57;59;60;
    61;62;63;64;66;67;68;69;73;74;75;76;78;79;81;84;86;87;86;86;85];

%X Distance for Longitudinal Profile
Queets_longitudinalprofile_x_full=[71.56901311;70.56901311;69.56901311;
    68.56901311;67.15479955;66.15479955;63.32637242;62.32637242;
    61.32637242;60.32637242;58.09030445;57.09030445;56.09030445;
    55.09030445;51.48475317;50.48475317;48.24868519;46.83447163;
    45.42025807;44.42025807;43.00604451;42.00604451;41.00604451;
    40.00604451;37.76997653;36.76997653;34.53390855;33.53390855;
    32.53390855;29.37163089;26.54320377;25.1289902;24.1289902;
    23.1289902;22.1289902;21.1289902;20.1289902;17.89292223;
```

```
    16.89292223;15.89292223;14.89292223;13.47870866;8.478708665;
    6.242640687;5.242640687;3.828427125;2.414213562;1.414213562;0];

Queets_longitudinalprofile_x=[43.00604451;42.00604451;41.00604451;
    40.00604451;37.76997653;36.76997653;34.53390855;33.53390855;
    32.53390855;29.37163089;26.54320377;25.1289902;24.1289902;
    23.1289902;22.1289902;21.1289902;20.1289902;17.89292223;
    16.89292223;15.89292223;14.89292223;13.47870866;8.478708665;
    6.242640687;5.242640687;3.828427125;2.414213562;1.414213562;0];

%Coordinates of Profile
%Full has zeros in sliding and uplift still present in it
Queets_x_full=[65;65;65;65;64;64;66;66;66;66;67;67;67;67;69;69;70;
    71;72;72;73;73;73;73;75;75;76;76;76;79;81;82;82;82;82;82;82;83;
    83;83;83;84;87;89;89;90;91;91;92];

Queets_y_full=[28;29;30;31;32;33;35;36;37;38;40;41;42;43;46;47;49;
    50;51;52;53;54;55;56;57;58;60;61;62;63;65;66;67;68;69;70;71;73;
    74;75;76;77;81;82;83;84;85;86;87];

Queets_x=[73;73;73;73;75;75;76;76;76;79;81;82;82;82;82;82;82;83;
    83;83;83;84;87;89;89;90;91;91;92];

Queets_y=[53;54;55;56;57;58;60;61;62;63;65;66;67;68;69;70;71;73;
    74;75;76;77;81;82;83;84;85;86;87];

%X Distance for Longitudinal Profile
Quinault_longitudinalprofile_x_full=[93.32331943;92.32331943;
    91.32331943;87.32331943;86.32331943;85.32331943;83.32331943;
    79.71776815;77.48170018;76.48170018;75.48170018;74.48170018;
    73.48170018;72.48170018;70.48170018;69.06748661;67.65327305;
    66.23905949;64.82484593;63.41063236;62.41063236;61.41063236;
    60.41063236;59.41063236;52.70242843;51.70242843;50.70242843;
    49.28821487;48.28821487;47.28821487;45.87400131;44.45978774;
    43.04557418;40.8095062;39.8095062;38.39529264;37.39529264;
    35.39529264;34.39529264;32.98107908;31.98107908;29.7450111;
    28.7450111;25.13945983;24.13945983;22.72524626;19.11969499;
    16.88362701;14.64755903;11.81913191;10.40491835;8.990704785;
    7.990704785;4.828427125;3.414213562;2;1;0];

Quinault_longitudinalprofile_x=[52.70242843;51.70242843;50.70242843;
    49.28821487;48.28821487;47.28821487;45.87400131;44.45978774;
    43.04557418;40.8095062;39.8095062;38.39529264;37.39529264;
    35.39529264;34.39529264;32.98107908;31.98107908;29.7450111;
    28.7450111;25.13945983;24.13945983;22.72524626;19.11969499;
    16.88362701;14.64755903;11.81913191;10.40491835;8.990704785;
    7.990704785;4.828427125;3.414213562;2;1;0];

%Coordinates of Profile
%Full has zeros in sliding and uplift still present in it
Quinault_x_full=[43;43;43;43;43;43;43;46;47;47;47;47;47;47;47;48;
    49;50;51;52;52;52;52;52;58;58;58;59;59;59;60;61;62;63;63;64;64;
    64;64;65;65;66;66;68;68;69;71;72;73;75;76;77;77;80;81;82;82;82];

Quinault_y_full=[32;33;34;38;39;40;42;44;46;47;48;49;50;51;53;54;
```

```
    55;56;57;58;59;60;61;62;65;66;67;68;69;70;71;72;73;75;76;77;78;
    80;81;82;83;85;86;89;90;91;94;96;98;100;101;102;103;104;105;
    106;107;108];

Quinault_x=[58;58;58;59;59;59;60;61;62;63;63;64;64;64;64;65;65;
    66;66;68;68;69;71;72;73;75;76;77;77;80;81;82;82;82];

Quinault_y=[65;66;67;68;69;70;71;72;73;75;76;77;78;80;81;82;83;
    85;86;89;90;91;94;96;98;100;101;102;103;104;105;106;107;108];


%Make plots of the figures – switch the names of the rivers so each
river is included
figure;
ph=plot(Quinault_longitudinalprofile_x_full,Quinault_totalerosion_full,
      'g*-');
hold on;
plot(Quinault_longitudinalprofile_x_full,Quinault_uplift_full,'b-');
title('Erosion and Contoured Uplift');
xlabel('Distance Along the Quinault River (km)');
ylabel('Uplift or Erosion (m)');
legend('Erosion','Uplift','Location','NorthEast');
legend('boxoff');
%saveas(ph,strcat(base_file_name,'_erosionvsuplift2.png'));

figure;
ph=plot(Quinault_longitudinalprofile_x_full,Quinault_uplift_full,'b-');
hold on;
plot(Quinault_longitudinalprofile_x_full,Quinault_pred_uplift_full_1,'r
      *-');
plot(Quinault_longitudinalprofile_x_full,Quinault_pred_uplift_full_10,'
      g*-');
title('Predicted vs. Total Uplift for l=0.1');
xlabel('Distance Along the Quinault River (km)');
ylabel('Uplift Over 10,000 yrs (m)');
legend('Uplift','Pred. Uplift l=0.1','Pred. Uplift
      l=1','Location','NorthEast');
legend('boxoff');
%saveas(ph,strcat(base_file_name,'_upliftvspreduplift_l_04.png'));

figure;
ph=plot(Quinault_longitudinalprofile_x_full,Quinault_uplift_full,'b-');
hold on;
plot(Quinault_longitudinalprofile_x_full,Quinault_pred_uplift_full_10,'
      r*-');
plot(Quinault_longitudinalprofile_x_full,Quinault_pred_uplift_full_10,'
      g*-');
title('Predicted vs. Total Uplift for l=1.0');
xlabel('Distance Along the Quinault River (km)');
ylabel('Uplift Over 10,000 yrs (m)');
legend('Uplift','Pred. Uplift l=1.0','Pred. Uplift
      l=1','Location','NorthEast');
legend('boxoff');
%saveas(ph,strcat(base_file_name,'_upliftvspreduplift_l_10.png'));

figure;
```

```
ph=plot(Quinault_longitudinalprofile_x_full,Quinault_uplift_full,'b-');
hold on;
plot(Quinault_longitudinalprofile_x_full,Quinault_pred_uplift_full_0,'r
      *-');
plot(Quinault_longitudinalprofile_x_full,Quinault_pred_uplift_full_10,'
      g*-');
title('Predicted vs. Total Uplift for l=0');
xlabel('Distance Along the Quinault River (km)');
ylabel('Uplift Over 10,000 yrs (m)');
legend('Uplift','Pred. Uplift l=0','Pred. Uplift
      l=1','Location','NorthEast');
legend('boxoff');
%saveas(ph,strcat(base_file_name,'_upliftvspreduplift_l_0.png'));
```